FRÉDÉRIC JEAN

GAIT ANALYSIS, MODELLING, AND COMPARISON FROM UNCONSTRAINED WALKS AND VIEWPOINTS

View-rectification of Body-part Trajectories from Monocular Video Sequences

Thèse présentée
à la Faculté des études supérieures et postdoctorales de l'Université Laval
dans le cadre du programme de doctorat en génie électrique
pour l'obtention du grade de Philosophiæ doctor (Ph.D.)

Faculté des sciences et de génie
UNIVERSITÉ LAVAL
QUÉBEC

2012

Résumé

L'analyse, la modélisation et la comparaison de la démarche de personnes à l'aide d'algorithmes de vision artificielle a récemment suscité beaucoup d'intérêt dans les domaines d'applications médicales et de surveillance. Il y a en effet plusieurs avantages à utiliser des algorithmes de vision artificielle pour faire l'analyse, la modélisation et la comparaison de la démarche de personnes. Par exemple, la démarche d'une personne peut être analysée et modélisée de loin en observant la personne à l'aide d'une caméra, ce qui ne requiert pas le placement de marqueurs ou de senseurs sur la personne. De plus, la coopération des personnes observées n'est pas requise, ce qui permet d'utiliser la démarche des personnes comme un facteur d'identification biométrique dans les systèmes de surveillance automatique.

Les méthodes d'analyse et de modélisation de la démarche existantes comportent toutefois plusieurs limitations. Plusieurs de ces méthodes nécessitent une vue de profil des personnes puisque ce point de vue est optimal pour l'analyse et la modélisation de la démarche. La plupart de ces méthodes supposent également une distance assez grande entre les personnes et la caméra afin de limiter les effets néfastes que la projection de perspective a sur l'analyse et la modélisation de la démarche. Par ailleurs, ces méthodes ne gèrent pas les changements de direction et de vitesse dans les marches. Cela limite grandement les marches pouvant être analysées et modélisées dans les applications médicales et les applications de surveillance.

L'approche proposée dans cette thèse permet d'effectuer l'analyse, la modélisation et la comparaison de la démarche de personnes à partir de marches et de points de vue non contraints. L'approche proposée est principalement constituée d'une méthode de rectification du point de vue qui permet de générer une vue fronto-parallèle (vue de profil) de la trajectoire imagée des membres d'une personne. Cette méthode de rectification de la vue est basée sur un modèle de marche novateur qui utilise la géométrie projective pour faire les liens spatio-temporels entre la position des membres dans la scène et leur

contrepartie dans les images provenant d'une caméra. La tête et les pieds sont les seuls membres nécessaires à l'approche proposée dans cette thèse. La position et le suivi de ces membres sont automatiquement effectués par un algorithme de suivi des membres développé dans le cadre de cette thèse. L'analyse de la démarche est effectuée par une nouvelle méthode qui extrait des caractéristiques de la démarche à partir de la trajectoire rectifiée des membres. Un nouveau modèle de la démarche basé sur la trajectoire rectifiée des membres est proposé afin de permettre la modélisation et la comparaison de la démarche en utilisant les caractéristiques dynamiques de la démarche.

L'approche proposée dans cette thèse est premièrement validée à l'aide de marches synthétiques comprenant plusieurs points de vue différents ainsi que des changements de direction. Les résultats de cette étape de validation montrent que la méthode de rectification de la vue fonctionne correctement, et qu'il est possible d'extraire des caractéristiques de la démarche valides à partir de la trajectoire rectifiée des membres. Par la suite, l'analyse, la modélisation et la comparaison de la démarche de personnes sont effectuées sur des marches réelles qui ont été acquises dans le cadre de cette thèse. Ces marches sont particulièrement difficiles à analyser et à modéliser puisqu'elles ont été effectuées près de la caméra et qu'elles comportent des changements de direction et de vitesse. Les résultats d'analyse de la démarche confirment que les caractéristiques de la démarche obtenues à l'aide de la méthode proposée sont réalistes et sont en accord avec les résultats présentés dans les études cliniques de la démarche. Les résultats de modélisation et de comparaison de la démarche démontrent qu'il est possible d'utiliser la méthode proposée pour reconnaître des personnes par leur démarche dans le contexte des applications de surveillance. Les taux de reconnaissance obtenus sont bons considérant la complexité des marches utilisées dans cette thèse.

Abstract

Gait analysis, modelling and comparison using computer vision algorithms has recently attracted much attention for medical and surveillance applications. Analyzing and modelling a person's gait with computer vision algorithms has indeed some interesting advantages over more traditional biometrics. For instance, gait can be analyzed and modelled at a distance by observing the person with a camera, which means that no markers or sensors have to be worn by the person. Moreover, gait analysis and modelling using computer vision algorithms does not require the cooperation of the observed people, which thus allows for using gait as a biometric in surveillance applications.

Current gait analysis and modelling approaches have however severe limitations. For instance, several approaches require a side view of the walks since this viewpoint is optimal for gait analysis and modelling. Most approaches also require the walks to be observed far enough from the camera in order to avoid perspective distortion effects that would badly affect the resulting gait analyses and models. Moreover, current approaches do not allow for changes in walk direction and in walking speed, which greatly constraints the walks that can be analyzed and modelled in medical and surveillance applications.

The approach proposed in this thesis aims at performing gait analysis, modelling and comparison from unconstrained walks and viewpoints in medical and surveillance applications. The proposed approach mainly consists in a novel view-rectification method that generates a fronto-parallel viewpoint (side view) of the imaged trajectories of body parts. The view-rectification method is based on a novel walk model that uses projective geometry to provide the spatio-temporal links between the body-part positions in the scene and their corresponding positions in the images. The head and the feet are the only body parts that are relevant for the proposed approach. They are automatically localized and tracked in monocular video sequences using a novel body parts tracking algorithm. Gait analysis is performed by a novel method that extracts standard

gait measurements from the view-rectified body-part trajectories. A novel gait model based on body-part trajectories is also proposed in order to perform gait modelling and comparison using the dynamics of the gait.

The proposed approach is first validated using synthetic walks comprising different viewpoints and changes in the walk direction. The validation results shows that the proposed view-rectification method works well, that is, valid gait measurements can be extracted from the view-rectified body-part trajectories. Next, gait analysis, modelling, and comparison is performed on real walks acquired as part of this thesis. These walks are challenging since they were performed close to the camera and contain changes in walk direction and in walking speed. The results first show that the obtained gait measurements are realistic and correspond to the gait measurements found in references on clinical gait analysis. The gait comparison results then show that the proposed approach can be used to perform gait modelling and comparison in the context of surveillance applications by recognizing people by their gait. The computed recognition rates are quite good considering the challenging walks used in this thesis.

Contents

List of Figures

List of Tables

List of Algorithms

List of Notations

$\mathsf{1}$	First foot
$\mathsf{2}$	Second foot
A	Identifier for the first part of a gait model
$\mathbf{b}_{\ell,c}[n]$	Bounding box corner c position for the body part $\ell \in \mathcal{L}$ at frame n
$b_{\ell,c,x}[n]$	x coordinate of the bounding box corner c for the body part $\ell \in \mathcal{L}$ at frame n
$b_{\ell,c,y}[n]$	y coordinate of the bounding box corner c for the body part $\ell \in \mathcal{L}$ at frame n
BL	Bounding box bottom-left corner
BR	Bounding box bottom-right corner
BS	Bottom-start point of a motion plane
BE	Bottom-end point of a motion plane
B	Identifier for the second part of a gait model
$\mathcal{C}$	The set of bounding box corner labels, $\mathcal{C} : \{\mathsf{TL}, \mathsf{TR}, \mathsf{BL}, \mathsf{BR}\}$
C	The number of gait half-cycles in an implicit continuous tracking interval, with $C = K - 1$
C_i	The number of gait half-cycles in the continuous tracking interval i, with $C_i = K_i - 1$
c	A bounding box corner label, $c \in \mathcal{C}$; A colour channel, $c \in \{1, 2, 3\}$; The index of a gait half-cycle, $c = 1, 2, \ldots, C$
D	The number of components of a gait feature vector, $D = 4Q$ or $D = 4(Q - 1)$
$d[n]$	The imaged distance between the feet at frame n
$d_{\text{med}}[n]$	The median-filtered distance between the feet at frame n
$\mathbf{E}_{\ell}[c]$	A 3-vector representing the 3-D position in the scene of the extremity $\ell \in \mathcal{L}_{\text{E}}$ for gait half-cycle c
$\mathbf{E}_{\mathsf{Q_a}}[c]$	The projection of the position $\mathbf{E}_{\mathsf{M}}[c]$ onto the stride line in the scene for gait half-cycle c
$\mathbf{E}_{\mathsf{Q_b}}[c]$	The projection of the position $\mathbf{E}_{\mathsf{M}}[c + 1]$ onto the stride line in the scene for gait half-cycle c
$\mathbf{e}_{\ell}[c]$	A 2-vector representing the imaged position of the extremity $\ell \in \mathcal{L}_{\text{E}}$ for gait half-cycle c

$\mathbf{e}_m[c]$	The imaged position of the extremity of the foot that is moving in the cth gait half-cycle
$\mathbf{e}_{\bar{m}}[c]$	The imaged position of the extremity of the foot that is not moving in the cth gait half-cycle
$\mathbf{e}_{\mathsf{Q_a}}[c]$	The projection of the position $\mathbf{e}_{\mathsf{M}}[c]$ onto the stride line in the image for gait half-cycle c
$\mathbf{e}_{\mathsf{Q_b}}[c]$	The projection of the position $\mathbf{e}_{\mathsf{M}}[c+1]$ onto the stride line in the image for gait half-cycle c
$\mathbf{e}_z[c]$	The imaged position of the foot extremity that is furthest from the horizontal vanishing point $\mathbf{w}[c]$ for a given gait half-cycle c
$\mathbf{e}_{\bar{z}}[c]$	The imaged position of the foot extremity that is closest to the horizontal vanishing point $\mathbf{w}[c]$ for a given gait half-cycle c
$\mathbf{e}'_{\mathsf{FS}}[i,c]$	The view-rectified position of the moving foot extremity at the beginning of the gait half-cycle c in continuous tracking interval i
$\mathbf{e}'_{\mathsf{FE}}[i,c]$	The view-rectified position of the moving foot extremity at the end of the gait half-cycle c in continuous tracking interval i
f	The focal length of the camera
f_{L}	Number of frames considered for background learning
f_{s}	Camera frame sampling rate in frames per second (fps)
f_{c}	Maximum gait cadence to detect (step/minute)
f_{U}	Background model update frequency (in frames)
$\mathcal{G}_y$	Set of gaps on image row y
G_{A}	The number of gait feature vectors of type A in a walk
G_{B}	The number of gait feature vectors of type B in a walk
$G_{\mathsf{A},r}$	The number of gait feature vectors of type A in a walk for subject r
$G_{\mathsf{B},r}$	The number of gait feature vectors of type B in a walk for subject r
$\mathbf{g}_{\mathsf{A}}$	A D-vector representing a gait feature vector of type A
$\mathbf{g}_{\mathsf{B}}$	A D-vector representing a gait feature vector of type B
$\mathbf{g}_{\mathsf{B}}$	The βth gait feature vector of type B in a walk
$\mathbf{g}_{\mathsf{A}}[\alpha]$	The αth gait feature vector of type A in a walk
$\mathbf{g}_{\mathsf{B}}[\beta]$	The βth gait feature vector of type B in a walk
$\mathbf{g}_{\mathsf{A},r}[\alpha]$	The αth gait feature vector of type A in a walk for subject r
$\mathbf{g}_{\mathsf{B},r}[\beta]$	The βth gait feature vector of type B in a walk for subject r
$\overline{\mathbf{g}}_{\mathsf{A}}$	The D-vector representing the gait model of type A in a walk
$\overline{\mathbf{g}}_{\mathsf{B}}$	The D-vector representing the gait model of type B in a walk
$\overline{\mathbf{g}}_{\mathsf{A},r}$	The D-vector representing the gait model of type A in a walk for subject r

$\overline{\mathbf{g}}_{\mathsf{B},r}$	The D-vector representing the gait model of type B in a walk for subject r
$\overline{\mathbf{g}}'_{\mathsf{A},r}$	The $(R-1)$-vector representing the gait model $\overline{\mathbf{g}}_{\mathsf{A}}$ projected into a lower dimensional feature space
$\overline{\mathbf{g}}'_{\mathsf{B},r}$	The $(R-1)$-vector representing the gait model $\overline{\mathbf{g}}_{\mathsf{B}}$ projected into a lower dimensional feature space
$\mathbf{H}$	A 3×3 homography matrix
$\mathbf{H}_{\mathrm{G}}$	The 3×3 homography matrix that metrically rectifies imaged points lying onto the ground plane
$\mathbf{H}_{\ell}[c]$	The 3×3 homography matrix that metrically rectifies the motion plane $\Pi_{\ell}[c]$
$\mathbf{H}_{\ell}[i,c]$	The 3×3 homography matrix that locally rectifies the motion plane $\Pi_{\ell}[i,c]$
$\widehat{\mathbf{H}}_{\ell}[c]$	The 3×3 homography matrix that locally rectifies the motion plane $\Pi_{\ell}[c]$
h	Height of a synthetic subject
$h[i,c]$	Height computed for the cth gait half-cycle of continuous tracking interval i
H	Head label
$\mathbf{I}$	A 3×3 identity matrix
I	Colour image; Also the number of continuous tracking intervals for a walk
$I[x,y,c,n]$	Pixel value in image I at position (x,y) for channel c and frame n
I_{B}	Binary image
$I_{\mathrm{B}}[x,y,n]$	Pixel value in binary image I_{B} at position (x,y) for frame n
I_{M}	Median background model image
$I_{\mathrm{M}}[x,y,c,n]$	Pixel median value at position (x,y) for channel c and frame n
$I_{\mathrm{U}}[x,y,n]$	Background update condition for pixel at position (x,y) and frame n
J	The number of angles describing the motion directions of the leading foot
j	The jth angles describing the motion direction of the leading foot, $j = 1,2,\ldots,J$
$\mathbf{K}$	A 3×3 matrix representing the camera intrinsic parameters
K	The number of key times in an implicit continuous tracking interval
K_i	The number of key times in the continuous tracking interval i
k	The index of a key time in a implicit continuous tracking interval, $k = 1,2,\ldots,K$
$\mathcal{L}$	The set of body-part labels, $\mathcal{L} : \{\mathsf{H},\mathsf{L},\mathsf{R}\}$ or $\mathcal{L} : \{\mathsf{H},1,2\}$
$\mathcal{L}_{\mathrm{E}}$	The set of extremity labels, $\mathcal{L}_{\mathrm{E}} : \{\mathsf{H},\mathsf{L},\mathsf{R},\mathsf{M}\}$, or $\mathcal{L}_{\mathrm{E}} : \{\mathsf{H},1,2,\mathsf{M}\}$

$\mathcal{L}_\Pi$	The set of plane labels, $\mathcal{L}_\Pi : \{\mathsf{H}, \mathsf{F}\}$
$\mathcal{L}_\mathrm{S}$	The set of sample labels, $\mathcal{L}_\mathrm{S} : \{\mathsf{H}, \mathsf{F}\}$
$\mathcal{L}_\mathrm{F}$	The set of foot labels, $\mathcal{L}_\mathrm{F} : \{\mathsf{L}, \mathsf{R}\}$ or $\mathcal{L}_\mathrm{F} : \{1, 2\}$
ℓ	A label; $\ell \in \mathcal{L}$, $\ell \in \mathcal{L}_\Pi$, $\ell \in \mathcal{L}_\mathrm{E}$, or $\ell \in \mathcal{L}_\mathrm{F}$
l	Label of the leading foot; $\ell \in \mathcal{L}_\mathrm{F}$
$\bar{l}$	Label of the trailing foot; $\ell \in \mathcal{L}_\mathrm{F}$
$\mathbf{l}$	A 3-vector representing a line
$\mathbf{l}_\mathrm{d}[c]$	A 3-vector representing the displacement line for gait half-cycle c
$\mathbf{l}_\mathrm{s}[c]$	A 3-vector representing the stride line for gait half-cycle c
$\mathbf{l}_{\mathsf{Q_a}}[c]$	A 3-vector representing the line perpendicular to the stride line $\mathbf{l}_\mathrm{s}[c]$ and passing through the position $\mathbf{e}_\mathsf{M}[c]$ for gait half-cycle c
$\mathbf{l}_{\mathsf{Q_b}}[c]$	A 3-vector representing the line perpendicular to the stride line $\mathbf{l}_\mathrm{s}[c]$ and passing through the position $\mathbf{e}_\mathsf{M}[c+1]$ for gait half-cycle c
$\mathbf{l}_\infty$	A 3-vector representing the vanishing line of the ground plane
$\mathbf{l}_\ell[c]$	A 3-vector representing the vanishing line of the motion plane $\Pi_\ell[c]$
$\mathbf{l}_{\ell,\mathsf{S}}[c]$	A 3-vector representing the vertical line at the start positions of the motion plane $\Pi_\ell[c]$
$\mathbf{l}_{\ell,\mathsf{E}}[c]$	A 3-vector representing the vertical line at the end positions of the motion plane $\Pi_\ell[c]$
$\mathbf{l}_{\ell,\mathsf{T}}[c]$	A 3-vector representing the vertical line at the top positions of the motion plane $\Pi_\ell[c]$
$\mathbf{l}_{\ell,\mathsf{B}}[c]$	A 3-vector representing the vertical line at the bottom positions of the motion plane $\Pi_\ell[c]$
$\mathbf{M}$	The 3×4 projection matrix of a camera
m	Label of the moving foot; $m \in \mathcal{L}_\mathrm{F}$
$\bar{m}$	Label of the still foot; $\bar{m} \in \mathcal{L}_\mathrm{F}$
N	Total number of frames in a video sequence
N_c	Number of frames in the cth gait half-cycle
$\mathbf{n}$	A 3-vector representing a plane' normal vector in the scenes
$\mathbf{n}_\ell[c]$	The 3-vector representing the normal vector of the motion plane $\Pi_\ell[c]$
$\mathbf{n}_\mathrm{G}$	The 3-vector representing the normal vector of the ground plane
n	Current frame number
$n_{\mathrm{E},i}$	Ending frame of the ith continuous tracking interval
$n_{\mathrm{S},i}$	Starting frame of the ith continuous tracking interval
n_k	The kth key frame number in an implicit continuous tracking interval
$n_{k,i}$	The kth key frame number in continuous tracking interval i
$\mathcal{O}$	Set of motion plane points, $\mathcal{O} : \{\mathsf{BS}, \mathsf{BE}, \mathsf{TS}, \mathsf{TE}\}$
$\mathbf{O}$	The initial position of the leading foot in the synthetic scene

$O(x, x^r_{\mathrm{S}}, x^r_{\mathrm{E}})$	Objective function for a coordinate x in the gap $[x^r_{\mathrm{S}}, x^r_{\mathrm{E}}]$ belonging to the longest path path $\mathcal{P}^*$
o	A motion plane point, $o \in \mathcal{O}$
$\mathcal{P}^k_y$	kth existing path of paths set $\mathcal{Q}_y$ in row y
$\mathcal{P}^*$	The longest path of background gaps between the legs
$\mathbf{P}_\ell[n]$	A 3-vector representing of the 3-D position in the scene of the body part $\ell \in \mathcal{L}$ at frame n
$\mathbf{p}_\ell[n]$	A 2-vector representing of imaged position of the body part $\ell \in \mathcal{L}$ at frame n
$p_{\ell,x}[n]$	The abscissa of the imaged position of the body part $\ell \in \mathcal{L}$ at frame n
$p_{\ell,y}[n]$	The ordinate of the imaged position of the body part $\ell \in \mathcal{L}$ at frame n
$\mathbf{p}_m[n]$	The imaged position of the foot that is moving in the previous frame $n-1$; Also, the imaged position of the foot that is moving in the implicit gait half-cycle c at frame n.
$\mathbf{p}_{\bar{m}}[n]$	The imaged position of the foot that is not moving in the previous frame $n-1$; Also, the imaged position of the foot that is not moving in the implicit gait half-cycle c at frame n
$\mathbf{p}_{\ell\mathsf{B}}[n]$	The imaged position of the foot extremity $\ell \in \mathcal{L}_{\mathrm{F}}$ at frame n
$\mathbf{p}_{m\mathsf{B}}[n]$	The imaged position of the foot extremity with label m, that is, the label of the foot moving in implicit gait half-cycle c
$\mathbf{p}_{\mathsf{HT}}[n]$	The imaged position of the top of the silhouette at frame n
$\mathbf{p}'_\ell[n]$	The view-rectified position of the body part $\ell \in \mathcal{L}$ at frame n
$\mathbf{p}'_{\mathsf{HT}}[n]$	The view-rectified position of the top of the silhouette at frame n
$\mathcal{Q}_y$	Set of paths existing in row y
Q	Number of samples
q	Sample index, $q = 1, 2, \ldots, Q$
$\mathbf{R}$	A 3×3 rotation matrix
$\mathbf{R}_x$	A 3×3 rotation matrix describing a rotation around the X axis
$\mathbf{R}_y$	A 3×3 rotation matrix describing a rotation around the Y axis
$\mathbf{R}_z$	A 3×3 rotation matrix describing a rotation around the Z axis
$\mathbf{R}_{\mathrm{G}}$	The 3×3 rotation matrix of the ground plane
R	Number of subjects
r	Index of a subject, $r = 1, 2, \ldots, R$
$\mathbf{S}_{\mathrm{B}}$	The $D \times D$ between-subject scatter matrix
$\mathbf{S}_{\mathrm{W}}$	The $D \times D$ within-subject scatter matrix
$\mathbf{S}_r$	The $D \times D$ scatter matrix for subject r
$\mathbf{s}_{\mathsf{H}}[i, c, q]$	A 2-vector representing the qth sample of the view-rectified head position in gait half-cycle c of interval i

$\mathbf{s}_{\mathsf{F}}[i,c,q]$	A 2-vector representing the qth sample of the view-rectified foot position in gait half-cycle c of interval i
$\mathbf{s}'_{\ell}[i,c,q]$	A 2-vector representing the qth sample of the position-based feature of $\ell \in \mathcal{L}_{\mathrm{S}}$ for gait half-cycle c and interval i
$\dot{\mathbf{s}}_{\ell}[i,c,q]$	A 2-vector representing the qth sample of the velocity-based feature of $\ell \in \mathcal{L}_{\mathrm{S}}$ for gait half-cycle c and interval i
$\mathcal{T}_{\ell,i}$	The trajectory of the body part $\ell \in \mathcal{L}$ for the continuous tracking interval i, which is defined as an ordered set of positions
$\mathcal{T}'_{\ell,i}$	The view-rectified trajectory of the body part $\ell \in \mathcal{L}$ for the continuous tracking interval i
$T[n]$	Timestamp of frame n
$T(t)$	Interpolated timestamp at non-integer frame number t
t	A non-integer valued frame number
t_k	The kth key time (non-integer frame number) in a walk (the continuous tracking interval is implicit)
$t_{k,i}$	The kth key time (non-integer frame number) of the continuous tracking interval i in a walk
t_c	The cth key time (non-integer frame number) in a walk (the continuous tracking interval is implicit)
$t_{c,i}$	The cth key time (non-integer frame number) of the continuous tracking interval i in a walk
TL	Bounding box top-left corner
TR	Bounding box top-right corner
TS	Top-start point of a motion plane
TE	Top-end point of a motion plane
u_0	Abscissa component of the camera principal point position
$\mathbf{v}[c]$	The vanishing point of the stride line for gait half-cycle c
$\mathbf{v}_{\perp}[c]$	The vanishing point which represent a direction perpendicular to $\mathbf{v}[c]$ for gait half-cycle c
$\mathbf{v}_{\mathrm{G}}[c]$	The vanishing point on the ground plane computed for gait half-cycle c
v_0	Ordinate component of the camera principal point position
$\mathbf{W}_{\mathsf{A}}$	The $D \times (R-1)$ matrix that projects the gait models of type A into a lower dimensional feature space
$\mathbf{W}_{\mathsf{B}}$	The $D \times (R-1)$ matrix that projects the gait models of type B into a lower dimensional feature space
W	Size of a search window for feet distance maxima detection
W_{med}	Size of a window for the median-filtering of the imaged feet distance
$\mathbf{w}[c]$	The vanishing point of the displacement line for gait half-cycle c

$\mathbf{X}_{\mathrm{c}}$	The 3-vector representing the 3-D position of the camera in the synthetic scene
$\overline{\mathbf{x}}_{\mathsf{A}}$	A D-vector representing a probe gait model of type A
$\overline{\mathbf{x}}_{\mathsf{B}}$	A D-vector representing a probe gait model of type B
$\overline{\mathbf{x}}'_{\mathsf{A}}$	The $(R-1)$-vector representing the probe gait model $\overline{\mathbf{x}}_{\mathsf{A}}$ projected into a lower dimensional feature space
$\overline{\mathbf{x}}'_{\mathsf{B}}$	The $(R-1)$-vector representing the probe gait model $\overline{\mathbf{x}}_{\mathsf{B}}$ projected into a lower dimensional feature space
X	The X axis in the scene
X_{L}	x coordinate of the left side of the legs region
X_{R}	x coordinate of the right side of the legs region
$x^j_{\mathrm{E},y}$	Ending coordinate of the jth gap in set $\mathcal{G}_y$ for row y
$x^k_{\mathrm{E},y}$	Ending coordinate of a gap in row y belonging to the kth gap in set $\mathcal{Q}_y$
x^r_{E}	Ending coordinate of the rth gap belonging to the longest path $\mathcal{P}^*$
$x_{\min}$	Leftmost coordinate of the gaps belonging to the longest path $\mathcal{P}^*$
$x_{\max}$	Rightmost coordinate of the gaps belonging to the longest path $\mathcal{P}^*$
$x^j_{\mathrm{S},y}$	Starting coordinate of the jth gap in set $\mathcal{G}_y$ for row y
$x^k_{\mathrm{S},y}$	Starting coordinate of a gap in row y belonging to the kth gap in set $\mathcal{Q}_y$
x^r_{S}	Ending coordinate of the rth gap belonging to the longest path $\mathcal{P}^*$
x^*	Optimal coordinate to divide the legs region in two parts
Y	The Y axis in the scene
Y_{B}	y coordinate of the bottom side of the legs region
Y_{T}	y coordinate of the top side of the legs region
Z	The Z axis in the scene
z	Label of the foot for which the extremity for a given gait half-cycle c is the furthest from the horizontal vanishing point $\mathbf{w}[c]$
$\bar{z}$	Label of the foot for which the extremity for a given gait half-cycle c is the closest to the horizontal vanishing point $\mathbf{w}[c]$
α	The index of a gait feature vector of type A, $\alpha = 1, 2, \ldots, G_{\mathsf{A}}$
α_x	Rotation angle around the X axis
α_y	Rotation angle around the Y axis
α_z	Rotation angle around the Z axis
β	The index of a gait feature vector of type B, $\beta = 1, 2, \ldots, G_{\mathsf{B}}$
$\gamma_{i,c,q}$	The qth frame number sample for gait half-cycle c in interval i
δ_{d}	A displacement on the ground plane
$\delta_{\mathrm{d}}[c]$	The displacement on the ground plane of a walker for the cth gait half-cycle

$\delta_{\mathrm{d}}[i,c]$	The displacement on the ground plane of a walker for the cth gait half-cycle in continuous tracking interval i
δ_{p}	A step length
$\delta_{\mathrm{p}}[k]$	The step length at the kth key time
δ_{s}	A stride length
$\delta_{\mathrm{s}}[c]$	The stride length for the cth gait half-cycle
$\delta_{\mathrm{s}}[i,c]$	The stride length for the cth gait half-cycle in continuous tracking interval i
δ_{w}	A stride width
$\delta_{\mathrm{w}}[k]$	The stride width at the kth key time
$\delta_{\mathrm{t}}[i,c]$	Duration of a gait half-cycle
$\delta_{\mathrm{t}}[i,c]$	Duration of the cth gait half-cycle in continuous tracking interval i
ϵ_{G}	The known length on the ground plane in scene units
ζ	Physical size of a camera pixel
η	Cadence computed for a walk
θ_j	The jth angle representing the motion direction of the leading foot
$\mathbf{\Lambda}$	A 3×3 isotropic scale matrix
$\mathbf{\Lambda}_{\mathrm{G}}$	The 3×3 isotropic scale matrix for the ground plane
λ	A scale factor
λ_{G}	The ground scale factor
ν_{H}	The vertical amplitude of the head motion as a percentage of the height h
ν_{F}	The vertical amplitude of the foot motion as a percentage of the height h
ξ_{A}	Minimum area for a connected region (pixels)
ξ_{B}	Minimum pixel value difference for a pixel to be considered as foreground
ξ_{HP}	Fraction of the pixels in the head region to count
ξ_{HR}	Height of the head region as a fraction of the silhouette bounding box height
ξ_{I}	Minimum interval duration (seconds)
ξ_{IH}	Minimum height of the silhouette bounding box as a fraction of the image height
ξ_{IW}	Minimum width of the silhouette bounding box as a fraction of the image width
ξ_{LR}	Height of the legs region as a fraction of the silhouette bounding box height
ξ_{LP}	Fraction of the pixels in the legs region to count in order to find a foot

ξ_{OF}	Maximum number of frames where the feet can be in an occlusion state (frames)
ξ_{OM}	Minimum number of counted pixel for the moving foot as a fraction of the of the number of foreground pixels in the legs region
ξ_{ON}	Minimal displacement between two consecutive frames for motion detection (pixels)
ξ_{OP}	Maximum number of counted pixel for the moving foot as a fraction of the of the number of foreground pixels in the legs region
$\xi_{\mathcal{P}}$	Minimum path length as a fraction of the legs region height
$\Pi_\ell[c]$	The motion plane $\ell \in \mathcal{L}_\Pi$ for gait half-cycle c in an implicit continuous tracking interval
$\Pi_\ell[i, c]$	The motion plane $\ell \in \mathcal{L}_\Pi$ for gait half-cycle c in continuous tracking interval i
$\boldsymbol{\pi}_{\ell,\mathsf{BS}}[c]$	The 2-vector representing the imaged bottom-start position of the motion plane $\Pi_\ell[c]$ for gait half-cycle c
$\boldsymbol{\pi}_{\ell,\mathsf{BE}}[c]$	The 2-vector representing the imaged bottom-end position of the motion plane $\Pi_\ell[c]$ for gait half-cycle c
$\boldsymbol{\pi}_{\ell,\mathsf{TS}}[c]$	The 2-vector representing the imaged top-start position of the motion plane $\Pi_\ell[c]$ for gait half-cycle c
$\boldsymbol{\pi}_{\ell,\mathsf{TE}}[c]$	The 2-vector representing the imaged top-end position of the motion plane $\Pi_\ell[c]$ for gait half-cycle c
$\Pi_{\mathsf{F}}[c]$	The imaged foot motion plane for gait half-cycle c
$\boldsymbol{\pi}_{\mathsf{F},\mathsf{BS}}[c]$	The 2-vector representing the imaged bottom-start position of the foot motion plane for gait half-cycle c
$\boldsymbol{\pi}_{\mathsf{F},\mathsf{BE}}[c]$	The 2-vector representing the imaged bottom-end position of the foot motion plane for gait half-cycle c
$\boldsymbol{\pi}_{\mathsf{F},\mathsf{TS}}[c]$	The 2-vector representing the imaged top-start position of the foot motion plane for gait half-cycle c
$\boldsymbol{\pi}_{\mathsf{F},\mathsf{TE}}[c]$	The 2-vector representing the imaged top-end position of the foot motion plane for gait half-cycle c
$\Pi_{\mathsf{H}}[c]$	The 2-vector representing the imaged head motion plane for gait half-cycle c,
$\boldsymbol{\pi}_{\mathsf{H},\mathsf{BS}}[c]$	The 2-vector representing the imaged bottom-start position of the head motion plane for gait half-cycle c
$\boldsymbol{\pi}_{\mathsf{H},\mathsf{BE}}[c]$	The 2-vector representing the imaged bottom-end position of the head motion plane for gait half-cycle c
$\boldsymbol{\pi}_{\mathsf{H},\mathsf{TS}}[c]$	The 2-vector representing the imaged top-start position of the head motion plane for gait half-cycle c
$\boldsymbol{\pi}_{\mathsf{H},\mathsf{TE}}[c]$	The 2-vector representing the imaged top-end position of the head motion plane for gait half-cycle c

$\widehat{\Pi}_\ell[c]$	The locally view-rectified version of the motion plane $\Pi_\ell[c]$
$\widehat{\boldsymbol{\pi}}_{\ell,o}[c]$	The 2-vector representing the point $o \in \mathcal{O}$ of the locally view-rectified motion plane $\widehat{\Pi}_\ell[c]$
$\widetilde{\overline{\boldsymbol{\pi}}}_{\ell,\mathsf{BS}}[c]$	The 2-vector representing the position of the point $\boldsymbol{\pi}_{\ell,\mathsf{BS}}[c]$ on the ground plane
$\widetilde{\overline{\boldsymbol{\pi}}}_{\ell,\mathsf{BE}}[c]$	The 2-vector representing the position of the point $\boldsymbol{\pi}_{\ell,\mathsf{BE}}[c]$ on the ground plane
$\Pi'_\ell[i,c]$	The metrically view-rectified version of the motion plane $\Pi_\ell[i,c]$
$\boldsymbol{\pi}'_{\ell,\mathsf{BS}}[i,c]$	The 2-vector representing the bottom-start position of the view-rectified motion plane $\Pi'_\ell[i,c]$
$\boldsymbol{\pi}'_{\ell,\mathsf{BE}}[i,c]$	The 2-vector representing the bottom-end position of the view-rectified motion plane $\Pi'_\ell[i,c]'$
$\boldsymbol{\pi}'_{\ell,\mathsf{TS}}[i,c]$	The 2-vector representing the top-start position of the view-rectified motion plane $\Pi'_\ell[i,c]'$
$\boldsymbol{\pi}'_{\ell,\mathsf{TE}}[i,c]$	The 2-vector representing the top-end position of the view-rectified motion plane $\Pi'_\ell[i,c]'$
$\rho_\ell[c]$	Aspect ratio of the locally view-rectified motion plane $\widehat{\Pi}_\ell[c]$
$\rho_{\mathsf{H}}[n]$	The normalized position of the head on the head displacement line segment
$\rho_{\mathsf{F}}[n]$	The normalized position of the foot on the stride line segment
$\tau[n]$	The normalized time at frame n in implicit gait half-cycle c
$\upsilon_\ell[c]$	The height of the motion plane $\Pi_\ell[c]$
υ_{med}	The median height of the motion planes in a walk
ϕ	Walking speed computed for a walk
Ψ	Size of the Gaussian kernel used to filter the body-part positions
$\boldsymbol{\Omega}$	A 3×3 matrix representing the image of the absolute conic (IAC)
$\omega_\ell[c]$	The width of the motion plane $\Pi_\ell[c]$ on the ground plane

Remerciements

J'aimerais remercier ici tous mes collègues et mes amis qui, de près ou de loin, ont contribué à l'achèvement de cette thèse de doctorat, soit par leurs encouragements, leurs conseils judicieux, ou par les connaissances qu'ils ont bien voulu partager avec moi. Je n'aurais pas pu mener à bien cette entreprise d'envergure et de longue haleine sans leur concours.

J'aimerais tout d'abord remercier le professeur Robert Bergevin, mon directeur de thèse, pour ses conseils, sa grande patiente, et son soutien tout au long de mes études doctorales. Je tiens également à remercier la professeure Alexandra Branzan Albu, ma codirectrice de thèse, pour son soutien, ses conseils, ses suggestions, et ses invitations à travailler sur mon doctorat à l'Université de Victoria à de nombreuses reprises.

Aussi, je remercie tous les étudiants et les professeurs du Laboratoire de Vision et Systèmes Numériques. Les conversations et les interactions avec plusieurs d'entre eux m'ont permis d'avoir de nouvelles idées et un regard nouveau sur mes travaux de doctorat. J'aimerais particulièrement remercier Jean-Nicolas Ouellet ainsi que le professeur Patrick Hébert pour leur aide et leurs conseils concernant la calibration de caméra et la géométrie projective. Je remercie également les étudiants du laboratoire SIMBIOSES de l'Université de Victoria qui m'ont accueilli à bras ouverts et qui m'ont permis d'améliorer considérablement mon anglais parlé et écrit.

Finalement, je tiens à remercier ma mère Sylvie, mon père Gilles, ma soeur Anne-Marie, ainsi que ma grand-mère Fernande pour leur soutien moral et leurs encouragements tout au long de mes études doctorales. Sans eux, je n'aurais jamais pu mener à bien ce doctorat.

"If we knew what it was we were doing, it would not be called research, would it?"

Albert Einstein

"See first, think later, then test. But always see first. Otherwise you will only see what you were expecting. Most scientists forget that."

Douglas Adams

"A common mistake people make when trying to design something completely foolproof is to underestimate the ingenuity of complete fools."

Douglas Adams, "Mostly Harmless"

"What we cannot reach by flying we must reach by limping... The Book says that it is no sin to limp."

Sigmund Freud, "XVIII, 64"

"I love deadlines. I like the whooshing sound they make as they fly by."

Douglas Adams

"Human beings, who are almost unique in having the ability to learn from the experience of others, are also remarkable for their apparent disinclination to do so."

Douglas Adams, "Last Chance to See"

"Nothing travels faster than the speed of light with the possible exception of bad news, which obeys its own special laws."

Douglas Adams, "The Hitchhiker's Guide to the Galaxy"

"The major difference between a thing that might go wrong and a thing that cannot possibly go wrong is that when a thing that cannot possibly go wrong goes wrong it usually turns out to be impossible to get at or repair."

Douglas Adams, "Mostly Harmless"

"What to do if you find yourself stuck with no hope of rescue: Consider yourself lucky that life has been good to you so far. Alternatively, if life hasn't been good to you so far, which given your present circumstances seems more likely, consider yourself lucky that it won't be troubling you much longer."

Douglas Adams, "The Hitchhiker's Guide to the Galaxy"

À ma mère Sylvie, mon père Gilles,
et ma soeur Anne-Marie.

Chapter 1

Introduction

"Our similarities are different."

Dale Berra

Walking is one of the most common daily actions performed by human beings. Despite its ubiquitousness, human locomotion is a complex action and it has been studied in great detail over the past century [1]. One of the first precise description of the normal human locomotion was made a century ago by A. A. Marks, an American who analyzed the walking process and illustrated it using eight different poses. Since then, the analysis of human locomotion has led to a terminology and collection of concepts that now constitute a wide field of study known as *gait* analysis and modelling. Today, this field of study is not only of interest to physicians, but also to physical therapists, neuroscientists, psychologists and engineers.

1.1 Definition of Gait

According to the Oxford Dictionary of English, gait is defined as "a person's manner of walking". One could also define gait as the set of movements performed when a person is walking. Interestingly, it was found that a person's gait can be represented by the motion of a set of 20 anatomical components [2]. Since the motion of these components is repeated over time, gait is said to be cyclic, that is, walking is a cyclic activity. This makes possible the temporal description of a person's gait by a sequence of events, or "key" times, that refer to specific spatial positions of some the components.

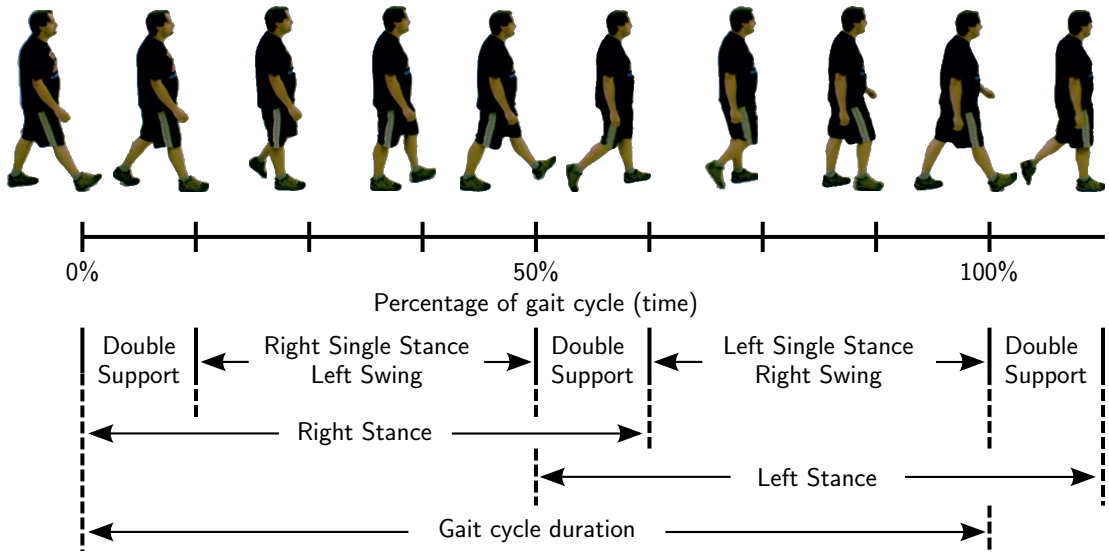

Figure 1.1 – Gait cycle temporal divisions. This is inspired of a figure presented in [3].

1.1.1 Terminology

A gait cycle is bounded temporally by the occurrence of two identical events during the walk. For instance, a gait cycle can be defined between the times where the right heel touches the ground (heel strike) as shown in Figure 1.1. This event is known as the *initial contact*, and is commonly used in the literature to define when a gait cycle begins and ends [1, 3]. The duration of a gait cycle is usually normalized to represent the percentage of completion of the cycle, that is, 0% refers to the beginning of the cycle, and 100% refers to the end.

The most important divisions (or phases) of the gait cycle are shown in Figure 1.1 and are discussed in detail in [1]. The *double support* phase (also called *double stance*) represents the time interval where both feet are in contact with the ground. It is followed by a *swing* phase of the left foot while the right foot is in a *single stance* phase. Another *double support* phase begins with the *initial contact* of the left foot, which occurs at around 50% of the gait cycle. The last half of the gait cycle is similar to the first half, with the right foot being in a *swing* phase and the left foot in a *single stance* phase. The *swing* phase accounts approximately for 38% of the gait cycle duration, while a *stance* phase, which includes two *double support* phases and a *single stance* phase, accounts for 62% of the gait cycle duration. It is worth noting that the *double support* phase duration decreases as the walk velocity increases. Moreover, the gait cycle of a running person consists only in *swing* phases and *single stance* phases, that is, there is no *double support* phases.

The most important spatial parameters of the gait are the *step length* and the *stride length*. The *step length* is the distance (in meters) between feet (heal to heal) at an initial contact, whereas the *stride length* is the distance (in meters) covered by a foot during a gait cycle (i.e. between two consecutive initial contacts). The *cadence* is a temporal parameter of the gait that is usually defined in steps per minute. It is used along with the *step length* to compute the *velocity* in meters per second (a spatio-temporal parameter of the gait). Regarding the direction of walk, it is usually referred to as the *line of progression*.

1.1.2 Gait Covariates

A person's gait can be influenced by the action of external factors, which are usually referred to as *covariates*. This means that movements performed during the walk will not always be the same because of the influence of these covariates. The most important gait covariates are [4, 5]:

- clothes (tight or loose clothes);
- footwear;
- surface type (grass, concrete, gravel, etc.);
- carried weight (backpack, suitcase, briefcase, bag, etc.);
- walk velocity;
- time (gait change over an extended period of time);
- emotional state [6].

The viewpoint from which gait is observed is also considered in the literature as a covariate [4, 5]. Although the viewpoint does not affect the gait itself, it does affect the way the gait *appears* in the images acquired from a fixed camera. This can have side effects on gait analyses that are performed using video sequences. Due to the perspective projection that is inherent in cameras, a person's gait can indeed appear distorted in the images. On the other hand, the perspective projection effects are negligible for the side view of a person walking relatively far away from a camera. The side view of a person, which is referred to as the fronto-parallel view in the literature, is actually the view from which most of the movements related to the gait are visible. It is therefore the viewpoint that is preferred for gait analysis. However, the fronto-parallel view is not always available, which is why the viewpoint is considered as a gait covariate.

1.2 Gait Modelling Applications

Gait modelling consists in extracting characteristics or a representation of the gait of a person or population. The nature of the characteristics or the representation can be application-dependent but usually takes the form of a set of parameters or a parametric function. The main purpose of building a gait model is to draw a general trend from the observations and to remove the small variations among the gait cycles of a person or population. Gait models are usually compared using some metrics (similarity or distance) in order to perform an application-dependent task.

Gait modelling and comparison is a very active research area and has found many practical applications. Medical applications are certainly the most common ones, although gait modelling has recently been considered for use in automatic surveillance applications. Some of these medical and surveillance applications are discussed in the following sections.

1.2.1 Medical Applications

Most medical applications consist in helping in the diagnosis of pathologies related to the human locomotion function. Some abnormalities in the gait patterns can be in fact considered as signs of the progression of some diseases [7, 8, 9]. The work presented in [7] proposes an approach based on computer vision to analyze the silhouettes of a walking person in order to categorize the walk style as normal walk, limping walk, line walk, swaying walk, or bending walk. Another computer vision-based approach [8] uses the silhouettes observed from a frontal view to build a model of the gait that makes possible the detection of subtle irregularities. By contrast, the method in [9] uses a motion capture system to extract gait features from joint motion trajectories, which are used to classify the gait as either with or without locomotion impairments.

Since the risk of fall in the elderly is more than ever a concern, some gait analysis methods were proposed to estimate the risks of falls and eventually to prevent it. The method proposed in [10] analyzes the gait of at risk elderlies by using a treadmill and a motion capture system. The minimum foot clearance[1] is analyzed in order to detect balance impairment and thus estimating the fall risks. In [12], the proposed method aims at building a remote system that would use computer vision techniques to analyze

[1]The minimum foot clearance (MFC) is the minimal distance between the foot and the ground when the velocity of the foot is at its maximum during the swing phase [11].

the gait of the elderly in their home and eventually to detect the moments when the risk of fall is high.

Some pathologies or physical conditions are directly associated with locomotion impairments, which affect the mobility and the posture of a person. This is the case for cerebral palsy [13] and knee osteoarthritis [14]. In [13], automatic gait analysis using a motion capture system is proposed as a way to assist in the diagnosis of cerebral palsy in early childhood. In the case of the method proposed in [14], knee osteoarthritis is detected and its severity is scored by analyzing gait data obtained from a force platform and an infrared camera system (special markers need to be placed on the subject's joints).

1.2.2 Surveillance Applications

Gait modelling and comparison has recently been considered in surveillance applications mainly because of the results shown by some early studies. A psychological study [15] first showed that people are able to recognize some biological activities (walking, running, bicycling, dancing, etc.) only by observing the motion of the moving lights (point-light displays) that are attached to the body joints of a person. Another study [16] using the same point-light displays system showed that it is also possible for people to recognize their friends by their walk, and more generally, the gender of a person. This is latter confirmed in the study presented in [17], which additionally concludes that gait can be used as a cue to the identity of a person. By modelling the gait of people using data obtained from various acquisition devices, one can compare the gait models and eventually matches the models corresponding to the same person. Since then, gait is considered as a biometric, like the fingerprints or the face of a person.

There are several works on surveillance applications that use gait as a way to recognize or classify people. In [18], human subjects are categorized as either "authorized" or "unauthorized" using the model of their gait, which is build using data from shoes with a pressure sensor, a tilt angle sensor, a gyroscope, a bend sensor and an accelerometer. A similar application is presented in [19], but it only uses the 3-D acceleration data acquired from a wearable device to model the gait. The method presented in [20] attempts to recognize people by their gait using foot motion data acquired from a motion capture system.

Gait modelling and recognition is also used in surveillance applications in combination with other biometrics. Some automatic surveillance systems, like the one presented in [21], are specifically designed to combine multiple biometrics in order to recognize

people. One of the main objectives of the system presented in [21] is to track pedestrians across a network of surveillance cameras using biometric such as face, appearance and gait. Gait and face recognition are usually combined together [22, 23] in surveillance applications since they are complementary to each other. Face recognition algorithms are indeed better suited for near frontal views, whereas gait recognition algorithms perform better with fronto-parallel views.

1.3 Computer Vision based Gait Modelling

Most of the medical and some surveillance applications discussed before rely on devices such as wearable sensors [14, 18, 19] or motion capture systems [9, 10, 13, 20]. The use of these devices complicates the acquisition process for both type of applications and absolutely necessitates cooperating subjects. Consequently, computer vision techniques have gained much interest due to their capability of performing gait analysis and modelling "at a distance". Acquiring gait data using a camera is indeed less intrusive (no wearable sensors or markers need to be placed on the subjects) and the cooperation of the subjects is not required in the case of surveillance applications.

Gait analysis and modelling approaches based on computer vision techniques can be divided in two categories: the *model-free* approaches (Section 1.3.1) and the *model-based* approaches (Section 1.3.2). Most of these gait modelling approaches are designed for surveillance applications, but some of them could be eventually extended in order to be used in medical applications (especially the model-based ones). Both model-free and model-based approaches are usually developed and tested using well established gait databases, which are specifically designed for computer vision-based gait modelling (Section 1.3.3).

1.3.1 Model-Free Approaches

Model-free approaches, which are also known as low-level, holistic, or appearance-based approaches, are mainly characterized by their gait model which often consists in a *representation* of *low-level data*. Most of these approaches model the gait as a representation of the binary silhouettes sequences obtained from a background subtraction algorithm. Although such low-level data contain information on both the *gait* and the *appearance* of a person, there is usually no effort made by model-free approaches to distinguish between the two kinds of information.

There are usually some post-processing steps performed on the obtained foreground binary images. For most of the model-free approaches, the biggest connected region in a foreground images is considered as the person's silhouette. These silhouettes are usually scaled to a predefined height H while maintaining the aspect ratio of their bounding box. Once they are scaled, the silhouettes are horizontally centred in a $H \times W$ image by either horizontally centring their scaled bounding box, or by centring the horizontal component of the silhouette's centroid. The scaled and centred silhouettes are typically contained within 128×88 pixels images.

One of the most well known gait model is the *Gait Energy Image* (GEI), which was first presented[2] in [25] and detailed in [26]. This gait model simply consists in an image defined as the average of all the silhouettes in a gait cycle. GEI is said to be a compact model and is robust to silhouette segmentation errors. The method in [27] proposes both supervised and unsupervised methods to select the most relevant parts of GEI in order to optimize gait recognition. In addition, some authors developed gait models that are inspired of or derived from GEI. This is the case of the method proposed in [28], which uses the variance of the silhouettes as a the gait model instead of the average of the silhouettes. The *Energy Deviation Images* are proposed as a model in [29] and are defined as the differences between the silhouettes and the GEI for a given gait cycle. The *Gait History Image* (GHI) proposed in [30] is another gait model that is similar to the GEI. In the GHI, the intensity value of a pixel depends on how many time the pixel changes for a foreground value and when those changes occur in the gait cycle.

There are some methods that consider key silhouettes [31] or even all the silhouettes [32] as a gait model, while other methods use low-level features extracted from the silhouettes. An example of the latter is the method described in [33], where a set of binary masks is used to compute the changes in the area of the silhouettes. Rather than using binary masks, the method in [34] defines an angular transform that computes the average pixels distance to the silhouette's centroid within angular sections. A more refined method presented in [35] first transforms the silhouettes non-linearly into a low-dimensional embedding using a Gaussian process latent variable model. The transformed silhouettes are then used to train a *Hidden Markov Model* (HMM), which is used as the gait model.

Some gait models are based on the contour of the silhouettes. A silhouette's contour is sometimes represented as a set of complex numbers obtained by sampling the silhouette's contour[3] at regular interval. The method presented in [36] uses this representation

[2]The model was also proposed at the same time by different authors under the name *Averaged Silhouettes* [24].

[3]The silhouette is centred beforehand on its centroid in the complex plane.

directly as a gait model, whereas the methods in [37] and [38] use the descriptors obtained respectively from Discrete Fourier Transforms (DFT) and Wavelets Transforms of each contour in a gait cycle. By contrast, the method in [39] computes the Discrete Fourier Transform on the set of complex contours in a gait cycle, and the gait model is defined as a Fourier Key Descriptor obtained by finding the component of the DFT having the maximum absolute value.

Some methods propose even simpler representations of the silhouettes to compute a model of the gait. The method proposed in [40] simply models the gait as the number of foreground pixels in each silhouette in a gait cycle. In [41], each silhouette is represented by a "width" vector (width of the silhouette at each row of the image), whereas in [42] and [43], the representation of the silhouette is the number of foreground pixels on each of row of the image. Another similar representation presented in [44] defines the gait model as the set of distances to the silhouette from the four borders of the bounding box.

There are some methods that use the silhouettes at their original size and position in the images. These methods use a volumetric representation from which a gait model is extracted. Each foreground frame in a gait cycle is usually kept to form a X-Y-T volume, where X and Y are the original image axis, and T is the time axis. The method presented in [45] proposes a gait model consisting in Gait Energy Images that are computed in the X-T plane over three different ranges of y values on the Y axis. X-Y-T volumes are used in [46] in order to perform frontal gait recognition. In this method, a X-Y-T volume is defined with the silhouette's edges over a gait cycle, and 3-D moments invariants of the volume are computed and used as a gait model.

Very few model-free methods do not use silhouettes to obtain a gait model. The method presented in [47] defines a gait model as a set of phase features that are obtained by optical-flow analysis. The method presented in [48] first uses the Laplacian of Gaussians operator to compute an edge map for each frame of a gait cycle, and then models the gait as the average of the Hough transform performed on each edge map.

1.3.2 Model-Based Approaches

In opposition to the model-free approaches, the model-based approaches model the gait using high-level data. These approaches define a spatial model of a person, that is, a model that represents the location of some of the body joints (neck, hips, knees, ankles, shoulders, elbows, wrists, etc.) and/or the location of some of the body parts (head, arms, legs, trunk, feet, hands, etc.). Some approaches also put constrains on the

location of the model parts with respect to each other. The model-parts locations are found in each frame by using low level data, and in some case, by using the previous model-parts locations. A gait model is then obtained by extracting features from the set of model-parts locations in a gait cycle.

Some model-based approaches only consider a limited number of body parts in order to model the gait. A typical example of this is the method proposed in [49], which only extracts the head, pelvis, and feet positions from predefined regions of the silhouettes. A gait model is then defined using the silhouette's height and the following distances : the distance between head and pelvis, the distance between feet, and the distances between the pelvis and each foot. A similar method presented in [50] analyzes the silhouette's contour shape and the bounding box in order to compute a gait model based on the person's height, strides length, and cadence. Using the silhouettes' skeleton, the method in [51] finds the position of some joints (head, neck, shoulder, pelvis, knees, and ankles), and computes angles between consecutive joints to model the gait of a person. The more sophisticated method presented in [52] (and further used in [53, 54, 55]) automatically extracts the ankles, the knees, and the hips positions using a motion template of the joints and a heel strike position detector. This motion template is derived from joints positions that are manually labelled in video sequences of many subjects. The angles between the joints are then computed and used as a gait model. In [56], the Velocity Hough Transform is proposed as a way to retrieve from the images the angle of the thigh, which is used as a gait model.

There exist model-based methods that consider many body parts in their spatial models. This is the case of the method described in [36], which models the gait by the fusion of the results obtained from a model-free and model-based method (see Section 1.3.1). The model-based method uses a spatial model consisting in 14 rigid parts that are positioned in the image with the help of learned motion and constrains models. However, only the angles of the legs and the thighs are used for gait modelling. The method described in [57], which is also used in [58], simply splits the silhouettes in seven regions representing the head, one of the arm, the torso, the thighs, and the legs. A gait model is build by first fitting an ellipse on each region, and then by computing the centroid, the orientation, and the aspect ratio of each ellipse. A five-links biped locomotion model is used in [59] to extract the ankles elevation, the ankles stride width, the knees elevation, and the knees stride width. A HMM is trained with these features and is used as the gait model. The method in [60] proposes a full-body layered deformable model that provides 22 parameters describing the human body (width, length, position, and orientation) over time. Other methods, as the one described in [61], simply uses manually defined binary masks representing the pixels belonging to body parts on the silhouettes. The gait model consists in the collection of

those binary masks and are directly used for gait comparison.

Other model-based approaches use a 3-D model of the human body to extract gait characteristics. The method in [62] represents each silhouette as a linear combination of prototype silhouettes, which in turn are used to compute the position of each of the 17 parts of a 3-D spatial model. The angles of the trunk, the thighs and the legs are computed and used as a gait model. Another method using a 10 joints 3-D model is presented in [63]. The luminance, edges and silhouettes acquired from multiple cameras are used in order to retrieve the position and the size of each part of the 3-D model, and a gait model is built by extracting the body parts length and the motion trajectory of the lower limbs.

1.3.3 Gait Databases

Many of the model-free and the model-based methods presented in the previous sections were tested on common gait databases. These gait databases consist in many video sequences of subjects walking in a given environment and under different walk conditions.

The HumanID Gait Challenge dataset[4] [5] is by far the most known and used gait database for computer vision based gait modelling and recognition. The database consists in a total of 1870 outdoor video sequences of 122 subjects who walk on an elliptic path. The acquisition setup is shown in Figure 1.2. The sequences are acquired by two cameras located at a distance of 15.85 m of the major axis of the path. The angle between the optical axis of the cameras is about 30 degrees. As reported by the authors, the view for the rear portion of the elliptic path is approximately fronto-parallel. Many gait covariates are considered in this database in order to provide realistic challenges to gait modelling and recognition algorithms. These covariates are the surface type (grass, concrete), the shoe-wear type (2), the weight carried (with or without carrying a briefcase), the viewpoint (2 cameras), and the time between the acquisitions (two different dates, six months apart). Moreover, twelve experiments of increasing difficulty are defined in the form of gallery/probe pairs, where a probe is a set of sequences that will be matched by a gait recognition algorithm to sequences in the gallery. Each experiment is defined such as the gallery sequences and the probe sequences differ with respect to one or more covariates.

The CASIA database [64] is also used by many researchers to develop and test gait

[4]It is sometime referred to as the USF gait database (University of South Florida).

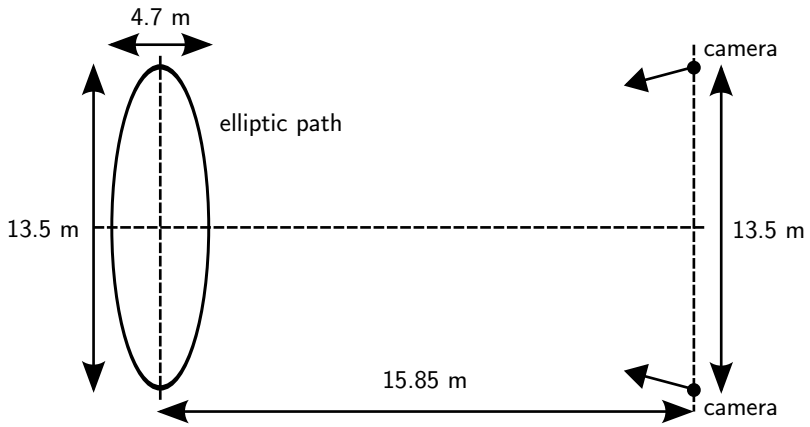

Figure 1.2 – The HumanID Gait database acquisition setup.

modelling and recognition algorithms. It consists in three parts, which are labelled Database A, Database B, and Database C. The Database A consists in 240 indoor video sequences of 20 subjects (12 sequences per subjects), where each subject walks in a straight line and is observed simultaneously from three cameras (4 sequences from a fronto-parallel view (90 degrees), 4 sequences from a frontal view (0 degree), and 4 sequences from a 45 degrees view). The Database B, which seems to be the most used of the three, consists in indoor video sequences of 124 subjects who are observed simultaneously from 11 cameras (0 degree to 180 degrees views) while walking on a straight line path. Three covariates are considered: the view, the clothing, and the carrying condition. Finally, the Database C consists in infra-red video sequences of 124 subjects observed from a fronto-parallel view at night. Four different walk conditions are considered: normal walk, normal walk with a bag, slow walk, and fast walk.

Another gait database that is extensively used is the SOTON [65] database (University of Southampton, UK). It consists in a small database and a large database. For the small database, 12 subjects walking on a straight line path are observed from four different views (fronto-parallel, frontal, oblique, and elevated). Some covariates are considered: slow/normal/fast walk, foot wears, worn coats, and carried bags. In the case of the large database, 116 subjects are observed repeatedly in both indoor and outdoor environments from two cameras (fronto-parallel and oblique views) while walking on a straight line path. The subjects are also observed from a fronto-parallel and an oblique view while walking on a treadmill.

The University of Maryland Database (UMD) [66] is worth noting since it was used by early works on gait modelling and recognition. The database #1 is comprised of outdoor video sequences of 25 subjects walking on a straight line. Two cameras are used to obtain four views of the walks: fronto-parallel views (toward left and toward

left) and frontal views (toward and away). The acquisition conditions of database #2 are similar to the ones in database #1 (outdoor, straight line walk), except that it involves 55 subjects observed from a fronto-parallel view and a frontal view.

Early gait modelling and recognition methods were also designed and tested on the CMU MoBo database [67] (Carnegie Mellon University Motion of Body Database). In this database, the subjects walk on a treadmill and are observed by six synchronized cameras, thus providing six different views (including the fronto-parallel view and the frontal view). The database provides the video sequences of the following four experiments for all of the 25 subjects: slow walk, fast walk, inclined walk, and walking with a ball.

1.4 Motivations

One may see that much effort has been made to model the gait under different acquisition conditions and gait covariates. Despite this progress, there are still some lingering issues and hypotheses that keep these methods from being used in real life scenarios, especially in the case of surveillance applications. The most important issues and hypotheses are:

Acquisition conditions : As most of computer vision-based algorithms, gait modelling and comparison methods usually suppose a controlled lighting and a static background. These assumptions usually come from the background subtraction algorithm that is used in most methods.

Number of people : Current methods rely on the fact that there is only one person observed at a time, that is, only one person is visible in an analyzed video sequence. A similar assumption is that a low-level person tracking algorithm is used beforehand in order to find and track people in the images over time. In real surveillance scenario, it is very likely that many people are going to be visible in the field of view of the camera. This is less an issue for medical applications since one person is usually considered at a time for gait analysis.

Inputs manipulation : For some databases (at least for the HumanID, CASIA, and SOTON databases), the silhouettes sequences for each subject are provided. However, those sequences were temporally segmented to only include frames where the silhouettes are complete, i.e. the frames where a subject enters and exits the field of view of the camera(s) were removed.

Gait features interpretability : Most gait modelling approaches do not extract gait

features that are interpretable, that is, features that have a physical meaning. This is especially true in the case of the model-free approaches. However, model-based approaches usually extract gait features that are interpretable, as seen in Section 1.3.2. Gait features interpretability is considered as an important characteristic [13] for medical applications that are used for the diagnosis of some pathologies.

Walking conditions : It is usually assumed that the observed people are always walking (they do not stop walking) and that their walk velocity is nearly constant. Moreover, subjects are usually asked to walk on a straight line (no change in the walk direction), on a predefined path, or on a treadmill[5]. Therefore, the gait models are extracted and compared using data coming from the same walk conditions, which is very unlikely in a real world scenario.

Viewpoint : Many gait modelling approaches consider the gait of a person observed at a distance from a fronto-parallel viewpoint, which is not always the case in real life scenarios. This issue is directly related to the "viewpoint" covariate that was discussed previously in Section 1.1.2.

Very few works have been made to tackle directly some of those issues. This is especially the case of the viewpoint issue, which is often underestimated or ignored by most of the gait modelling and comparison approaches. Indeed, most of the approaches are at best *view-dependent*, that is, they compare gait models extracted from the *same view* (or a *similar view*) and for the *same walking path*. Moreover, subjects are usually considered walking on a straight line since a change in the walk direction would lead to a change in the viewpoint. This can been seen in the design of most of the gait database (CASIA, SOTON, UMD), excepted for the HumanID Gait Challenge database in which the subjects walk on an elliptic path. However, it seems[6] that only the rear portion of the elliptic path is used, and as reported by the authors of the database, the view for that portion of the path is approximately fronto-parallel.

Another assumption made by most approaches is that subjects are observed "at a distance", i.e. the distance between them and the camera is such that they can be considered as planar objects by computer vision algorithms. This assumption is referred to as *weak perspective* and can be considered valid for most of the outdoor surveillance scenario. However, weak perspective cannot be assumed in the case where subjects are close to the camera, as in most indoor surveillance and medical applications. Most of the approaches for gait modelling and comparison are not designed to cope with

[5]It is unclear whether a treadmill could impose a certain gait as well as a certain velocity.

[6]The authors of the USF database present the results of their gait recognition algorithm (baseline) only for the rear portion of the elliptic path. It is unclear if the whole elliptic path is used by other works in the literature since their results are usually compared to the ones obtained with the baseline algorithm.

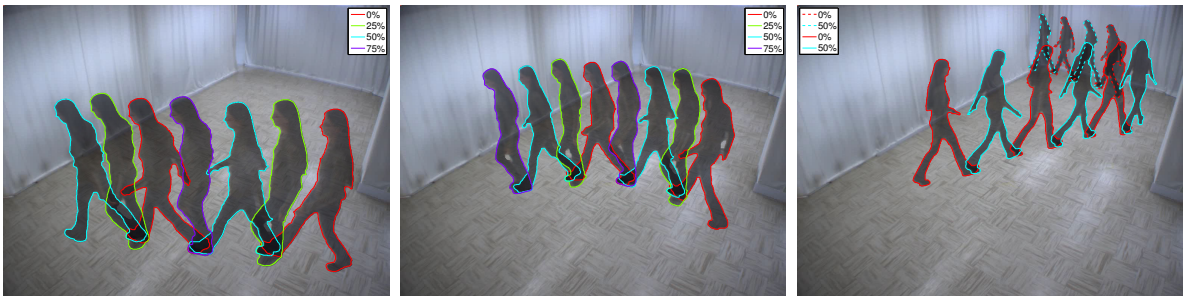

(a) (b) (c)

Figure 1.3 – Example of perspective distortion in the silhouettes of a subject. In (a), the subject walks close to the camera on a straight line. In (b) the subject performs a smooth change of direction, and in (c), a more marked change of direction. The silhouette's contour colour represents its temporal occurrence in a gait cycle, as indicated in the legend (% of gait cycle duration).

perspective projection effects that are present in such conditions.

An example of this is shown in Figure 1.3, where the silhouettes of a person are shown for three different experiments. The first experiment, shown in Figure 1.3(a), consists in a person walking close to the camera on a straight line. In the second experiment (Figure 1.3(b)), the person walks close to the camera but performs a smooth change in the walk direction. In the last experiment (Figure 1.3(c)), the person walks away from the camera and performs at some point a more marked change in the walk direction. The silhouettes' contour are coloured so that they represent the time they occur in a gait cycle. Silhouettes that have the same contour colour should have a *similar shape* since they represent the *same posture* of the person but for different gait cycles. One may verify that the posture is the same by closely examining the legs and the arms positions in the image. The silhouettes' shape would be very similar in the case of weak perspective, that is, when the person is observed far away from the camera and that the angle between the line of progression and the camera optical axis is perpendicular (i.e. a fronto-parallel view). However, one may see that this is not the case in the examples shown here since weak perspective does not apply; The silhouettes' shape appears different for the same postures. Differences in the silhouettes' shapes are even present in the first experiment where the view is almost fronto-parallel. These differences are even more marked across the gait cycles of the different experiments. The "distortion" effect can be explained by the fact that the person continuously exposes a different portion of her body as she moves across the field of view of the camera. Therefore, the *projected* silhouette's contours are different.

In such conditions, model-free approaches would build "distorted" gait models since most of them rely on the whole silhouettes or on the silhouettes' contour. This means that the gait models of the same person would not be necessarily similar, even if the models are built from *different views* of the *same walk* (i.e. from synchronized views). Only the model-based methods that recover the 3-D positions of the body parts are intrinsically immune to the perspective projection effects. However, some of these 3-D methods require more than one camera while others do not recover 3-D positions of the body parts in real-time. These may be seen as limitations in both surveillance and medical applications given that real-time is often a requirement and that using more than one camera is complex as well as expensive. The model-based methods that recover 2-D positions of the body parts in the image are also affected by perspective projection effects. Nonetheless this thesis will show, among other things, that is it possible to remove projective distortion from the 2-D positions of body parts, thus allowing gait modelling and comparison between different views.

1.5 Contributions

This thesis aims at addressing some of the issues that were discussed in the previous section. The emphasis is mainly on addressing the *viewpoint* issue, which is considered here as the most important issue in current gait analysis, modelling and comparison approaches. An aspect of the *walking conditions* issue is also addressed since the changes in the walk direction are handled in this thesis. Moreover, some efforts are made to develop fully automatic algorithms that do not require manual intervention, thus addressing the *inputs manipulation* issue. Finally, the *gait features interpretability* issue is also addressed in this work by proposing gait models consisting of features that have a physical meaning.

Given that very few works in the literature have addressed these issues directly, the present work provides several significant contributions. The first contribution consists in a novel walk model based on projective geometry that provides the spatio-temporal links between a normal walk performed in the scene and the corresponding imaged walk. This walk model is used in a novel, automatic view-rectification method that generates a metric fronto-parallel viewpoint of body-part trajectories. Another contribution consists in generating two novel gait models based on the body-part positions and velocities extracted from the view-rectified body-part trajectories. The features used in these models have a physical meaning, which allows for both human and machine-based interpretations. A method for generating 3-D synthetic walks with changes in the walk direction is also proposed in order to validate the view-rectification method. Finally,

a novel gait database consisting in real unconstrained walks is proposed in this thesis. The walks in the gait database include changes in the walk direction as well as changes in the walking speed.

1.6 Proposed Approach Overview

Figure 1.4 shows an overview of the proposed approach. It consists in five different steps: Acquisition, tracking, view-rectification, gait analysis, and gait modelling and comparison.

In the *acquisition* step, colour frames from a camera are first acquired and then processed by a background subtraction algorithm. This means that a certain amount of static frames representing the scene background have to be acquired before a person shows up in the field of view of the camera. The outputs of this block are the colour frames and the foreground binary frames obtained from the background subtraction algorithm and morphological filtering. The image presented in the acquisition block shows the colour frames that correspond to a key time in the double support phase of each gait cycles.

The *tracking* step first consists in analyzing the binary foreground frames in order to extract the silhouettes of the person. Next, the position of the feet and the head is found by analyzing the resulting silhouette. Feet correspondence is then performed using the current and the past positions of the feet. The outputs of this block are the 2-D imaged trajectories of the head and the feet, that is, the 2-D positions in the frames over time. The image in the tracking block shows the complete trajectories of the person's head and feet.

The most important contributions of this thesis lie in the *view-rectification* step. A fronto-parallel view of the body part trajectories is generated (left graphics) by first determining the *image* of the "motion planes" (right image). An imaged motion plane is defined as the projection in the camera image of the plane in the scene in which the motion of a body part lies. In the case of the head, the imaged motion planes are shown in transparency in the view-rectification block (the imaged motion planes of the feet are not shown here). A body-part's motion plane is defined in each gait half-cycle, where a gait half-cycle is defined between the occurrences of two consecutive double support phases. A metric, *view-rectifying transformation* is then computed for each motion plane by performing projective geometry calculations. This transformation makes an imaged motion plane appear as if it was observed from a fronto-parallel view. Applying

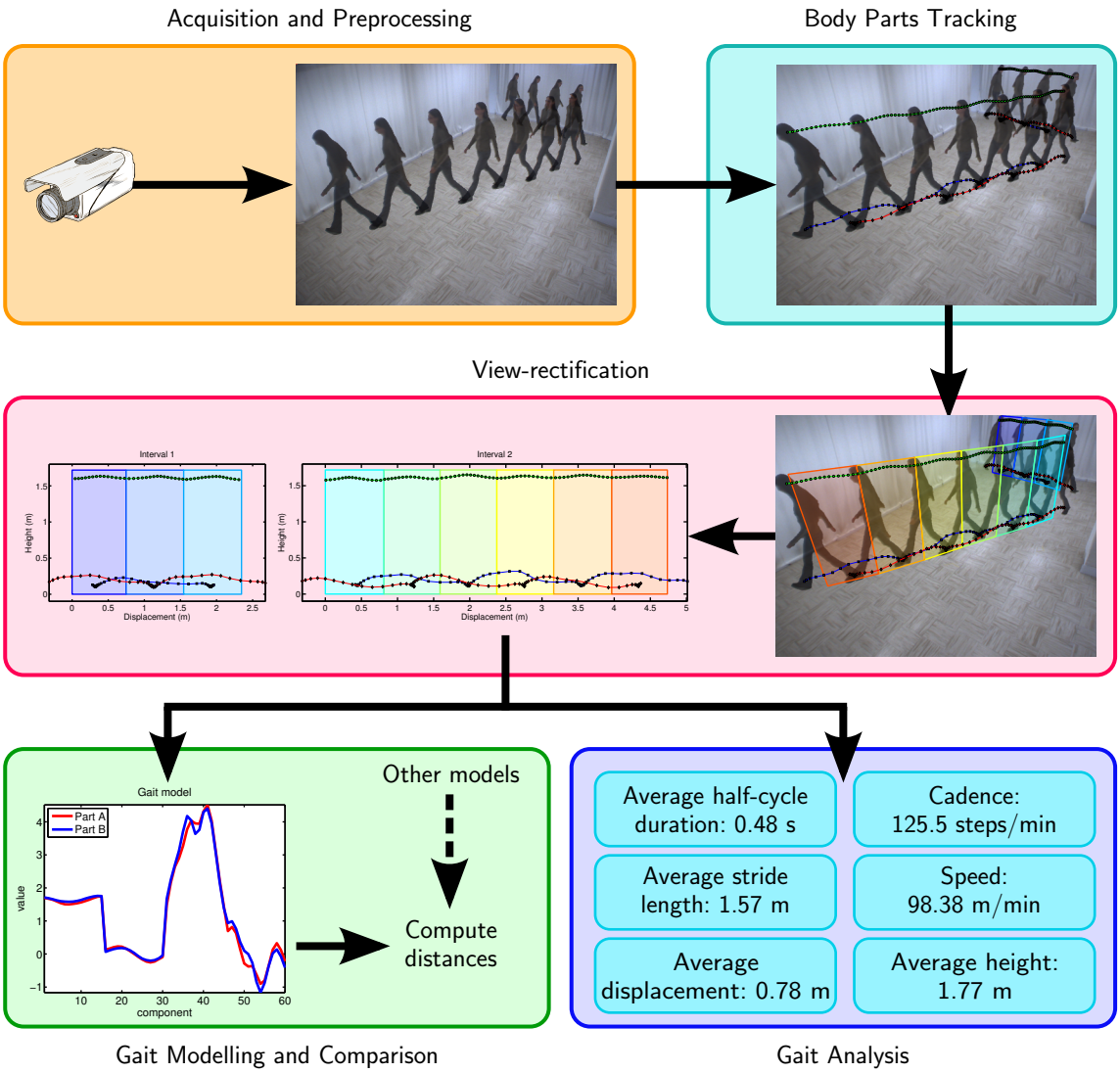

Figure 1.4 – Approach overview.

these transformations to the corresponding body-part trajectories effectively generates a fronto-parallel view of the walk. The left graphics of the view-rectification block shows the *view-rectified* feet and head trajectories as well as the *view-rectified* head motion planes. The output of this block is the view-rectified body-part trajectories, which are used by the *gait analysis* step and the *gait modelling and comparison* step.

In the *gait analysis* step, gait measurements are extracted from the view-rectified body-part trajectories. Gait measurements such as stride lengths, displacements, and height are computed on a gait half-cycle basis using the view-rectified body-part extremities. Other gait measurements such as the half-cycle durations and cadence are computed using the number of detected gait half-cycles and the time intervals in which they are defined. The walking speed is obtained from the computed displacements and

gait half-cycle durations.

The last step consists in performing *gait modelling and comparison* using the view-rectified body-part trajectories. Two gait models are computed from the view-rectified trajectories. The first gait model is based on the view-rectified positions of the head and feet, while the second gait model is based on the velocities of the head and feet (only the velocity-based gait model is shown in the gait modelling and comparison block). Each gait model is formed of two parts, each part representing the gait when the left and the right foot is moving, respectively. An improved representation of the gait models is then learned from a subset of walks using a off-the-shelf machine learning technique. The improved gait models are then compared by computing the Euclidean distance between each corresponding model part. Gait modelling and comparison can be used to perform gait recognition and identification, that is, recognizing people by their gait (surveillance applications).

1.7 Document Structure

This thesis is organized so that it closely follows the structure of the proposed approach presented in the previous section. The Chapter 2 first describes both the acquisition and the body parts tracking steps. The view-rectification method is next detailed in the Chapter 3, followed by the gait analysis, modelling and comparison methods in Chapter 4. The experimental results are then presented and discussed in Chapter 5. Finally, Chapter 6 concludes by outlining the thesis contributions and by proposing directions for the future work.

Chapter 2

Body Parts Tracking

"Our nature consist in motion;
complete rest is death."

Blaise Pascal

As discussed in Section 1.4, model-based approaches are better suited than model-free approaches to perform gait modelling and comparison. Indeed, model-based approaches only retrieve *gait* information, unlike the model-free approaches where *appearance* information is also retrieved. Moreover, it will be shown latter in this thesis that it is possible with a model-based approach to perform gait analysis, modelling, and comparison from unconstrained walks and viewpoints.

Model-based approaches needs the body parts to be localized and tracked in each frame of a video sequence according to a predefined part-based human model. This chapter therefore presents the body parts tracking algorithm that was developed as part of this thesis in order to perform model-based gait modelling and comparison. The acquisition and pre-processing step outlined in Section 1.6 is also presented in this chapter since it provides the inputs used by the proposed body parts tracking algorithm.

A short literature review on body parts tracking approaches is first presented. It is followed by a brief overview of the pre-processing step and the body parts tracking algorithm. The proposed algorithm is subsequently detailed along with the pre-processing steps. The last part of this chapter describes some post-processing operations performed on the body-part trajectories obtained using the proposed body parts tracking algorithm. The chapter is concluded by discussing the real-time performance and limitations of the body parts tracking algorithm.

2.1 Literature Review

Localizing and tracking the body parts of people in video sequences is a research area in itself [68]. Most approaches in the literature targets a wide range of applications by recovering the pose of people either in single images [69] or in video sequences. The poses are intended to be used for motion analysis, activity recognition, and human-computer interaction. The approaches discussed here are the ones that focus on recovering body-part positions during walking or similar activities.

The first step of a body parts tracking algorithm consists in determining the *initial* positions of the body parts in the first frame of a video sequence. Given that the initial positions accuracy can greatly influence the tracking process, some algorithms require *manual initialization* of the body-part positions [70, 71] or require *user feedback* [72] during the body parts tracking process. The method presented in [70] requires the user to specify the positions of 18 predefined joints in the first image of a video sequence. Similarly, the body part model used in [71] must be rescaled according to the size of the body parts in the image, which are manually measured by a human operator beforehand. Human intervention is necessary in the method presented in [72], where the user has to manually correct the algorithm estimates of the body-part positions during the first few seconds of a video sequence. Manual initialization or intervention from a human operator for a body parts tracking algorithm is clearly inappropriate in typical gait modelling applications.

In most cases, considering all the possible configurations of a complex human model in each frame of a video sequence might not be possible nor desirable. This is why some approaches consider a *side-view human model* in order to limit the number of possible configurations [36, 51, 56, 57, 59, 60, 73, 74]. However, these approaches provide meaningful body part positions only when the viewpoint is fronto-parallel, which is not practicable in the case of unconstrained walks.

Some approaches locate the body-part positions on a *frame-by-frame* basis without establishing body parts *correspondence* between consecutive frames [49, 50, 57]. These tracking approaches can only be used to extract static gait characteristics since the motion performed by each body parts cannot be recovered.

Motion templates are used in some approaches in order to track the body parts for a normal walk [52, 73, 74, 71, 75]. These motion templates typically represent the positions over time of some (or all) the body parts for a normal walk. A motion template is defined by manually labelling the typical position of the body parts during

a gait cycle for several video sequences of normal subjects. Once the motion template has been defined, it is "fitted" onto the walk of an individual using cues from some low level data such as silhouettes [71, 75], edges [73, 71], or interest points [52, 74] obtained with feature points detectors. Approaches using motion templates are said to be robust to temporary self-occlusion[1] and to noisy low level data. Besides the learning phase that must be undergone in such approaches, the use of a motion template in gait modelling applications has other drawbacks. For instance, motion template approaches cannot easily cope with walk velocity variations occurring in unconstrained walk, which can lead to inaccurate body-part positions. Moreover, most of these approaches are limited to a fronto-parallel viewpoint since their motion template is strictly learned from fronto-parallel sequences [52, 73, 74, 71]. The approach presented in [75] addresses this viewpoint issue by using a mixture of view-dependent motion templates, but it requires for the learning phase many video sequences of each considered view. Finally, motion template approaches somehow make the obtained body-part positions follow an averaged motion that might not necessarily reflects all the peculiarities of a person's gait.

2.2 Body Parts Tracking Approach

The body part tracking approach proposed in this thesis is designed in such a way that it does not suffer from the drawbacks of the previously discussed approaches. It is based on a three parts human model (head and two feet) where the parts are detected and tracked across the frames of a monocular video sequence. The proposed body parts tracking approach has the following properties:

- No manual initialization or motion template are needed
- Body-part positions can be found for wide range of viewpoints
- Foot occlusions are handled and body parts correspondence between frames is established
- Body-part positions are found in real-time

Four assumptions are made in the proposed approach. The first one is that the subjects are observed in a scene with a static background. The second assumption is that the subjects appear upright in the image. Also, the walking surface is assumed to be planar and level. Finally, it is assumed here that there is only one subject visible at any time in the field of view of the camera. These are common assumptions made in body part tracking approaches as well as gait analysis, modelling and comparison

[1] A self-occlusion means that a body part is partly of fully hidden by another body part.

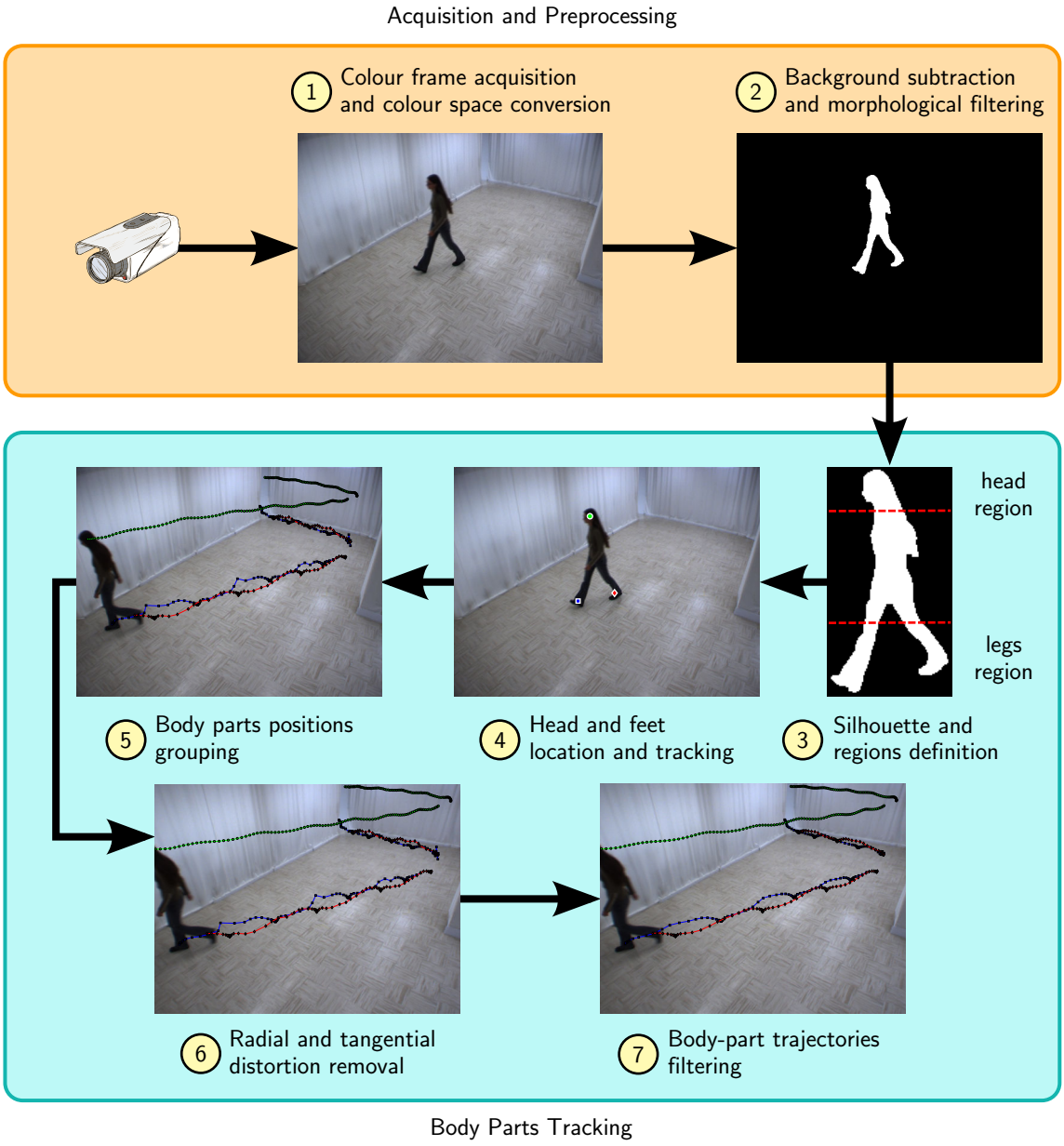

Figure 2.1 – Acquisition, pre-processing, and body parts tracking approaches.

approaches [64, 65].

An overview of the proposed body parts tracking approach is presented in Figure 2.1, along with an overview of the acquisition and pre-processing approach. The later is included here since it consists only in a few standard steps and its output is only used by the body parts tracking approach. The first step of the acquisition and pre-processing algorithm consists in acquiring colour *RGB* frames from a monocular camera. The acquired colour *RGB* frames are then converted in another colour space to ease

background subtraction and morphological filtering performed in step 2. The output of step 2 is a binary image where black and white pixels belong to background and foreground respectively.

The first step of the body parts tracking method consists in determining the foreground region corresponding to the silhouette of the subject (step 3). Two regions are then defined in the silhouette, which are used in step 4 to locate and track the head and the feet respectively. It is possible to perform step 1 to 4 in real-time in order to acquire the head and the foot positions as soon as a frame has been acquired from the camera. Step 5 to 7 are considered as post-processing of the obtained body-part positions and hence are performed when the subject is no longer visible in the field of view of the camera. In step 5, the positions of the body parts are grouped into *intervals* of contiguous tracking of the head and the feet. The set of positions of a body part in such intervals are referred here to as the *trajectory* of the body part. Body-part trajectories can then be corrected for radial and tangential distortion (step 6). Finally, the body-part trajectories are filtered in step 7 in order to compensate for noisy body-part positions.

The acquisition and pre-processing steps (step 1 and 2) are presented in Section 2.3, while step 3 is described in Section 2.4. The head and the feet tracking algorithms are presented in Section 2.5 and 2.6 respectively (step 4). The post-processing steps 5, 6, and 7 are presented in Section 2.7.

2.3 Acquisition and Pre-processing

The specific colour space, background subtraction algorithm and morphological operators that are presented in the following sections have been found experimentally to provide the best results on the video sequences of the gait database used in this thesis. For instance, shadows or reflections on the floor are mostly absent from the obtained binary images, and the obtained silhouettes are sharp.

2.3.1 Colour Space Conversion

The colour frames acquired from the camera are represented in the RGB (Red Green Blue) colour space. Many colour spaces were tested in this work in order to facilitate background subtraction [76]: Grey scale, RGB, normalized RGB, YC_bC_r (Luma,

blue Chroma, red Chroma), *HSI* (Hue, Saturation, Intensity), CIE[2] *XYZ*, and CIE $L^*a^*b^*$. Experiments on the video sequences used in this thesis showed that the CIE $L^*a^*b^*$ colour space provides sharper silhouettes when used along with the background subtraction algorithm described in Section 2.3.2.

Each frame of a video sequence is converted [76] from the *RGB* colour space to the $L^*a^*b^*$ colour space before being processed by the background subtraction algorithm. Figure 2.2 shows the result of the conversion of the *RGB* frame shown in step 1 of Figure 2.1. The L^*, a^*, and b^* channels are shown in 2.2(a), 2.2(b), and 2.2(c) respectively, while a colour representation of the converted frame is shown in 2.2(d).

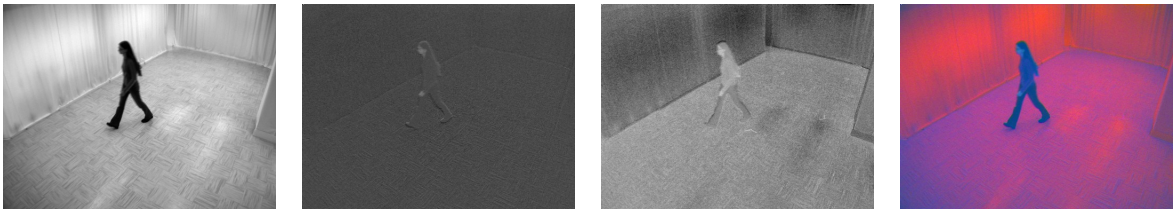

(a) (b) (c) (d)

Figure 2.2 – Colour conversion from *RGB* space to CIE $L^*a^*b^*$ space. The L^*, a^* and b^* channels for the image in step 1 in Figure 2.1 are shown in (a), (b), and (c) respectively. In (d), a colour representation of the $L^*a^*b^*$ image is shown, where the red, green and blue channels represent the L^*, a^* and b^* channels respectively.

2.3.2 Background Subtraction and Morphological Filtering

Many background subtraction algorithms were also tested here: *Adaptive Median* [77], *Running Gaussian Average* [78], *Gaussian Mixture Model* [79], *Eigenbackground* [80], *Adaptive Gaussian Mixture Model* [81], and *Temporal Median* [82]. The combination of the *Adaptive Median* algorithm with the $L^*a^*b^*$ colour space provided the best results on the video sequences used in this thesis. Indeed, the obtained silhouettes are sharp and cast shadows are not detected as foreground.

The *Adaptive Median* algorithm [77] basically consists in dynamically modelling the scene background at frame n using an estimated *median image* $I_{\mathrm{M}}[x, y, c, n]$, where x and y represent a pixel position in the image and c is the channel number ($c = 1 \rightarrow L^*$, $c = 2 \rightarrow a^*$, and $c = 3 \rightarrow b^*$). For each colour frame $I[x, y, c, n]$, $n = 1, 2, \ldots, N$, a

[2]CIE: *Commission Internationale d'Éclairage*.

binary image $I_{\mathrm{B}}[x, y, n]$ can be obtained in the following way:

$$I_{\mathrm{B}}[x, y, n] = \begin{cases} 1 & \text{if } \left|I[x, y, c, n] - I_{\mathrm{M}}[x, y, c, n]\right| > \xi_{\mathrm{B}} \quad \forall c \in \{1, 2, 3\} \\ 0 & \text{otherwise,} \end{cases} \tag{2.1}$$

where ξ_{B} is a threshold that must be manually adjusted for a given scene background and lightning conditions, and 1 and 0 represent foreground and background respectively. The median background model is computed for each frame n in the following way:

$$I_{\mathrm{M}}[x, y, c, n] = \begin{cases} I[x, y, c, n] & \text{if } n = 1 \\ I_{\mathrm{M}}[x, y, c, n-1] + 1 & \text{if } I[x, y, c, n] > I_{\mathrm{M}}[x, y, c, n] \text{ and } I_{\mathrm{U}}[x, y, n] \\ I_{\mathrm{M}}[x, y, c, n-1] - 1 & \text{if } I[x, y, c, n] < I_{\mathrm{M}}[x, y, c, n] \text{ and } I_{\mathrm{U}}[x, y, n] \\ I_{\mathrm{M}}[x, y, c, n-1] & \text{otherwise,} \end{cases} \tag{2.2}$$

where the *update condition* $I_{\mathrm{U}}[x, y, n]$ is defined as

$$I_{\mathrm{U}}[x, y, n] = \begin{cases} \text{true} & \text{if } (n \bmod f_{\mathrm{U}}) = 0 \text{ and } (n \leq f_{\mathrm{L}} \text{ or } I_{\mathrm{B}}[x, y, n] = 0) \\ \text{false} & \text{otherwise.} \end{cases} \tag{2.3}$$

The algorithm parameters f_{U} and f_{L} represent respectively the update frequency and the number of frames to be considered in the initial learning phase. Hence, the value of a pixel at position (x, y) in the median background model can be updated each f_{U} frame if either the algorithm is still in its learning phase ($n \leq f_{\mathrm{L}}$) or the pixel was labelled as background in the current frame ($I_{\mathrm{B}}(x, y, n) = 0$).

The value of a pixel for a given channel in the median model image is increased by one if the corresponding pixel in the current image has a greater value, or decreased by one if it has a smaller value. This simple procedure estimates the median of the observed pixel values since about half of the values will be smaller than the estimated value and the other half will be greater than the estimated value. This background subtraction algorithm is robust to outliers (median estimate) and its low complexity makes it a good choice to perform background subtraction in real-time. It is important to note that the first f_{L} frames must represent a static scene, that is, no subject is visible in the field of view of the camera.

Figure 2.3 shows an example of background subtraction. An input frame in the $L^*a^*b^*$ colour space is shown in Figure 2.3(a). The binary image obtained with the background subtraction algorithm is shown in Figure 2.3(b), and the relevant portion of the binary image is shown in Figure 2.3(c). Morphological operations are performed on this binary image in order to remove isolated pixels and connected regions that are too small. First, two morphological erosions followed by two morphological dilatations

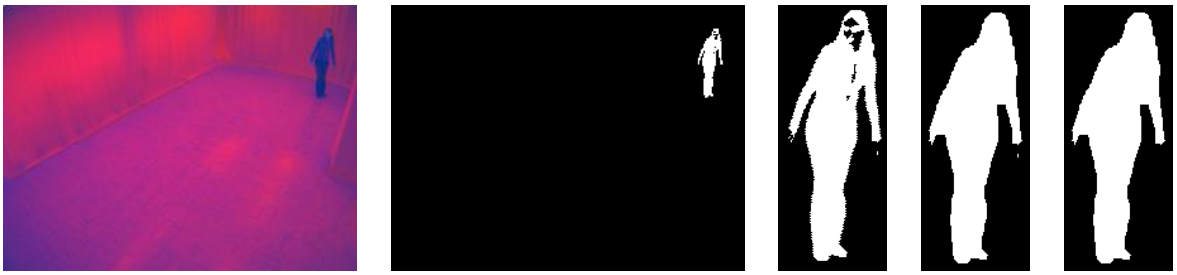

(a) (b) (c) (d) (e)

Figure 2.3 – Background subtraction and morphological filtering. In (a), a frame represented in the $L^*a^*b^*$ colour space. In (b), binary image obtained from background subtraction with its relevant portion shown (c). In (d), the result of applying morphological dilatations and erosions on the binary image, and in (e), the remaining connected regions after area filtering.

Figure 2.4 – Results of background subtraction and morphological filtering for 30 frames of a video sequence. Only the relevant portion of the binary frames are shown.

are performed using a 3×3 square structural element (Figure 2.3(d)). Next, the 8-connected pixels regions are filtered according to their area (number of pixels), that is, connected components having an area smaller than $\xi_{\text{A}} = 50$ pixels are removed (Figure 2.3(e)). Results of background subtraction and morphological filtering are shown for many frames in Figure 2.4.

2.4 Silhouette and Regions Definition

The first step of the body parts tracking approach consists in determining whether a person silhouette is analyzable in each binary image obtained from the previous step. First, the silhouette of the person is obtained as the largest connected region in the binary image. Moreover, this largest connected region is a valid silhouette only if the size of its bounding box is at least 3% of the image width and 15% of the image height ($\xi_{\text{IW}} = 0.03$ and $\xi_{\text{IH}} = 0.15$). This permits to reject the frames where the silhouette of a subject would be too small to be able to locate and track the head and the feet. A

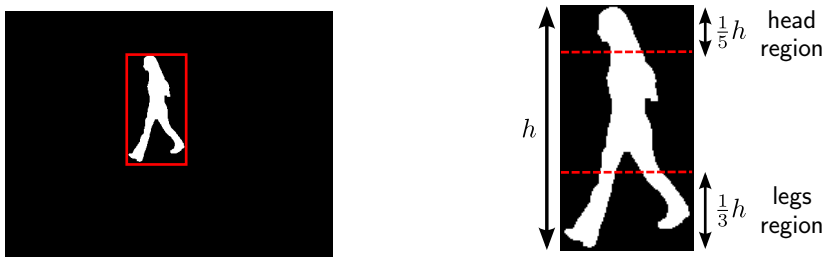

(a) (b)

Figure 2.5 – Silhouette and regions definition. In (a), the silhouette is defined as the largest connected region in a binary image obtained from the acquisition and pre-processing steps. In (b), two regions of the silhouette are defined according to the bounding box height.

frame is also rejected if the silhouette has some of its pixels on the image border, which could mean that the subject is not completely visible in the field of view of the camera. Figure 2.5(a) shows the silhouette that is found for the colour frame shown in step 1 of Figure 2.1.

Once a valid silhouette and its bounding box are found, two regions are defined with respect to the bounding box height (see Figure 2.5(b)). The first region corresponds to the region where one would expect the head to be located given that the person is assumed upright in the image. The height of the head region is defined as one fifth of the bounding box height starting from the top ($\xi_{\mathrm{HR}} = \frac{1}{5}$). The second region corresponds to the part of the silhouette where the legs are located, and its height is defined as one third of the bounding box height starting from the bottom ($\xi_{\mathrm{LR}} = \frac{1}{3}$). Each body part will be searched in its corresponding region. The thresholds ξ_{IW}, ξ_{IH}, ξ_{HR}, and ξ_{LR} were found by observations.

2.5 Head Location

The head position only needs to be determined on a frame-by-frame basis since it does not occlude or interact with other body parts during the walk. The head position can be represented in two simple ways: As the position of the highest pixel of the silhouette, or as a centroid of a region corresponding to the head. The latter position has some advantages over the former one. For instance, the position of the highest pixel is less robust to spurious pixels in the silhouette contour than the head region centroid. Moreover, the position of the head region centroid can be seen as an approximation of the *projection* in the image of the centroid of the 3-D volume occupied by the head.

(a) (b)

Figure 2.6 – Head location. In (a), a close-up on the upper region of the silhouette. In (b), two third of silhouette foreground pixels in the head region were counted (shown in grey). The centroid of this subset of foreground pixels represents the head position (black circle).

By contrast, the position of the highest pixel might represent quite different positions on the head depending on the viewpoint. Therefore, the centroid of the head region provides a more robust representation of the head position across the frames of a video sequence.

For a frame n, the head position $\mathbf{p}_{\mathsf{H}}[n]$ is obtained by computing the centroid of a subset of the foreground pixels in the head region of the silhouette as shown in Figure 2.6. The head bounding box is computed as well and is represented by the four corners $\mathbf{b}_{\mathsf{H,TL}}[n]$ (top-left), $\mathbf{b}_{\mathsf{H,TR}}[n]$ (top-right), $\mathbf{b}_{\mathsf{H,BL}}[n]$ (bottom-left), and $\mathbf{b}_{\mathsf{H,BR}}[n]$ (bottom-right) of the pixels subset bounding box. This pixel subset is obtained by counting the foreground pixels row by row from the top until two third ($\xi_{\mathrm{HP}} = \frac{2}{3}$) of the foreground pixels in the head region is reached (see Figure 2.6(b)). This "pixels counting" algorithm will also be used for computing the foot positions.

2.6 Foot Location and Tracking

Unlike the head, the feet need to be *tracked* since they occlude each other during the swing phase of a gait cycle. This means that the correspondence between the foot positions in consecutive frames must be established. Therefore, a specific algorithm was developed in order to locate and track the feet.

The foot location and tracking method is presented in Figure 2.7. The legs region is used as input, and the output for the current frame n is the positions of the two feet $\mathbf{p}_1[n]$ and $\mathbf{p}_2[n]$ (foot 1 and foot 2) along with the four corners of their bounding box: $\{\mathbf{b}_{1,\mathsf{TL}}[n], \mathbf{b}_{1,\mathsf{TR}}[n], \mathbf{b}_{1,\mathsf{BL}}[n], \mathbf{b}_{1,\mathsf{BR}}[n]\}$ and $\{\mathbf{b}_{2,\mathsf{TL}}[n], \mathbf{b}_{2,\mathsf{TR}}[n], \mathbf{b}_{2,\mathsf{BL}}[n], \mathbf{b}_{2,\mathsf{BR}}[n]\}$. The first step of the method is to divide the legs region into two parts, each part containing a leg (legs separation, Section 2.6.1). The failure or the success of this operation determines

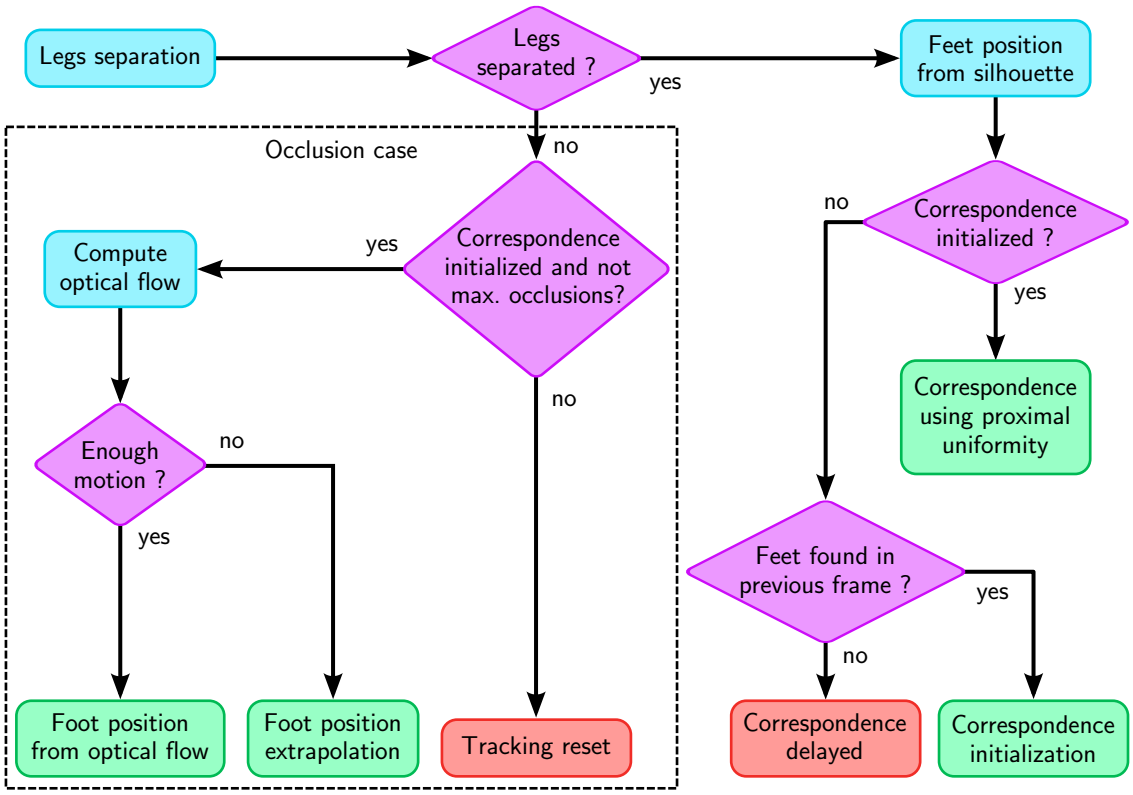

Figure 2.7 – Foot location and tracking method.

whether the feet are considered in occlusion or not.

If the legs can be successfully separated (no occlusion), then a foot position is found for each leg using the same pixels counting method that is used for the head (Section 2.6.2). Next, the correspondence is established using proximal uniformity [83] in the case where foot correspondence is already initialized. Foot correspondence is initialized only if the feet were found in the previous frame. Otherwise, foot correspondence initialization is delayed until the next frame.

In the case where the legs cannot be separated, the feet are considered in occlusion. If foot correspondence is not initialized or the feet have been in occlusion for more than a certain number of frames, the tracking algorithm is reset, that is, foot positions will not be found until the legs can be separated again. Otherwise, an attempt to find the position of the *moving foot* is made by computing optical flow in the legs region, and the *still foot* is assigned the position it had in the previous frame (Section 2.6.3). The moving foot position is determined using the pixels counting algorithm on the moving part of the silhouette in the legs region only if there is enough motion. If there is not enough motion in the legs region, the moving foot position is linearly extrapolated.

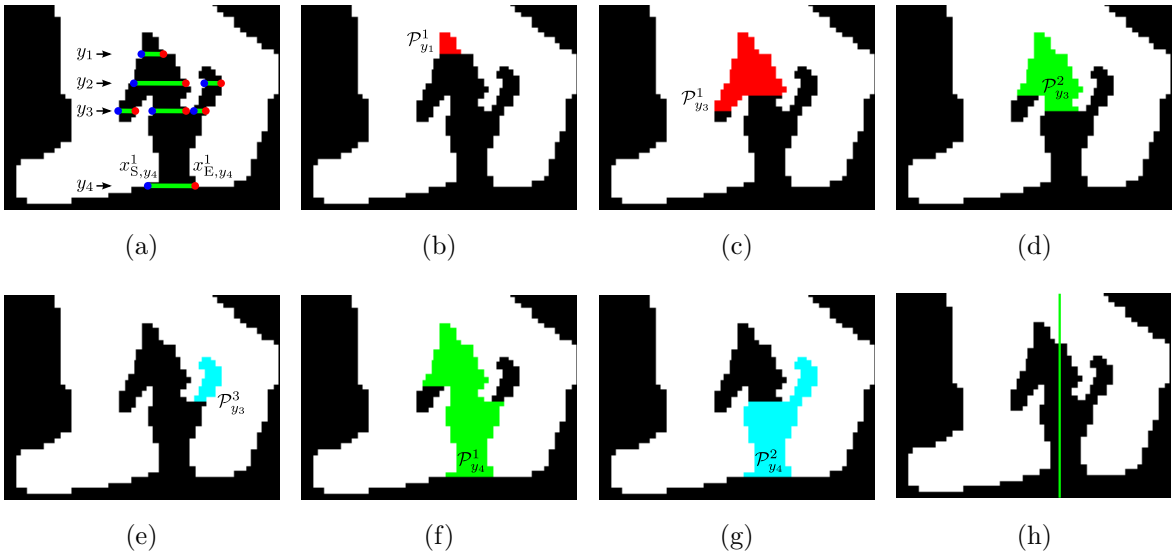

Figure 2.8 – Legs separation process for a noisy legs region. In (a), the gaps in four rows y_1, y_2, y_3, and y_4 are shown in green, with their starting and ending positions represented by a red and a blue point respectively. In (b), the gaps belonging to the path $\mathcal{P}^1_{y_1}$ in row y_1 are shown in red. The gaps belonging to the three paths $\mathcal{P}^1_{y_3}$, $\mathcal{P}^2_{y_3}$, and $\mathcal{P}^3_{y_3}$ in row y_3 are shown in (c), (d), and (e) respectively. In (f) and (g), the gaps belonging to the two paths $\mathcal{P}^1_{y_4}$ and $\mathcal{P}^2_{y_4}$ in row y_4 are shown. The path $\mathcal{P}^1_{y_4}$ is the longest path among all the paths of all rows. It is used to find the position where the legs region will be divided in two parts, as shown in (h).

2.6.1 Legs Separation

Figure 2.8 shows an example with the different steps of the legs separation process. Separating the legs is achieved by scanning each row of pixels of the legs region and searching for foreground-background-foreground transition patterns. The background in these patterns potentially represents the gaps between the legs, which can be further used to separate the legs. A gap is represented in each row by an interval of consecutive background pixels delimited by foreground pixels at both ends. Denoting $I_{\mathrm{B}}(x, y)$ as the value of the pixel at position (x, y) in the legs region, which is defined for $x = X_{\mathsf{L}} \dots X_{\mathsf{R}}$ and $y = Y_{\mathsf{T}} \dots Y_{\mathsf{B}}$, the set $\mathcal{G}_y$ of background gaps in row y is defined as :

$$\begin{aligned} \mathcal{G}_y : \Big\{ [x^j_{\mathrm{S},y}, x^j_{\mathrm{E},y}] \mid\ & I_{\mathrm{B}}(x^j_{\mathrm{S},y} - 1, y) - I_{\mathrm{B}}(x^j_{\mathrm{S},y}, y) = 1 \text{ and} \\ & I_{\mathrm{B}}(x^j_{\mathrm{E},y} + 1, y) - I_{\mathrm{B}}(x^j_{\mathrm{E},y}, y) = 1 \text{ and} \\ & \forall x \in [x^j_{\mathrm{S},y}, x^j_{\mathrm{E},y}]\ I_{\mathrm{B}}(x, y) = 0 \Big\} \end{aligned} \tag{2.4}$$

Algorithm 2.1: Paths detection

for $y = Y_{\mathsf{T}}, Y_{\mathsf{T}}+1, \ldots, Y_{\mathsf{B}}$ **do**
  $\mathcal{Q}_y \leftarrow \{\}$
  for $j = 1, 2, \ldots, |\mathcal{G}_y|$ **do**
    Flag $= 0$
    for $k = 1, 2, \ldots, |\mathcal{Q}_{y-1}|$ **do**
      if $[x^j_{\mathrm{S},y}, x^j_{\mathrm{E},y}]$ overlaps with $[x^k_{\mathrm{S},y}, x^k_{\mathrm{E},y}]$ **then**
        $\mathcal{Q}_y \leftarrow \mathcal{Q}_y \cup \{\mathcal{P}^k_{y-1} \cup \{[x^j_{\mathrm{S},y}, x^j_{\mathrm{E},y}]\}\}$
        Flag $= 1$
      end if
    end for
    if Flag $= 0$ **then**
      $\mathcal{Q}_y \leftarrow \mathcal{Q}_y \cup \{\{[x^j_{\mathrm{S},y}, x^j_{\mathrm{E},y}]\}\}$
    end if
  end for
end for

where $x^j_{\mathrm{S},y}$ and $x^j_{\mathrm{E},y}$ are the starting and ending position of the jth gap in row y. The first two conditions make a gap start on a foreground-background transition and end on a background-foreground transition (foreground positions are not part of the gap). The last condition defines a gap as an interval of consecutive background pixels. The gaps that are found in this way for row y are denoted $[x^j_{\mathrm{S},y}, x^j_{\mathrm{E},y}]$, where $j = 1, 2, \ldots, |\mathcal{G}_y|$. Figure 2.8(a) shows the gaps that are found for four rows in a noisy region of the legs.

Once all the gaps are found on each row y of the legs region, overlaps between these gaps and the ones of the previous row $(y-1)$ are searched in order to identify vertically connected background gaps. At a given row y, the upward connected gaps form a *path* $\mathcal{P}_y$. The longest path among all paths of all rows will be considered as representing the main background gap between the legs, and a position will be computed from this path in order to divide vertically the legs region in two parts. Algorithm 2.1 is used to detect all the paths in all the rows of the legs region. In this algorithm, a set $\mathcal{Q}_y$ of paths is defined for each row y, and each path is denoted $\mathcal{P}^k_y$, $k = 1 \ldots |\mathcal{Q}_y|$. An example of paths that are found using this algorithm is shown in Figures 2.8(b) to 2.8(g) for three rows y_1, y_3, and y_4. The background gap represented by a path at a given row is shown by colouring all the gaps belonging to it.

In the path detection algorithm, the gap $[x^k_{\mathrm{S},y-1}, x^k_{\mathrm{E},y-1}]$ belonging to a path $\mathcal{P}^k_{y-1}$ (in row $y-1$) is checked for an overlap with a gap $[x^j_{\mathrm{S},y}, x^j_{\mathrm{E},y}]$ in current row y. If there is an overlap, then a path consisting in the gap $[x^j_{\mathrm{S},y}, x^j_{\mathrm{E},y}]$ and the gaps in path $\mathcal{P}^k_{y-1}$ is added to the set of paths $\mathcal{Q}_y$. A path $\mathcal{P}^k_{y-1}$ that overlaps with more than one gap in row

y is thus "duplicated". In Figures 2.8(c) and 2.8(d), the paths $\mathcal{P}^1_{y_3}$ and $\mathcal{P}^2_{y_3}$ have many gaps in common since there is a row between y_2 and y_3 where a gap was overlapping with two gaps in the next row.

Once all the paths are found in all rows, the longest path, $\mathcal{P}^*$ must be found in order to divide the legs region in two parts :

$$\mathcal{P}^* = \arg\max_{\mathcal{P}^k_y} \left(\left| \mathcal{P}^k_y \right| \right), \quad y \in [Y_\mathsf{T}, Y_\mathsf{B}], \; k \in [1, |\mathcal{Q}_y|] \tag{2.5}$$

where $\left|\mathcal{P}^k_y\right|$ is the number of gaps in the path $\mathcal{P}^k_y$, that is, the "length" of the path. In Figure 2.8, the longest path among all paths in all rows is the path $\mathcal{P}^* = \mathcal{P}^1_{y_4}$, which is shown in Figure 2.8(f). The path $\mathcal{P}^*$ is considered as representing the gap between the two legs only if it has a length that is greater than a fraction $\xi_\mathcal{P} = 0.2$ of the height $(Y_\mathsf{B} - Y_\mathsf{T})$ of the legs region. If $|\mathcal{P}^*| < \xi_\mathcal{P}(Y_\mathsf{B} - Y_\mathsf{T})$, then legs are not separated and the feet are considered to be in occlusion. Otherwise, the path is used to find a position where the legs region will be vertically divided in two parts, each part being meant to contain one leg. The position is computed by first determining the minimum and maximum x position $x_{\min}$ and $x_{\max}$ among all the gaps belonging to the path $\mathcal{P}^*$:

$$\begin{aligned} x_{\min} &= \min_r \left(x^r_\mathrm{S}\right) \quad r = 1, 2, \ldots, |\mathcal{P}^*| \\ x_{\max} &= \max_r \left(x^r_\mathrm{E}\right) \quad r = 1, 2, \ldots, |\mathcal{P}^*| \end{aligned} \tag{2.6}$$

where $[x^r_\mathrm{S}, x^r_\mathrm{E}]$ is a gap in $\mathcal{P}^*$. Then, an optimal separation position x^* is searched in the range $[x_{\min}, x_{\max}]$ by maximizing the output of an *objective* function O for all gaps belonging the longest path $\mathcal{P}^*$:

$$x^* = \arg\max_{x \in [x_{\min}, x_{\max}]} \left(\sum_{r=1}^{|\mathcal{P}^*|} O(x, x^r_\mathrm{S}, x^r_\mathrm{E}) \right) \tag{2.7}$$

where the objective function $O(x, x^r_\mathrm{S}, x^r_\mathrm{E})$ is defined as

$$O(x, x^r_\mathrm{S}, x^r_\mathrm{E}) = \begin{cases} x - x^r_\mathrm{S} & \text{if } |x - x^r_\mathrm{S}| < |x^r_\mathrm{E} - x| \\ x^r_\mathrm{E} - x & \text{otherwise.} \end{cases} \tag{2.8}$$

For a given gap $[x^r_\mathrm{S}, x^r_\mathrm{E}]$, the objective function O is designed to have a maximal value at the position $x = \frac{1}{2}(x^r_\mathrm{S} + x^r_\mathrm{E})$, that is, the middle of the gap. The value of the function for a position x is simply the *signed distance* to the closest gap end. This means that the distance is negative if the x position is outside the gap. The x^* position obtained with Equation 2.7 is considered as the best position in the background gap between the legs to divide of the legs region in two parts. It actually represents a vertical line whose position is a trade-off between maximizing the distance to foreground pixels and minimizing the number of foreground pixels the vertical line intercepts. The first part of the legs region is then defined in the range $[X_\mathsf{L}, x^*]$ while the second part is defined in the range $[x^* + 1, X_\mathsf{R}]$. An example of legs separation is shown in Figure 2.8(h).

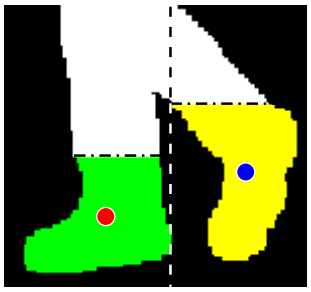

Figure 2.9 – Foreground pixels counting from the bottom of each leg region until 25% of the number of foreground pixels in the legs region is reached. The centroid of the obtained pixels subset is considered as the foot position. The pixels subset of each leg region is shown in green and in yellow, along with its centroid (red and blue circles).

2.6.2 Foot Location and Correspondence without Occlusion

In the case where the legs region is successfully divided in two parts, a foot position if computed in both parts. This case correspond to the right branch in Figure 2.7, which begins with the "Feet position from silhouette" step. The same pixels counting algorithm used for the head (Section 2.5) is used here to compute the centroid of a subset of the foreground pixel in each leg region. As for the head, the centroid is considered here has an estimation of the projection in the image of the 3-D centroid of the volume occupied by a foot.

Figure 2.9 shows the foot positions that are obtained with this algorithm. The pixels are counted from the bottom of a *leg region* until one fourth ($\xi_{\text{LP}} = \frac{1}{4}$) of the number of foreground pixels in the *legs region* in reached. The centroids obtained from the leg regions are then considered as the foot positions, which are denoted here as $\mathbf{p}_1[n]$ and $\mathbf{p}_2[n]$ for current frame n. A bounding box is also computed from each pixels subset in order to represent the rectangular area occupied by each foot.

Once the foot positions are found in the current frame n, foot correspondence must be established with the foot positions obtained in the previous frame $n-1$. A different correspondence algorithm is used depending on whether foot correspondence is established between frames $n-1$ and $n-2$ or not. One of this algorithm (proximal uniformity) needs the correspondence to be established between frame $n-1$ and frame $n-2$ in order to establish correspondence between frame n and $n-1$. The correspondence thus needs to be *initialized* at some point by another algorithm (see "Correspondence using proximal uniformity" and "Correspondence initialization" in Figure 2.7).

In the case where the correspondence was not established in the previous frame,

an attempt is made to *initialize* foot correspondence in the current frame n only if the foot positions were found in the previous frame $n-1$. Otherwise, correspondence initialization is not possible for the current frame and is delayed until the next frame (see "Correspondence delayed" in Figure 2.7). The correspondence initialization is performed by associating the closest foot positions in current and previous frames (closest point algorithm). The foot positions $\mathbf{p}_1[n]$ and $\mathbf{p}_2[n]$ are *swapped* if necessary to reflect this foot association:

$$\begin{aligned}\mathbf{p}_1[n] \longleftrightarrow \mathbf{p}_2[n] \text{ if } & \\ & \big\|\mathbf{p}_1[n]-\mathbf{p}_2[n-1]\big\| < \big\|\mathbf{p}_2[n]-\mathbf{p}_2[n-1]\big\| \text{ and} \\ & \big\|\mathbf{p}_1[n]-\mathbf{p}_2[n-1]\big\| < \big\|\mathbf{p}_1[n]-\mathbf{p}_1[n-1]\big\| \\ & \text{or if} \\ & \big\|\mathbf{p}_2[n]-\mathbf{p}_1[n-1]\big\| < \big\|\mathbf{p}_1[n]-\mathbf{p}_1[n-1]\big\| \text{ and} \\ & \big\|\mathbf{p}_2[n]-\mathbf{p}_1[n-1]\big\| < \big\|\mathbf{p}_2[n]-\mathbf{p}_2[n-1]\big\|\end{aligned} \tag{2.9}$$

where $\|\cdot\|$ is the vector norm. In the unlikely case where $\mathbf{p}_1[n]$ and $\mathbf{p}_2[n]$ are at equal distance from $\mathbf{p}_1[n-1]$ and $\mathbf{p}_2[n-1]$, the correspondence initialization is simply delayed until the next frame to avoid a wrong correspondence. The correspondence initialization algorithm provides good correspondence if the feet are far enough from each other and if the motion between the two frames is small. This is the case here since the correspondence initialization is performed only when the legs are separated in two consecutive frames. The feet are therefore relatively far from each other in both frames, and the motion between the frames is relatively small.

In the case where the foot correspondence is established between frames $n-1$ and $n-2$ (correspondence is initialized), the motion correspondence algorithm developed by Rangarajan & Shah [83] is used to establish foot correspondence between frames n and $n-1$. As for the correspondence initialization, the foot positions $\mathbf{p}_1[n]$ and $\mathbf{p}_2[n]$ will be swapped (if necessary) according to the association made by the motion correspondence algorithm.

Moving feature points correspondence is established in [83] by assuming that a point follows a smooth trajectory and has a small spatial displacement between each frame. These two assumptions hold here since 1) the typical frame rate used for gait analysis and modelling is about 30 frames per second, which lead to small spatial displacement, and 2), a foot motion is smooth during walking. The motion correspondence algorithm provides some robustness to the proposed approach since foot correspondence can be preserved in case of a noisy silhouette (e.g. the bottom part of a leg is not present in the silhouette).

Figure 2.10 shows examples of foot location and tracking for frames where the feet

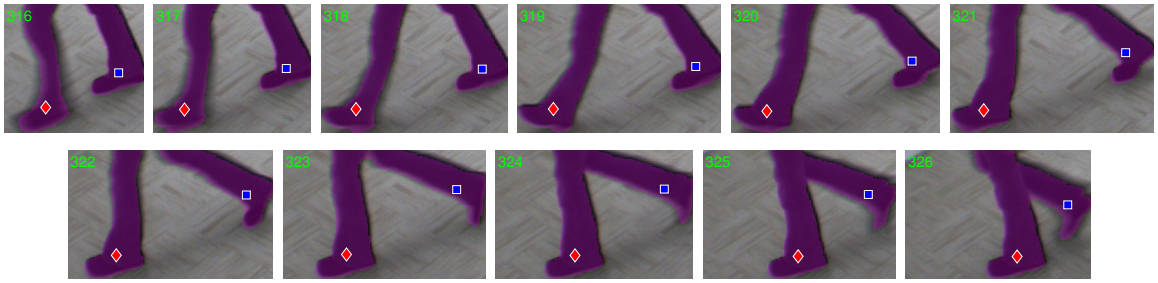

Figure 2.10 – Examples of foot location and tracking without occlusion. The silhouette is overlaid in pink in the frames, and the foot positions are represented by a blue square and a red diamond. One can see that foot correspondence is established in all frames, that is, the blue square and the red diamond belong to the same foot across the frames.

are not in occlusion. The legs in these frames can be separated since there are a valid background paths. One may see that foot correspondence is established in each frame, that is, a foot position is represented by the same symbol across the frames.

2.6.3 Foot Location and Correspondence with Occlusion

Feet are considered to be in an occlusion state in the current frame n when the legs can not be separated with the method presented in Section 2.6.1. An attempt is made to find a position for the *moving foot* only if the foot correspondence is initialized and if the feet have not been been in occlusion for more than ξ_{OF} consecutive frames. Otherwise, foot positions will not be found until the legs can be separated again in the following frames (see "Tracking reset" in Figure 2.7). Foot correspondence must have been initialized in the occlusion case since the foot positions for frame $n-1$ and $n-2$ are needed in order to determine which foot is moving in the current frame. The maximum number of consecutive frames is set to $\xi_{\text{OF}} = 10$ in this thesis in order to limit the number of extrapolations that are made when there is not enough motion in the legs region.

As discussed in Section 1.1.1, there is only one foot moving at a time during human locomotion. Moreover, the velocity of the moving foot is maximal during the time interval where occlusion is most likely to happen, that is, when the feet are the closest to each other. It is then possible to detect parts of the moving foot by analyzing the optical flow of the legs region. In order to determine which foot is moving in the previous frame, the difference between each foot x coordinate in the frames $(n-1)$ and

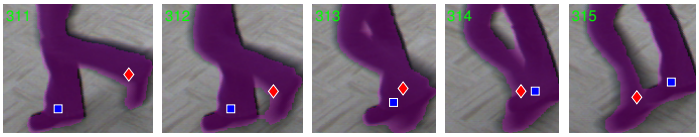

Figure 2.11 – Examples of foot location and tracking with occlusion. The silhouette is overlaid in pink in the frames, and the foot positions are represented by a blue square and a red diamond. In frames 311 and 315, the feet are not in occlusion since the legs can be separated by analyzing the legs region of the silhouette. Frame 312 to 314 correspond to occlusion frames since there is no background gaps between the legs (frame 313), or the height of the background paths is not long enough (frames 312 and 314).

$(n-2)$ are compared:

$$m = \begin{cases} 1 & \text{if } \left|p_{1,x}[n-1] - p_{1,x}[n-2]\right| > \left|p_{2,x}[n-1] - p_{2,x}[n-2]\right| \\ 2 & \text{otherwise,} \end{cases} \tag{2.10}$$

where m is the label of the moving foot. In the case of the *still foot*, which is denoted $\bar{m}$, its position in frame n is simply considered as its position in frame $n-1$: $\mathbf{p}_{\bar{m}}[n] = \mathbf{p}_{\bar{m}}[n-1]$. The pixels belonging to the moving foot are found by first computing the optical flow in the legs region using the method developed by Horn & Schunck [84] ("Compute optical flow" in Figure 2.7). Since this method only works for grey scale data, a grey scale conversion of the original *RGB* image in the legs region is performed for the current and the previous frames. A binary mask of the legs region is then computed by finding the pixel positions where the optical flow norm is greater than $\xi_{\text{ON}} = 10$ pixels. Two morphological dilations are applied to the resulting mask followed by a logical `and` operator with the silhouette legs region of the current frame. The final mask consist in pixels positions where there is significant motion in the legs region of the silhouette.

The position of the moving foot $\mathbf{p}_m[n]$ is obtained by using the pixels counting algorithm on the mask ("Foot position from optical flow" in Figure 2.7). Up to 25% of the number of pixels in the silhouette legs region are counted in the mask, starting from the bottom ($\xi_{\text{OP}} = \frac{1}{4}$). The centroid of the counted pixels is used as the position of the moving foot only if the number of counted pixels is at least 0.2% of the number of pixels in the silhouette legs region ($\xi_{\text{OM}} = 0.002$). Otherwise, the moving foot position will be linearly extrapolated using its two previous positions: $\mathbf{p}_m[n] = 2\,\mathbf{p}_m[n-1] - \mathbf{p}_m[n-2]$ ("Foot position extrapolation" in Figure 2.7).

Figure 2.11 shows examples of foot location and tracking for some frames where the feet are in occlusion. Frames 311 and 315 represent the positions of the feet before and after the occurrence of feet occlusion in frames 312 to 314. The positions computed

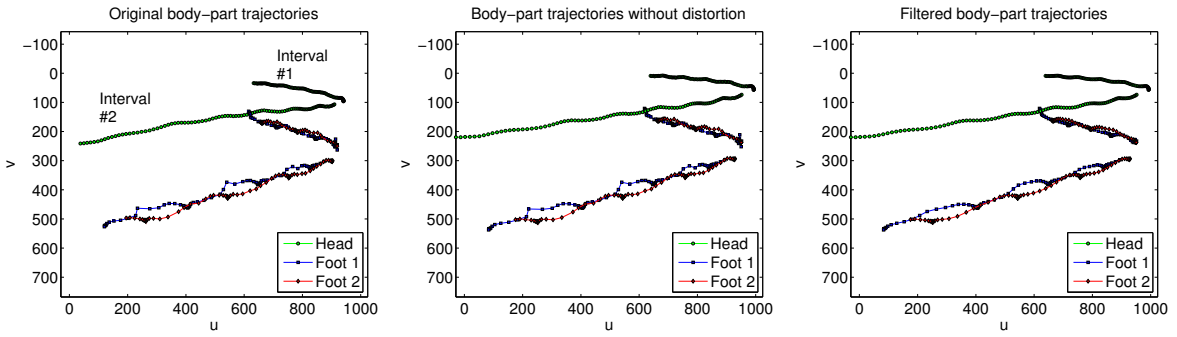

(a) (b) (c)

Figure 2.12 – Body-part positions post-processing. In (a), the body parts positions are grouped to form trajectories which are defined for a time interval of continuous tracking. In (b), radial and tangential distortion are removed from the body part trajectories. In (c), Gaussian filtering is used to smooth the body-part trajectories.

for the moving foot are consistent with the ones obtained when there is no occlusion. Foot correspondence is implicit in the case of feet occlusion since only the moving foot is searched in the legs region.

2.7 Body Parts Positions Post-processing

Figure 2.12 shows the results of each of the post-processing step performed on the body-part positions obtained for the example presented in Figure 2.1. The first post-processing step, which is detailed in Section 2.7.1, consist in grouping the body-part positions into continuous tracking intervals. Distortion removal is the second post-processing step and is described in Section 2.7.2. Finally, the body part trajectories filtering step is presented in Section 2.7.3.

2.7.1 Grouping Positions into Continuous Tracking Intervals

In order to facilitate the analysis and the modelling of the gait, the body-part positions are grouped into *continuous tracking intervals*, which are defined temporally as contiguous frames intervals where both the head and the feet are successfully localized and tracked. A video sequence can be temporally segmented into a set of I continuous tracking intervals, where each interval is defined as $[n_{\mathrm{S},i}, n_{\mathrm{E},i}]$, with $n_{\mathrm{S},i}$ and $n_{\mathrm{E},i}$ being the interval starting and ending frame number respectively ($i = 1, 2, \ldots, I$). An interval

i is defined as too short if $(n_{\mathrm{E},i} - n_{\mathrm{S},i})/f_{\mathrm{s}} < \xi_{\mathrm{I}}$, where f_{s} is the acquisition frame rate (in frames per second), and ξ_{I} is a threshold in seconds. In this thesis, an interval is considered too short if its duration is less than one second ($\xi_{\mathrm{I}} = 1$).

The *time serie* consisting in the positions of a body part for a given frame range is referred here to as the *body part trajectory*. Thus, the body part trajectory of the body part $\ell \in \{\mathsf{H}, 1, 2\}$ for the continuous tracking interval i is defined as the set of ordered positions $\mathcal{T}_{\ell,i} : \{\mathbf{p}_\ell[n] \,|\, n \in [n_{\mathrm{S},i}, n_{\mathrm{E},i}]\}$. In the rest of this thesis, a body part trajectory will be referred to as the positions $\mathbf{p}_\ell[n]$ for a given frame range.

Figure 2.12(a) shows an example where continuous tracking intervals are identified for a complete video sequence. The first event that causes an interval to be defined in this example is the reset at some point of the feet tracking algorithm. Interval #1 is then defined from the time where the first positions of the body part are found (when the subject was completely in the field of view of the camera) to the time where the feet tracking is reset. In the case of interval #2, it is defined from the time where the feet tracking recovered to the time where the subject exited the field of view of the camera. The positions in each trajectory in Figure 2.12(a) are plotted with a symbol specific to each body part. Each plotted position is linked by a line segment with the previous and the next positions. This helps to see the progression in time of a body part as well its relative velocity in the image.

2.7.2 Removing Radial and Tangential Distortion

Radial and tangential distortions can be removed from the body part trajectories if the camera was properly calibrated, that is, radial and tangential distortions were taken into account during the calibration process. This step could be performed instead on the whole frames acquired from the camera, but that would require to perform a transformation for all pixel positions in the frames as well as interpolating pixel values. It is therefore faster and simpler to locate and track the body parts in the distorted frames and then to remove the distortion from the body part trajectories.

The distortion model used here is the one proposed by Heikkilä [85], where the radial and tangential distortion parameters are each represented by two coefficients. Distortion removal is performed on all the body part trajectories of each interval in a video sequence. Figure 2.12(b) shows body part trajectories for which radial and tangential distortion are removed. The trajectories seem to have been stretched outwards with respect to the image centre compared to the original trajectories shown in Figure 2.12(a).

2.7.3 Body Parts Trajectory Filtering

Filtering permits to compensate for the noise that may be present in the body-part trajectory. This is especially true for the feet trajectories where the quality of the positions computed by the tracking algorithm during feet occlusion depends on the degree of occlusion in the legs region.

Each body part position $\mathbf{p}_\ell[n]$ is filtered using a Gaussian kernel of size Ψ and standard deviation σ as follow:

$$\breve{\mathbf{p}}_\ell[n] = \frac{\sum_{j=-\psi}^{\psi} \mathbf{p}_\ell[n+j]\, e^{\frac{-j^2}{2\sigma^2}}}{\sum_{j=-\psi}^{\psi} e^{\frac{-j^2}{2\sigma^2}}}, \quad n \in [n_{\mathrm{S},i} + \psi, n_{\mathrm{E},i} - \psi]\,,\ \psi = \lfloor \Psi/2 \rfloor\,, \tag{2.11}$$

where $\breve{\mathbf{p}}_\ell[n]$ denotes the filtered position. The kernel size Ψ is computed such as the filter covers about 98.76% of the area of a Gaussian with standard deviation σ, that is, $\Psi = 5\sigma$. In this thesis, a standard deviation of $\sigma = 1$ is used for the Gaussian kernel, which leads to a kernel size of $\Psi = 5$. The positions in intervals $[n_{\mathrm{S},i}, n_{\mathrm{S},i} + \psi)$ and $(n_{\mathrm{E},i} - \psi, n_{\mathrm{E},i}]$ are not filtered, that is, they remain unchanged: $\breve{\mathbf{p}}_\ell[n] = \mathbf{p}_\ell[n]$. The filtered body-part positions will simply be referred as to $\mathbf{p}_\ell[n]$ in the rest of this thesis.

2.8 Conclusion

The body parts tracking algorithm presented in this chapter permits to obtain the positions of the head and the feet for frames in which there is a valid silhouette. Foot correspondence is established between each consecutive frames of a video sequence, thus allowing identification of each foot with arbitrary labels 1 (foot 1) and 2 (foot 2) for the whole sequence. Post-processing step provides filtered and undistorted body-part trajectories that are defined for continuous tracking interval.

The proposed algorithm can compute the position of the body parts in each frame of a video sequence in real-time. Table 2.1 shows the performance statistics of a *C++* implementation of the algorithm on the database used in this thesis. The processing times do not include the pre-processing and the post-processing steps described in this chapter. A total of 95438 frames having a resolution of 1024×768 were used to compute these statistics. One may see that the mean processing time is below 33 ms (30 fps), the frame rate at which the video sequences were acquired.

	Mean	Std	Median	Min	Max
ms/frame	8.9	19.4	5.9	1.3	171.6

Table 2.1 – Real-time performance statistics of the body parts tracking algorithm.

There are some limitations to the proposed body parts tracking algorithm. For instance, the algorithm is not able to compute the positions of the body parts for viewpoints in the range $[-40°, 40°]$, where $0°$ is the frontal view. This range of viewpoints is problematic since the legs cannot be separated most of the time and the feet occlusion last for too many frames. An example of this can be seen for the frames 214 to 238 in Figure 2.4. A second limitation is that the algorithm relies heavily on the silhouettes in order to find the position of the body parts. In the case where a silhouette does not contains one of the body parts (e.g. the pixels belonging to a body part are not in the silhouette), the computed position will not be representative of the real body part position. The position errors can be diminished to some degree by the filtering step discussed in Section 2.7.3, but cannot be completely eliminated.

Gait analysis, modelling and comparison will be performed using the trajectories of the body parts. Since these trajectories are view-dependent, they must be first transformed so that they appear to be observed from a fronto-parallel view. This is the main subject of the next chapter.

Chapter 3

View-rectification

"Sometimes only a change of viewpoint
is needed to convert a tiresome duty
into an interesting opportunity."

Alberta Flanders

As discussed in Section 1.4, invariance to the *viewpoint* is one of the most important issue of gait analysis and modelling approaches. Indeed, most approaches consider only a *fronto-parallel view* of people walking at a distance since this viewpoint is well suited for gait analysis and modelling. Moreover, the fronto-parallel viewpoint permits to perform gait analysis and modelling at a distance without being affected too much by the *perspective projection* effects.

However, perspective projection effects cannot be ignored for arbitrary viewpoints or for walks that are performed close to the camera. Silhouette-based gait analysis and modelling approaches are especially affected in these cases since the observed contour points on the silhouettes may not correspond to the same physical points for two different frames (see Section 1.4). Model-based approaches are also affected by perspective projection effects, but the body-part positions mostly correspond to the same physical positions for two different frames. This is the main reason for the use of a model-based approach in this thesis as well as for the development of a body parts tracking algorithm in Chapter 2.

It will be shown in this chapter that it is possible to recover a fronto-parallel view of imaged body-part trajectories obtained for non-frontal walks. A *view-rectification* process is performed to make the imaged body-part trajectories appear as if they were

observed from a fronto-parallel view. The view-rectification process requires some hypotheses on how the walk is performed, along with the knowledge of the camera intrinsic parameters, the ground vanishing line, and, optionally, the ground scale factor.

In this chapter, a literature review on viewpoint invariant gait analysis and modelling is first presented. It is followed by a brief overview of the proposed approach. Each step of the view-rectification algorithm is then subsequently detailed. The chapter is concluded by discussing the properties, the advantages, and the limitations of the proposed approach.

3.1 Literature Review

As discussed previously in Section 1.4, very few gait analysis, modelling and comparison approaches are designed to cope with viewpoint changes. Some of the approaches that are specifically designed to perform view-invariant gait analysis, modelling and comparison are based on multi-view acquisition systems [86, 87]. For instance, the approach in [86] decomposes the view factor, the body configuration factor and the gait style of walking people using data acquired from multiple views (from four to six views). A supervised manifold learning algorithm is used in [87] in order to maximize the difference between the subjects while minimizing the effects of the different viewpoints (from two to eleven views). Unfortunately, the use of a multiple views acquisition system to learn a view-independent model of each person's gait is not a practical option in the case of real-time surveillance in public area since there is usually only one camera per observed area. Although it is possible to use a multiple views acquisition system in the case of medical applications, this is undesirable since those systems are expensive and can be difficult to operate for a physician.

In other approaches, predefined static gait features are instead extracted from monocular video sequence using knowledge of the environment and the camera [49, 50]. The approach in [49] extracts measurements (distance between the head and the pelvis, distance between the feet and bounding box height) directly from the silhouettes and then applies a depth compensation factor to these measurements. However, this depth compensation factor is only valid for a given view and has to be estimated using a subject with known height. A camera calibrated with respect to the ground is used in [50] in order to estimate the strides length, the cadence and the height of a person from an arbitrary view. However, the extrinsic camera parameters must be known in order to estimate those gait features directly from the camera image. Moreover, the approaches of [49, 50] are limited to the extraction of static, predefined features, and

thus cannot be easily adapted to the extraction of dynamic gait features.

View-invariant gait modelling and comparison is performed in [88] by considering only the *frame range* in the compared gait video sequences where the *viewpoint range* is the same. Although this approach avoids some of the problem due to perspective distortion, one cannot assumes that a common viewpoint range between two given video sequences always exists. Moreover, this approach does not fully exploit all the gait cycles in the video sequences in order to perform gait modelling and comparison.

Generation of a fronto-parallel view of the silhouettes has been proposed by a number of authors in the literature [58, 89, 90]. In these works, the silhouettes computed from a video sequence are transformed using either rotations [89, 90] or homographies [58]. The transforms are computed by either estimating the direction of the walk in the image [89, 90], or by estimating the homography induced by the pair of parallel lines that represent the trajectory of the upper and lower points of the silhouettes [58]. These approaches assume that the walk is performed on a straight line, and that the observed person can be considered as a planar object, that is, the walk is performed far from the camera. These assumptions do not hold for walks with changes in direction or for walks that are performed close to the camera. As discussed in Section 1.4, the silhouettes in such conditions are distorted by perspective projection and thus should not be used for gait features extraction.

The most comprehensive view-invariant gait analysis, modelling and comparison approach to date is the one described in [55, 91, 92, 93]. A fronto-parallel view of the positions of the ankle, knee and hip joints is recovered using a single non-calibrated camera. The approach is based on the following assumptions: the subjects walk in a straight line at a constant velocity, the joints of a leg lie in a plane in the scene, and the distance between adjacent joints remains constant during walk. Since gait is a cyclic motion, the observation of multiple gait cycles from a single camera is similar to the observation of a single gait cycle from multiple cameras related by a translation in the direction of the walk. Therefore, the positions of the joints in the images lie in an auto-epipolar configuration. A fronto-parallel view of the joint trajectories can then be generated by using epipolar geometry. The earliest version [91, 92, 93] of this method relied on marker placed on the subject's legs in order to recover the positions of the joints in the images. As for the most recent version [55], it uses a joint tracking algorithm [52] based on a motion template, which was discussed previously in Section 2.1. Although this approach is perfectly sound, it restricts the possible surveillance scenarios since it relies on assumptions such as constant velocity and straight line walks. Although this approach could be used in medical scenarios, it could be problematic to have some patient walk at a constant velocity in restrained acquisition room.

3.2 View-rectification Approach Overview

The approach proposed in this thesis consists in performing a *view-rectification* of the imaged body-part trajectories, that is, a fronto-parallel view of imaged body-part trajectories is generated. These generated body-part trajectories are referred to as the *view-rectified* body-part trajectories, and are suitable for view-invariant gait analysis and modelling. The proposed method does not suffer from the limitations of the methods discussed in the previous section since

- only a single camera is necessary;
- static and dynamic features can be extracted from the rectified body-part trajectories;
- all complete gait half-cycles can be used for gait analysis and modelling;
- subjects are not considered as planar objects;
- walk can be performed close to the camera as well as far from the camera;
- changes in the walking direction are handled;
- changes in the walking speed are also handled.

The following assumptions are made in the proposed view-rectification approach :

1. The camera is fixed;
2. The surface of walk is flat and level, i.e. people are not walking on an inclined or uneven surface;
3. People walk normally, i.e. people are not walking backwards, running, jumping, or doing any other activity that is not related to walking;
4. People stay upright while they are walking, i.e. they do not bend;
5. The motion of each body part is planar during each gait half-cycle, i.e. the body-part positions lie in a plane during a given half-cycle.

Assumptions 1, 2, 3, and 4 are common to most approaches that perform gait analysis and modelling using computer vision techniques. Assumption 5 is similar to the one in [55, 91, 92, 93], but is assumed here to be true only within each gait half-cycle instead of the whole walk. In the case of the proposed approach, these five assumptions also provide constraints that are used to define a model of a typical walk, which will be discussed in Section 3.3.

Figure 3.1 shows an overview of the proposed view-rectification approach. The approach uses as input the head and the feet trajectories obtained, e.g. using the body parts tracking method described in Chapter 2. The first step of the proposed

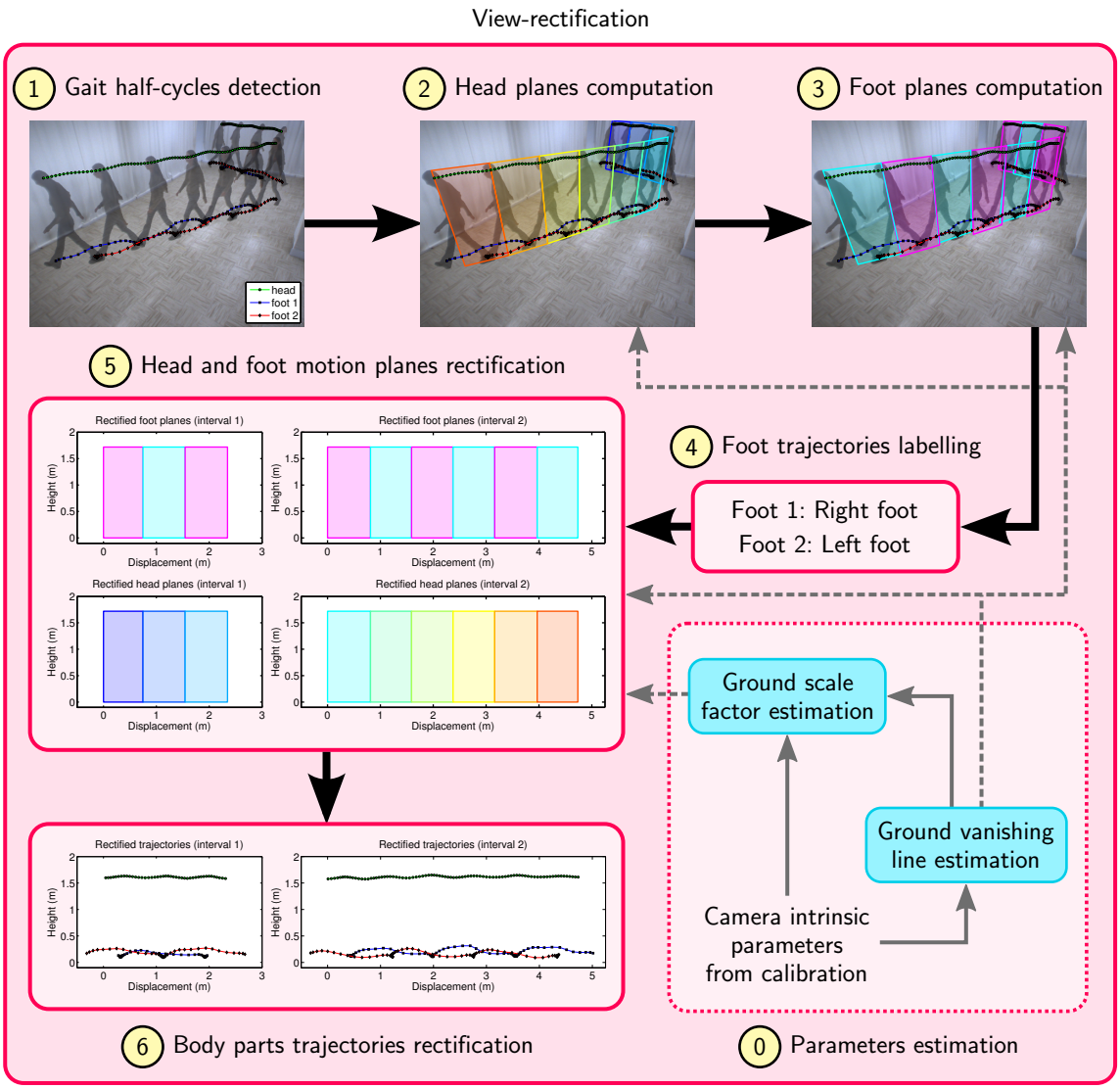

Figure 3.1 – Overview of the view-rectification approach. The plain arrows show the order in which each step must be performed, while the dashed arrows point to the steps that need a certain parameter of the proposed approach.

approach consists in temporally segmenting the trajectories into *gait half-cycles*. Next, the constraints provided by the *walk model* are considered in Step 2 and 3 in order to compute the *imaged head and foot motion planes*, which are the image of the two *scene planes* in which the head and the foot motion is performed for each gait half-cycle. The *label* of the foot trajectories (left or right) are then deduced in Step 4 using the imaged head motion planes. In Step 5, each head and foot motion planes is *metrically rectified* in order to make it appear as if it was observed from a fronto-parallel view. Finally, the *view-rectified body-part trajectories* are computed in Step 6 by using the homography induced by the imaged motion planes and their rectified counterpart.

The parameters that are needed for the proposed approach are estimated in Step 0. This step needs to be performed only once for a given camera setup, and thus can be performed once the camera is fixed and calibrated. The main parameter to be estimated is the *ground vanishing line*, which is defined as the line in the image representing the horizon of the ground plane. It is estimated automatically by using the imaged body-part trajectories obtained from a small set of walks. An optional parameter that can be estimated is the *ground scale factor*, which permits to compute the view-rectified body-part trajectories in *scene units*, that is, in meters. The estimation of the ground scale factor necessitates some known distance(s) between points on the ground plane, and these points must be manually identified in the image. This is an optional parameter since scene units are not needed for the comparison of measurements or gait models.

The remainder of this chapter is organized as follows. The proposed walk model is presented in Section 3.3. Next, the method for gait half-cycles detection (Step 1) is presented in Section 3.4. Computation of the head and the feet motion planes (Step 2 and 3) is described in Section 3.5, followed by the presentation of the foot trajectories labelling method (Step 4) in Section 3.6. The rectification of the motion planes and the rectification of the body-part trajectories are presented in Section 3.7 and Section 3.8 respectively. Finally, the estimation of the parameters (Step 0) is presented in Section 3.9.

3.3 Walk Model

The proposed view-rectification approach is based on a model of the walk that describes some of the constraints imposed on the body-part positions for a typical walk. The walk model is mainly used here in order to compute the imaged motion planes in which each body-part motion is performed during a gait half-cycle. Using the walk model described in this section along with projective geometry concepts provides a spatio-temporal link between a normal walk performed in the scene and the corresponding imaged walk. The walk model will also be used to compute gait measurements such as the strides length, the steps length, and the displacement (the distance a person has travelled).

Figure 3.2 presents the proposed 3-D walk model, which was defined on the basis of human walk observations made in medical references [94, 95, 96, 97]. In order to simplify its visualization, the walk model is shown from a side view in Figure 3.2(a) and a top view in Figure 3.2(b). The positions shown in the model are 3-D points representing either a body-part extremity (top of the head or a foot contact point on the ground) or a position derived from body-part extremities (feet middle points). Here, these 3-D

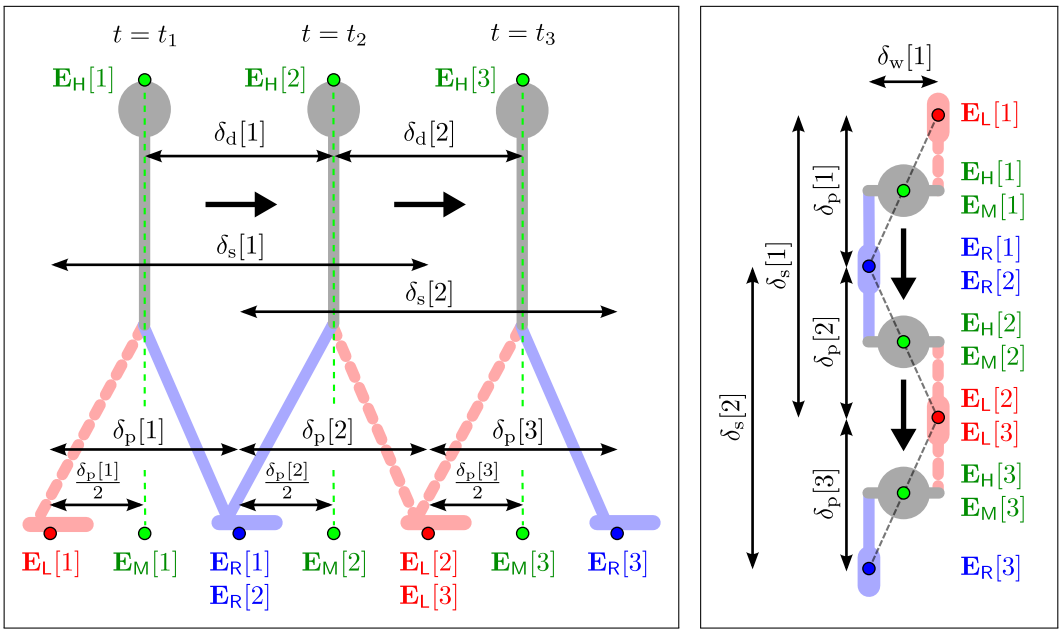

(a) Side view (b) Top view

Figure 3.2 – The proposed walk model is shown from two different viewpoints for a straight line walk performed from left to right. The positions of the body-part extremities ($\mathbf{E}_\mathsf{H}$, $\mathbf{E}_\mathsf{L}$, and $\mathbf{E}_\mathsf{R}$) are defined for the three key times of a gait cycle, that is, the beginning (t_1), the middle (t_2) and the end (t_3). A stick model shows how the body parts relate to each other at each key times of the gait cycle. Features related to the gait are also shown: stride length (δ_s), step length (δ_p), displacement (δ_d), and stride width (δ_w).

positions are referred to as extremities and are denoted $\mathbf{E}_\ell$, where ℓ represent the label of the extremities ($\ell \in \{\mathsf{H}, \mathsf{L}, \mathsf{R}, \mathsf{M}\}$, i.e. "Head", "Left foot", "Right foot", "Middle point"). A stick model shows how these extremities relate to each other at some key times in a gait cycle. The trunk and the head are shown as a grey segment and a grey circle respectively, whereas the left leg and the right leg are shown as a red dashed line and a blue line respectively. The positions of the head and the feet mass centre are not shown here since only the positions of extremities are needed in the proposed walk model. Also, the notation used in this thesis consists in using bold capital letter for 3-vector representing 3-D points (i.e. positions) in the scene, and bold small letter for 2-vector representing 2-D imaged points. For instance, the 3-D extremity position $\mathbf{E}_\ell$ would be imaged as a 2-D position $\mathbf{e}_\ell$

The extremities positions in Figure 3.2 are shown for three key times, namely at the beginning ($t = t_1$), the middle ($t = t_2$) and end ($t = t_3$) of a gait cycle. As explained in Section 1.1.1, these key times represent the beginning of double support phases, which are the time interval where both feet are in contact with the ground. Since the

beginning of a double support phase might occur between two frames, that is, at a non-integer frame number, the continuous variable t is used here instead of the discrete variable n in order to make this distinction clear. The position of an extremity for the kth key time t_k is denoted $\mathbf{E}_\ell[k]$, since the extremities are only defined for key times. At times t_1 and t_3, the right leg is the *leading* leg and the left leg is the *trailing* leg, whereas the left leg is *leading* and the right leg is *trailing* at time t_2 [94]. In the first gait half-cycle, which is defined within the time interval $[t_1, t_2]$, the left foot moves from position $\mathbf{E}_\mathsf{L}[1]$ to position $\mathbf{E}_\mathsf{L}[2]$, whereas the right foot position remains unchanged, that is, $\mathbf{E}_\mathsf{R}[1] = \mathbf{E}_\mathsf{R}[2]$. During the second gait half-cycle, which is defined within the time interval $[t_2, t_3]$, the right foot moves from position $\mathbf{E}_\mathsf{R}[2]$ to position $\mathbf{E}_\mathsf{R}[3]$, and the left foot position remains unchanged ($\mathbf{E}_\mathsf{R}[2] = \mathbf{E}_\mathsf{R}[3]$). During both gait half-cycles, the head and the trunk are continuously moving forward. One should note that there is no assumption in the walk model regarding the shape of the body-part trajectories during a gait half-cycle. Indeed, only the positions of specific body-part extremities are considered at specific key times.

Important gait features are also depicted in Figure 3.2, namely the step lengths (δ_p), stride lengths (δ_s), and the stride width (δ_w). A *step length* is defined as the distance on the ground between the leading and the trailing foot, and is computed in the direction of the walk [94] as shown in Figure 3.2(b). A step length is denoted $\delta_\mathrm{p}[k]$ since it can be computed on a key time basis, that is, it can be computed for each key time t_k in a walk. A *stride length* is defined as the distance travelled by the moving foot during a gait half-cycle. It is denoted here as $\delta_\mathrm{s}[c]$, that is, the stride length for the cth gait half-cycles. The variable c is used here instead of variable k to stress the fact that a stride length can only be computed on a gait half-cycle basis, and not on a key time basis. One may see that the variables k and c are closely related: if one considers that there are K key times for a given walk ($k = 1, 2, \ldots, K$), then there are exactly $C = K - 1$ gait half-cycles, since a gait half-cycle is bounded by two consecutive key times ($c = 1, 2, \ldots, C$). In Figure 3.2, $\delta_\mathrm{s}[1]$ denotes the stride length for the left foot, which is the foot moving in half-cycle $c = 1$, and $\delta_\mathrm{s}[2]$ denotes the stride length for the right foot, which is the foot moving in half-cycle $c = 2$. The *stride width*, $\delta_\mathrm{w}[k]$, is defined as the distance between the feet in the direction *perpendicular* to the direction of walk at each key time, as shown in Figure 3.2(b). The stride width is presented here only for completeness and won't be used in the proposed method.

Some relations can be established between the gait features and extremities positions. For instance, the head-trunk position at a key time is about half a step length behind the leading foot [94], and therefore half a step length in front of the trailing foot (see Figure 3.2(a)). From a top view, the symmetry of the body during the double support phase makes the head and the feet positions collinear, as shown by the black

dashed lines in Figure 3.2(b). Thus, the perpendicular projection on the ground of the head extremity corresponds to the middle point between the feet extremity, which is denoted here as $\mathbf{E}_{\mathsf{M}}[k]$. This projection is represented by the vertical green dashed lines in Figure 3.2(a). The feet middle points can be used to compute a person's displacement $\delta_{\mathrm{d}}[c]$ during the gait half-cycle c as

$$\delta_{\mathrm{d}}[c] = \big\|\mathbf{E}_{\mathsf{M}}[c+1] - \mathbf{E}_{\mathsf{M}}[c]\big\|. \tag{3.1}$$

One should note here that the variable c needs to be used to index the feet middle points in order to define this relation, albeit the feet middle points are defined on a key time basis. One may convince oneself that this relation holds by noting that $\delta_{\mathrm{d}}[1] = \big\|\mathbf{E}_{\mathsf{M}}[2] - \mathbf{E}_{\mathsf{M}}[1]\big\|$ in Figure 3.2. It is also possible to see from Figure 3.2(b) that the displacement is half the stride length $\delta_{\mathrm{s}}[c]$:

$$\delta_{\mathrm{d}}[c] = \frac{\delta_{\mathrm{p}}[c]}{2} + \frac{\delta_{\mathrm{p}}[c+1]}{2} = \frac{\delta_{\mathrm{s}}[c]}{2}. \tag{3.2}$$

This result can be deduced by observing that in the case of a straight line walk, the stride length is the sum of the step lengths $\delta_{\mathrm{p}}[c]$ and $\delta_{\mathrm{p}}[c+1]$.

An important property of human walk is that the step lengths can be different for the left and the right foot, but the strides length must be the same for both feet in order to perform a straight line walk [94, 96]. This implies that there is a change in the direction of walk when the left and the right strides are not of the same length. The foot that is moving during a gait half-cycle travels towards the direction aimed at, or towards an intermediate direction in the case of a smooth change of direction. A walk can thus be segmented into linear walk segment on a gait half-cycle basis. Since the proposed walk model is defined on a gait half-cycle basis, it is valid for straight line walks as well as walks with changes in direction.

Figure 3.3 shows a top view of the walk model in the case of a walk with changes in direction. Here, the extremities positions are shown for 5 key times, that is, 2 complete gait cycles (4 half-cycles). The direction of walk is changed by 30° at each half-cycle. One may notice that the left strides length (red dashed lines) are shorter than the right strides length (blue dashed lines). Compared to the strides performed for a straight line walk, a person actually has to perform shorter strides with her left foot and longer strides with her right foot in order to change the direction of walk to the left. Another observation that can be made is that a stride length is no longer the sum of two step lengths, as the step lengths are computed in the direction of the walk for the corresponding half-cycle. Since the direction of the walk changes at each gait half-cycle, a stride length is indeed function of both the step lengths and the stride width for a given half-cycle. Apart from this, the relations between the strides length and the extremities positions discussed previously still hold in the case of a walk with

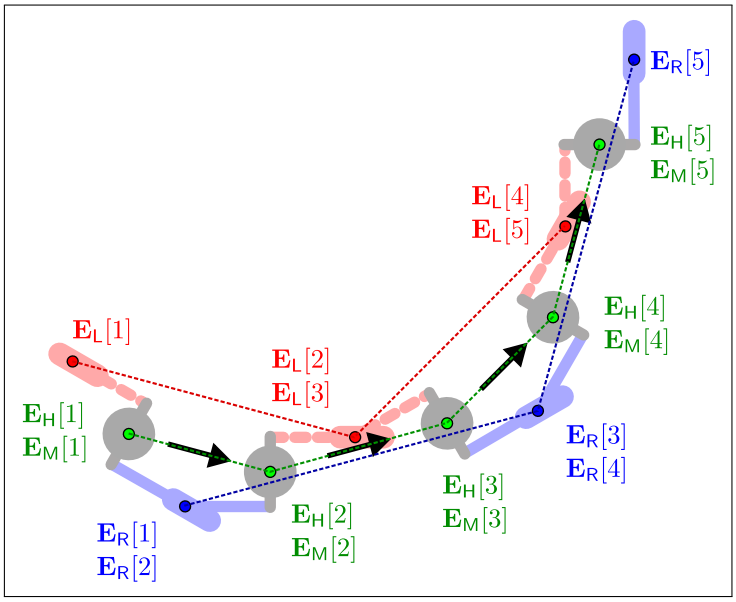

Figure 3.3 – Top view of the walk model for a walk with changes in direction. The extremities positions are shown for 5 key times. The direction of walk (black arrows) is changed by 30° at each gait half-cycle.

changes in direction. For instance, the displacement during a half-cycle is still half the stride length. This can be seen in Figure 3.3 by first observing that the triangles $\triangle\mathbf{E}_{\mathsf{L}}[c]\mathbf{E}_{\mathsf{L}}[c{+}1]\mathbf{E}_{\mathsf{R}}[c]$ and $\triangle\mathbf{E}_{\mathsf{M}}[c]\mathbf{E}_{\mathsf{M}}[c{+}1]\mathbf{E}_{\mathsf{R}}[c]$, are always similar (here $c \in \{1, 2, 3, 4\}$). Given that the base of those triangles is defined as

$$\delta_{\mathrm{s}}[c] = \big\|\mathbf{E}_{\mathsf{L}}[c+1] - \mathbf{E}_{\mathsf{L}}[c]\big\| \;\text{ and }\; \delta_{\mathrm{d}}[c] = \big\|\mathbf{E}_{\mathsf{M}}[c+1] - \mathbf{E}_{\mathsf{M}}[c]\big\|, \tag{3.3}$$

and that the relations between the two other sides are, from Equation 3.1,

$$\begin{aligned} \big\|\mathbf{E}_{\mathsf{M}}[c] - \mathbf{E}_{\mathsf{R}}[c]\big\| &= \frac{1}{2}\big\|\mathbf{E}_{\mathsf{L}}[c] - \mathbf{E}_{\mathsf{R}}[c]\big\| \;\text{ and} \\ \big\|\mathbf{E}_{\mathsf{M}}[c+1] - \mathbf{E}_{\mathsf{R}}[c]\big\| &= \frac{1}{2}\big\|\mathbf{E}_{\mathsf{L}}[c+1] - \mathbf{E}_{\mathsf{R}}[c]\big\|, \end{aligned} \tag{3.4}$$

it follows that $\delta_{\mathrm{d}}[c] = \frac{1}{2}\delta_{\mathrm{s}}[c]$. Moreover, it is possible to see from this result that the direction of the displacement will always be parallel to the direction aimed at by the person's moving foot. Thus, the head and the moving foot trajectories in the scene are parallel during a gait half-cycle. This observation is used thoroughly in the proposed view-rectification approach.

The proposed walk model, which consists in the relations and the constraints discussed in this section, will be used to compute, on a half-cycle basis, the image of the planes in which each imaged body-part motion is performed. In order to do so, the gait half-cycles must first be detected using the imaged body-part trajectories.

3.4 Gait Half-Cycles Detection

As mentioned previously, a gait half-cycle is defined as a time interval bounded by the starting time of two consecutive double support phases. Therefore, detecting the gait half-cycles in a walk implies detecting the starting time of the double support phases. By definition, the double support phase starts at the moment in time when the heel of the moving foot makes contact with the ground. However, detecting the moment in time where the heel touches the ground is a not a trivial computer vision task. Another noticeable moment in time during the double support phase is the one where the feet are furthest apart. This moment in time, which is referred here to as *key time*, can be detected by analyzing the time-series of the distance between the imaged feet positions in a video sequence. The key times can be obtained by first computing the distance between the feet in each frame, and then by determining the K *key frames* n_k for which the distance is maximal when compared to neighbouring frames. The key times t_k, which are non integer frame numbers, can then be interpolated from the obtained key frames n_k, $k = 1, 2, \ldots, K$.

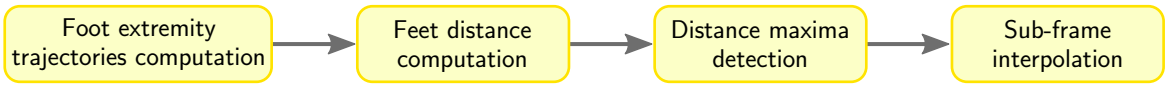

Figure 3.4 – Gait half-cycles detection algorithm.

Figure 3.4 shows the four steps of the proposed gait half-cycles detection algorithm, which is detailed in the following subsections. The first step consists in computing the foot extremity trajectories in each continuous tracking interval. Next, the foot extremity trajectories are used to compute the distance between the feet, which is then analyzed in order to find the key frames. Finally, the key times are computed using sub-frame interpolation and are used to define the gait half-cycles.

3.4.1 Foot Extremity Trajectories Computation

As discussed in Chapter 2, the body parts tracking method provides for each frame n the position of the head and the feet $\mathbf{p}_{\mathsf{H}}[n]$, $\mathbf{p}_1[n]$, and $\mathbf{p}_2[n]$, as well as the bounding box of the region where each body part is located, $\mathbf{b}_{\ell,c}[n]$, $\ell \in \{\mathsf{H}, 1, 2\}$ and $c \in \{\mathsf{TL}, \mathsf{TR}, \mathsf{BL}, \mathsf{BR}\}$. However, the body part tracking algorithm does not provide the trajectory of each foot extremity. Therefore, the trajectory of each foot extremity, which is denoted as $\mathbf{p}_{\ell\mathsf{B}}[n]$, $\ell \in \{1, 2\}$, is computed directly from the position of the

Figure 3.5 – Example of foot extremity computation for a frame. The foot positions are represented by a square and a diamond, and the computed foot extremity positions are represented as triangles. The foot bounding boxes are shown using plain lines.

foot centre of mass along with the corresponding foot bounding box:

$$\widetilde{\mathbf{p}}_{\ell\mathsf{B}}[n] = \underbrace{\begin{bmatrix} 1 \\ 0 \\ -p_{\ell,x}[n] \end{bmatrix}}_{\mathbf{l}_\mathrm{v}} \times \underbrace{\left(\widetilde{\mathbf{b}}_{\ell,\mathsf{BL}}[n] \times \widetilde{\mathbf{b}}_{\ell,\mathsf{BR}}[n]\right)}_{\mathbf{l}_\mathrm{h}} = \mathbf{l}_\mathrm{v} \times \mathbf{l}_\mathrm{h}, \tag{3.5}$$

where the operator $\times$ denotes the cross product, and the tilde denotes that the positions are in homogeneous coordinates [98], that is,

$$\widetilde{\mathbf{p}}_{\ell\mathsf{B}}[n] = \lambda \begin{bmatrix} \mathbf{p}_{\ell\mathsf{B}}[n] \\ 1 \end{bmatrix} \text{ for any } \lambda \neq 0. \tag{3.6}$$

One must note that a line can also be represented in homogeneous coordinates, that is, a line $l_1 x + l_2 y + l_3 = 0$ in the image can be represented as a vector $\mathbf{l} = \lambda[l_1 \; l_2 \; l_3]^\mathsf{T}$ for any $\lambda \neq 0$. Moreover, a line joining two points can be defined as the cross product of the homogeneous representation of the two points. Also, the intersection point of two lines can be defined as the cross product of the homogeneous representation of the lines. These two results come from the duality of points and lines in the projective space $\mathbb{P}^2$ [98], which is the projective space considered when working in the camera image plane. The position of a foot extremity is thus simply computed as the intersection point of two lines $\mathbf{l}_\mathrm{v}$ and $\mathbf{l}_\mathrm{h}$. The line $\mathbf{l}_\mathrm{v}$ is the vertical line $x = p_{\ell,x}[n]$ that passes through the point $\mathbf{p}_\ell[n]$(i.e. the foot position), whereas the line $\mathbf{l}_\mathrm{h}$ is defined as the line joining the bottom corners of the foot bounding box, $\mathbf{b}_{\ell,\mathsf{BL}}[n]$ and $\mathbf{b}_{\ell,\mathsf{BR}}[n]$. The line $\mathbf{l}_\mathrm{h}$ represents the bottom of the foot region and the foot extremity can be considered as a point on this line. The foot extremity position for a given frame n is thus computed by finding the point on line $\mathbf{l}_\mathrm{h}$ that has the same abscissa as the foot position.

Figure 3.5 shows the foot extremity positions obtained using Equation 3.5 for an

example frame. The foot positions are shown along with the bounding boxes and the computed foot extremity positions. One should note that the line $\mathbf{l}_{\mathrm{h}}$, representing the bottom side of the bounding box, might not be perfectly horizontal in some case, especially for bounding boxes close to the image border. This is due to the distortion removal that is performed on bounding boxes corners position (Section 2.7.2). As discussed in the following sections, the foot extremity trajectories are used to compute the distance between the feet as well as to define the planes of motion.

3.4.2 Feet Distance Computation

The distance between the feet for a frame n is defined within a continuous tracking interval i as the discrete function $d[n]$:

$$d[n] = \frac{\sum_{j=-\psi}^{\psi} \left\| \mathbf{p}_{1\mathsf{B}}[n+j] - \mathbf{p}_{2\mathsf{B}}[n+j] \right\| e^{\frac{-j^2}{2\sigma^2}}}{\sum_{j=-\psi}^{\psi} e^{\frac{-j^2}{2\sigma^2}}}, \quad n \in [n_{\mathrm{S},i} + \psi, n_{\mathrm{E},i} - \psi], \tag{3.7}$$

where $\psi = \lfloor \Psi/2 \rfloor$, Ψ is the size of a Gaussian kernel used for filtering, and $n_{\mathrm{S},i}$ and $n_{\mathrm{E},i}$ are respectively the starting and the ending frame of the continuous tracking interval i. The filtering parameters used here are the same as for the body-part trajectory filtering described in Section 2.7.3, that is, $\sigma = 1$, $\Psi = 5$. For the frame ranges $[n_{\mathrm{S},i}, n_{\mathrm{S},i} + \psi)$ and $(n_{\mathrm{E},i} - \psi, n_{\mathrm{E},i}]$, the distance is unfiltered and is simply defined as $d[n] = \left\| \mathbf{p}_{1\mathsf{B}}[n] - \mathbf{p}_{2\mathsf{B}}[n] \right\|$. The unfiltered distances correspond to frames that can not be detected as key frames by the algorithm described below.

Figure 3.6 shows an example of feet distance computation for the walk shown in step 1 of Figure 3.1. The filtered and the unfiltered distances between the feet are shown in order to see the effect of filtering. One thing that can be noticed is the effect of perspective projection on the imaged distance between the feet, that is, the distance between the feet becomes larger as the person walks closer to the camera. Fortunately, this will have no impact on the maxima detection as the maxima clearly stand out in the distance time-series.

3.4.3 Distance Maxima Detection

The detection of the distance maxima is performed by finding the frames for which the distance is maximal in a search window. The size W of this window is defined as a

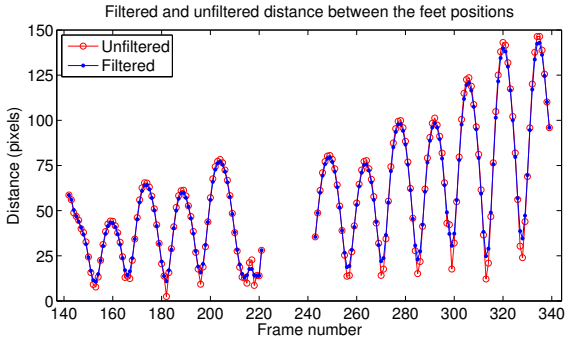

Figure 3.6 – Example of feet distance computation. The unfiltered and the filtered distances between the feet are shown for two continuous tracking intervals. The gaps from frame 222 to frame 242 represents the time range where the feet could not be tracked.

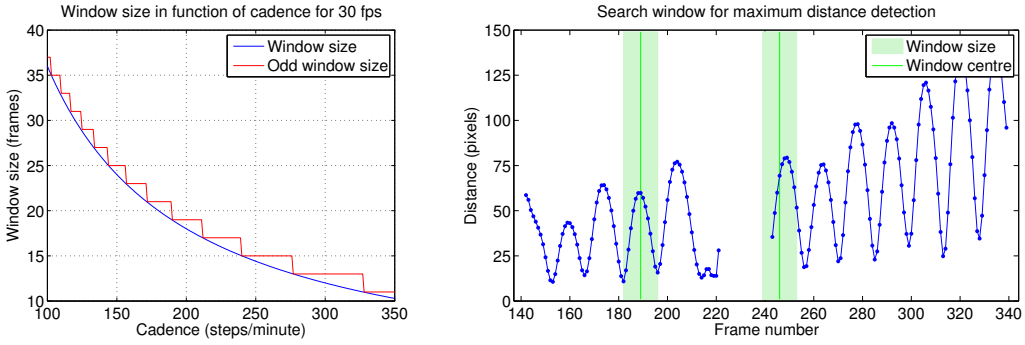

(a) (b)

Figure 3.7 – Search window for distance maxima detection. In (a), the size of the search window is shown as a function of the cadence for $f_s = 30$ fps. In (b), a search window of size $W = 15$ is centred on frames 189 and 246 for the filtered distance previously shown in Figure 3.6. The size of the search window was computed with $f_c = 240$ steps/min.

function of the frame sampling rate f_s (in frames per second) and a maximal bound on the cadence f_c (in steps per minute):

$$W = \text{odd}\,(2 \times 60 f_s / f_c) = 2 \left\lceil \frac{(2 \times 60 f_s / f_c) + 1}{2} \right\rceil - 1, \tag{3.8}$$

where the function odd($\cdot$) rounds up to the nearest odd number in order to obtain a more convenient window that can be centred on a frame. The value $60 f_s / f_c$ simply represents the minimal (non-integer) number of frames between two steps, that is, the minimal number of frames between two feet distance maxima. For a cadence greater than f_c, this means there would be more than one distance maxima in the window, and thus only one of the distance maxima would be detected. A search window defined in function of a maximum bound on the cadence will detect feet distance maxima for walks with cadence up to f_c.

Figure 3.7(a) shows the size of a search window as a function of the cadence for

a standard frame rate of 30 fps ($f_s = 30$). The window size computed as $120 f_s / f_c$ is shown as a blue continuous curve, whereas the window size computed with Equation 3.8 is shown as a red discontinuous curve. It is possible to see that for a given maximal bound f_c, the actual maximal cadence that can be detected using a odd sized window is less than or equal to f_c. For instance, the maximal cadence that can be detected with $f_c = 150$ is $120 f_s / W = 120 \times 30/25 = 144$ steps/min. Although it is theoretically possible to detect distance maxima that are $w = \lfloor W/2 \rfloor$ frames apart from each other using a search window of size W, it might not be possible in practice if the distance value of the maxima are not equal. For this reason, one would set the maximal bound f_c to a value greater that the maximum expected cadence. A safe value for f_c is two times the maximal expected cadence since the search window borders would fall close to distance minima in the case of a walk with the maximal expected cadence. This can be seen in Figure 3.7(b), which shows a search window centred on two frames for the filtered distance previously shown in Figure 3.6. Here, a window size of $W = 15$ has been obtained by setting $f_c = 240$ steps/min, that is, two times the subject's cadence, which is in the order of 120 steps/min. If a window size of $W = 31$ ($f_c = 120$) was used instead, one may see in Figure 3.7(b) that no distance maximum could be detected at frame 189 because of the presence of greater distances within the search window (e.g. frames 174 and 204). By setting f_c to two times the maximal expected cadence, one may see that both window borders effectively fall on the minimum between the consecutive maxima, and thus all the distance maxima can be detected.

Using two times the expected cadence value for f_c increases the possibility of detecting noisy distances as maxima, however. To overcome this possibility, the detected maxima are accessed by verifying that they are also maximal in a median-filtered version of the distance time series. The median filtering removes isolated distance maxima that would have been smoothed, but not removed, by the Gaussian filtering. The median-filtered distance, denoted $d_{\text{med}}[n]$, is computed from the filtered distance signal $d[n]$ as

$$d_{\text{med}}[n] = \underset{j}{\text{median}} \left(d[j] \right), \quad j \in [n - w_{\text{med}}, n + w_{\text{med}}], \quad n \in [n_{\text{S},i}, n_{\text{E},i}], \tag{3.9}$$

where $w_{\text{med}} = \lfloor W_{\text{med}}/2 \rfloor$, and $W_{\text{med}} = \lfloor W/2 \rfloor$, that is, half the search window size. Zero-padding is performed on the distance signal $d[n]$ in order to obtain a median distance $d_{\text{med}}[n]$ for each frame $n \in [n_{\text{S},i}, n_{\text{E},i}]$ in a continuous tracking interval i.

Algorithm 3.1 shows the detailed procedure to perform distance maxima detection on each continuous tracking interval of a walk. The frame on which the search window is first centred is $n_{\text{S},i} + \lfloor W/4 \rfloor$, and not $n_{\text{S},i} + \lfloor W/2 \rfloor$ as one would expect. The main reason for this is that the first distance maximum occurring in an interval would mostly never be detected, as the feet tracking always starts after a feet occlusion, that is, close to a feet

Algorithm 3.1: Distance maxima detection.

1: $w = \lfloor W/2 \rfloor$
2: **for** $i = 1, 2, \ldots, I$ **do** $\Rightarrow$ *for each continuous tracking interval*
3: $K_i = 0$
4: $j = n_{\mathrm{S},i} + \lfloor W/4 \rfloor$ $\Rightarrow$ *initial search frame*
5: **while** $j \leq (n_{\mathrm{E},i} - \lfloor W/4 \rfloor)$ **do**
6: $\alpha = \max(n_{\mathrm{S},i}, j - w)$ $\Rightarrow$ *first frame in search window*
7: $\beta = \min(j + w, n_{\mathrm{E},i})$ $\Rightarrow$ *last frame in search window*
8: $d^* = \max_l (d[l])$ for $l \in [\alpha, \beta]$ $\Rightarrow$ *distance maximum*
9: $d^*_{\mathrm{m}} = \max_l (d_{\mathrm{m}}[l])$ for $l \in [\alpha, \beta]$ $\Rightarrow$ *median distance maximum*
10: **if** $d[j] = d^*$ **and** $d_{\mathrm{m}}[j] = d^*_{\mathrm{m}}$ **then** $\Rightarrow$ *distance maximum detected*
11: $K_i = K_i + 1$, $k = K_i$
12: $n_{k,i} = j$ $\Rightarrow$ *key frame number*
13: $j = j + w + 1$
14: **else** $\Rightarrow$ *no distance maximum detected*
15: $j = j + 1$
16: **end if**
17: **end while**
18: **end for**
19: **return** K_i for $i = 1, 2, \ldots, I$ $\Rightarrow$ *number of key frames in each interval*
20: **return** $n_{k,i}$ for $k = 1, 2, \ldots, K_i$ $\Rightarrow$ *key frames for each interval*

distance maximum (see Section 2.6.2). For instance, the distance maximum at frame 249 in Figure 3.7 would not be detected if the search started at frame $n_{\mathrm{S},i} + \lfloor W/2 \rfloor = 243 + 7 = 250$. But by starting the search at $n_{\mathrm{S},i} + \lfloor W/4 \rfloor = 243 + 3 = 246$, as shown by the window centred on this frame in Figure 3.7, the distance maximum at frame 249 is detected when the search window is centred on it. The same reasoning holds in the case of the last frame searched in an interval, which is frame $n_{\mathrm{E},i} - \lfloor W/4 \rfloor$. Only the frame for which a distance exists are considered in the search window, hence the computation at lines 6 and 7 of the first and the last valid frame number (α and β) within the search window. One may also note that a maximum distance is detected at a given frame only if it is a maximum distance within the search window for both the Gaussian filtered distance and the median filtered distance (line 10). Once a maximum is detected, the search is continued $w + 1$ frames further, as there cannot be another distance maximum in the following w frames (line 13). Otherwise, the search is performed on the next frame (line 15). Finally, the algorithm returns the detected maximum distance frames, $n_{k,i}$, as well as the number K_i of detected maxima for a given interval i.

Figure 3.8 shows the distance maxima detected for two walks performed by two

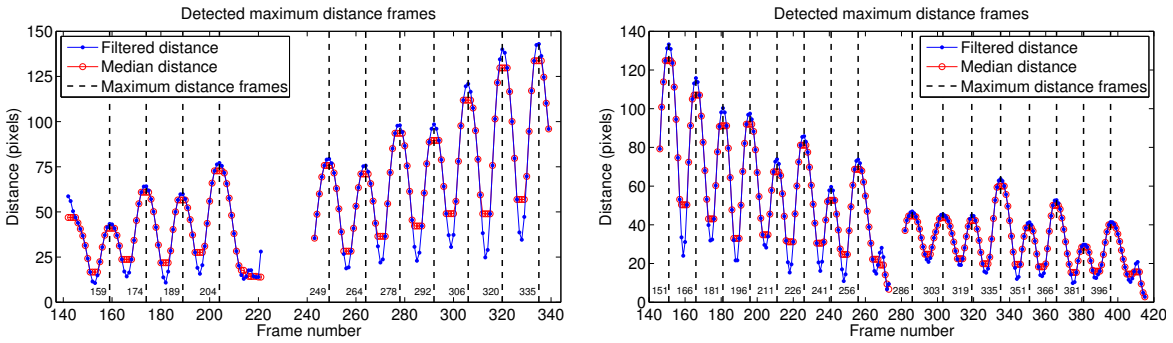

(a) (b)

Figure 3.8 – Examples of detected distance maxima for two walks performed by two different subjects. Both the Gaussian filtered (blue curve) distance and the median filtered (red curve) distance are shown, along with the frames (key frames) for which a distance maximum was detected (vertical dashed lines).

different subjects. It is possible to see that all maxima were correctly detected in both cases, and that false maxima were discarded. For instance, no maximum was detected around frame 217 in Figure 3.8(a) and around frame 411 in Figure 3.8(b) since the search window is wide enough to filter them out. Moreover, the noisy distance around frame 270 in Figure 3.8(b) was discarded because the median distance is not maximal for this frame. Indeed, the median filtered distance is useful in cases where the feet distance is highly noisy for a few consecutive frames.

3.4.4 Sub-frame Interpolation

The key times $t_{k,i}$ can be computed once the key frames $n_{k,i}$ (maximum distance frames) have been obtained. Each key frame $n_{k,i}$ is refined to non-integer key times $t_{k,i}$ by performing a parabolic (second order polynomial) interpolation:

$$t_{k,i} = n_{k,i} + \frac{d[n_{k,i}-1] - d[n_{k,i}+1]}{2\big(d[n_{k,i}+1] - 2d[n_{k,i}] + d[n_{k,i}-1]\big)}. \tag{3.10}$$

The distance values at the previous frame $n_{k,i}-1$ and the next frame $n_{k,i}+1$ are used along with the distance value at frame $n_{k,i}$ to fit a parabola on the three points $\big(-1, d[n_{k,i}-1]\big)$, $\big(0, d[n_{k,i}]\big)$ and $\big(1, d[n_{k,i}+1]\big)$, as shown in Figure 3.9(a). The use of -1, 0, and 1 instead of $n_{k,i}-1$, $n_{k,i}$, and $n_{k,i}+1$ simplifies the parabola fitting process and permits to compute the location of the parabola's maximum with respect to the key frame $n_{k,i}$. This relative location is represented by the second term of Equation 3.10 and its value is a fraction of a frame number. For instance, the maximum of the fitted parabola in Figure 3.9(a) is located at -0.35 frame of the key frame 249, that

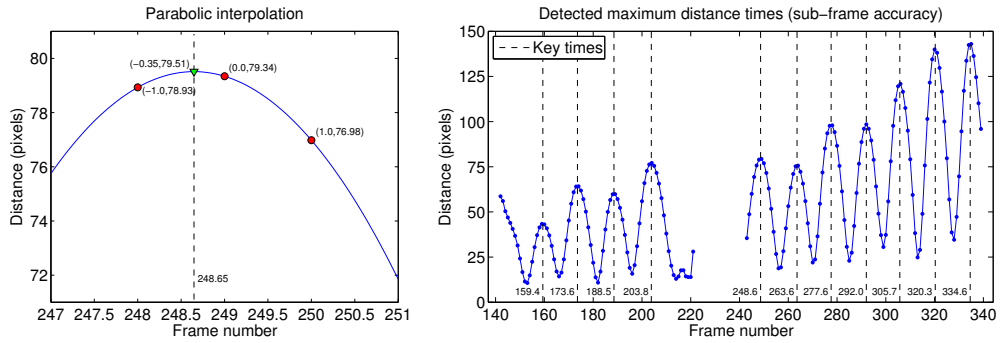

(a) (b)

Figure 3.9 – Example of key times obtained from sub-frame interpolation for the key frames shown in Figure 3.8(a). In (a), sub-frame interpolation for the key frame 249. The feet distance for frames 248, 249 and 250 are shown as red circles. The fitted parabola is shown as a continuous blue curve, and its maximum is shown as a green triangle. The obtained key time is 248.65 (black vertical dashed line) as the parabola maximum is located at -0.35 frame from the key frame 249. In (b), the obtained key times are shown as black vertical dashed lines.

is, at *key time* 248.65. The obtained sub-frame values are named *key times* in order to differentiate them from the discrete, integer-valued frame numbers. Figure 3.9(b) shows the key times obtained with sub-frame interpolation for the key frames in Figure 3.8(a).

Once the K_i key times in the continuous tracking interval i have been obtained, the gait half-cycles can be defined as the time intervals $[t_{c,i}, t_{c+1,i}]$, for $c = 1, 2, \ldots, C_i$. Thus, there is exactly $C_i = K_i - 1$ gait half-cycles, and exactly $\lfloor C_i/2 \rfloor$ *complete* gait cycles. Defining the gait half-cycle as a function of the key times instead of the key frames simplifies the assignment of the frames that falls on the half-cycle boundaries. For instance, the frames assigned to half-cycle $[t_{c,i}, t_{c+1,i}]$ are the frames in discrete interval $[\lceil t_{c,i} \rceil, \lfloor t_{c+1,i} \rfloor]$. This is useful for the definition of the motion planes as well as for the rectification of the body-part trajectories.

3.5 Motion Planes Computation

As discussed previously, the approach proposed in this thesis consists in rectifying the imaged body-part trajectories on a gait half-cycle basis. It is assumed that the motion of a body part is planar during a gait half-cycle, that is, the positions of the body part in each frame of the gait half-cycle lie in a plane in the scene (Assumption no.5). Two

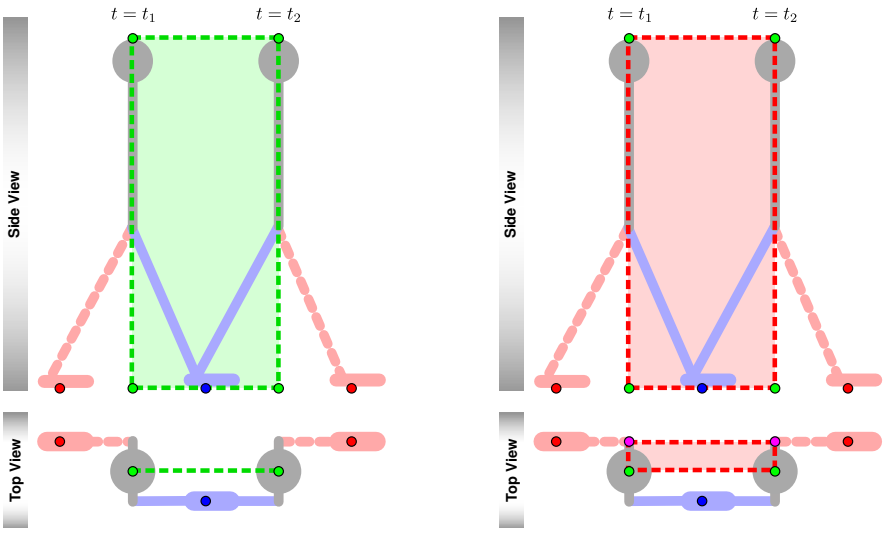

(a) (b)

Figure 3.10 – Planes of motion during a gait half-cycle. In (a), the head motion plane, and in (b), the moving foot motion plane. The points lying in these planes are linked using dashed lines in order to show that they form a rectangle in the scene. The head motion plane is perpendicular to the ground plane, whereas the foot motion plane is slightly slanted with respect to the head motion plane.

motion planes are considered during a gait half-cycle, that is, the head motion plane and the moving foot motion plane. These motion planes are depicted in Figure 3.10 from a side view and a top view. The head motion plane is perpendicular to the ground plane and passes through the head extremities and the feet middle points for the two key times t_1 and t_2. As for the foot motion plane, it is slightly slanted with respect to the head motion plane and it passes through the head extremities and two points lying on the stride line, which is the line joining the foot extremity at key times t_1 and t_2. These two points are actually the projection of the feet middle points on the stride line, as shown in Figure 3.10(b). Also, one can see that the four points in both motion planes form a rectangle in the scene.

Although no motion plane can be computed for the still foot in a given gait half-cycle (the foot is not moving), the positions of this foot can be considered to lie in both the previous and the next foot motion plane, that is, the motion planes defined in the previous and the next gait half-cycle. More details will be provided on the definition of the scene motion planes in the following subsections.

The main idea of the proposed approach is to identify the image of the motion planes for each gait-half-cycle of a walk. The imaged motion planes are obtained by identifying the image of four points that are known to lie on them. The arrangement

of the four imaged points in the image will, in general, be a trapezoid, which provides information on the orientation of the plane in the scene with respect to the camera. This information can be used to compute an homography that transforms the imaged plane (trapezoid) into a rectified plane for which the four points form a rectangle with the same proportions as the rectangle in the scene. This homography can then be used in order to get a rectified view of the corresponding body-part trajectory.

The method used to compute the imaged motion planes on a gait half-cycle basis is presented in Figure 3.11. Three steps must first be performed in order to compute the head motion plane. The obtained head motion plane is then used along with the result of two other steps in order to compute the plane of motion of the moving foot. In both cases, the knowledge of the intrinsic camera parameters is necessary, as well as the ground vanishing line. The computation of the head motion plane and the foot motion plane is described in Section 3.5.1 and 3.5.2, respectively.

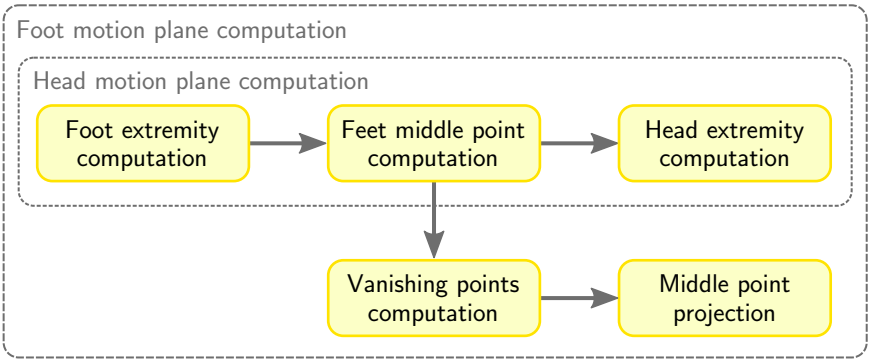

Figure 3.11 – Method for the computation of the planes of motion on a gait half-cycle basis.

3.5.1 Head Motion Plane Computation

The actual motion of the head during a gait cycle is quite complex: it has a sinusoidal component for each of the three orthogonal directions of motion, which are the vertical direction, the lateral direction, and the direction of walk [95]. Since the lateral motion of the head is mainly visible from a frontal view, it will be ignored here. The motion of the head is thus considered to lie entirely in the *plane of progression*, which is the vertical plane aligned with the direction of walk that corresponds closely to the body sagittal plane [94]. The four 3-D points that are known to lie in this motion plane during a gait half-cycle c are the head extremities $\mathbf{E}_{\mathsf{H}}[c]$ and $\mathbf{E}_{\mathsf{H}}[c+1]$, and the feet middle points $\mathbf{E}_{\mathsf{M}}[c]$ and $\mathbf{E}_{\mathsf{M}}[c+1]$ (see walk model in Figure 3.2). One may see that the two vertical lines joining the points $\mathbf{E}_{\mathsf{M}}[c]$, $\mathbf{E}_{\mathsf{H}}[c]$ and $\mathbf{E}_{\mathsf{M}}[c+1]$, $\mathbf{E}_{\mathsf{H}}[c+1]$ are parallel lines, which are perpendicular to the ground plane. Similarly, the two horizontal lines joining

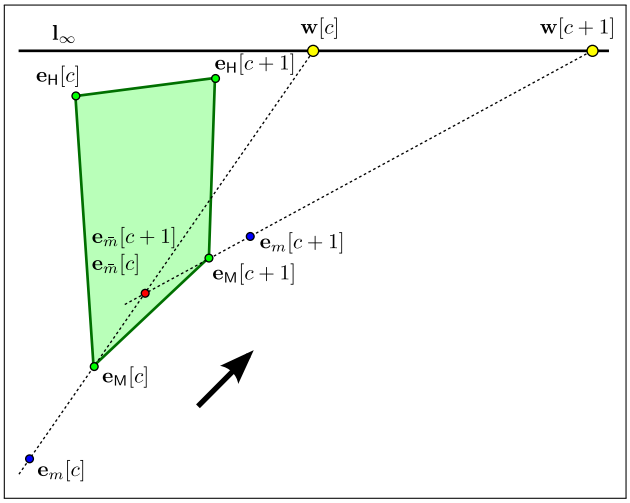

Figure 3.12 – Computation of the head motion plane for a gait half-cycle. Here, m and $\bar{m}$ represent the label of the moving foot and the still foot respectively.

the points $\mathbf{E}_\mathsf{M}[c]$, $\mathbf{E}_\mathsf{M}[c+1]$ and $\mathbf{E}_\mathsf{H}[c]$, $\mathbf{E}_\mathsf{H}[c+1]$ are parallel lines, which are also parallel to the ground plane. These lines form a rectangle in the scene and will be imaged as as trapezoid, unless the viewpoint is exactly fronto-parallel, in which case it will be imaged as a rectangle. Computing the imaged head motion plane thus corresponds to computing the position of the imaged points $\mathbf{e}_\mathsf{M}[c]$, $\mathbf{e}_\mathsf{M}[c+1]$, $\mathbf{e}_\mathsf{H}[c]$, and $\mathbf{e}_\mathsf{H}[c+1]$. It will be shown shortly that the position of these four imaged points, along with the imaged lines they support, provides all the information needed to compute the orientation of the plane of motion with respect to the camera.

Figure 3.12 presents a schematic of an imaged head motion plane and the four imaged points that lie into it for a gait half-cycle c. The imaged head motion plane is shown as a green trapezoid, which is defined by the imaged points $\mathbf{e}_\mathsf{M}[c]$, $\mathbf{e}_\mathsf{M}[c+1]$, $\mathbf{e}_\mathsf{H}[c]$, and $\mathbf{e}_\mathsf{H}[c+1]$. The imaged feet middle points $\mathbf{e}_\mathsf{M}[c]$ and $\mathbf{e}_\mathsf{M}[c+1]$ are computed using the ground vanishing line $\mathbf{l}_\infty$, a cross ratio that is deduced from the walk model, and the imaged feet extremities $\mathbf{e}_m[c]$, $\mathbf{e}_m[c+1]$, $\mathbf{e}_{\bar{m}}[c]$, and $\mathbf{e}_{\bar{m}}[c+1]$, where m and $\bar{m}$ represent respectively the label of the moving foot and the still foot for gait half-cycle c. The head extremities $\mathbf{e}_\mathsf{H}[c]$ and $\mathbf{e}_\mathsf{H}[c+1]$ are then computed using the obtained feet middle points, the interpolated positions of the head mass centre at time t_c and t_{c+1}, and the interpolated head bounding boxes. Figure 3.12 will be referenced in the following sections, which present the details of the steps for computing the four imaged points of the imaged head motion plane.

3.5.1.1 Foot Extremity Computation

In order to compute the position of the imaged feet middle points $\mathbf{e}_{\mathsf{M}}[c]$ and $\mathbf{e}_{\mathsf{M}}[c+1]$, the positions of the imaged foot extremities $\mathbf{e}_{\mathsf{1}}[c]$, $\mathbf{e}_{\mathsf{1}}[c+1]$, $\mathbf{e}_{\mathsf{2}}[c]$, and $\mathbf{e}_{\mathsf{2}}[c+1]$ must first be determined. One could simply determine the imaged foot extremities by interpolating them at non-integer key times t_c and t_{c+1} from the foot extremity trajectories $\mathbf{p}_{\mathsf{1B}}[n]$ and $\mathbf{p}_{\mathsf{2B}}[n]$ obtained with Equation 3.5. However, in practice, these interpolated foot extremity positions would not satisfy the walk model constraint $\mathbf{e}_{\bar{m}}[c] = \mathbf{e}_{\bar{m}}[c+1]$, that is, the still foot extremities would not be exactly the same at times t_c and t_{c+1}. This is because the still foot in a gait half-cycle actually moves a little bit between time t_c and t_{c+1}. The imaged foot extremities thus have to be determined so that the walk model constraint $\mathbf{e}_{\bar{m}}[c] = \mathbf{e}_{\bar{m}}[c+1]$ is satisfied in all gait half-cycles, while ensuring that the computed foot extremities are reliable.

In order to compute each foot extremity in a gait half-cycle c, the label m and $\bar{m}$ of the moving and the still foot must first be determined:

$$(m, \bar{m}) = \begin{cases} (1,2) & \text{if } \|\mathbf{p}_{\mathsf{1B}}[\lceil t_c \rceil] - \mathbf{p}_{\mathsf{1B}}[\lfloor t_{c+1} \rfloor]\| > \|\mathbf{p}_{\mathsf{2B}}[\lceil t_c \rceil] - \mathbf{p}_{\mathsf{2B}}[\lfloor t_{c+1} \rfloor]\| \\ (2,1) & \text{otherwise,} \end{cases} \tag{3.11}$$

The moving foot is thus simply identified as the foot for which the distance between the foot extremity positions at frames $\lceil t_c \rceil$ and $\lfloor t_{c+1} \rfloor$ is the greatest. One must note that whenever the variable m and $\bar{m}$ are used, they are referring to the label of the moving and the still foot in the gait half-cycle c.

The extremity position of the still foot at time t_c and t_{c+1} is computed as the average position of the foot extremity positions in the gait half-cycle c:

$$\mathbf{e}_{\bar{m}}[\kappa] = \frac{1}{N_c} \sum_{n=\lceil t_c \rceil}^{\lfloor t_{c+1} \rfloor} \mathbf{p}_{\bar{m}\mathsf{B}}[n], \quad \text{for } \kappa \in \{c, c+1\}, \tag{3.12}$$

where $N_c = \lfloor t_{c+1} \rfloor - \lceil t_c \rceil + 1$ (the number of frames in gait half-cycle c), and $\mathbf{p}_{\bar{m}\mathsf{B}}[n]$ is the extremity position of the foot with the label represented by $\bar{m}$ (the still foot in gait half-cycle c) at frame n. The variable κ is used here to stress that the extremity position is defined as a function of c, the index of the considered gait half-cycle. Moreover, there are only two values of κ that can be used with this function for a given gait half-cycle c, that is, $\kappa = c$, and $\kappa = c+1$. One can see that the constraint $\mathbf{e}_{\bar{m}}[c] = \mathbf{e}_{\bar{m}}[c+1]$ is imposed here.

Similarly, the extremity position of the moving foot at time t_c and t_{c+1} is computed

as follows:

$$\mathbf{e}_m[\kappa] = \frac{1}{\beta - \alpha + 1} \sum_{n=\alpha}^{\beta} \mathbf{p}_{m\mathsf{B}}[n], \quad \text{for } \kappa \in \{c, c+1\}, \tag{3.13}$$

where $\mathbf{p}_{m\mathsf{B}}[n]$ is the extremity position of the foot with the label represented by m (the moving foot in gait half-cycle c), and α, β are defined as

$$\alpha = \begin{cases} \lceil t_c \rceil - \min(\lfloor N_c/2 \rfloor, \lceil t_c \rceil - n_{\mathrm{S},i}) & \text{if } c = 1,\ \kappa = c \\ \lceil t_{c+1} \rceil & \text{if } c = 1,\ \kappa = c+1 \\ \lceil t_{c-1} \rceil & \text{if } c = C,\ \kappa = c \\ \lceil t_{c+1} \rceil & \text{if } c = C,\ \kappa = c+1 \\ \lceil t_{c-1} \rceil & \text{if } 1 < c < C-1,\ \kappa = c \\ \lceil t_{c+1} \rceil & \text{if } 1 < c < C-1,\ \kappa = c+1 \end{cases} \tag{3.14}$$

and

$$\beta = \begin{cases} \lfloor t_c \rfloor & \text{if } c = 1,\ \kappa = c \\ \lfloor t_{c+2} \rfloor & \text{if } c = 1,\ \kappa = c+1 \\ \lfloor t_c \rfloor & \text{if } c = C,\ \kappa = c \\ \lfloor t_{c+1} \rfloor + \min(\lfloor N_c/2 \rfloor, n_{\mathrm{E},i} - \lfloor t_{c+1} \rfloor) & \text{if } c = C,\ \kappa = c+1 \\ \lfloor t_c \rfloor & \text{if } 1 < c < C-1,\ \kappa = c \\ \lfloor t_{c+2} \rfloor & \text{if } 1 < c < C-1,\ \kappa = c+1. \end{cases} \tag{3.15}$$

The computed extremity position is the average of the moving foot extremity positions from frame α to frame β. Since the foot is moving in the gait half-cycle c, the foot extremity positions from frame $\lceil t_c \rceil$ to frame $\lfloor t_{c+1} \rfloor$ cannot be used to compute the moving foot extremities at times t_c and t_{c+1}. Therefore, the foot extremities at times t_c and t_{c+1} are computed using the foot extremity positions in the previous and the next gait half-cycle, respectively. Indeed, the foot that is moving in gait half-cycle c is not moving in the previous gait half-cycle $c-1$ and the next gait half-cycle $c+1$. The frame indexes α and β are thus defined according to the different cases. For instance, when $\kappa = c$, the average of the foot extremity positions of the previous gait half-cycle $c-1$ is computed, whereas the average of the foot extremity positions of the next gait half-cycle $c+1$ is computed when $\kappa = c+1$. There are two special cases, that is, when $c = 1$, $\kappa = c$, and when $c = C$, $\kappa = c+1$. The frame range used in these cases depends on how many frames are available before the first gait half-cycle or after the last gait half-cycle. Since these frames are not part of a complete gait half-cycle, caution is taken by considering only at most $\lfloor N_c/2 \rfloor$ of them. By choosing this number of frames, one assumes that the duration of the incomplete gait half-cycle is at least half the duration of gait half-cycle $c = 1$ or $c = C$. The exact number of considered frames depends on the first frame $n_{\mathrm{S},i}$ or the last frame $n_{\mathrm{E},i}$ of the continuous tracking interval i.

Using Equations 3.12 and 3.13 thus permits to obtain the foot extremity positions $\mathbf{e}_1[c]$, $\mathbf{e}_1[c+1]$, $\mathbf{e}_2[c]$, and $\mathbf{e}_2[c+1]$ for a given gait half-cycle c by considering which foot is moving during the gait half-cycle. These equations will give consistent results across the gait half-cycles. For instance, if the foot 1 is moving and foot 2 is still in gait half-cycle c, then the foot 1 was still and the foot 2 was moving in gait half-cycles $c-1$. This means that:

- For gait half-cycle $c-1$, the foot extremity positions $\mathbf{e}_1[c-1]$ and $\mathbf{e}_1[c]$ are computed with Equation 3.12, and foot extremities $\mathbf{e}_2[c-1]$ and $\mathbf{e}_2[c]$ are computed with Equation 3.13.
- For gait half-cycle c, the foot extremity positions $\mathbf{e}_1[c]$ and $\mathbf{e}_1[c+1]$ are computed with Equation 3.13, and foot extremities $\mathbf{e}_2[c]$ and $\mathbf{e}_2[c+1]$ are computed with Equation 3.12;

One can see that the foot extremity positions $\mathbf{e}_1[c]$ computed for gait cycles $c-1$ and c are the same, since the same foot extremity positions from frame $\lceil t_{c-1} \rceil$ to frame $\lfloor t_c \rfloor$ are used to compute the average extremity position. Also, the foot extremity positions $\mathbf{e}_2[c]$ computed for gait cycle $c-1$ and c are the same, since the same foot extremity positions from frame $\lceil t_c \rceil$ to frame $\lfloor t_{c+1} \rfloor$ are used to compute the average extremity position.

Figure 3.13 shows some examples of computed foot extremities. In Figure 3.13(a), the computed foot extremities are shown for a given key time. The foot extremities for each key time of a walk are shown in 3.13(b). One can see that the computed extremities represent well the ground position of the feet at each key time of the walk.

3.5.1.2 Feet Middle Point Computation

The imaged feet middle point at time t_c can be computed once the foot extremities positions have been interpolated. One should recall that the feet middle point get its name from the fact that it is located on the middle of the line segment joining the foot extremity positions (Figure 3.2(b)). However, the feet middle point is not necessarily imaged as the middle point of the line segment passing through the imaged foot extremities because of the perspective projection. The imaged feet middle point must then be computed by using projective geometry techniques.

It is possible from the walk model to compute a *projective invariant*, that is, a measurement that does not change under perspective projection. This means that the

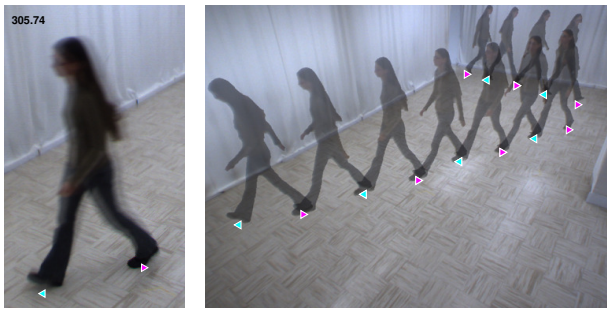

(a) (b)

Figure 3.13 – Example of foot extremities computation. In (a), the computed foot extremities for key time 305.74 are shown as a cyan and magenta triangles over a silhouette interpolated from frames 305 and 306. In (b), the computed foot extremities are shown for each key time of a walk.

measurement is the same in both the scene and the images obtained from a camera. This projective invariant is named the *cross-ratio*, which is a ratio of ratio of lengths usually computed from the position of four collinear points [98]. One should note that the points dimensionality (1-D, 2-D or 3-D) is irrelevant when computing the cross-ratio since only the relative distance between the points is considered.

Given four points $\mathbf{x}_1$, $\mathbf{x}_2$, $\mathbf{x}_3$, $\mathbf{x}_4$, the cross-ratio R is computed as

$$R = \frac{\Delta_{13}/\Delta_{23}}{\Delta_{14}/\Delta_{24}} = \frac{\Delta_{13}\Delta_{24}}{\Delta_{14}\Delta_{23}}, \tag{3.16}$$

where $\Delta_{ab} = \|\mathbf{x}_a - \mathbf{x}_b\|$. In the case where the points $\mathbf{x}_1$, $\mathbf{x}_2$, $\mathbf{x}_3$, and $\mathbf{x}_4$ are imaged under a projective transformation as the points $\mathbf{x}'_1$, $\mathbf{x}'_2$, $\mathbf{x}'_3$, and $\mathbf{x}'_4$ respectively, the cross-ratio R' computed on the imaged points will be the same, that is, $R' = R$. One should note that the cross-ratio permits one of the points to be at infinity. For instance, if the point $\mathbf{x}_4$ was located at infinity, it can be shown that the cross-ratio would simply be defined as $R = \Delta_{13}/\Delta_{23}$.

Figure 3.14(a) presents an arrangement of the four collinear points $\mathbf{x}_1$, $\mathbf{x}_2$, $\mathbf{x}_3$, and $\mathbf{x}_4$. This arrangement correspond to the one in the walk model, that is, the points $\mathbf{x}_1$ and $\mathbf{x}_3$ represents the foot extremities positions, and the point $\mathbf{x}_2$ represents the feet middle point. It is possible to compute the cross-ratio of this point arrangement by assuming the existence of a point $\mathbf{x}_4$ located at infinity on the ground plane and collinear with the three other points. The cross-ratio value of the points arrangement is

$$R = \frac{\Delta_{13}\Delta_{24}}{\Delta_{14}\Delta_{23}} = \frac{\Delta_{13}\infty}{\infty\Delta_{23}} = \frac{\Delta_{13}}{\Delta_{13}/2} = 2 \tag{3.17}$$

since $\Delta_{23} = \Delta_{13}/2$ according to the walk model. Knowing the cross-ratio of this ar-

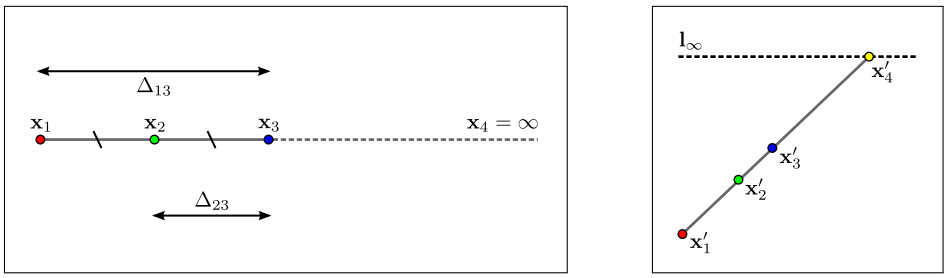

(a) Collinear points arrangement (b) Perspective view

Figure 3.14 – Cross-ratio of four collinear points, with one of the point being located at infinity. In (a), the points $\mathbf{x}_1$, $\mathbf{x}_2$, $\mathbf{x}_3$ are arranged as in the walk model. The points $\mathbf{x}_1$ and $\mathbf{x}_3$ represent the foot extremities positions, and the point $\mathbf{x}_2$ represents the feet middle points. The point $\mathbf{x}_4$ is at infinity and is considered collinear with the three other points. In (b), a possible perspective view of the points shown in (a). The point $\mathbf{x}_4$ has a finite position in this view ($\mathbf{x}'_4$) and can be computed as the crossing point between the vanishing line $\mathbf{l}_\infty$ of the ground plane and the line joining the imaged points $\mathbf{x}'_1$ and $\mathbf{x}'_3$.

rangement of points in the walk model is useful since the cross-ratio will be the same for the imaged points. Moreover, it is possible to determine the position of a point in the arrangement given the position of the three other points and the cross-ratio of the points arrangement.

Figure 3.14(b) shows a possible perspective view of the points arrangement presented in Figure 3.14(a). It is supposed here that the position of the imaged point $\mathbf{x}'_2$ cannot be computed from the image, and thus must be computed using the known cross-ratio and the position of the imaged points $\mathbf{x}'_1$, $\mathbf{x}'_3$, and $\mathbf{x}'_4$. The position of the imaged points $\mathbf{x}'_1$ and $\mathbf{x}'_3$ are known since they represent the positions of the foot extremities. The point $\mathbf{x}_4$, which is located at infinity on the ground plane, is imaged as a finite point $\mathbf{x}'_4$ in this perspective view. Under a projective transformation, all points located at infinity are indeed imaged as finite points, which are called *vanishing points*. Moreover, the points located at infinity on a plane in the scene are imaged on a line, which is called the *vanishing line* (or the horizon line) of the plane [98]. Also, a projective transformation preserves the points collinearity, which means that collinear points in the scene are imaged as collinear points in the image. Therefore, the location of the imaged point $\mathbf{x}'_4$ can be computed as the intersection point of the ground vanishing line and the line joining the points $\mathbf{x}'_1$ and $\mathbf{x}'_3$.

Since the relative order of collinear points are in practice preserved under a projective transformation, the imaged point $\mathbf{x}'_2$ will be located somewhere between the imaged points $\mathbf{x}'_1$ and $\mathbf{x}'_3$. Using the known cross ratio $R' = R = 2$ of this points arrangement,

the distance Δ'_{12} between the point $\mathbf{x}'_1$ and $\mathbf{x}'_2$ can be computed as follow:

$$\begin{aligned} R' = 2 &= \frac{\Delta'_{13}\Delta'_{24}}{\Delta'_{14}\Delta'_{23}} \\ 2 &= \frac{\Delta'_{13}(\Delta'_{14} - \Delta'_{12})}{\Delta'_{14}(\Delta'_{13} - \Delta'_{12})} \\ 2\Delta'_{13}\Delta'_{14} - 2\Delta'_{14}\Delta'_{12} &= \Delta'_{13}\Delta'_{14} - \Delta'_{13}\Delta_{12} \\ -2\Delta'_{14}\Delta'_{12} + \Delta'_{13}\Delta_{12} &= -2\Delta'_{13}\Delta'_{14} + \Delta'_{13}\Delta'_{14} \\ \Delta'_{12}(-2\Delta'_{14} + \Delta'_{13}) &= -\Delta'_{13}\Delta'_{14} \\ \Delta'_{12} &= \frac{\Delta'_{13}\Delta'_{14}}{2\Delta'_{14} - \Delta'_{13}}. \end{aligned} \tag{3.18}$$

This algebraical development is based on the substitution of Δ'_{24} and Δ'_{23} by $\Delta'_{14} - \Delta'_{12}$ and $\Delta'_{13} - \Delta'_{12}$ respectively. Once obtained, the distance Δ'_{12} can be used to compute the position of the point $\mathbf{x}'_2$ as

$$\mathbf{x}'_2 = \mathbf{x}'_1 + \Delta'_{12}\frac{\mathbf{x}'_4 - \mathbf{x}'_1}{\|\mathbf{x}'_4 - \mathbf{x}'_1\|}. \tag{3.19}$$

The point $\mathbf{x}'_2$ is thus simply defined as the point at a distance of Δ'_{12} from point $\mathbf{x}'_1$ in the direction of point $\mathbf{x}'_4$. As one may see in Figure 3.14(b), the point $\mathbf{x}'_2$ is not the middle point of points $\mathbf{x}'_1$ and $\mathbf{x}'_3$. Because of the perspective effect, the point $\mathbf{x}'_2$ is closer to the point $\mathbf{x}'_3$ than the point $\mathbf{x}'_1$.

In order to compute the position of the feet middle point $\mathbf{e}_{\mathsf{M}}[c]$ using Equation 3.19, one must first determine the image of the point at infinity that is collinear with the foot extremities $\mathbf{e}_m[c]$ and $\mathbf{e}_{\bar{m}}[c]$ for a half-cycle c. This point is denoted $\mathbf{w}[c]$ in the schematic presented in Figure 3.12 and is defined as the intersection point between the ground vanishing line $\mathbf{l}_\infty$ and the line joining the foot extremities $\mathbf{e}_m[c]$ and $\mathbf{e}_{\bar{m}}[c]$:

$$\widetilde{\mathbf{w}}[c] = \mathbf{l}_\infty \times \left(\widetilde{\mathbf{e}}_1[c] \times \widetilde{\mathbf{e}}_2[c]\right) \tag{3.20}$$

Next, one must determine which feet extremity acts as the point $\mathbf{x}'_1$ and $\mathbf{x}'_3$ in the collinear points arrangement. This is necessary because the order of the points is important when using cross-ratios. Since the point $\mathbf{x}'_1$ in the arrangement is the furthermost from the point $\mathbf{x}'_4$, one can simply determine the labels z and $\bar{z}$ of the foot extremity corresponding respectively to points $\mathbf{x}'_1$ and $\mathbf{x}'_3$ as

$$(z, \bar{z}) = \begin{cases} (1, 2) & \text{if } \|\mathbf{w}[c] - \mathbf{e}_1[c]\| > \|\mathbf{w}[c] - \mathbf{e}_2[c]\| \\ (2, 1) & \text{otherwise.} \end{cases} \tag{3.21}$$

The foot extremities positions acting as $\mathbf{x}'_1$ and $\mathbf{x}'_3$ are thus $\mathbf{e}_z[c]$ and $\mathbf{e}_{\bar{z}}[c]$ respectively. It is now possible to compute the distance of the imaged feet middle point with respect

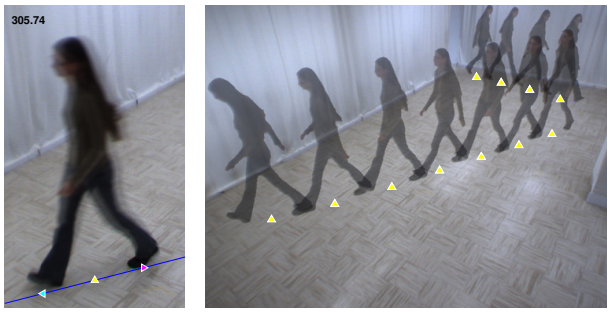

(a) (b)

Figure 3.15 – Example of feet middle points computation. In (a), the computed feet middle point for key time 305.74 is shown as an upward yellow triangle, along with the foot extremities (cyan and magenta triangles). In (b), the computed feet middle points are shown for each key time of a walk.

to the foot extremity position $\mathbf{e}_z[c]$ using Equation 3.18:

$$\Delta'_{z\mathsf{M}} = \|\mathbf{e}_{\mathsf{M}}[c] - \mathbf{e}_z[c]\| = \frac{\|\mathbf{e}_{\bar{z}}[c] - \mathbf{e}_z[c]\| \ \|\mathbf{w}[c] - \mathbf{e}_z[c]\|}{2\,\|\mathbf{w}[c] - \mathbf{e}_z[c]\| - \|\mathbf{e}_{\bar{z}}[c] - \mathbf{e}_z[c]\|}. \tag{3.22}$$

Finally, the position of the feet middle point $\mathbf{e}_{\mathsf{M}}[c]$ at time t_c can be computed using Equation 3.19:

$$\mathbf{e}_{\mathsf{M}}[c] = \mathbf{e}_z[c] + \Delta'_{z\mathsf{M}} \frac{\mathbf{w}[c] - \mathbf{e}_z[c]}{\|\mathbf{w}[c] - \mathbf{e}_z[c]\|}, \tag{3.23}$$

and by substituting Equation 3.22 in Equation 3.23, one obtains

$$\mathbf{e}_{\mathsf{M}}[c] = \mathbf{e}_z[c] + \big(\mathbf{w}[c] - \mathbf{e}_z[c]\big) \frac{\|\mathbf{e}_{\bar{z}}[c] - \mathbf{e}_z[c]\|}{2\,\|\mathbf{w}[c] - \mathbf{e}_z[c]\| - \|\mathbf{e}_{\bar{z}}[c] - \mathbf{e}_z[c]\|}. \tag{3.24}$$

An example of a feet middle point computed using Equation 3.24 is shown in Figure 3.15(a). Since the viewpoint for the frame in this example is close to a fronto-parallel view, the obtained feet middle point seems to be located close to the middle point of the two imaged foot extremities. One should note that this would not be the case for viewpoints that are not fronto-parallel. The feet middle points computed at each key time of a walk are shown in Figure 3.15(b).

3.5.1.3 Head Extremity Computation

The computation of the head extremity at a key time t_c can be performed once the feet middle point has been obtained. From the walk model, on can see that the feet middle point corresponds to the orthogonal projection of the head extremity on the ground plane. Therefore, the feet middle point, the head mass centre and the head

extremity are collinear and are joined by a vertical line that is perpendicular to the ground plane. The image of this line, which is referred here to as the vertical orientation line, can already be computed since the imaged feet middle point and the imaged head mass centre are already known at this stage. Since the position of the imaged head extremity lie on this line, it can be computed as the intersection point between the vertical orientation line and the line passing through the position of the top of the silhouette in the image. The position of the top of the silhouette is defined here as the x component of the head mass centre and the y component of the topmost point on the silhouette. One must notice that in the general case, the position of the top of the silhouette in the image does not correspond to the imaged head extremity since the silhouette does not necessarily appear vertical in the image. The method proposed here provides a more realistic position for the head extremity and does not consider it merely as the top position of the silhouette.

The trajectory of the top of the silhouette $\mathbf{p}_{\mathsf{HT}}[n]$ is first computed from the head mass centre and the head bounding box:

$$\widetilde{\mathbf{p}}_{\mathsf{HT}}[n] = \begin{bmatrix} 1 \\ 0 \\ -p_{\mathsf{H},x}[n] \end{bmatrix} \times \left(\widetilde{\mathbf{b}}_{\mathsf{H,TL}}[n] \times \widetilde{\mathbf{b}}_{\mathsf{H,TR}}[n] \right), \tag{3.25}$$

where $\widetilde{\mathbf{b}}_{\mathsf{H,TL}}[n]$ and $\widetilde{\mathbf{b}}_{\mathsf{H,TR}}[n]$ are the top-left and top-right corner of the head bounding box (in homogeneous coordinates), and $p_{\mathsf{H},x}[n]$ is the abscissa of the position of the head mass centre. This equation is very similar to Equation 3.5, which is used to compute the foot extremity position. The top of the silhouette $\mathbf{p}_{\mathsf{HT}}[n]$ obtained with Equation 3.25 represents the intersection point between the vertical line passing through the head mass centre and the line joining the top corners of the head bounding box. Figure 3.16(a) shows an example of position of the top of a silhouette obtained with Equation 3.25 for two consecutive frames.

Next, the position of the head mass centre and the position of the top of the silhouette is determined at time t_c. Since the head does not move a lot between two frames, a linear interpolation is used to compute these positions. The head mass centre at time t_c is thus defined as

$$\mathbf{p}_{\mathsf{H}}(t_c) = \mathbf{p}_{\mathsf{H}}\left[\lfloor t_c \rfloor\right] + (t_c - \lfloor t_c \rfloor)\left(\mathbf{p}_{\mathsf{H}}\left[\lceil t_c \rceil\right] - \mathbf{p}_{\mathsf{H}}\left[\lfloor t_c \rfloor\right]\right), \tag{3.26}$$

and the position of the top of the silhouette is defined as

$$\mathbf{p}_{\mathsf{HT}}(t_c) = \mathbf{p}_{\mathsf{HT}}\left[\lfloor t_c \rfloor\right] + (t_c - \lfloor t_c \rfloor)\left(\mathbf{p}_{\mathsf{HT}}\left[\lceil t_c \rceil\right] - \mathbf{p}_{\mathsf{HT}}\left[\lfloor t_c \rfloor\right]\right). \tag{3.27}$$

An example of the interpolated mass centre and the position of the top of the silhouette is presented in Figure 3.16(b).

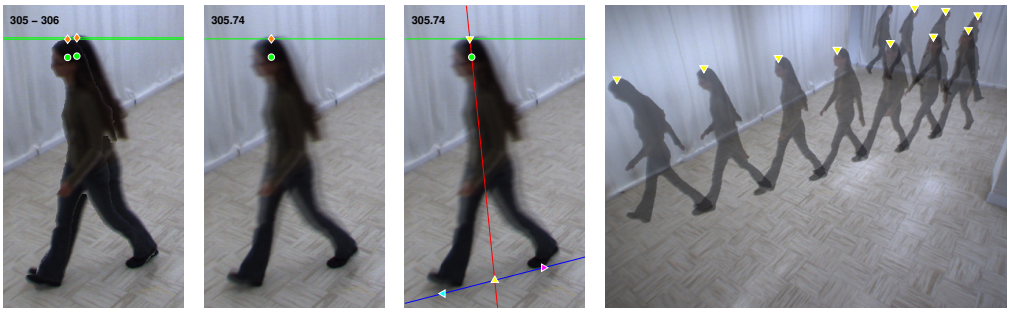

(a) (b) (c) (d)

Figure 3.16 – Computation of the imaged head extremity. In (a), the positions of the head mass centre and the top of the silhouette for frames 305 and 306 are shown as green circles and orange diamond respectively. In (b), the interpolated positions of the head mass centre and the top of the silhouette are shown over an interpolated silhouette at key time 305.74. In (c), the computed head extremity is shown as an downward yellow triangle. The green line represents the y component of the top of the silhouette. In (d), the computed head extremities are shown for each key time of a walk (one of the extremities is too close to the image border to be shown here).

Finally, the head extremity position $\mathbf{e}_{\mathsf{H}}[c]$ at time t_c is computed as the intersection point of the horizontal line passing through $\mathbf{p}_{\mathsf{HT}}(t_c)$ and the line joining the feet middle point $\mathbf{e}_{\mathsf{M}}[c]$ and the head mass centre $\mathbf{p}_{\mathsf{H}}(t_c)$:

$$\widetilde{\mathbf{e}}_{\mathsf{H}}[c] = \begin{bmatrix} 0 \\ 1 \\ -p_{\mathsf{HT},y}(t_c) \end{bmatrix} \times \big(\widetilde{\mathbf{e}}_{\mathsf{M}}[c] \times \widetilde{\mathbf{p}}_{\mathsf{H}}(t_c)\big), \tag{3.28}$$

where $\widetilde{\mathbf{e}}_{\mathsf{H}}[c]$ is the homogeneous coordinates representation of $\mathbf{e}_{\mathsf{H}}[c]$, and $p_{\mathsf{HT},y}(t_c)$ is the y component of the top of the silhouette at time t_c. An example of head extremity position is shown in Figure 3.16(c). One may see that the line joining the feet middle point, the head mass centre, and the head extremity represents quite well the vertical orientation of the person in the image. Figure 3.16(d) shows the head extremities obtained at each key time of a walk.

The imaged head motion planes are defined once the head extremity positions and the feet middle points have been computed for all key times in a continuous tracking interval. The notation i will be omitted here since the continuous tracking interval is implicit. Thus, for each gait half-cycle $c = 1, 2, \ldots, C$, an imaged head motion plane $\Pi_{\mathsf{H}}[c]$ is defined by the set

$$\Pi_{\mathsf{H}}[c] : \big\{\boldsymbol{\pi}_{\mathsf{H,BS}}[c], \boldsymbol{\pi}_{\mathsf{H,BE}}[c], \boldsymbol{\pi}_{\mathsf{H,TS}}[c], \boldsymbol{\pi}_{\mathsf{H,TE}}[c]\big\} \equiv \big\{\mathbf{e}_{\mathsf{M}}[c], \mathbf{e}_{\mathsf{M}}[c+1], \mathbf{e}_{\mathsf{H}}[c], \mathbf{e}_{\mathsf{H}}[c+1]\big\}, \tag{3.29}$$

where $\boldsymbol{\pi}_{\mathsf{H,BS}}[c]$, $\boldsymbol{\pi}_{\mathsf{H,BE}}[c]$, $\boldsymbol{\pi}_{\mathsf{H,TS}}[c]$, $\boldsymbol{\pi}_{\mathsf{H,TE}}[c]$ are new variable names that refer respectively to the bottom-start (BS), bottom-end (BE), top-start (TS), and top-end (TE) points.

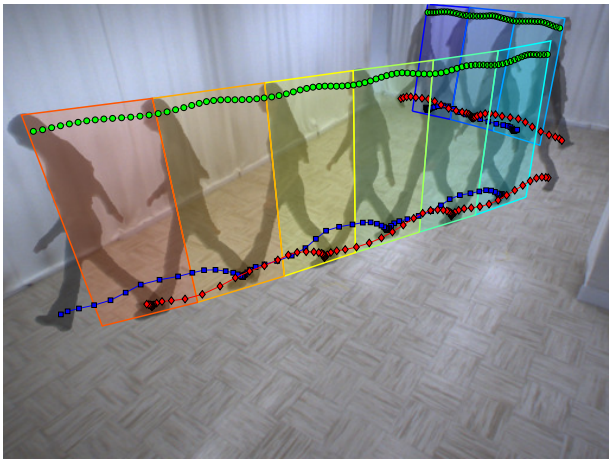

Figure 3.17 – Example of the head motion planes obtained for a walk. The head motion planes are shown for the two continuous tracking intervals obtained from the video sequence of this walk. The planes are outlined as trapezoids of different colours, where the colour shade correspond to the order of occurrence in time (from blue to red). A trapezoid is defined by the head extremities and feet middle points obtained for two consecutive key times.

One should note that as for the head motion planes in the scene, two 'consecutive' imaged planes $\Pi_{\mathsf{H}}[c]$ and $\Pi_{\mathsf{H}}[c+1]$ share two points, that is, the feet middle point $\mathbf{e}_{\mathsf{M}}[c+1]$ and the head extremity $\mathbf{e}_{\mathsf{H}}[c+1]$.

Figure 3.17 presents the head motion planes that were computed for the walk used as an example so far. The trapezoidal-shaped planes are shown as four line segments, that is, two line segments joining the head extremities with the feet middle points computed at the same key time, and two line segments joining consecutive head extremities and feet middle points. The colour used to outline a plane represents its order of occurrence in time such that the blue and the red colours represents the beginning and the ending of the walk respectively. One must note that only one of the line segments joining a head extremity point to a feet middle point is visible for a given plane (excepted for the last plane) since consecutive planes have these points in common. The planes in a continuous tracking interval look like a 'folding screen' that one could 'unfold' in order to remove all changes in the walk direction and to observe it from a fronto-parallel view. This is actually what will be performed by the plane rectification process, which will be described latter in Section 3.7. The plane rectification process can be performed once the head and the foot motion planes are computed for a walk.

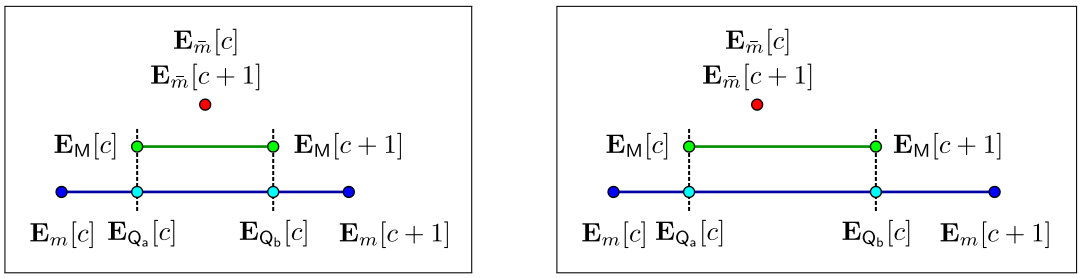

Figure 3.18 – Top view of the walk model for a gait half-cycle c. In (a), the step length at key time t_c is equal to the step length t_{c+1}. In (b), the step length t_{c+1} is greater than the step length t_c.

3.5.2 Foot Motion Plane Computation

The motion of a foot during a gait half-cycle is more complex than the head motion, as one may have noticed so far in the figures showing the body-part trajectories. As for the head motion, the directions of motion for the foot are the vertical direction and the direction of walk. Therefore, the foot moves along a line joining the foot extremity position $\mathbf{E}_m[c]$ and $\mathbf{E}_m[c+1]$ during a gait half-cycle. Also, during the same gait half-cycle, the head moves along a line from position $\mathbf{E}_{\mathsf{H}}[c]$ to position $\mathbf{E}_{\mathsf{H}}[c+1]$. The former line is referred here to as the *stride line*, whereas the latter line is referred to as the *head displacement line*. These two lines are parallel in the scene, and one may assume that the motion of the moving foot is performed in the plane where both of these lines lie. This motion plane is thus slightly slanted compared to the head motion plane, and it is assumed here that the departure of the foot motion from this plane is negligible for walks with smooth changes in the walk direction. There are already four 3-D points that are known to lie on the foot motion plane, that is, the points $\mathbf{E}_{\mathsf{H}}[c]$, $\mathbf{E}_{\mathsf{H}}[c+1]$, $\mathbf{E}_m[c]$, and $\mathbf{E}_m[c+1]$. One pair of parallel lines can be obtained from these points, that is, the head displacement line and the stride line. However, one needs to observe two pairs of lines in the image to define an imaged plane, with the lines in each pair representing parallel lines in the plane (the reason for this will be discussed in Section 3.7).

One way of obtaining another pair of parallel lines in the foot plane is to consider two new points that lie on the stride line. These two new points are denoted $\mathbf{E}_{\mathsf{Q_a}}[c]$ and $\mathbf{E}_{\mathsf{Q_b}}[c]$, and correspond to the perpendicular projection of the feet middle points on the stride line, as shown in Figures 3.18(a) and 3.18(b). The new points are positioned according to the length of the steps at key times t_c and t_{c+1}. The case where the step length at key time t_c is equal to the step length at t_{c+1} is depicted in Figure 3.18(a). The points $\mathbf{E}_{\mathsf{Q_a}}[c]$ and $\mathbf{E}_{\mathsf{Q_b}}[c]$ are located at a distance of a quarter of the stride length

from the points $\mathbf{E}_m[c]$ and $\mathbf{E}_m[c+1]$ respectively (hence the labels $\mathsf{Q_a}$ and $\mathsf{Q_b}$). In the more general case where the steps length are different at key times t_c and t_{c+1}, the points position on the stride line will depend on the difference between the steps length, as depicted in Figure 3.18(b). One should note that the distance between the points $\mathbf{E}_{\mathsf{Q_a}}[c]$ and $\mathbf{E}_{\mathsf{Q_b}}[c]$ is half the stride length in both cases since this is the distance between the feet middle points $\mathbf{E}_{\mathsf{M}}[c]$ and $\mathbf{E}_{\mathsf{M}}[c+1]$ (see Equation 3.3 and 3.4 in Section 3.3).

Although the points $\mathbf{E}_{\mathsf{Q_a}}[c]$ and $\mathbf{E}_{\mathsf{Q_b}}[c]$ do not directly represent a characteristic of the gait or a body-part position, they will be useful here for two reasons. First, it is possible with these points to define two parallel lines lying in the foot motion plane: one line joining the points $\mathbf{E}_{\mathsf{Q_a}}[c]$ and $\mathbf{E}_{\mathsf{H}}[c]$, and another line joining the points $\mathbf{E}_{\mathsf{Q_b}}[c]$ and $\mathbf{E}_{\mathsf{H}}[c+1]$. The image of the foot motion plane can thus be defined using the image of this pair of lines along with the image of the head displacement line and the image of the stride line. Secondly, the points $\mathbf{E}_{\mathsf{Q_a}}[c]$ and $\mathbf{E}_{\mathsf{Q_b}}[c]$, along with the head extremities $\mathbf{E}_{\mathsf{H}}[c]$ and $\mathbf{E}_{\mathsf{H}}[c+1]$, help resolve the issue of determining the relative position of the head and the feet trajectories once they have been independently view-rectified. This issue will be discussed in more details in Section 3.7.

Figure 3.19 presents a schematic of the computation of the imaged foot motion plane for a gait half-cycle c occurring in time interval $[t_c, t_{c+1}]$. As for the head motion plane, computing the imaged foot motion plane corresponds to computing the position of the imaged points $\mathbf{e}_{\mathsf{Q_a}}[c]$, $\mathbf{e}_{\mathsf{Q_b}}[c]$, $\mathbf{e}_{\mathsf{H}}[c]$, and $\mathbf{e}_{\mathsf{H}}[c+1]$. Here, only the points $\mathbf{e}_{\mathsf{Q_a}}[c]$ and $\mathbf{e}_{\mathsf{Q_b}}[c]$ need to be computed, as the points $\mathbf{e}_{\mathsf{H}}[c]$ and $\mathbf{e}_{\mathsf{H}}[c+1]$ have already been computed in Section 3.5.1.3. The imaged point $\mathbf{e}_{\mathsf{Q_a}}[c]$ and $\mathbf{e}_{\mathsf{Q_b}}[c]$ are computed by first determining the vanishing point of the *ground displacement line* $\mathbf{l}_{\mathrm{d}}[c]$, which is the line joining $\mathbf{e}_{\mathsf{M}}[c]$ and $\mathbf{e}_{\mathsf{M}}[c+1]$, using the ground vanishing line $\mathbf{l}_\infty$. The vanishing point $\mathbf{v}[c]$ is common to all lines in the image that are parallel in the scene with the ground displacement line, which includes the stride line $\mathbf{l}_{\mathrm{s}}[c]$. Next, the vanishing point $\mathbf{v}_\perp[c]$, which is common to all lines that are perpendicular to the ground displacement line in the scene, is determined using the calibration matrix $\mathbf{K}$ and the ground vanishing line $\mathbf{l}_\infty$. Using the vanishing point $\mathbf{v}_\perp[c]$, it is possible to define two lines $\mathbf{l}_{\mathsf{Q_a}}[c]$ and $\mathbf{l}_{\mathsf{Q_b}}[c]$ that pass through the feet middle points $\mathbf{e}_{\mathsf{M}}[c]$ and $\mathbf{e}_{\mathsf{M}}[c+1]$ respectively. The intersection point of these two lines with the stride line finally provide the imaged point $\mathbf{e}_{\mathsf{Q_a}}[c]$ and $\mathbf{e}_{\mathsf{Q_b}}[c]$. These steps are detailed in the following sections.

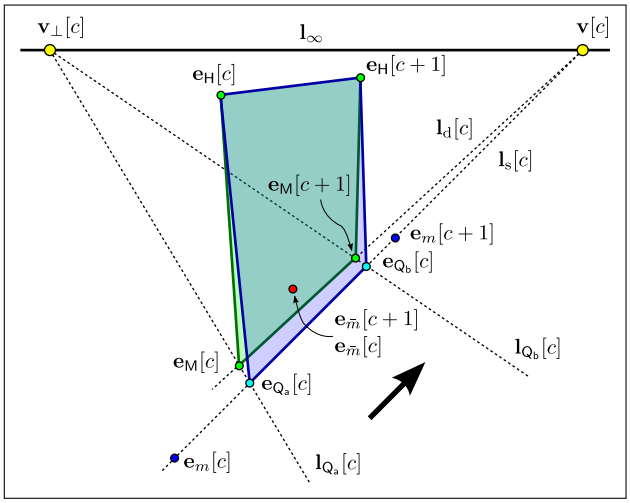

Figure 3.19 – Computation of the foot motion plane for a gait half-cycle. The foot motion plane is shown in blue. The head motion plane for the same gait half-cycle is shown in green. Here, the viewpoint and the direction of walk (black arrow) makes the head motion plane appear behind the foot motion plane.

3.5.2.1 Vanishing Points Computation

The main idea of determining the vanishing points $\mathbf{v}[c]$ and $\mathbf{v}_\perp[c]$ is to perform a projection of the feet middle points on the stride line as depicted in Figure 3.18. The knowledge of the vanishing point $\mathbf{v}_\perp[c]$ permits to determine the image of the dashed lines in Figure 3.18, which represent the direction of the projection of the feet middle points on the stride line. This direction of projection is perpendicular in the walk model, but will not appear perpendicular in the image because of the perspective effect.

The first step consists in computing the ground displacement line $\mathbf{l}_\mathrm{d}[c]$, which is the line joining the imaged points $\mathbf{e}_\mathsf{M}[c]$ and $\mathbf{e}_\mathsf{M}[c+1]$:

$$\mathbf{l}_\mathrm{d}[c] = \widetilde{\mathbf{e}}_\mathsf{M}[c] \times \widetilde{\mathbf{e}}_\mathsf{M}[c+1]. \tag{3.30}$$

This line lies on the ground place in the scene since it joins two foot extremities, which are positions defined on the ground plane. The point at infinity on this line also lies on the ground plane, and is thus imaged as a vanishing point $\mathbf{v}[c]$ on the ground vanishing line. The vanishing point $\mathbf{v}[c]$ can then be defined as the intersection point between the ground vanishing line $\mathbf{l}_\infty$ and the ground displacement line $\mathbf{l}_\mathrm{d}[c]$:

$$\widetilde{\mathbf{v}}[c] = \mathbf{l}_\mathrm{d}[c] \times \mathbf{l}_\infty, \tag{3.31}$$

where $\widetilde{\mathbf{v}}[c]$ is the homogeneous representation of the vanishing point. One should note that this vanishing point is common to all imaged lines that are parallel to the ground

displacement line in the scene, which also includes lines that do not lie on the ground plane.

There is in the scene an infinity of parallel line sets that are perpendicular to the ground displacement line, and thus there is an infinity of vanishing points representing directions perpendicular to ground displacement line. The vanishing point that is of interest here,$\mathbf{v}_{\perp}[c]$, is the vanishing point that represents a direction perpendicular to the ground displacement line and that is located on the ground plane. The vanishing point $\mathbf{v}_{\perp}[c]$ is thus a point on the ground vanishing line $\mathbf{l}_{\infty}$, that is,

$$\mathbf{l}_{\infty} \cdot \widetilde{\mathbf{v}}_{\perp}[c] = \mathbf{l}_{\infty}^{\mathsf{T}} \, \widetilde{\mathbf{v}}_{\perp}[c] = 0, \tag{3.32}$$

where the operator $(\,\cdot\,)$ denotes the inner product. This relation provides one constraint on the unknown vanishing point $\mathbf{v}_{\perp}[c]$, but two constraints are needed. The other constraint needed here is that the vanishing point $\mathbf{v}_{\perp}[c]$ represents a direction perpendicular to the direction represented by the vanishing point $\mathbf{v}[c]$. It is known from projective geometry [98] that two vanishing points representing orthogonal directions must satisfy to the following constraint:

$$\widetilde{\mathbf{v}}^{\mathsf{T}}[c] \; \mathbf{\Omega} \; \widetilde{\mathbf{v}}_{\perp}[c] = 0, \tag{3.33}$$

where $\mathbf{\Omega}$ is a 3×3 matrix called the *Image of the Absolute Conic* (IAC), which is an imaged complex points conic that is related to the camera intrinsic parameters by the following relation:

$$\mathbf{\Omega} = (\mathbf{K}\mathbf{K}^{\mathsf{T}})^{-1}, \tag{3.34}$$

where $\mathbf{K}$ is a 3×3 matrix representing the camera intrinsic parameters. The vanishing point $\mathbf{v}_{\perp}[c]$ can then be determined by solving a linear system of the form $\mathbf{A}\,\mathbf{x} = \mathbf{0}$:

$$\begin{bmatrix} \mathbf{l}_{\infty}^{\mathsf{T}} \\ \widetilde{\mathbf{v}}^{\mathsf{T}}[c] \; \mathbf{\Omega} \end{bmatrix} \begin{bmatrix} x_1 \\ x_2 \\ x_3 \end{bmatrix} = \begin{bmatrix} 0 \\ 0 \end{bmatrix}, \tag{3.35}$$

where $\widetilde{\mathbf{v}}_{\perp}[c] = \mathbf{x}$ and $\mathbf{A}$ is a 2×3 matrix of rank 2. One must note that only two equations are needed here since the vanishing point is defined up to a scale in homogeneous coordinates. An exact solution can be obtained for $\mathbf{x}$ by performing a *Singular Value Decomposition* of the matrix $\mathbf{A}$, that is, $\mathbf{A} = \mathbf{U}\mathbf{D}\mathbf{V}^{\mathsf{T}}$, and then taking as the solution the singular vector (a column vector of matrix $\mathbf{V}$) that corresponds to the smallest singular value in diagonal matrix $\mathbf{D}$.

3.5.2.2 Middle Points Projection

Once the vanishing point $\mathbf{v}_{\perp}[c]$ has been determined, the imaged points $\mathbf{e}_{\mathsf{Q_a}}[c]$ and $\mathbf{e}_{\mathsf{Q_b}}[c]$ can easily be computed as the intersection between the stride line $\mathbf{l}_{\mathsf{s}}[c]$ and the lines

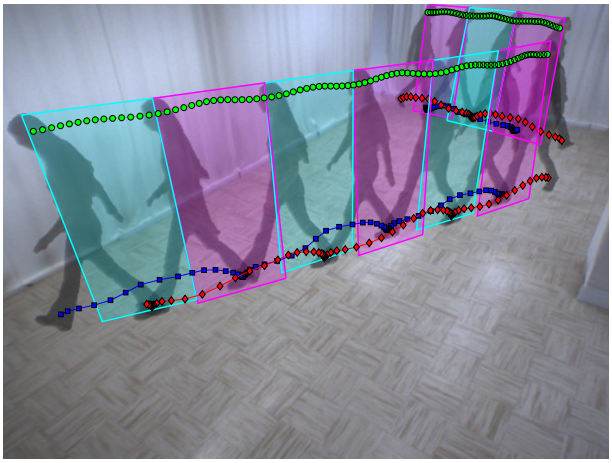

Figure 3.20 – Example of the foot motion planes obtained for a walk. The foot motion planes are shown for the two continuous tracking intervals obtained from the video sequence of this walk. The planes are displayed for foot 1 and 2 as cyan and magenta trapezoids respectively.

$\mathbf{l}_{\mathsf{Q_a}}[c]$ and $\mathbf{l}_{\mathsf{Q_b}}[c]$ respectively. The lines $\mathbf{l}_{\mathsf{Q_a}}[c]$ and $\mathbf{l}_{\mathsf{Q_b}}[c]$ are first determined as the lines joining the vanishing point $\mathbf{v}_{\perp}[c]$ and the foot middle points $\mathbf{e}_{\mathsf{M}}[c]$ and $\mathbf{e}_{\mathsf{M}}[c+1]$:

$$\mathbf{l}_{\mathsf{Q_a}}[c] = \widetilde{\mathbf{v}}_{\perp}[c] \times \widetilde{\mathbf{e}}_{\mathsf{M}}[c], \tag{3.36}$$

$$\mathbf{l}_{\mathsf{Q_b}}[c] = \widetilde{\mathbf{v}}_{\perp}[c] \times \widetilde{\mathbf{e}}_{\mathsf{M}}[c+1]. \tag{3.37}$$

The imaged points $\mathbf{e}_{\mathsf{Q_a}}[c]$ and $\mathbf{e}_{\mathsf{Q_b}}[c]$ are then computed as

$$\widetilde{\mathbf{e}}_{\mathsf{Q_a}}[c] = \mathbf{l}_{\mathsf{s}}[c] \times \mathbf{l}_{\mathsf{Q_a}}[c], \tag{3.38}$$

$$\widetilde{\mathbf{e}}_{\mathsf{Q_b}}[c] = \mathbf{l}_{\mathsf{s}}[c] \times \mathbf{l}_{\mathsf{Q_b}}[c]. \tag{3.39}$$

Finally, a foot motion plane $\Pi_{\mathsf{F}}[c]$ is defined for the gait half-cycle c as the set

$$\Pi_{\mathsf{F}}[c] : \left\{\boldsymbol{\pi}_{\mathsf{F,BS}}[c], \boldsymbol{\pi}_{\mathsf{F,BE}}[c], \boldsymbol{\pi}_{\mathsf{F,TS}}[c], \boldsymbol{\pi}_{\mathsf{F,TE}}[c]\right\} \equiv \left\{\mathbf{e}_{\mathsf{Q_a}}[c], \mathbf{e}_{\mathsf{Q_b}}[c], \mathbf{e}_{\mathsf{H}}[c], \mathbf{e}_{\mathsf{H}}[c+1]\right\}. \tag{3.40}$$

One must remember that only one foot plane is defined for each gait-half-cycle c. If foot 1 is moving in half-cycle c, then its motion plane is $\Pi_{\mathsf{F}}[c]$, and $\Pi_{\mathsf{F}}[c+1]$ is the motion plane of foot 2, $\Pi_{\mathsf{F}}[c+2]$ the motion plane of foot 1, etc.

Figure 3.20 shows the foot motion planes that were obtained for the walk used as an example so far. The trapezoidal-shaped planes are shown as four line segments, that is, two line segments joining the head extremities with the corresponding projected feet middle points, and two line segments joining consecutive head extremities and projected feet middle points. The colour used to outline a plane represents its foot label, that is, cyan for foot 1 and magenta for foot 2. One may see that the bottom part of consecutive foot motion planes are not connected, since consecutive planes correspond to different feet, and each foot moves in a different plane.

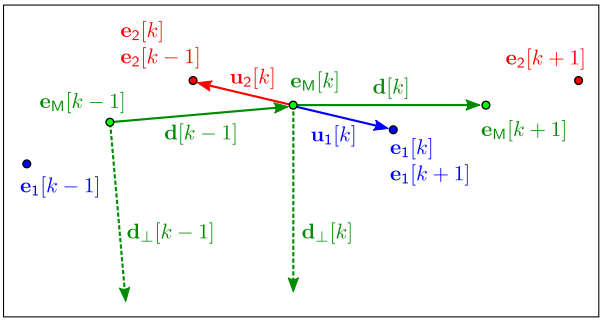

Figure 3.21 – Schematic for foot trajectories labelling. The imaged positions of the foot extremities $\mathbf{e}_1$, $\mathbf{e}_2$, and the feet middle points $\mathbf{e}_M$ are depicted for three key times. $k-1$, k, and $k+1$. The imaged direction of the walk between two key times is represented by a vector $\mathbf{d}$. The vectors $\mathbf{u}_1$ and $\mathbf{u}_2$ represent the position of the corresponding foot extremity with respect to the feet middle point. See text for details.

Once the head and the foot motion planes are computed, the imaged motion planes can be view-rectified in order to make them appear as from a fronto-parallel view. Before entering into the details of the view-rectification process, an algorithm that performs foot trajectories labelling will be presented since it can be performed as soon as the motions planes are computed for a given continuous tracking interval.

3.6 Foot Trajectories Labelling

As mentioned previously, the foot trajectories were arbitrarily labelled as 1 or 2 for each continuous tracking interval by the body part tracking method. However, it is often useful for gait analysis and modelling to know which foot is the right foot and which foot is the left foot. A method is therefore proposed in this thesis to automatically determine the label R (right) or L (left) for the foot trajectories in a given continuous tracking interval. This method can be performed as soon as the head motion planes have been computed for a continuous tracking interval. Foot trajectories labelling is thus performed independently on each continuous tracking interval (the notation i will be dropped here for clarity).

Figure 3.21 presents how one can infer on a key time basis the label of a foot trajectory directly from the *imaged* foot extremities and feet middle points. One must first recall that the feet middle points were also considered as the imaged ground positions of a walker at a given key time k. Thus, it is possible to define the *imaged displacement direction* as the vector $\mathbf{d}[k] = \mathbf{e}_M[k+1] - \mathbf{e}_M[k]$ between key times k and $k+1$. For a key time k, the right foot extremity should then be located on the right side of the

vector $\mathbf{d}[k]$ (with respect to the direction pointed to). For instance, the foot extremity $\mathbf{e}_1[k]$ in Figure 3.21 is clearly on the right side of vector $\mathbf{d}[k]$, whereas the foot extremity $\mathbf{e}_2[k]$ is on the left side. Since the foot extremities $\mathbf{e}_1[k]$ and $\mathbf{e}_2[k]$ are relevant for the time interval $[t_{k-1}, t_k]]$, the foot label can also be inferred by considering the displacement vector $\mathbf{d}[k-1]$. In this case, the foot extremity $\mathbf{e}_1[k]$ is on the right side of vector $\mathbf{d}[k-1]$, and the foot extremity $\mathbf{e}_2[k]$ is on the left side. One may conclude here that the foot trajectories 1 and 2 correspond to the right and left foot trajectories respectively.

The side on which the foot extremities $\mathbf{e}_1[k]$ and $\mathbf{e}_2[k]$ are located with respect to the vector $\mathbf{d}[k]$ (or $\mathbf{d}[k-1]$) can be determined by performing an inner product of two vectors. As shown in Figure 3.21, two vectors can be computed from the foot extremities and the foot middle point at key time k:

$$\mathbf{u}_1[k] = \mathbf{e}_1[k] - \mathbf{e}_\mathsf{M}[k], \tag{3.41}$$

$$\mathbf{u}_2[k] = \mathbf{e}_2[k] - \mathbf{e}_\mathsf{M}[k]. \tag{3.42}$$

Also, the perpendicular vector pointing toward the right side of the displacement vector $\mathbf{d}[k]$ can be computed as the vector

$$\mathbf{d}_\perp[k] = \begin{bmatrix} d_y[k] \\ -d_x[k] \end{bmatrix}, \tag{3.43}$$

where $d_x[k]$ and $d_y[k]$ are the x and y components of vector $\mathbf{d}[k]$. The vector $\mathbf{d}_\perp[k]$ thus corresponds to a 90° clockwise rotation of the vector $\mathbf{d}[k]$. One may see that if a foot extremity $\mathbf{e}_\ell[k]$ ($\ell \in \{1, 2\}$) is located on the right side of the vector $\mathbf{d}[k]$, then the inner product $\mathbf{u}_\ell[k] \cdot \mathbf{d}_\perp[k]$ is greater than 0, whereas the inner product $\mathbf{u}_\ell[k] \cdot \mathbf{d}_\perp[k]$ is less than 0 if it is located on the left side. It is possible to see in Figure 3.21 that $\mathbf{u}_1[k] \cdot \mathbf{d}_\perp[k] > 0$, $\mathbf{u}_1[k] \cdot \mathbf{d}_\perp[k-1] > 0$, $\mathbf{u}_2[k] \cdot \mathbf{d}_\perp[k] < 0$, and $\mathbf{u}_2[k] \cdot \mathbf{d}_\perp[k-1] < 0$. Therefore, a foot trajectory ℓ corresponds to the right foot trajectory if $\mathbf{u}_\ell[k] \cdot \mathbf{d}_\perp[k] > 0$, or corresponds to the left foot trajectory if $\mathbf{u}_\ell[k] \cdot \mathbf{d}_\perp[k] < 0$.

The foot trajectories labelling process would not be robust if it was based solely on one or two observations performed at one key time in a continuous tracking interval. Indeed, bad foot labelling can happen at some key times when the foot extremities are noisy, or when there is a sudden change in the direction of walk. The main idea of the proposed foot trajectories labelling method is to consider the labelling performed for all key times in a continuous tracking interval. A voting process is performed in order to determine which of the foot trajectory 1 or 2 is more likely to be the right foot trajectory. The proposed voting process is detailed in Algorithm 3.2. Two accumulators A_1 and A_2 are used to count the number of times the foot extremities 1 and 2 have been labelled as the right foot. Also, a variable V is used to count the number of consistent labellings that has been performed. A consistent labelling has been performed at key

Algorithm 3.2: Voting process for foot trajectories labelling.

$V = 0$
$A_1 = 0$, $A_2 = 0$
for $k = 1 \dots K$ **do**
  if $k = 1$ **then** $\Rightarrow$ *special case: first key time*
    if $\mathbf{u}_1[1] \cdot \mathbf{d}_\perp[1] > 0$ and $\mathbf{u}_2[1] \cdot \mathbf{d}_\perp[1] < 0$ **then**
      $A_1 = A_1 + 1$, $V = V + 1$
    else if $\mathbf{u}_2[1] \cdot \mathbf{d}_\perp[1] > 0$ and $\mathbf{u}_1[1] \cdot \mathbf{d}_\perp[1] < 0$ **then**
      $A_2 = A_2 + 1$, $V = V + 1$
    end if
  else if $k = K$ **then** $\Rightarrow$ *special case: last key time*
    if $\mathbf{u}_1[K] \cdot \mathbf{d}_\perp[K-1] > 0$ and $\mathbf{u}_2[K] \cdot \mathbf{d}_\perp[K-1] < 0$ **then**
      $A_1 = A_1 + 1$, $V = V + 1$
    else if $\mathbf{u}_2[K] \cdot \mathbf{d}_\perp[K-1] > 0$ and $\mathbf{u}_1[K] \cdot \mathbf{d}_\perp[K-1] < 0$ **then**
      $A_2 = A_2 + 1$, $V = V + 1$
    end if
  else $\Rightarrow$ *general case:* $1 < k < K$
    if $\mathbf{u}_1[k] \cdot \mathbf{d}_\perp[k-1] > 0$ and $\mathbf{u}_2[k] \cdot \mathbf{d}_\perp[k-1] < 0$ **then**
      $A_1 = A_1 + 1$, $V = V + 1$
    else if $\mathbf{u}_2[k] \cdot \mathbf{d}_\perp[k-1] > 0$ and $\mathbf{u}_1[k] \cdot \mathbf{d}_\perp[k-1] < 0$ **then**
      $A_2 = A_2 + 1$, $V = V + 1$
    end if
    if $\mathbf{u}_1[k] \cdot \mathbf{d}_\perp[k] > 0$ and $\mathbf{u}_2[k] \cdot \mathbf{d}_\perp[k] < 0$ **then**
      $A_1 = A_1 + 1$, $V = V + 1$
    else if $\mathbf{u}_2[k] \cdot \mathbf{d}_\perp[k] > 0$ and $\mathbf{u}_1[k] \cdot \mathbf{d}_\perp[k] < 0$ **then**
      $A_2 = A_2 + 1$, $V = V + 1$
    end if
  end if
end for

time k if one of the foot extremities has been labelled as the right foot and the other extremity has been labelled as the left foot. In the general case $1 < k < K$, the location of foot extremities at key time k are determined with respect to displacement vectors $\mathbf{d}[k]$ and $\mathbf{d}[k-1]$. There are two special case, namely the case where $k = 1$, and the case $k = K$, where the location of the foot extremities are determined with only one displacement vector, that is, vector $\mathbf{d}[1]$ if $k = 1$ and vector $\mathbf{d}[K-1]$ if $k = K$.

Once the voting process is performed, the foot trajectories can be labelled as follow:

$$(1, 2) \rightarrow \begin{cases} (\mathsf{R}, \mathsf{L}) & \text{if } \frac{A_1}{V} \geq \frac{A_2}{V}, \\ (\mathsf{L}, \mathsf{R}) & \text{if } \frac{A_1}{V} < \frac{A_2}{V}. \end{cases} \tag{3.44}$$

The ratios A_1/V and A_2/V corresponds to the probability of the foot trajectories $\mathsf{1}$ and $\mathsf{2}$ to be the right foot trajectory respectively. In the case where the both probabilities are equal, an arbitrary labelling is performed, as nothing better can be performed with

the information at hand. The labelling of the foot trajectories will be used to perform gait analysis and modelling in Chapter 4.

3.7 Metric Motion Planes Rectification

The view-rectification approach proposed in this thesis aims at making the imaged body-part trajectories appear as if observed from a fronto-parallel view. In order to achieve this, the imaged motion planes of the body parts were computed for each gait half-cycle in Section 3.5. Each imaged motion plane is defined by four points, which are the images of four points that are known to lie in these planes in the scene. It is known that these four points form a rectangle in the scene, and that the image of these four points form a trapezoid shape in the image if observed from a non fronto-parallel viewpoint. The first step of the proposed view-rectification approach is thus to generate, for each imaged motion plane, a fronto-parallel view of the motion plane. This step is referred here to as the *metric rectification* of the motion planes. The term *metric* means that measurements performed on a rectified plane will correspond to the measurements that one could performs on the original plane in the scene. By default, the rectified motion planes will be defined up to a scale, that is, the units in the rectified plane will be arbitrary. This means that angles and ratio of lengths measured in the rectified plane will correspond to the measurements that could be made in the scene. For instance, the four known points lying in a *rectified plane* will form a rectangle for which the aspect ratio will correspond to the aspect ratio of the corresponding rectangle in the scene. It will be seen later that the scale factor can be fixed in order to define the rectified motion planes in scene units (e.g. in meters).

Figure 3.22 presents an overview of the proposed method for metric rectification of the motion planes. The steps of the proposed method are shown as yellow boxes and are performed on a video sequence basis, that is, after the imaged motion planes are computed for all continuous tracking intervals in a video sequence. A preliminary step is shown as a blue box and consists in performing a metric rectification of the *ground plane*. Although the ground plane rectification is simply performed once for a given camera setup, it is presented here since it helps presenting the view-rectification process of the motion planes. The first step of the proposed method consists in estimating the metric information of each motion plane, that is, the aspect ratio, the width, and the height in either arbitrary units or scene units. The second step of the proposed method consists in computing the rectified planes while ensuring their position with respect to each other reflect what would be observed in the scene from a fronto-parallel viewpoint. The last step consists in computing the transformation (homography) that maps each

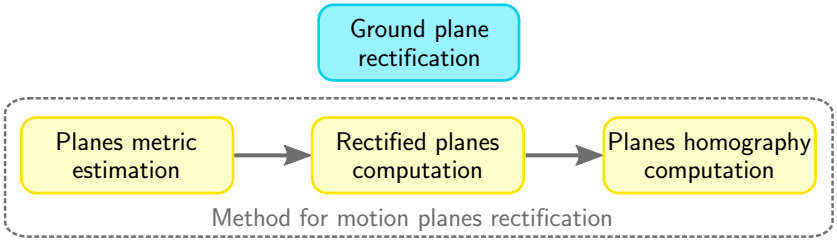

Figure 3.22 – Method for the rectification of the planes of motion for a complete walk.

imaged motion planes to its rectified counterpart.

3.7.1 Ground Plane Rectification

The method proposed for motion planes rectification needs the transform that rectifies the imaged ground plane. The ground plane rectification process only depends on the camera setup, that is, it depends on the camera intrinsic parameters, the orientation of the camera with respect to the ground plane, and optionally, the scale factor that permits to make measurements in scene units. Therefore, the rectification of the ground plane can be performed as soon as the ground vanishing line and the camera intrinsic parameters are known. The rectification of the ground plane is detailed here as it is closely related to the process of motion plane rectification.

It is known in projective geometry [98] that an imaged plane can be metrically rectified if one knows the camera intrinsic parameters and the plane's vanishing line in the image. First, the plane's normal vector $\mathbf{n}$ with respect to the camera's Euclidean coordinate frame must be computed as follow:

$$\mathbf{n} = \frac{\mathbf{K}^\mathsf{T}\mathbf{l}}{\|\mathbf{K}^\mathsf{T}\mathbf{l}\|}, \tag{3.45}$$

where $\mathbf{K}$ is the 3×3 matrix representing the camera intrinsic parameters, and $\mathbf{l}$ is the vanishing line of the considered plane in the image. A plane can be metrically rectified by considering a synthetic pure rotation of the camera that makes the plane parallel to the *camera image plane*. This 3-D synthetic rotation of the camera can be described by an homography $\mathbf{H}$ defined as

$$\mathbf{H} = \mathbf{K}\mathbf{R}\mathbf{K}^{-1}, \tag{3.46}$$

where $\mathbf{H}$ is a 3×3 matrix, and $\mathbf{R}$ is a 3×3 rotation matrix defined as

$$\mathbf{R} = \begin{bmatrix} \mathbf{r}_1 & \mathbf{r}_2 & \mathbf{n} \end{bmatrix}^\mathsf{T}. \tag{3.47}$$

The rotation matrix is designed such that $\mathbf{Rn} = [0\ 0\ 1]^\mathsf{T}$, that is, the normal $\mathbf{n}$ is rotated to lie along the camera optical axis, which can be described by the vector $[0\ 0\ 1]^\mathsf{T}$ in the camera's Euclidean coordinate frame. The vectors $\mathbf{r}_1$, $\mathbf{r}_2$, and $\mathbf{n}$ in the rotation matrix must form a triad of orthonormal vectors. Two arbitrary vectors $\mathbf{r}_1$ and $\mathbf{r}_2$ can be found to satisfy this condition by first performing the *Singular Value Decomposition* $\mathbf{n}^\mathsf{T} = \mathbf{UDV}^\mathsf{T}$ and then by defining $\mathbf{r}_1$ and $\mathbf{r}_2$ as the last two column vectors of matrix $\mathbf{V}$. One must note that the homography $\mathbf{H}$ will metrically rectify the plane up to a similarity transform, that is, up to an isotropic[1] scale factor and a rigid transformation (2-D rotation and translation) in the image plane. If one has a way to determine the scale factor, which is denoted λ, the homography $\mathbf{H}$ can be further refined as

$$\mathbf{H} = \mathbf{\Lambda KRK}^{-1}, \tag{3.48}$$

where the 3×3 matrix $\mathbf{\Lambda}$ is defined as

$$\mathbf{\Lambda} = \begin{bmatrix} \lambda & 0 & 0 \\ 0 & \lambda & 0 \\ 0 & 0 & 1 \end{bmatrix}. \tag{3.49}$$

The plane can be rectified up to a rigid transformation in this case.

The homography that metrically rectifies the ground plane is denoted $\mathbf{H}_\mathrm{G}$ and is obtained using Equation 3.48. One should note that the ground vanishing line $\mathbf{l}_\infty$ is considered to be known here. Also, if the ground scale factor is unknown, then $\lambda = 1$, $\mathbf{\Lambda} = \mathbf{I}_{3\times3}$ (the identity matrix), and thus Equation 3.48 becomes identical to Equation 3.46. The method to compute the ground vanishing line and the ground scale factor will be described later in Sections 3.9.1 and 3.9.2 respectively.

An example of ground plane rectification is shown in Figure 3.23. In Figure 3.23(a), a frame from the camera is shown, and the ground vanishing line is depicted as a blue line. Also, four points were manually specified in the image and represents the image of four corners of a group of 3×3 square tiles on the floor. These points are used here only to show the effect of the rectification on the ground plane, and thus are not used in anyway in the rectification process. One may see that because of perspective projection, the group of tiles does not appear as a square in the image. The computed homography $\mathbf{H}_\mathrm{G}$ was applied on the image and on the four points in order to show the effect of the ground plane rectification, and the result is shown in Figure 3.23(b). The resulting image was cropped in order to show only the pixels that belong to the floor. One may see that the resulting image is a top view of the floor and that the group of tiles now appears as a square. The ground plane is said to be metrically rectified since ratios

[1] A scale factor that is the same for all axes.

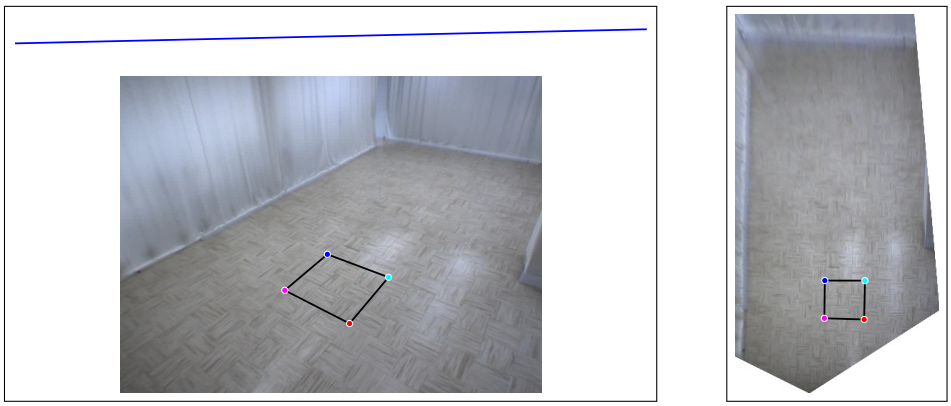

(a) (b)

Figure 3.23 – Example of metric rectification of the ground plane. In (a), the ground vanishing line is shown as a blue line. Given the orientation of the camera with respect to the ground plane and its field of view, the ground vanishing line is located above the image. Four points are shown over the image and represents the four corners of a 3×3 group of square tiles on the ground. In (b), the image from the camera is rectified according to the rectifying homography. The image was cropped to show only the part of the image representing the floor. The four corners points were also rectified according to the same homography. The rectification is metric since the 3×3 group of tiles appears as a square on the rectified ground plane.

of lengths and angles on the rectified ground plane are recovered. The transform that rectifies the ground plane will be used in the proposed method to compute the distance travelled on the ground plane for each gait half-cycle. This distance corresponds to the width of the rectangle formed by the four points that are known to lie in the head and the foot motion planes.

3.7.2 Motion Planes Metric Estimation

As mentioned in the previous section, the motion planes rectification process is closely related to the ground plane rectification process. The difference lies in the fact that the motion planes are all related in some way, and therefore the rectification process must preserve the relations between the motion planes. For instance, a given head motion plane $\Pi_{\mathsf{H}}[c]$ is related to the previous head motion plane $\Pi_{\mathsf{H}}[c-1]$ and the next head motion plane $\Pi_{\mathsf{H}}[c+1]$ since $\boldsymbol{\pi}_{\mathsf{H,BS}}[c] = \boldsymbol{\pi}_{\mathsf{H,BE}}[c-1]$, $\boldsymbol{\pi}_{\mathsf{H,TS}}[c] = \boldsymbol{\pi}_{\mathsf{H,TE}}[c-1]$, $\boldsymbol{\pi}_{\mathsf{H,BE}}[c] = \boldsymbol{\pi}_{\mathsf{H,BS}}[c+1]$, and $\boldsymbol{\pi}_{\mathsf{H,TE}}[c] = \boldsymbol{\pi}_{\mathsf{H,TS}}[c-1]$ (see Equation 3.29 in Section 3.5.1.3). Also, a given foot motion plane $\Pi_{\mathsf{F}}[c]$ is related to the other foot motion planes $\Pi_{\mathsf{F}}[c-1]$ and $\Pi_{\mathsf{F}}[c+1]$ since $\boldsymbol{\pi}_{\mathsf{F,TS}}[c] = \boldsymbol{\pi}_{\mathsf{F,TE}}[c-1]$ and $\boldsymbol{\pi}_{\mathsf{F,TE}}[c] = \boldsymbol{\pi}_{\mathsf{F,TS}}[c+1]$. A foot motion plane $\Pi_{\mathsf{F}}[c]$ is related to the head motion plane $\Pi_{\mathsf{H}}[c]$ as well since $\boldsymbol{\pi}_{\mathsf{F,TS}}[c] = \boldsymbol{\pi}_{\mathsf{H,TS}}[c]$

and $\boldsymbol{\pi}_{\mathsf{F},\mathsf{TE}}[c] = \boldsymbol{\pi}_{\mathsf{H},\mathsf{TE}}[c]$ (see Equation 3.40 in Section 3.5.2.2). These relations can be preserved by combining the metric information of all the motion planes in a walk. The metric information of a motion plane consists in the aspect ratio and either the width or the height of the corresponding rectangle in the scene. The first step of the proposed plane rectification method thus consists in estimating the metric information of each motion plane.

The aspect ratio of a motion plane's rectangle can be estimated after having performed a *local rectification* of the plane by applying a homography transform computed using Equation 3.46. A local rectification means here that the plane is rectified only in order to estimate its rectangle aspect ratio. In order to perform a local rectification, the vanishing line $\mathbf{l}_\ell[c]$ of a given motion plane $\Pi_\ell[c]$, $\ell \in \{\mathsf{H},\mathsf{F}\}$, must be first computed:

$$\mathbf{l}_\ell[c] = \big(\mathbf{l}_{\ell,\mathsf{S}}[c] \times \mathbf{l}_{\ell,\mathsf{E}}[c]\big) \times \big(\mathbf{l}_{\ell,\mathsf{B}}[c] \times \mathbf{l}_{\ell,\mathsf{T}}[c]\big), \tag{3.50}$$

where the lines $\mathbf{l}_{\ell,\mathsf{S}}[c]$, $\mathbf{l}_{\ell,\mathsf{E}}[c]$, $\mathbf{l}_{\ell,\mathsf{B}}[c]$, and $\mathbf{l}_{\ell,\mathsf{T}}[c]$ are computed from the four imaged points of the motion plane. These lines correspond to the "starting" (S) line, the "ending" (E) line, the "bottom" line (B), and the "top" line (T) in the motion plane, and are computed as follow:

$$\mathbf{l}_{\ell,\mathsf{S}}[c] = \widetilde{\boldsymbol{\pi}}_{\ell,\mathsf{BS}}[c] \times \widetilde{\boldsymbol{\pi}}_{\ell,\mathsf{TS}}[c], \tag{3.51}$$
$$\mathbf{l}_{\ell,\mathsf{E}}[c] = \widetilde{\boldsymbol{\pi}}_{\ell,\mathsf{BE}}[c] \times \widetilde{\boldsymbol{\pi}}_{\ell,\mathsf{TE}}[c], \tag{3.52}$$
$$\mathbf{l}_{\ell,\mathsf{B}}[c] = \widetilde{\boldsymbol{\pi}}_{\ell,\mathsf{BS}}[c] \times \widetilde{\boldsymbol{\pi}}_{\ell,\mathsf{BE}}[c], \tag{3.53}$$
$$\mathbf{l}_{\ell,\mathsf{T}}[c] = \widetilde{\boldsymbol{\pi}}_{\ell,\mathsf{TS}}[c] \times \widetilde{\boldsymbol{\pi}}_{\ell,\mathsf{TE}}[c], \tag{3.54}$$

where $\widetilde{\boldsymbol{\pi}}_{\ell,\mathsf{BS}}[c]$, $\widetilde{\boldsymbol{\pi}}_{\ell,\mathsf{BE}}[c]$, $\widetilde{\boldsymbol{\pi}}_{\ell,\mathsf{TS}}[c]$, and $\widetilde{\boldsymbol{\pi}}_{\ell,\mathsf{TE}}[c]$ are the homogeneous coordinates representation of the points. The lines $\mathbf{l}_{\ell,\mathsf{B}}[c]$ and $\mathbf{l}_{\ell,\mathsf{T}}[c]$ are known to be the image of horizontal parallel lines in the scene, and thus intersect on a vanishing point. Similarly, the lines $\mathbf{l}_{\ell,\mathsf{S}}[c]$ and $\mathbf{l}_{\ell,\mathsf{E}}[c]$ are known to be the image of vertical parallel lines in the scene, and intersect on a different vanishing point. These two observations are true for head planes as well as foot planes. One should notice these specific four points were chosen in the head and foot motion planes since they lead to two pairs of parallel lines. These pairs of lines provide two vanishing points, which are used to compute the vanishing line of the motion plane. Figure 3.24 shows an example of the obtained vanishing line for a head motion plane. The two pairs of parallel lines (dashed lines) are shown along with the two vanishing points. As for the ground plane, one may think of the vanishing line of a motion plane as its "horizon" line.

Once the vanishing line of a motion plane $\Pi_\ell[c]$ has been obtained, the *locally rectified motion plane* $\widehat{\Pi}_\ell[c]$ can be computed using the homography transform $\widehat{\mathbf{H}}_\ell[c]$. This homography is computed with Equation 3.46 by using the vector normal to the motion

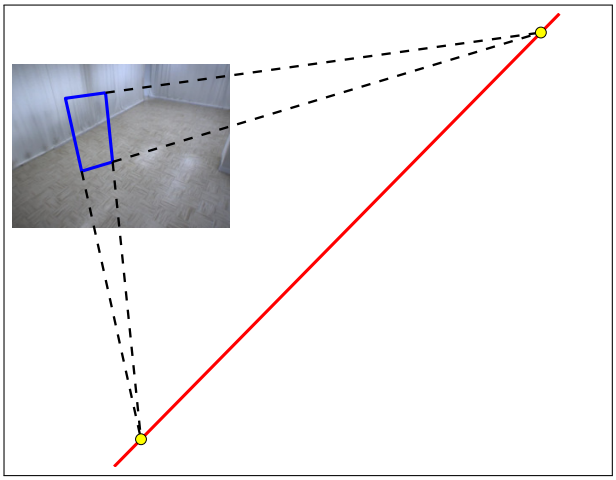

Figure 3.24 – Example of vanishing line for a head motion plane. The vanishing line is defined using the horizontal and the vertical vanishing points (yellow circles), which are respectively the intersection of the horizontal lines and the vertical lines (dashed lines) of the motion plane shown in blue.

plane:

$$\mathbf{n}_\ell[c] = \frac{\mathbf{K}^\mathsf{T}\mathbf{l}_\ell[c]}{\|\mathbf{K}^\mathsf{T}\mathbf{l}_\ell[c]\|}. \tag{3.55}$$

The locally rectified plane $\widehat{\Pi}_\ell[c]$ is defined by computing the rectified points $\widehat{\boldsymbol{\pi}}_{\ell,o}[c]$, $o \in \{\mathsf{TS}, \mathsf{TE}, \mathsf{BS}, \mathsf{BE}\}$:

$$\widetilde{\widehat{\boldsymbol{\pi}}}_{\ell,o}[c] = \widehat{\mathbf{H}}_\ell[c]\ \widetilde{\boldsymbol{\pi}}_{\ell,o}[c], \tag{3.56}$$

where $\widetilde{\widehat{\boldsymbol{\pi}}}_{\ell,o}[c]$ is the homogeneous coordinates representation of the point $\widehat{\boldsymbol{\pi}}_{\ell,o}[c]$. One must note that the locally rectified plane is defined up to a similarity transformation, which means that the distances between the rectified points are defined in arbitrary units. Nevertheless, the aspect ratio of the corresponding rectangle in the scene can be computed from locally rectified points since an aspect ratio is invariant to a similarity transformation. The aspect ratio is computed as

$$\rho_\ell[c] = \frac{\|\widehat{\boldsymbol{\pi}}_{\ell,\mathsf{TS}}[c] - \widehat{\boldsymbol{\pi}}_{\ell,\mathsf{BS}}[c]\|}{\|\widehat{\boldsymbol{\pi}}_{\ell,\mathsf{BE}}[c] - \widehat{\boldsymbol{\pi}}_{\ell,\mathsf{BS}}[c]\|}, \tag{3.57}$$

that is, the ratio of the rectangle's height and width in the locally rectified motion plane.

One should note that the locally rectified motion planes are each defined on a different, arbitrary scale, and thus the lengths that are computed in a locally rectified motion plane (rectangle width and height for instance) are not comparable with the lengths computed in another locally rectified motion plane. In order to get metric information on a common scale for all motion planes, the width of each motion plane's rectangle is

computed on the rectified ground plane. Indeed, the imaged points $\boldsymbol{\pi}_{\ell,\mathsf{BS}}[c]$ and $\boldsymbol{\pi}_{\ell,\mathsf{BE}}[c]$ are known to lie in the motion planes and in the ground plane. It is thus possible to compute the position $\overline{\boldsymbol{\pi}}_{\ell,\mathsf{BS}}[c]$ and $\overline{\boldsymbol{\pi}}_{\ell,\mathsf{BE}}[c]$ of these two points in the rectified ground plane as follow:

$$\widetilde{\overline{\boldsymbol{\pi}}}_{\ell,\mathsf{BS}}[c] = \mathbf{H}_{\mathrm{G}}\, \widetilde{\boldsymbol{\pi}}_{\ell,\mathsf{BS}}[c], \tag{3.58}$$

$$\widetilde{\overline{\boldsymbol{\pi}}}_{\ell,\mathsf{BE}}[c] = \mathbf{H}_{\mathrm{G}}\, \widetilde{\boldsymbol{\pi}}_{\ell,\mathsf{BE}}[c]. \tag{3.59}$$

The distance between these two points thus corresponds to the rectangle's width of the motion plane $\Pi_\ell[c]$ on the rectified ground plane and is defined as

$$\omega_\ell[c] = \left\| \overline{\boldsymbol{\pi}}_{\ell,\mathsf{BE}}[c] - \overline{\boldsymbol{\pi}}_{\ell,\mathsf{BS}}[c] \right\|. \tag{3.60}$$

Given the aspect ratio and the rectangle's width of a motion plane, the rectangle's height of a motion plane, $\upsilon_\ell[c]$, can be computed as

$$\upsilon_\ell[c] = \rho_\ell[c]\, \omega_\ell[c]. \tag{3.61}$$

One must notice that the size of the motion plane's rectangle is defined in the units of the ground plane. As mentioned previously, these units are either scene units or arbitrary units, depending on whether the ground scale factor was determined or not.

Once again, it is important to note that the local rectification is performed here only to recover the metric information of each motion plane in a video sequence. The locally rectified motion planes cannot be used as the final rectified planes since local rectification does not preserve the relations between adjacent motion planes. Therefore, the metric information recovered from each motion plane needs to be combined in order to compute the rectified motion planes.

3.7.3 Rectified Motion Planes Computation

As seen previously, the four points that are known to lie in each motion plane form a rectangle in the scene, and this rectangle is imaged as a rectangle if the viewpoint is fronto-parallel. This means that the four points must form a rectangle in the rectified motion planes since the rectification process consists in generating a fronto-parallel view of the walk. Also, the motion planes must be rectified such that the relations with the neighbouring motion planes are preserved, that is, the points they have in common in the scene must still be common points once the motion planes are rectified. Defining the rectified motion planes thus consists in computing the rectified position of the four points by combining the metric information computed for each plane.

It is possible to see from the walk model that the motion planes' rectangles can be considered of the same height during a walk. Indeed, the person's height does not change during the walk (hypothesis no.4, page 44), but the *apparent height*, that is, the distance from the top of the head to the floor, slightly changes according to the step length at each gait half-cycle. The maximal height difference consists in the difference between the real person's height (when the person stands still) and the apparent height for the longest step the person can take. Since it is assumed here that the person is always walking (hypothesis no.3, page 44), the difference in the rectangle's height will be neglected, which means that the apparent height will be considered the same for all gait half-cycles in all intervals of a walk.

Another observation that can be made from the walk model is that the height of a foot motion plane's rectangle is not much greater than the height of a head motion plane's rectangle. The foot motion plane is only slightly slanted with respect to the head motion plane. Moreover, the foot motion plane's rectangle and the head motion plane's rectangle in a given gait half-cycle coincide when imaged from a fronto-parallel view (see Figure 3.10). This means that these two rectangles will be the same in the rectified head and foot motion planes, that is, the rectangles will share the same four rectified points. Therefore, the rectified foot motion plane for a gait half-cycle c, which is denoted $\Pi'_{\mathsf{F}}[c]$, is equal to the rectified head motion plane $\Pi'_{\mathsf{H}}[c]$.

Given the previous observations, the rectified motion planes for both the head and the foot are computed as follows. First, a common height must be determined for all the motion planes' rectangles. This common height, which is denoted here as υ_{med}, is defined as the median of the height of all the planes' rectangles of a walk:

$$\upsilon_{\text{med}} = \underset{i,c,\ell}{\text{median}}\, \upsilon_\ell[i,c], \tag{3.62}$$

where $i = 1, 2, \ldots, I$, $c = 1, 2, \ldots, C_i$, and $\ell \in \{\mathsf{H}, \mathsf{F}\}$. The notation $\upsilon_\ell[i,c]$ is used here since the interval number must be made explicit (the same will apply in the following). The median height is chosen over the average height since it provides more robustness to outliers, which can occur when metric information is computed from imaged planes with noisy points positions.

The next step consists in defining the rectified planes by computing their rectified points using Algorithm 3.3. In this algorithm, the rectified head plane $\Pi'_{\mathsf{H}}[i,c]$ and the rectified foot plane $\Pi'_{\mathsf{F}}[i,c]$ for a gait half-cycle c in interval i are defined with rectangles that are υ_{med} tall and $\omega_{\mathsf{H}}[i,c]$ wide. Here, the width that was obtained in Section 3.7.2 for the head plane's rectangle is chosen as the width for both head and foot planes' rectangle. The reason is that the rectangle width obtained for the head and the foot planes are equal by definition, that is $\omega_{\mathsf{H}}[i,c] = \omega_{\mathsf{F}}[i,c]$ (see Section 3.5.2).

Algorithm 3.3: Rectified Motion Planes Computation.

for $i = 1, 2, \ldots, I$ **do** ⇒ *For all intervals*
  $\delta = 0$ ⇒ *The first plane starts at position* $x = 0$
  for $c = 1, 2, \ldots, C_i$ **do** ⇒ *For all gait half-cycles in interval* i
    $\boldsymbol{\pi}'_{\mathsf{H,BS}}[i,c] = \boldsymbol{\pi}'_{\mathsf{F,BS}}[i,c] = \begin{bmatrix} \delta \\ 0 \end{bmatrix}$ ⇒ *Bottom start point*
    $\boldsymbol{\pi}'_{\mathsf{H,TS}}[i,c] = \boldsymbol{\pi}'_{\mathsf{F,TS}}[i,c] = \begin{bmatrix} \delta \\ \upsilon_{\text{med}} \end{bmatrix}$ ⇒ *Top start point*
    $\boldsymbol{\pi}'_{\mathsf{H,BE}}[i,c] = \boldsymbol{\pi}'_{\mathsf{F,BE}}[i,c] = \begin{bmatrix} \delta + \omega_{\mathsf{H}}[i,c] \\ 0 \end{bmatrix}$ ⇒ *Bottom end point*
    $\boldsymbol{\pi}'_{\mathsf{H,TE}}[i,c] = \boldsymbol{\pi}'_{\mathsf{F,TE}}[i,c] = \begin{bmatrix} \delta + \omega_{\mathsf{H}}[i,c] \\ \upsilon_{\text{med}} \end{bmatrix}$ ⇒ *Top end point*
    $\delta = \delta + \omega_{\mathsf{H}}[i,c]$ ⇒ *Next plane starts where the current plane ends*
  end for
end for

One should note that the rectified planes are defined in a 2-D Euclidean space. The abscissa represents the displacement of the subject, from left to right, with the starting position being zero. The ordinate represents the height, from bottom to top, with zero being the ground level. For each interval, the plane in the first half-cycle has its point $\boldsymbol{\pi}_{\mathsf{H,BS}}$ at the origin $(0, 0)$. It is important to stress again that the rectified head and foot planes in a gait half-cycle are the same, that is, the rectangles coincide. The four points of the planes in a gait half-cycle c of interval i are defined such that the relation with the previous and the next planes are preserved:

$$\begin{aligned} \boldsymbol{\pi}'_{\ell,\mathsf{BS}}[i,c] &= \boldsymbol{\pi}'_{\ell,\mathsf{BE}}[i,c-1], \quad \boldsymbol{\pi}'_{\ell,\mathsf{TS}}[i,c] = \boldsymbol{\pi}'_{\ell,\mathsf{TE}}[i,c-1], \\ \boldsymbol{\pi}'_{\ell,\mathsf{BE}}[i,c] &= \boldsymbol{\pi}'_{\ell,\mathsf{BS}}[i,c+1], \quad \boldsymbol{\pi}'_{\ell,\mathsf{TE}}[i,c] = \boldsymbol{\pi}'_{\ell,\mathsf{TS}}[i,c+1], \end{aligned} \tag{3.63}$$

for $\ell \in \{\mathsf{H}, \mathsf{F}\}$. One may see that the rectified motion planes in each interval are defined from left to right and that their position reflect the order of occurrence of the gait half-cycles. This means that each walk will be rectified such that it appears to have been observed from a fronto-parallel and performed from left to right for the complete video sequence. This common representation will facilitate gait analysis and comparison.

Figure 3.25 presents the rectified motion planes obtained for the imaged head and foot motion planes shown in Figures 3.17 and 3.20, respectively. The rectified head and foot motion planes (rectangles) are shown separately since they coincide. The colour of each plane corresponds to the colour used for the imaged planes of Figures 3.17 and 3.20. One may see that the rectified planes are defined from left to right, even in the case of the interval #2 where the walk was performed from right to left.

The axes in this example are in meters since the scale factor of the ground plane

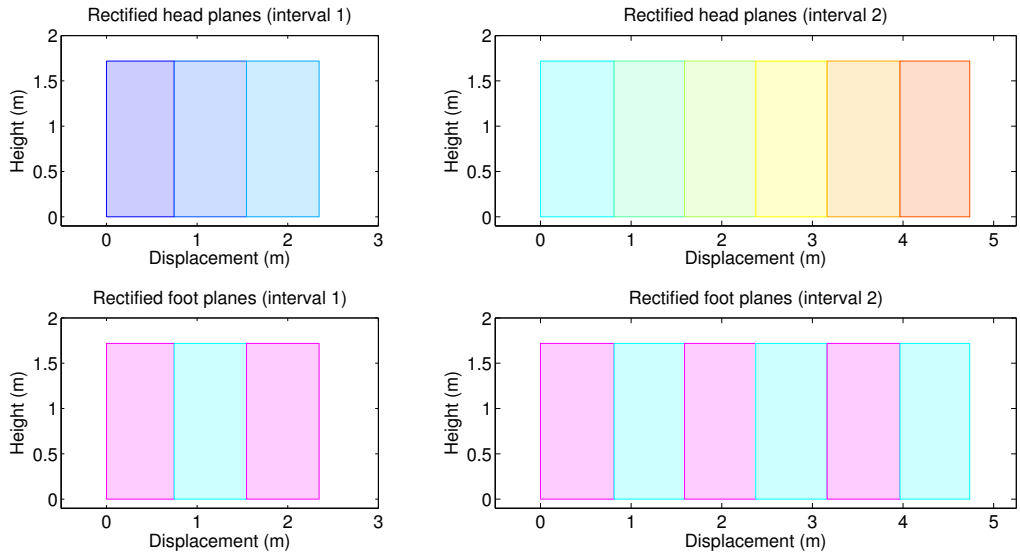

Figure 3.25 – Example of rectified head and foot motion planes. The top row shows the rectified head planes for the two intervals of the example video sequence, while the bottom row shows the corresponding rectified foot motion planes.

is known, which permits to perform real measurements on the walk. For instance, the person's apparent height in this example is about 1.75 m, and the displacement for the first gait half-cycle of interval #1 is about 0.75 m. In the case where the scale factor is unknown, the axes have arbitrary units, given the unknown scale. Although real measurements cannot be performed in that case, comparison can be performed between rectified walks. For instance, it would be possible to determine that a given person appears to be x times taller than another person, or that her average displacement per half-cycle is y times shorter than another person.

As one may see, the rectified plane already provides some information about a person's gait. More information can be extracted if the body-part trajectories are also rectified. In order to obtain the rectified body-part trajectories, the homography that maps a given imaged plane to its rectified counterpart must first be computed.

3.7.4 Motion Planes Homography Computation

The transform that maps the points in a plane into another plane is called an homography and can be mathematically represented by a 3×3 matrix when a 2-D Euclidean space is considered [98]. For a given gait half-cycle c in interval i, an imaged motion plane $\Pi_\ell[i, c]$, $\ell \in \{\mathsf{H}, \mathsf{F}\}$, can be mapped to its corresponding rectified motion plane

$\Pi'_{\mathsf{H}}[i,c]$ by a homography $\mathbf{H}_\ell[i,c]$ defined such that

$$\widetilde{\boldsymbol{\pi}}'_{\ell,o}[i,c] = \mathbf{H}_\ell[i,c]\,\widetilde{\boldsymbol{\pi}}_{\ell,o}[i,c], \quad \forall\, o \in \{\mathsf{TS},\mathsf{TE},\mathsf{BS},\mathsf{BE}\}. \tag{3.64}$$

Each of the four pairs of corresponding points between the imaged and the rectified planes provides two constraints on the homography, which has 8 degrees of freedom. It is thus possible to build a linear system $\mathbf{Ah} = \mathbf{0}$, where $\mathbf{h}$ is the vector form of the homography matrix, and $\mathbf{A}$ is the 8×9 matrix defined [98] as

$$\mathbf{A} = \begin{bmatrix}
\pi_{\mathsf{BS},x} & \pi_{\mathsf{BS},y} & 1 & 0 & 0 & 0 & -\pi_{\mathsf{BS},x}\pi'_{\mathsf{BS},x} & -\pi_{\mathsf{BS},y}\pi'_{\mathsf{BS},x} & -\pi'_{\mathsf{BS},x} \\
0 & 0 & 0 & \pi_{\mathsf{BS},x} & \pi_{\mathsf{BS},y} & 1 & -\pi_{\mathsf{BS},x}\pi'_{\mathsf{BS},y} & -\pi_{\mathsf{BS},y}\pi'_{\mathsf{BS},y} & -\pi'_{\mathsf{BS},y} \\
\pi_{\mathsf{TS},x} & \pi_{\mathsf{TS},y} & 1 & 0 & 0 & 0 & -\pi_{\mathsf{TS},x}\pi'_{\mathsf{TS},x} & -\pi_{\mathsf{TS},y}\pi'_{\mathsf{TS},x} & -\pi'_{\mathsf{TS},x} \\
0 & 0 & 0 & \pi_{\mathsf{TS},x} & \pi_{\mathsf{TS},y} & 1 & -\pi_{\mathsf{TS},x}\pi'_{\mathsf{TS},y} & -\pi_{\mathsf{TS},y}\pi'_{\mathsf{TS},y} & -\pi'_{\mathsf{TS},y} \\
\pi_{\mathsf{BE},x} & \pi_{\mathsf{BE},y} & 1 & 0 & 0 & 0 & -\pi_{\mathsf{BE},x}\pi'_{\mathsf{BE},x} & -\pi_{\mathsf{BE},y}\pi'_{\mathsf{BE},x} & -\pi'_{\mathsf{BE},x} \\
0 & 0 & 0 & \pi_{\mathsf{BE},x} & \pi_{\mathsf{BE},y} & 1 & -\pi_{\mathsf{BE},x}\pi'_{\mathsf{BE},y} & -\pi_{\mathsf{BE},y}\pi'_{\mathsf{BE},y} & -\pi'_{\mathsf{BE},y} \\
\pi_{\mathsf{TE},x} & \pi_{\mathsf{TE},y} & 1 & 0 & 0 & 0 & -\pi_{\mathsf{TE},x}\pi'_{\mathsf{TE},x} & -\pi_{\mathsf{TE},y}\pi'_{\mathsf{TE},x} & -\pi'_{\mathsf{TE},x} \\
0 & 0 & 0 & \pi_{\mathsf{TE},x} & \pi_{\mathsf{TE},y} & 1 & -\pi_{\mathsf{TE},x}\pi'_{\mathsf{TE},y} & -\pi_{\mathsf{TE},y}\pi'_{\mathsf{TE},y} & -\pi'_{\mathsf{TE},y}
\end{bmatrix} \tag{3.65}$$

One must first note that ℓ, i, and c have been dropped here for clarity. Also, the variables $\pi_{o,x}$ and $\pi_{o,x}$ are respectively the x and y component of the point $\boldsymbol{\pi}_o$, with $o \in \{\mathsf{TS},\mathsf{TE},\mathsf{BS},\mathsf{BE}\}$. The linear system can be solved for $\mathbf{h}$ by performing a *Singular Value Decomposition* of the matrix $\mathbf{A}$, that is, $\mathbf{A} = \mathbf{UDV}^{\mathsf{T}}$, and then taking as the solution the singular vector (a column of matrix $\mathbf{V}$) that correspond to the smallest singular value in diagonal matrix $\mathbf{D}$. The head and the foot planes homography matrices $\mathbf{H}_{\mathsf{H}}[i,c]$ and $\mathbf{H}_{\mathsf{F}}[i,c]$ are thus computed in this way for each gait half-cycles c in each interval i of a video sequence. Each homography matrix will be used to rectify the corresponding body-part trajectories in the corresponding gait half-cycle and interval.

3.8 Body-part Trajectories Rectification

As discussed previously, it is assumed here that each body-part trajectory lies in a plane (Hypothesis no.5, Section 3.2). The image of the head and the foot motion planes were defined for each gait half-cycle c in each interval i. Thus, each motion plane is defined for the time interval $[t_{i,c}, t_{i,c+1}]$. The rectified planes were defined using the metric information computed for the imaged planes. Finally, the homography that maps an imaged motion plane to its rectified counterpart was computed. Therefore, rectifying a body-part trajectory within a gait half-cycle c consists in applying the corresponding homography on each imaged position of the body part in the discrete frame interval $[\lceil t_{i,c} \rceil, \lfloor t_{i,c+1} \rfloor]$.

Algorithm 3.4: Still Foot Rectification.

if $c = 1$ **then**
  $\widetilde{\mathbf{p}}'_{\bar{m}}[n] = \mathbf{H}_{\mathsf{F}}[i, c+1]\,\widetilde{\mathbf{p}}_{\bar{m}}[n], \quad n \in [\lceil t_{i,c} \rceil, \lfloor t_{i,c+1} \rfloor]$
else if $c = C_i$ **then**
  $\widetilde{\mathbf{p}}'_{\bar{m}}[n] = \mathbf{H}_{\mathsf{F}}[i, c-1]\,\widetilde{\mathbf{p}}_{\bar{m}}[n], \quad n \in [\lceil t_{i,c} \rceil, \lfloor t_{i,c+1} \rfloor]$
else
  $a = \lfloor (\lceil t_{i,c} \rceil + \lfloor t_{i,c+1} \rfloor)/2 \rfloor$
  $\widetilde{\mathbf{p}}'_{\bar{m}}[n] = \mathbf{H}_{\mathsf{F}}[i, c-1]\,\widetilde{\mathbf{p}}_{\bar{m}}[n], \quad n \in [\lceil t_{i,c} \rceil, a]$
  $\widetilde{\mathbf{p}}'_{\bar{m}}[n] = \mathbf{H}_{\mathsf{F}}[i, c+1]\,\widetilde{\mathbf{p}}_{\bar{m}}[n], \quad n \in [a+1, \lfloor t_{i,c+1} \rfloor]$
end if

The rectification of head and the moving foot trajectories is straightforward. The rectified trajectory of the head $\mathbf{p}'_{\mathsf{H}}[n]$ within gait half-cycle c of interval i is computed as

$$\widetilde{\mathbf{p}}'_{\mathsf{H}}[n] = \mathbf{H}_{\mathsf{H}}[i, c]\,\widetilde{\mathbf{p}}_{\mathsf{H}}[n], \quad n \in [\lceil t_{i,c} \rceil, \lfloor t_{i,c+1} \rfloor], \tag{3.66}$$

where $\widetilde{\mathbf{p}}'_{\mathsf{H}}[n]$ is the homogeneous representation of the rectified head trajectory, $c = 1, 2, \ldots, C_i$, and $i = 1, 2, \ldots, I$. The rectified trajectory of the moving foot $\mathbf{p}'_m[n]$ within gait half-cycle c of interval i is computed as

$$\widetilde{\mathbf{p}}'_m[n] = \mathbf{H}_{\mathsf{F}}[i, c]\,\widetilde{\mathbf{p}}_m[n], \quad n \in [\lceil t_{i,c} \rceil, \lfloor t_{i,c+1} \rfloor]. \tag{3.67}$$

where $\widetilde{\mathbf{p}}'_m[n]$ is the homogeneous representation of the rectified trajectory of the moving foot.

The positions of the still foot within a given gait half-cycle c can be rectified using the homography of the previous gait half-cycle $c-1$, the homography of the next gait half-cycle $c+1$, or both homographies. One should note that even if the still foot is considered as not moving in a given gait half-cycle, it will in practice move a little bit at the beginning and at the end of the gait half-cycle. This is due to the fact that at the beginning of the gait half-cycle, the foot just touched the ground, and thus still has to move a little more to be in full contact with the ground. The opposite event occurs at the end of the gait half-cycle, that is, the foot starts to move until it completely gets off the ground. It is therefore better to compute the rectified positions of the still foot since it permits to obtain continuous, rectified trajectories for each foot. The rectified positions $\widetilde{\mathbf{p}}'_{\bar{m}}[n]$ of the still foot in a given gait half-cycle c of interval i is computed using Algorithm 3.4. This algorithm mainly deals with the cases of the first and the last gait half-cycles, where the homography of the next and the previous gait half-cycle is used, respectively, to compute the rectified positions. In the normal case, the rectified positions of the first half of the gait half-cycle c are computed with the homography of the previous gait half-cycle $c-1$, while the rectified positions of the second half of the gait half-cycle c are computed with the homography of the next gait half-cycle $c+1$. This is consistent with the fact that the foot still moves a little bit at the beginning of

the gait half-cycle c and that this motion is performed in the previous motion plane in gait half-cycle $c-1$, whereas the motion performed at the end of the gait-half-cycle c is performed in the foot motion plane computed in the next gait half-cycle $c+1$. One must note that the still foot positions can be rectified only if there is at least two gait half-cycles in the considered interval i.

It is also possible to rectify the trajectory of the top of the head $\mathbf{p}_{\mathsf{HT}}[n]$ using Equation 3.66 since the positions of the top of the head are in the same motion plane as the head mass centre. The rectified trajectory of the top of the head will be referred to as $\mathbf{p}'_{\mathsf{HT}}[n]$. Also, the two positions of the moving foot extremity in gait half-cycle c of interval i, $\mathbf{e}_m[i,c]$ and $\mathbf{e}_m[i,c+1]$, are rectified using the foot plane homography $\mathbf{H}_{\mathsf{F}}[i,c]$ as follow:

$$\widetilde{\mathbf{e}}'_{\mathsf{FS}}[i,c] = \mathbf{H}_{\mathsf{F}}[i,c]\,\widetilde{\mathbf{e}}_m[i,c], \tag{3.68}$$

$$\widetilde{\mathbf{e}}'_{\mathsf{FE}}[i,c] = \mathbf{H}_{\mathsf{F}}[i,c]\,\widetilde{\mathbf{e}}_m[i,c+1], \tag{3.69}$$

where $\widetilde{\mathbf{e}}_m[i,c]$, $\widetilde{\mathbf{e}}_m[i,c+1]$ are the homogeneous coordinates of the moving foot extremity positions at the beginning and at the end of the gait half-cycle c in interval i, and $\widetilde{\mathbf{e}}'_{\mathsf{FS}}[i,c]$, $\widetilde{\mathbf{e}}'_{\mathsf{FE}}[i,c]$ are the corresponding homogeneous coordinate of the rectified foot extremity positions (F for foot, S for start, and E for end). The variables $\mathbf{e}'_{\mathsf{FS}}[i,c]$ and $\mathbf{e}'_{\mathsf{FE}}[i,c]$ thus represent the rectified extremity positions of the foot that is moving (the foot with the label represented by m) in gait half-cycle c if interval i. The rectified trajectory of the top of the head and the rectified moving foot extremity positions are used in Chapter 4 to perform gait analysis.

Figure 3.26 shows the rectified head and foot trajectories corresponding to the imaged trajectories shown in Figure 3.17. Here, only the trajectories for the head and the foot mass centre are shown. By comparing the imaged and the rectified trajectories, one may see that the rectified trajectories appears to have been observed from a fronto-parallel viewpoint, and that the walk appears to be performed from left to right. Also, it is possible to see that the stride lengths appear more similar for the rectified foot trajectories than for the imaged foot trajectories. Finally, the rectified head trajectory has the typical sinusoidal shape that one would expect by observing a walk from a fronto-parallel viewpoint.

3.9 Parameters Estimation

The proposed view-rectification approach necessitates the use of a few parameters that need to be determined beforehand. These parameters are the camera intrinsic param-

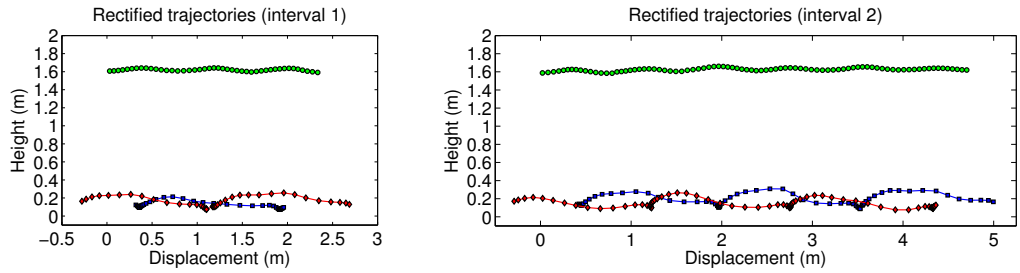

Figure 3.26 – Example of rectified head and foot trajectories. The rectified trajectories are shown separately for each interval of the example video sequence.

eters, the imaged ground vanishing line, and optionally the ground scale factor. The camera intrinsic parameters, along with the radial and tangential distortion parameters, are obtained by conventional camera calibration. More details about this calibration process are provided in Section B.3. The imaged ground vanishing line and the ground scale factor are determined by using the methods proposed in Sections 3.9.1 and 3.9.2, respectively. One must note that the parameters are totally independent of the walks that are going to be observed through the camera setup. Nonetheless, some of these parameters can be estimated automatically from the observation of a number of walks as it will be seen shortly.

3.9.1 Ground Vanishing Line Estimation

One could estimate the ground vanishing line by determining at least two vanishing points in the image that represent points at infinity on the ground plane in the scene. As seen previously, a vanishing point can be found in the image as the intersection point of a group of imaged lines that are parallel with each others in the scene. If these lines are parallel to the ground plane in the scene, then the vanishing point lies on the vanishing line of the ground plane. Therefore, at least two groups of lines are necessary to estimate the ground vanishing line. The direction of the groups of lines must be different in order to obtain different vanishing points from which the vanishing line can be estimated.

Although the ground vanishing line could be estimated by manually determining groups of lines in the image, a fully automatic method is proposed here. The proposed method uses the imaged body-part trajectories from several walk sequences, which can be walk sequences from the same subject or from different subjects. In this thesis, a subset of the video sequences from the proposed gait database[2] are used to estimate

[2]The proposed gait database will be presented in Chapter 5 and detailed in Appendix B

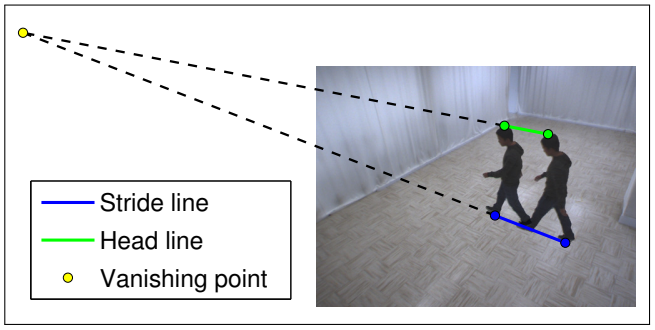

Figure 3.27 – Example of vanishing point computation for a gait half-cycle. The blue and the green line segments represent respectively the stride line and the head displacement line. The line segments' endpoints are the moving foot contact points and the position of the top of the head.

the ground vanishing line. One should note that the ground vanishing line needs only to be estimated once for a fixed camera setup since the location and the orientation of this line in the camera image depends only on the position and the orientation of the camera with respect to the ground plane.

It is possible to see from a walk model that for a gait half-cycle c, the stride line, which is joining the moving foot extremities $\mathbf{E}_m[c]$ and $\mathbf{E}_m[c+1]$, and the head displacement line, which is joining the head extremities $\mathbf{E}_{\mathsf{H}}[c]$ and $\mathbf{E}_{\mathsf{H}}[c+1]$, are both parallel to the ground plane in the scene and are parallel to each other. This means that the image of these two lines can be used to compute a vanishing point corresponding to a point at infinity on the ground plane in the scene. A vanishing point $\mathbf{v}_{\mathrm{G}}[c]$ can therefore be computed for each gait half-cycle as follows:

$$\widetilde{\mathbf{v}}_{\mathrm{G}}[c] = \underbrace{\left(\widetilde{\mathbf{p}}_{\mathsf{HT}}(t_c) \times \widetilde{\mathbf{p}}_{\mathsf{HT}}(t_{c+1})\right)}_{\text{head line}} \times \underbrace{\left(\mathbf{e}_m[c] \times \mathbf{e}_m[c+1]\right)}_{\text{stride line}}, \tag{3.70}$$

where $\widetilde{\mathbf{v}}_{\mathrm{G}}$ is the homogeneous coordinates representation of $\mathbf{v}_{\mathrm{G}}$, $\mathbf{e}_m[c]$ is the homogeneous coordinates representation of the moving foot extremity at time t_c, and $\widetilde{\mathbf{p}}_{\mathsf{HT}}(t_c)$ is the interpolated position of the top of the silhouette at time t_c. One should note that both $\mathbf{p}_{\mathsf{HT}}(t_c)$ and $\mathbf{e}_m[c]$ were computed only from the raw, imaged body-part trajectories and the body-part bounding boxes, and thus, neither of them depends on the knowledge of the ground vanishing line. The position of the top of the silhouette acts here as an approximation of the head extremity, as the latter depends on the foot middle points, which in turn depends on the ground vanishing line. Figure 3.27 shows an example of a ground vanishing point obtained for a gait half-cycle. The line segments defined by the positions of the top of the head and the foot contact points on the floor are shown along with the point were the head displacement line and the stride line intersect, that is, a ground vanishing point.

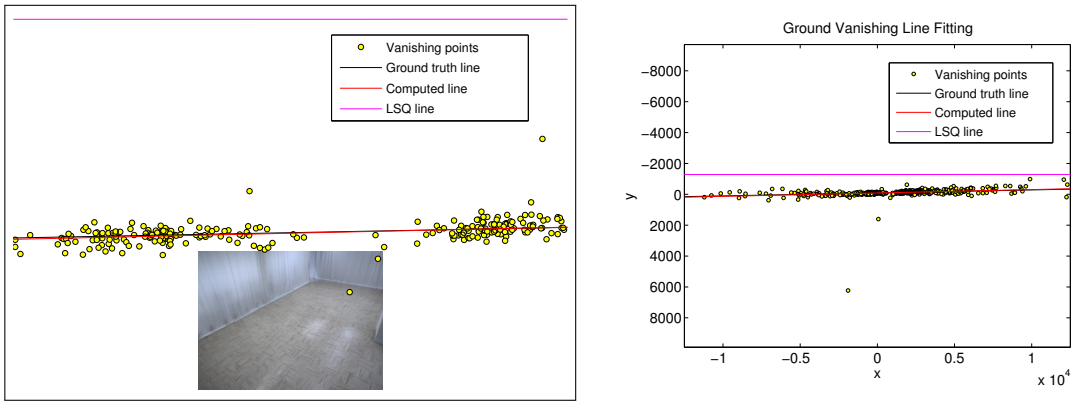

(a) (b)

Figure 3.28 – Robust fitting of the ground vanishing line over the ground vanishing points. In (a), the computed vanishing line is shown with respect to the camera image, along with some of the ground vanishing points, the ground truth vanishing line and the vanishing line computed using a simple least squares fitting (LSQ). In (b), more of the ground vanishing points are shown along with the lines, without the camera image. One can see that the LSQ line is influenced by outlier vanishing points, while the computed line is not.

Many ground vanishing points can thus be obtained by considering several walks, that is, by computing a vanishing point for each gait half-cycle in each interval of each walk. Computing these vanishing points for a given walk only necessitates a few processing steps, which consists mainly in detecting the gait half-cycles (Section 3.4) in each interval, and then computing the position of the top of the head (Equation 3.27) and the foot extremities (Section 3.5.1.1) at each key times t_c. The vanishing points obtained from several walks are used in a line fitting process in order to estimate the ground vanishing line. One must note that the computed vanishing points are prone to the noise that might be present in the body-part trajectories. The ground vanishing line is thus fitted on the ground vanishing points using a robust regression method based on *iteratively reweighted least squares* [99]. The method implementation used in this thesis is the `robustfit` MATLAB® function, which uses a bi-square weighting function by default.

The ground vanishing line obtained with the proposed method for the gait database used in this thesis is presented in Figure 3.28. Here, 100 video sequences (10 walks performed by 10 different subjects) were used to obtain a total of 558 ground vanishing points. One must note that only a subset of the vanishing points could be shown in Figures 3.28(a) and 3.28(b) as some of them have a large abscissa value. Figure 3.28(a) shows the computed line and the vanishing points with respect to the camera image whereas Figure 3.28(b) shows more vanishing point but without the camera image. For comparison and validation purposes, the *ground truth* vanishing line of the ground plane is shown along with the line that can be obtained with a simple least squares line fitting

on the vanishing points. The ground truth line was obtained by first manually fitting lines on some of the floor tiles in the image. The two groups of lines that are found represent perpendicular directions on the floor (the tiles are square), which permits to compute the two vanishing points necessary to obtain the ground truth vanishing line. One can see from these Figures that the computed vanishing line is very close to the ground truth one. The computed vanishing line is $y = -0.0219x - 87.2$, the ground truth line is $y = -0.0192x - 91.7$, and the line obtained with a simple least squares fitting is $y = 5.72 \times 10^{-5}x - 1284$. As one would expect, the leverage of the outlier points made the least squares fitted line very different from the ground truth line.

One can see from these results that it is possible to automatically estimate the ground vanishing line for a given camera setup. The proposed method will work as long as the input walks lead to *different* vanishing points, that is, the walk directions are not all the same. Otherwise, the vanishing points would be located in the same area of the image space since they coarsely represent the same direction, and thus the line fitting process would not be reliable.

3.9.2 Ground Scale Factor Estimation

The estimation of the ground scale factor is the only part of the proposed view-rectification method that needs manual input from a user. This only needs to be performed once for a given camera setup, and can thus be easily performed along with camera calibration. As discussed previously, the ground scale factor is an optional parameter that is used by the proposed method to obtain rectified trajectories in scene units, that is, in meters. In the case where the ground scale factor is not defined, the view-rectified trajectories are in arbitrary units, which means that only relative comparison of the trajectories obtained from the camera setup can be performed. The ground scale factor is thus useful to obtain real measurements as well as to compare rectified trajectories obtained from different camera setups (each camera setup has its own ground scale factor).

The ground scale factor can be determined if one can identify in the image some points that are known to lie on the ground plane and for which the distance to each other is known in the scene. In the case of the database used in this thesis, such points in the image can be found by considering the tiles on the floor, as shown in Figure 3.29. Using a graphical user interface, a user fits lines on each side of a floor tile in the image by manually adjusting two endpoints (cyan points). These lines, which are denoted $\mathbf{l}_1$, $\mathbf{l}_2$, $\mathbf{l}_\mathrm{a}$, and $\mathbf{l}_\mathrm{b}$, are then used to compute the position in the image of the four corners of the tile $\mathbf{u}_{1\mathrm{a}}$, $\mathbf{u}_{1\mathrm{b}}$, $\mathbf{u}_{2\mathrm{a}}$, and $\mathbf{u}_{2\mathrm{b}}$ (red points). As it will be shown shortly, the ground

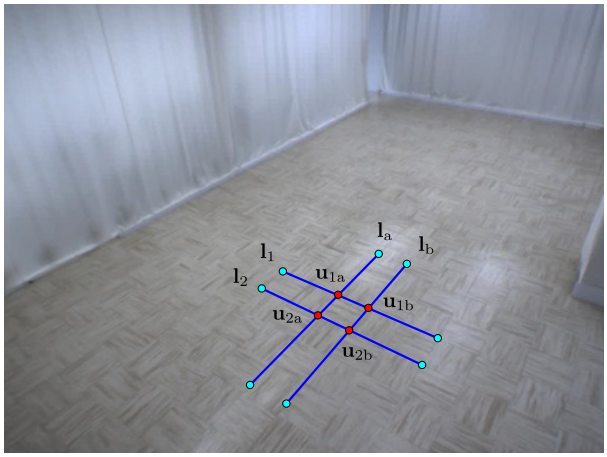

Figure 3.29 – Identification of points in the image on ground plane. Here, a user fits a line on each side of an imaged tile by manually specifying two points for each line (cyan points) using a graphical user interface. The lines $\mathbf{l}_1$, $\mathbf{l}_2$, $\mathbf{l}_\mathrm{a}$, and $\mathbf{l}_\mathrm{b}$ are then used to compute position of the tile's corners in the image (red points), which are denoted $\mathbf{u}_{1\mathrm{a}}$, $\mathbf{u}_{1\mathrm{b}}$, $\mathbf{u}_{2\mathrm{a}}$, and $\mathbf{u}_{2\mathrm{b}}$.

scale factor can be determined using these four points since the distance between them is known in the scene, that is, the tile side length is 304.8 mm (12 inches). One should note that the user is asked to fit lines on the tile sides instead of fitting points directly on the tile corners since lines are easier to fit and to assess visually than points.

The points $\mathbf{u}_{x\alpha}$, where $x = \{1, 2\}$ and $\alpha = \{\mathrm{a}, \mathrm{b}\}$, are computed as the intersection of lines $\mathbf{l}_x$ and $\mathbf{l}_\alpha$:

$$\widetilde{\mathbf{u}}_{x\alpha} = \mathbf{l}_x \times \mathbf{l}_\alpha, \tag{3.71}$$

where $\widetilde{\mathbf{u}}_{x\alpha}$ is the homogeneous coordinate representation of $\mathbf{u}_{x\alpha}$. The rectified position $\overline{\mathbf{u}}_{x\alpha}$ of each point $\mathbf{u}_{x\alpha}$ can then be computed in the rectified ground plane using Equation 3.46:

$$\widetilde{\overline{\mathbf{u}}}_{x\alpha} = \mathbf{K}\mathbf{R}_\mathrm{G}\mathbf{K}^{-1}\,\widetilde{\mathbf{u}}_{x\alpha}, \tag{3.72}$$

where $\widetilde{\overline{\mathbf{u}}}_{x\alpha}$ is the homogeneous coordinate representation of $\overline{\mathbf{u}}_{x\alpha}$. The rotation matrix $\mathbf{R}_\mathrm{G}$ is defined as in Equation 3.47,

$$\mathbf{R}_\mathrm{G} = \begin{bmatrix} \mathbf{r}_1 & \mathbf{r}_2 & \mathbf{n}_\mathrm{G} \end{bmatrix}^\mathsf{T}, \tag{3.73}$$

where the ground normal vector $\mathbf{n}_\mathrm{G}$ is defined as in Equation 3.45, that is,

$$\mathbf{n}_\mathrm{G} = \frac{\mathbf{K}^\mathsf{T}\mathbf{l}_\infty}{\|\mathbf{K}^\mathsf{T}\mathbf{l}_\infty\|}, \tag{3.74}$$

using the ground vanishing line $\mathbf{l}_\infty$ that can be obtained as described in Section 3.9.1.

One can see that the rectification process is defined up to a similarity transform, and thus the distance between the rectified tile corners $\overline{\mathbf{u}}_{x\alpha}$ are defined in arbitrary units.

Since the length of the tile side is known in the scene, one can compute the *ground scale factor* λ_{G} converting these arbitrary units to the scene units as

$$\lambda_{\mathrm{G}} = \frac{\epsilon_{\mathrm{G}}}{\bar{\epsilon}}, \tag{3.75}$$

where ϵ_{G} is the known length of a tile side in scene units (here, $\epsilon_{\mathrm{G}} = 0.3048$ m), and $\bar{\epsilon}$ is the length in arbitrary units of the tile side on the rectified ground plane. Since the tile on the rectified ground plane will most likely not be perfectly square, the length $\bar{\epsilon}$ is defined as the average length of the four sides of the tile:

$$\bar{\epsilon} = \frac{1}{4}\big(\|\overline{\mathbf{u}}_{1\mathrm{a}} - \overline{\mathbf{u}}_{1\mathrm{b}}\| + \|\overline{\mathbf{u}}_{1\mathrm{a}} - \overline{\mathbf{u}}_{2\mathrm{a}}\| + \|\overline{\mathbf{u}}_{2\mathrm{a}} - \overline{\mathbf{u}}_{2\mathrm{b}}\| + \|\overline{\mathbf{u}}_{1\mathrm{b}} - \overline{\mathbf{u}}_{2\mathrm{b}}\|\big). \tag{3.76}$$

Given the ground scale factor λ_{G}, it is possible to compute the homography $\mathbf{H}_{\mathrm{G}}$ that directly rectifies the ground plane in scene units as in Equation 3.48:

$$\mathbf{H}_{\mathrm{G}} = \mathbf{\Lambda}_{\mathrm{G}}\mathbf{K}\mathbf{R}_{\mathrm{G}}\mathbf{K}^{-1}, \tag{3.77}$$

where the 3×3 scale matrix $\mathbf{\Lambda}_{\mathrm{G}}$ is defined here as

$$\mathbf{\Lambda}_{\mathrm{G}} = \begin{bmatrix} \lambda_{\mathrm{G}} & 0 & 0 \\ 0 & \lambda_{\mathrm{G}} & 0 \\ 0 & 0 & 1 \end{bmatrix}. \tag{3.78}$$

Any imaged point that is known to lie on the ground plane can thus be directly rectified using the homography $\mathbf{H}_{\mathrm{G}}$. The position of the rectified points will be in scene units, and the distance computed between any pair of rectified points will be equal to the distance that could be measured in the scene. This is actually what is performed in Section 3.7.2 with the bottom points of the motion plane, which are known to lie on the ground plane.

The proposed method for the estimation of the ground scale factor can be used in any camera setup ans scene. One only needs to identify in the camera image at least two points that are known to lie on the ground plane and for which the distance is known in the scene. For instance, one could place a ruler on the ground and identify the position in the camera image of the ruler endpoints. Then, the endpoints are rectified using Equation 3.72, and the ground scale factor is computed with Equation 3.75 using the known ruler length in the scene and the distance between the two rectified endpoints.

3.10 Conclusion

The view-rectification approach presented in this chapter permits to rectify imaged body-part trajectories so that they appear to have been observed from a fronto-parallel

viewpoint. The proposed method first determines the key times in the walk, that is, the times when the feet are furthest apart. These key times are then used to define the gait half-cycles. The imaged head and foot motion planes are determined for each gait half-cycles using the body-part extremities computed from the imaged head and foot trajectories. The rectified body-part trajectories are obtained by transforming the imaged body-part trajectories using the homographies that metrically rectify the motion planes.

The proposed method has many advantages over previous ones that can be summarized as follows:

- it only requires a few common assumptions compared to the existing methods in the literature;
- it makes use of a walk model that is mostly based on observations from clinical studies. The walk model defines constraints on how the walk can be performed and thus permits to compute the motion planes;
- it deals with changes in the walk direction as well as changes in walking speed since no assumptions are made on either the speed or the walk direction;
- it only requires as input data the imaged trajectories of the head and the feet along with the bounding box of each body part at each frame;
- it does not depend on a specific body parts tracking algorithm, that is, any body parts tracking algorithm could be used as long as it provides both the trajectories and the bounding box of the head and the feet;
- it requires only a small number of parameters that are easily set:
    - the vanishing line can be estimated directly from the imaged body-part trajectories of a set of walks;
    - the camera intrinsic parameters can be obtained using a off-the-shelf camera calibration method;
    - the optional ground scale factor can be estimated using manual inputs from the user during the camera calibration process. This computation is performed only once for a given camera setup;
    - the maximum cadence f_c of the walks can be set to the maximum expected cadence on the walks that will be processed;
    - the standard deviation σ of the Gaussian filtering process can be set according to the level of noise in the body-part trajectories;
- it permits to express the rectified body-part trajectory in scene units in the case the ground scale factor is determined;
- it is entirely automatic and does not necessitate any input from a human user in order to process a walk sequence obtained from a calibrated camera.

The proposed method could be extended in order to perform a view-rectification of other body-part trajectories as well. For instance, if one could determine the imaged position of the knees at each frame, it would be possible to perform a view-rectification of their trajectories using the homographies of the foot motion planes since the knees are known to lie in the foot motion planes. Also, if one could determine the imaged positions of the hands at each frame, it would be possible to define hand motion planes[3] for each hand as it was done for each foot.

An obvious limitation of the proposed method is that it cannot work on perfectly frontal walks since the imaged motion plane would appear as a line in the image, and thus the planes metric could not be computed (the plane's vanishing line is confounded with the plane itself). In practice, view-rectification of near frontal view would also not work well since the imaged body-part positions are close the plane's vanishing line in the image, which means that even weak noise in the imaged body-part positions could result in strong noise in the rectified body-part positions. In this thesis, there is no body parts tracking performed in most such cases, and thus no view-rectification is performed.

The proposed walk model has another limitation regarding fast changes in walk direction. Indeed, a fast change in walk direction leads to motions that are not lying in planes in the scene. For instance, the motion of the moving foot cannot lie in a plane in such a case since the foot has to avoid colliding with the still foot. Moreover, the moving foot cannot pass on the other side of the still foot since this is physically impossible. Therefore, the 3-D trajectory of the moving foot in such case is not planar, and the imaged trajectory does not lie in the motion planes computed by the proposed view-rectification method. This means that in the case of a fast change in the walk direction, the resulting rectified trajectories will be deformed and thus will not represent the motion that has actually been performed in the scene. In this thesis, it is assumed that changes of direction may be present but are limited in speed and intensity.

Finally, one should notice that in the case of a walk with changes in walk direction, there may be discontinuities in the rectified foot trajectories. Although this may sound like a limitation, it is actually a feature of the proposed method. The reason is the proposed method has been designed to recover the actual motion performed by the head and the feet along with the spatial relation of the moving foot with respect to the head during each gait half-cycle. The proposed rectification method thus recovers the stride lengths along with the person displacement on the ground plane. Since the left and right strides length are not equal when a person changes its walk direction, it is not

[3]Further assumptions would have to be made on the hands motion since this motion is not as constrained as the foot motion during walking.

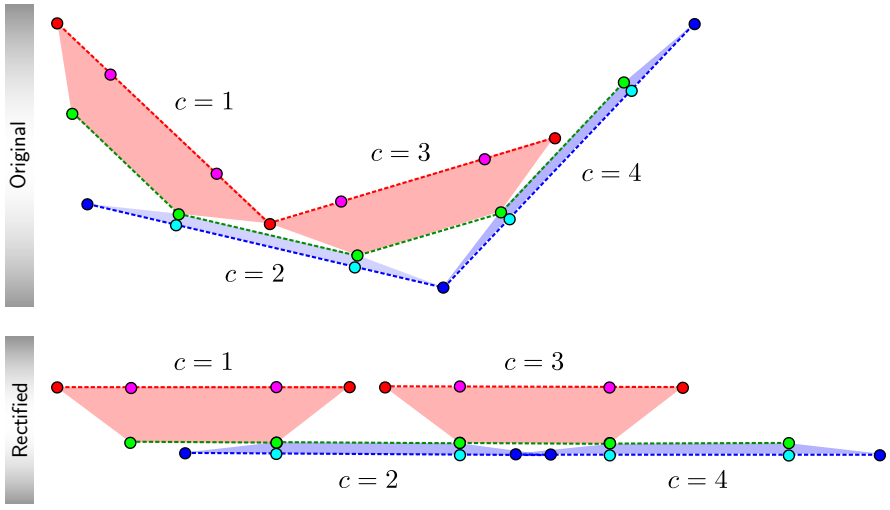

Figure 3.30 – Schematic representation of the foot trajectories discontinuities. The original extremities positions on the ground plane according the walk model are shown in the top figure for two gait cycles of a walk with two changes in the walk direction. The extremities positions are the right foot extremities (blue points), the left foot extremities (red points), the feet middle points (green points), and the projected middle points (magenta and cyan points). The stride lines and the displacement lines are also shown as red, blue and green dashed lines. Blue and red trapezoids are used here to link all the points for which the spatial relation is maintained by the rectification process. The schematic presenting the effect of the view-rectification method is shown on the bottom figure. There is a gap for the left foot during cycle 2, and an overlap for the right foot during cycle 3, since the left strides are shorter than the right strides.

possible to generate a side view of the feet trajectories that would not be disconnected between consecutive gait half-cycles.

Figure 3.30 depicts how such discontinuities may result from the view-rectification process. A top view of the positions of the extremities on the ground plane is shown, along with a top view of the position of these rectified extremities. Here, the strides length of the left foot are shorter than the strides length of the right foot. As mentioned previously, the effect of the rectification process is to "unfold" the walk with respect to the head planes, which are represented here by the displacement lines (green dashed lines). In order to preserve the spatial relation between the extremities and the strides length at each gait half-cycle, the foot extremities must be "detached". Here, the left foot (red) extremity is detached during cycle 2, which leads to two different positions of that foot extremity in the rectified walk. This thus forms a discontinuity, which occurs in the rectified left foot trajectory as a sudden gap in the middle of cycle 2. A similar effect occurs for the right foot, that is, the right foot (blue) extremity is detached during cycle 3. In that case, the discontinuity occurs in the right foot trajectory as a sudden

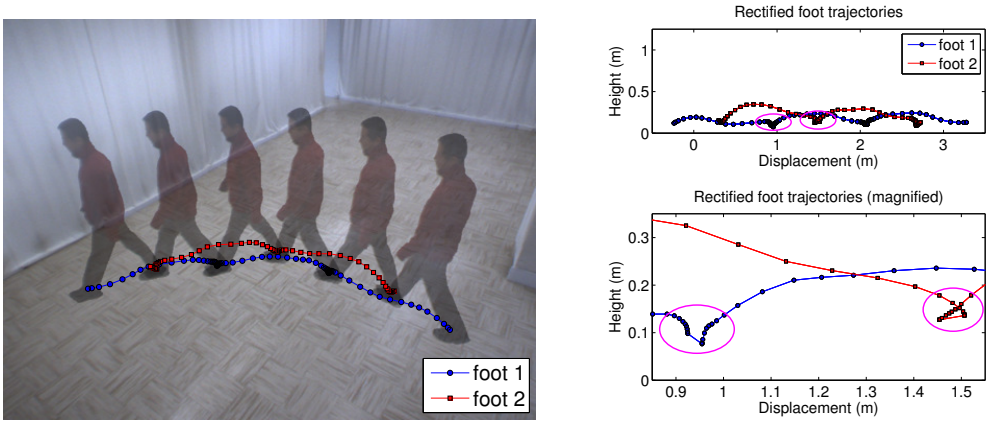

(a) (b)

Figure 3.31 – Example of discontinuities in the rectified foot trajectories. In (a), the original foot trajectories of a walk where the subject continuously change its walk direction are shown. The strides length of the left foot (foot 1) are shorter than the strides lengths of the right foot (foot 2). In (b), the complete rectified foot trajectories obtained with the proposed method are shown in the top figure, with magenta ellipses showing where discontinuities occur in the foot trajectories. A magnification of the discontinuities of the rectified foot trajectories is shown in the bottom figure.

overlap in the middle of cycle 3.

Figure 3.31 shows an example of such discontinuities for a real walk with a slow change in the walk direction. The imaged foot trajectories are shown in Figure 3.31(a). In this walk, the left strides are shorter than the right strides since the person performs a left change in walk direction. The complete rectified foot trajectories are shown at the top of Figure 3.31(b). Two magenta ellipses indicate the positions where the discontinuities occur in the rectified trajectories. The bottom part of Figure 3.31(b) shows a magnification of the trajectories to make the discontinuities more visible. The gap in left foot trajectory (blue) and the overlap in the right foot (red) trajectory are visible. It is important to realize that nothing can be done to remove these discontinuities if the stride lengths and the spatial relation of the head and the feet are to be preserved on a gait half-cycle basis. The proposed view-rectification method has been purposely designed on the basis that gait analysis and modelling is usually performed on a gait cycle basis or a gait half-cycle basis.

View-rectification of body-part trajectories using the proposed method will permit to perform view-invariant gait analysis and comparison since the rectified trajectories are free of the perspective distortion effect arising from observing people walking from non fronto-parallel viewpoints. The following chapter describes gait analysis and modelling methods that use as input the view-rectified body-part trajectories.

Chapter 4

Gait Analysis, Modelling, and Comparison

"I still believe in the possibility of a model of reality - that is to say, of a theory which represents things themselves and not merely the probability of their occurrence."

Albert Einstein

As previously discussed in Section 1.2, there are two main applications for gait analysis and modelling: medical applications and surveillance applications. In medical applications, an individual's gait is analyzed in order to detect pathologies related to human locomotion. This can be done by extracting measurements for each gait cycle, or by modelling the gait and comparing it to specific gait models that represent different pathologies or different conditions of a pathology. In surveillance applications, an individual's gait is modelled and compared to other individuals' gait for recognition purposes. Most of the gait analysis and modelling approaches in the literature target surveillance applications. This make these approaches hardly applicable to medical applications since they focus only on the extraction of gait features with high discriminating power.

It will be shown in this chapter that the rectified trajectories of the head and the feet, along with the rectified extremities and the rectified motion planes, are well suited for performing gait analysis, modelling, and comparison, and thus that the approach proposed in this thesis can be used in both medical and surveillance applications. Gait analysis is performed by extracting typical gait measurements (cadence, stride length, displacement, speed) from the rectified body-part extremities and the rectified motion

planes. Also, a dynamic gait model is computed from the view-rectified body-part trajectories. Gait models are then compared using off-the-shelf machine learning techniques.

This chapter is structured as follows. Section 4.1 presents the proposed gait analysis method. Next, a method for building a dynamic gait model is presented in Section 4.2. The method for comparing gait models is then described in Section 4.3. The chapter is concluded in Section 4.4.

4.1 Gait Analysis

Gait analysis is discussed here as a collection of gait measurements that are used in clinical gait analysis [3, 94, 95, 96, 97]. The purpose of this section is to show that the most common gait measurements can be extracted from the rectified body-part extremities and the rectified motion planes, and thus that the approach proposed in this thesis can be used for gait analysis.

The most common gait measurements that are considered here are the *stride length*, the *cadence*, and the *walking speed*. Other gait measurements are also considered, such as the *displacement* and the *gait half-cycle duration*, since they are needed to compute the cadence and the walking speed. Although a person's height is not a gait characteristic, its calculation is performed here since it is a useful measurement. The method used to compute these gait measurements are presented in the following sections.

4.1.1 Stride Length Computation

As mentioned previously in Section 3.3, the stride length δ_s is defined as the distance travelled by a foot during a gait half-cycle. It can be computed for a gait half-cycle c in interval i as

$$\delta_s[i,c] = \left\| \mathbf{e}'_{\mathsf{FS}}[i,c] - \mathbf{e}'_{\mathsf{FE}}[i,c] \right\|, \tag{4.1}$$

where $\mathbf{e}'_{\mathsf{FS}}[i,c]$ and $\mathbf{e}'_{\mathsf{FE}}[i,c]$ are the view-rectified moving foot extremity position at the beginning and at the end of the gait half-cycle c of interval i, respectively. The stride length is thus the distance between the view-rectified extremities of the moving foot for a given half-cycle in a tracking interval.

4.1.2 Displacement Computation

The displacement of a person corresponds to the distance travelled by the person's body in a gait half-cycle. The displacement δ_{d} during a gait half-cycle is defined as the distance between the rectified feet middle points, which are defined at the beginning and at the end of the gait half-cycle. As explained in Section 3.5.1.3, the feet middle points are used to define the head motion plane, that is, the bottom-start point $\boldsymbol{\pi}_{\mathsf{H,BS}}$ and the bottom-end point $\boldsymbol{\pi}_{\mathsf{H,BE}}$. Thus the rectified feet middle points correspond to the points $\boldsymbol{\pi}'_{\mathsf{H,BS}}$ and $\boldsymbol{\pi}'_{\mathsf{H,BE}}$ of the rectified head motion plane. The person's displacement during gait half-cycle c in interval i is then computed as

$$\delta_{\mathrm{d}}[i,c] = \left\| \boldsymbol{\pi}'_{\mathsf{H,BE}}[i,c] - \boldsymbol{\pi}'_{\mathsf{H,BS}}[i,c] \right\|, \tag{4.2}$$

that is, the distance between the rectified feet middle points.

4.1.3 Gait Half-cycle Duration Computation

The duration of a gait half-cycle c in interval i could be computed as $t_{i,c+1} - t_{i,c}$. However, the resulting duration would be expressed as a non-integer number of frames, which is not convenient since one needs to consider the camera frame rate to interpret the computed duration. It is thus better to compute the gait half-cycle duration in usual units, that is, in seconds.

Some cameras provide a *timestamp* for each acquired frame. Each timestamp represents either the elapsed time in seconds since the acquisition process started, or the actual time when each frame was acquired. These timestamps can thus be used to compute the gait-half cycle duration in seconds. The timestamp for a frame index n is denoted here as $T[n]$. In the case where no timestamp are provided by the camera, a timestamp can then be approximated as

$$T[n] = \frac{(n-1)}{f_{\mathrm{s}}}, \tag{4.3}$$

where f_{s} is the known camera acquisition frame rate. In this case, the timestamps for frames $n = 1, 2, \ldots, N$ are $0, \frac{1}{f_{\mathrm{s}}}, \frac{2}{f_{\mathrm{s}}}, \ldots, \frac{N}{f_{\mathrm{s}}}$.

Since the timestamps are only known for integer frame indexes, an interpolation must be performed in order to obtain the timestamps for non-integer frame indexes. A linear interpolation can be performed to obtain a timestamp at a non-integer frame index t as follows:

$$T(t) = T[\lfloor t \rfloor] + (t - \lfloor t \rfloor)(T[\lceil t \rceil] - T[\lfloor t \rfloor]). \tag{4.4}$$

As usual, the notation $T(\,\cdot\,)$ denotes the fact that the timestamps are expressed as a function of a continuous variable, while the notation $T[\,\cdot\,]$ denotes the fact that the timestamps are expressed as a function of a discrete variable.

Finally, the duration of gait half-cycle c in interval i is computed using the interpolated timestamps at key times $t_{i,c}$ and $t_{i,c+1}$:

$$\delta_{\mathrm{t}}[i,c] = T(t_{i,c+1}) - T(t_{i,c}). \tag{4.5}$$

4.1.4 Cadence Computation

A person's cadence is usually expressed as the number of steps performed in one minute (steps/min). One must note that one step is performed for each gait half-cycle, and thus the total number of steps performed during a walk is $\sum_{i=1}^{I} C_i$, where C_i is the number of gait half-cycle in the continuous tracking interval i. Therefore, the cadence η for a given walk is computed as

$$\eta = 60\,\frac{\sum\limits_{i=1}^{I} C_i}{\sum\limits_{i=1}^{I}\sum\limits_{c=1}^{C_i} \delta_{\mathrm{t}}[i,c]}, \tag{4.6}$$

where the denominator is the duration of the walk in seconds, and the factor 60 is used to convert units from steps/s to steps/min.

4.1.5 Speed Computation

Similarly to the cadence, a person's walking speed is usually expressed as the distance travelled in one minute, which is expressed in m/min. The walking speed ϕ for a given walk is computed as

$$\phi = 60\,\frac{\sum\limits_{i=1}^{I}\sum\limits_{c=1}^{C_i} \delta_{\mathrm{d}}[i,c]}{\sum\limits_{i=1}^{I}\sum\limits_{c=1}^{C_i} \delta_{\mathrm{t}}[i,c]}, \tag{4.7}$$

where the numerator is the total distance travelled during the walk in meters, and the denominator is the total duration of the walk in seconds. The factor 60 is used to convert the units from m/s to m/min.

4.1.6 Height Computation

A person's height can be computed for each gait half-cycle c of interval i. Height is usually measured as the distance from the ground to the extremity of the head while the person stands up still. Here, since the person is walking, the distance from the ground to the extremity of the head is always changing. The height is minimal at the key times (when the feet are furthest apart), and maximal somewhere close to the middle of a gait half-cycle (when the feet are the closest to each others). The height h of a person can then be approximated on a gait half-cycle basis as the maximum observed height:

$$h[i,c] = \max_n \big(p'_{\mathsf{HT},y}[n]\big), \quad n \in [\lceil t_{i,c} \rceil \,, \lfloor t_{i,c+1} \rfloor] \,, \tag{4.8}$$

where $p'_{\mathsf{HT},y}[n]$ is the y component of the rectified position of the top of the head at frame n. The rectified trajectory of the top of the head is considered here as an approximation to the head extremity since the latter can only be computed at each key time. One must note that the y component of the position $p_{\mathsf{HT},y}[n]$ directly approximates the height for frame n since the rectified motion planes were defined such that their bottom points have their y component equal to zero. Thus, the y component of the positions in all rectified trajectories and extremities directly represents the distance from the ground.

4.2 Gait Modelling

In this thesis, a novel gait model is proposed in order to perform gait modelling and comparison. The proposed gait model is based on the extraction of features from rectified body-part trajectories. This makes the proposed model unique since most gait models proposed in the literature are based on features extracted from silhouettes, as discussed in Section 1.3. The gait model described here will be used to show that the approach proposed in this thesis, which consists in using a metric view-rectification of the imaged body-part trajectories, is well suited for gait modelling and comparison.

The proposed gait model is defined on a gait half-cycle basis and is made of two parts: the first part models the gait half-cycles where the left foot is moving (part A), and the second part models the gait half-cycles where the right foot is moving (part B). Therefore, all gait half-cycles of a walk where the left foot is moving are used to build the part A, and all gait half-cycles of a walk where the right foot is moving are used to build the part B. Defining the gait model this way allows for detecting potential differences in the movement of the right and left body parts. For instance, this can be useful to model the gait of a limping person, or of a patient rehabilitating from stroke.

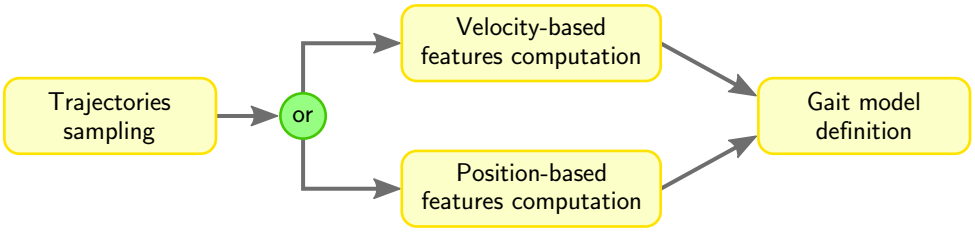

Figure 4.1 – Gait modelling overview.

An overview of the proposed method for gait modelling is presented in Figure 4.1. The first step consists in sampling the body-part trajectories in order to get the same number of positions in each gait half-cycle. Next, gait features are extracted using one of the two proposed methods, that is, gait features are either based on the position or on the velocity of the body parts. Finally, the gait model is defined using the extracted features. The method for body-part trajectories sampling is described in Section 4.2.1, and the methods for gait features extraction are described in Section 4.2.2. The definition of the gait model is detailed in Section 4.2.3.

4.2.1 View-rectified Body-part Trajectories Sampling

In order to obtain gait features that have the same number of components for all gait half-cycles, the body-part trajectories must be sampled, and a fixed, predetermined number of samples must be used for all gait models. Thus, Q sampled positions will be computed for the rectified head trajectory and the rectified moving foot trajectory in each gait half-cycle c of each tracking interval i. It must be noted that the trajectory of the still foot is not used in the proposed gait model, and therefore it is not sampled. The sampled positions computed from the head and the moving foot trajectories are respectively denoted $\mathbf{s}_{\mathsf{H}}[i,c,q]$ and $\mathbf{s}_{\mathsf{F}}[i,c,q]$, where $i = 1,2,\ldots,I$, $c = 1,2,\ldots,C_i$, and $q = 1,2,\ldots,Q$. They are computed by first temporally dividing the frame range of gait half-cycle c into $Q-1$ equal parts, which leads to Q frame indexes denoted $\gamma_{i,c,q}$:

$$\gamma_{i,c,q} = \lceil t_{i,c} \rceil + (q-1)\frac{\lfloor t_{i,c+1} \rfloor - \lceil t_{i,c} \rceil}{Q-1}, \tag{4.9}$$

for $q = 1,2,\ldots,Q$. One should note that $\gamma_{i,c,1} = \lceil t_{i,c} \rceil$ and $\gamma_{i,c,Q} = \lfloor t_{i,c+1} \rfloor$, that is, the first and the last frame indexes of gait half-cycle c (integer frame indexes), whereas the frames indexes $\gamma_{i,c,q}$ for $q = 2,3,\ldots,Q-1$ are in general non-integer frame indexes. The view-rectified head and foot trajectories are interpolated for these frame indexes

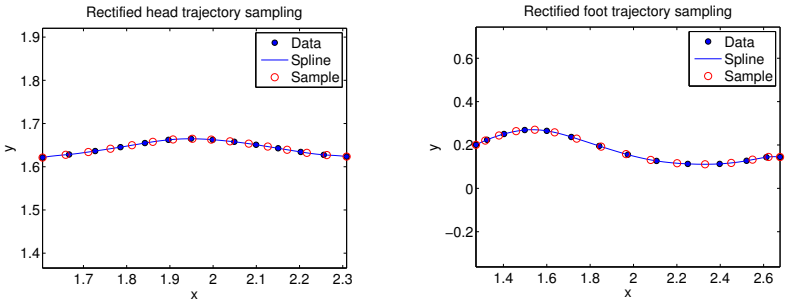

(a) (b)

Figure 4.2 – Example of sampled head and foot trajectories for a gait half-cycle. In (a), the sampled head trajectory, and in (b), the sampled foot trajectory. The view-rectified positions are shown as blue dots, the spline is shown as a continuous blue curve, and the sampled positions are shown as red circles. In this example, there are $Q = 16$ sampled positions.

using a cubic spline interpolation [100]:

$$\mathbf{s}_{\mathsf{H}}[i, c, q] = \text{spline}\big(\mathcal{T}'_{\mathsf{H},i}, \gamma_{i,c,q}\big), \tag{4.10}$$

$$\mathbf{s}_{\mathsf{F}}[i, c, q] = \text{spline}\big(\mathcal{T}'_{m,i}, \gamma_{i,c,q}\big), \tag{4.11}$$

where $\mathcal{T}'_{\mathsf{H},i}$ and $\mathcal{T}'_{m,i}$ are defined as

$$\mathcal{T}'_{\mathsf{H},i} : \big\{\mathbf{p}'_{\mathsf{H}}[n] \mid n \in [n_{\mathrm{S},i}, n_{\mathrm{E},i}]\big\}, \tag{4.12}$$

$$\mathcal{T}'_{m,i} : \big\{\mathbf{p}'_{m}[n] \mid n \in [n_{\mathrm{S},i}, n_{\mathrm{E},i}]\big\}, \tag{4.13}$$

which are the whole view-rectified trajectories in interval i for the head and the foot with label m, where m is defined as the label (L or R) of the foot moving in gait half-cycle c. The operator $\text{spline}(\mathcal{T}, \gamma)$ interpolates a 2-D position at non-integer frame γ by computing a cubic spline on the ordered set of 2-D positions in trajectory $\mathcal{T}$. One must note that a 2-D cubic spline interpolation simply consists in performing two independent 1-D cubic spline interpolations on the components x and y of the 2-D positions.

Figure 4.2 shows an example of sampled head and foot positions for a gait half-cycle where the number of samples per gait half-cycle is set to $Q = 16$. It is possible to see that the first and last samples in each case correspond to the first and the last positions of the body part in the given gait half-cycle, respectively. Also, one must note that the samples were designed to be equally spaced on the time axis, which makes them not necessarily equally spaced on the x and y axes. One may think of the qth sample as the position of the body part at $100\frac{q-1}{Q-1}$ % of a gait half-cycle.

4.2.2 Gait Features Computation

Gait features are extracted on a gait half-cycle basis from the sampled positions obtained with the method discussed in Section 4.2.1. Two types of features are proposed in this thesis: position-based features, and velocity-based features. These two types of features are designed to represent the dynamics of the gait, and thus, only the sampled positions of the head and the moving foot in a gait half-cycle are considered. The positions of the still foot in a gait half-cycle are not used to extract gait features since there is no motion performed by the foot, and thus there is no features representing the dynamic aspect of the gait to extract from them. The computation of the position-based features is described in Section 4.2.2.1, while the computation of the velocity-based feature is described in Section 4.2.2.2.

4.2.2.1 Position-based Features Computation

The position-based features are actually the sampled head and moving foot positions for which the mean position is removed:

$$\mathbf{s}'_\ell[i,c,q] = \mathbf{s}_\ell[i,c,q] - \frac{1}{Q}\sum_{q=1}^{Q}\mathbf{s}_\ell[i,c,q], \tag{4.14}$$

where $\ell \in \{\mathsf{H},\mathsf{F}\}$, and $q = 1,2,\ldots,Q$. It is possible to see that the mean of the positions $\mathbf{s}'_\ell[i,c,q]$ is $[0,\ 0]^\mathsf{T}$. The positions $\mathbf{s}'_\ell[i,c,q]$ in a given gait half-cycle c are used as gait features since they are no more related to the origin of the rectified trajectory space. It is possible for instance to compare the qth sampled position $\mathbf{s}'_\ell[i,c_1,q]$ in half-cycle c_1 to the corresponding qth sampled position $\mathbf{s}'_\ell[i,c_2,q]$ in gait half-cycle c_2.

4.2.2.2 Velocity-based Features Computation

The velocity-based features are computed from the sampled head and moving foot positions as

$$\dot{\mathbf{s}}_\ell[i,c,q] = \frac{\mathbf{s}_\ell[i,c,q+1] - \mathbf{s}_\ell[i,c,q]}{T(\gamma_{i,c,q+1}) - T(\gamma_{i,c,q})} \quad \text{for } q = 1,2,\ldots,Q-1, \tag{4.15}$$

where $T(\gamma_{i,c,q+1})$ and $T(\gamma_{i,c,q})$ are the timestamps computed with Equation 4.4 at non-integer frames $\gamma_{i,c,q+1}$ and $\gamma_{i,c,q}$, respectively. The velocity vector $\dot{\mathbf{s}}_\ell[i,c,q]$ thus represents both the speed and the travelling direction of the body part from the qth sampled position to the $(q+1)$th sampled position.

Algorithm 4.1: Gait feature vectors definition.

$G_{\mathsf{A}} = 0$
$G_{\mathsf{B}} = 0$
for $i = 1, 2, \ldots, I$ **do** ⇒ *for each continuous tracking interval*
  for $c = 1, 2, \ldots, C_i$ **do** ⇒ *for each gait half-cycle*
    if $m = \mathsf{L}$ **then** ⇒ *moving foot is the left foot*
      $G_{\mathsf{A}} = G_{\mathsf{A}} + 1$
      $\mathbf{g}_{\mathsf{A}}[G_{\mathsf{A}}] = \mathrm{cat}\big(\{\dot{\mathbf{s}}_{\mathsf{H}}[i, c, q]\}_q, \{\dot{\mathbf{s}}_{\mathsf{F}}[i, c, q]\}_q\big)$
    else if $m = \mathsf{R}$ **then** ⇒ *moving foot is the right foot*
      $G_{\mathsf{B}} = G_{\mathsf{B}} + 1$
      $\mathbf{g}_{\mathsf{B}}[G_{\mathsf{B}}] = \mathrm{cat}\big(\{\dot{\mathbf{s}}_{\mathsf{H}}[i, c, q]\}_q, \{\dot{\mathbf{s}}_{\mathsf{F}}[i, c, q]\}_q\big)$
    end if
  end for
end for

4.2.3 Gait Model Definition

Once the gait features have been computed from the sampled body-part positions (position-based or velocity-based features), it is possible to define the *two-part* gait model. The proposed gait model is said to be constituted of two parts since there is a gait model defined for each type of gait half-cycle, that is, one model for gait half-cycles where the left foot is moving (part A) and one model for gait half-cycles where the right foot is moving (part B). Each part of the gait model will always be considered independently, since they are considered here as potentially different.

For a given walk sequence, the first step for the definition of the two-part gait model is to create a feature vector for each gait half-cycle. A gait feature vector is created according to Algorithm 4.1, and is denoted either $\mathbf{g}_{\mathsf{A}}$ or $\mathbf{g}_{\mathsf{B}}$ depending on the type of gait half-cycle it comes from. There are G_{A} gait features vectors for part A and G_{B} gait feature vectors for part B defined for a given walk sequence, and thus $G_{\mathsf{A}} + G_{\mathsf{B}} = \sum_{i=1}^{I} C_i$. Each gait feature vector is defined as the concatenation of the sampled gait features (here the velocity-based gait features are used) for the head and for the moving foot. The notation $\{\dot{\mathbf{s}}_\ell[i, c, q]\}_q$ denotes the set of all velocity samples for the body part $\ell \in \{\mathsf{H}, \mathsf{F}\}$ in gait half-cycle c of interval i, where $q = 1, 2, \ldots, Q - 1$. One must note that the gait feature vectors can also be defined using the position-based gait features by using $\mathbf{s}'_\ell$ instead of $\dot{\mathbf{s}}_\ell$, and by considering $q = 1, 2, \ldots, Q$. The operator $\mathrm{cat}(\{\,\cdot\,\}, \{\,\cdot\,\})$ concatenates the velocity-based gait feature samples for the head and the

foot into a single vector as follows:

$$\begin{aligned}\mathrm{cat}\big(\{\dot{\mathbf{s}}_{\mathsf{H}}[i,c,q]\}_q, \{\dot{\mathbf{s}}_{\mathsf{F}}[i,c,q]\}_q\big) = \Big(&\dot{s}_{\mathsf{H},x}[i,c,1],\ldots,\dot{s}_{\mathsf{H},x}[i,c,Q-1],\\ &\dot{s}_{\mathsf{H},y}[i,c,1],\ldots,\dot{s}_{\mathsf{H},y}[i,c,Q-1],\\ &\dot{s}_{\mathsf{F},x}[i,c,1],\ldots,\dot{s}_{\mathsf{F},x}[i,c,Q-1],\\ &\dot{s}_{\mathsf{F},y}[i,c,1],\ldots,\dot{s}_{\mathsf{F},y}[i,c,Q-1]\Big)^{\mathsf{T}},\end{aligned} \tag{4.16}$$

where $\dot{s}_{\ell,x}$ and $\dot{s}_{\ell,y}$ are the x and y sampled velocity components of the body part $\ell \in \{\mathsf{H},\mathsf{F}\}$. In the case of the position-based gait features, the concatenation is performed as follows:

$$\begin{aligned}\mathrm{cat}\big(\{\mathbf{s}'_{\mathsf{H}}[i,c,q]\}_q, \{\mathbf{s}'_{\mathsf{F}}[i,c,q]\}_q\big) = \Big(&s'_{\mathsf{H},x}[i,c,1],\ldots,s'_{\mathsf{H},x}[i,c,Q],\\ &s'_{\mathsf{H},y}[i,c,1],\ldots,s'_{\mathsf{H},y}[i,c,Q],\\ &s'_{\mathsf{F},x}[i,c,1],\ldots,s'_{\mathsf{F},x}[i,c,Q],\\ &s'_{\mathsf{F},y}[i,c,1],\ldots,s'_{\mathsf{F},y}[i,c,Q]\Big)^{\mathsf{T}},\end{aligned} \tag{4.17}$$

where $s'_{\ell,x}$ and $s'_{\ell,y}$ are the x and y sampled position components of the body part $\ell \in \{\mathsf{H},\mathsf{F}\}$. The gait feature vectors $\mathbf{g}_{\mathsf{A}}$, $\mathbf{g}_{\mathsf{B}}$ have $D = 4(Q-1)$ components when the velocity-based gait features are used, and $D = 4Q$ components when the position-based gait features are used.

Once the gait feature vectors are obtained for all the gait half-cycles of a walk, the two-part gait model is defined as the two average gait feature vectors $\overline{\mathbf{g}}_{\mathsf{A}}$ and $\overline{\mathbf{g}}_{\mathsf{B}}$:

$$\overline{\mathbf{g}}_{\mathsf{A}} = \frac{1}{G_{\mathsf{A}}}\sum_{\alpha=1}^{G_{\mathsf{A}}}\mathbf{g}_{\mathsf{A}}[\alpha], \tag{4.18}$$

$$\overline{\mathbf{g}}_{\mathsf{B}} = \frac{1}{G_{\mathsf{B}}}\sum_{\beta=1}^{G_{\mathsf{B}}}\mathbf{g}_{\mathsf{B}}[\beta]. \tag{4.19}$$

For a walk performed by a given subject, the two-part gait model is thus defined as an average gait half-cycle of type A and an average gait half-cycle of type B, which are based on either the position or the velocity of the body parts.

Figure 4.3 shows an example of a position-based gait model and an example of a velocity-based gait model, both of which were computed from the view-rectified body-part trajectories shown in Figure 3.26. The two-part gait model obtained using position-based gait features is shown in Figures 4.3(a) and 4.3(b), and the two-part gait model obtained using velocity-based gait features is shown in Figures 4.3(c) and 4.3(d). Part A of a gait model ($\overline{\mathbf{g}}_{\mathsf{A}}$) is shown as a red curve , whereas part B of a gait model ($\overline{\mathbf{g}}_{\mathsf{B}}$) is

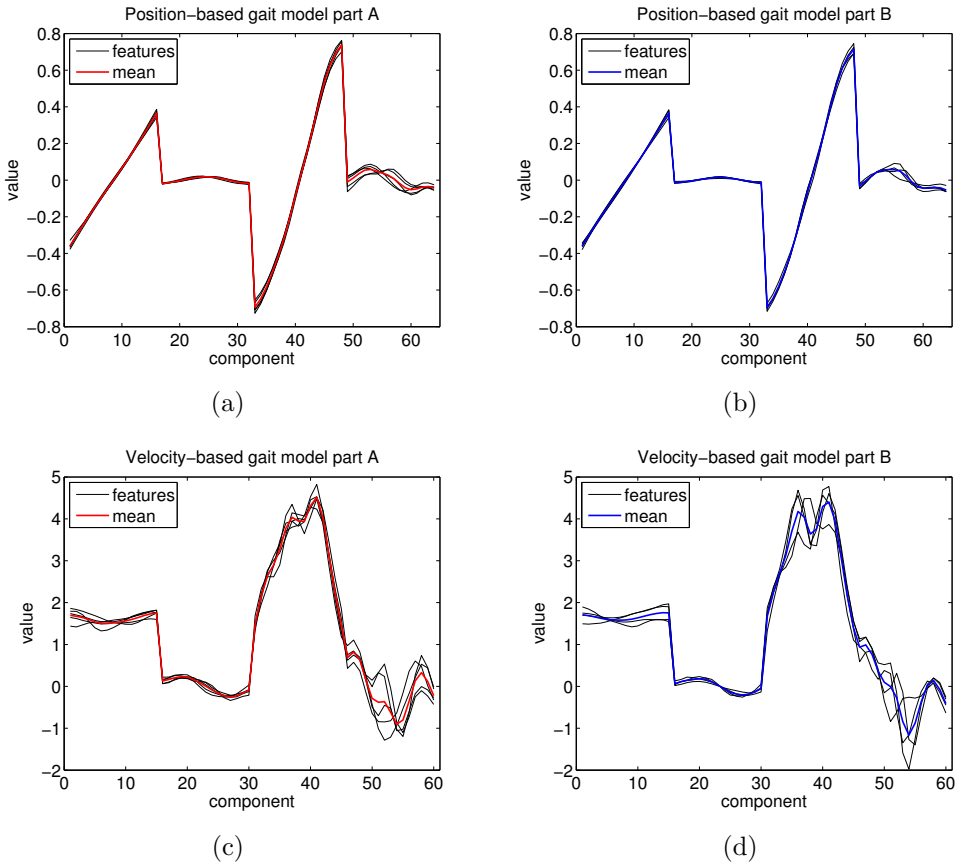

Figure 4.3 – Example of a position-based gait model and a velocity-based gait model. Parts A and B of the position-based gait model are shown in (a) and (b), respectively. Parts A and B of the velocity-based gait model are shown in (c) and (d), respectively. Each black curve represents a gait feature vector ($\mathbf{g}_{\mathsf{A}}[\alpha]$ or $\mathbf{g}_{\mathsf{B}}[\beta]$) computed for a gait half-cycle. The average gait feature vectors $\overline{\mathbf{g}}_{\mathsf{A}}$ and $\overline{\mathbf{g}}_{\mathsf{B}}$ are shown as a red curve and a blue curve, respectively. The red curve in (a) and the blue curve in (b) form the position-based gait model for the walk, while the red curve in (c) and the blue curve in (d) form the velocity-based gait model for the walk.

shown as a blue curve. Each black curve in the figures represents a gait feature vector ($\mathbf{g}_{\mathsf{A}}[\alpha]$ or $\mathbf{g}_{\mathsf{B}}[\beta]$) computed for a gait half-cycle of the walk. It is possible to see that the part A and the part B of a gait model are similar in the case of this walk. Also, one can notice that there is more variance across the gait half-cycles for the velocity-based features. One of the reasons for this is that the derivative is sensitive to the noise in the body-part positions. Another reason is that the walking speed was not constant, that is, the person had to decelerate in order to turn, and then had to accelerate to continue walking on a straight line (see Figure 3.17).

4.3 Gait Model Comparison

Gait model comparison consists in computing a distance between two gait models. A gait model is usually compared to many other gait models in order to classify it in one of a certain number R of known classes (categories), where each class is represented by one or more gait models. The gait model to be classified is called the probe, whereas the set of gait models representing the different classes is called the gallery. For surveillance applications, there would be one class for each person to recognize, and thus the gait model(s) associated to each class would represent a specific person's gait. A probe gait model, which comes from a person to be identified, would then be compared to the gait model(s) of each subject (class), and the class for which the distance is the smallest would be assigned to the probe model. In the case of medical applications, each class could represents, for instance, a different pathology related to the gait. Therefore, each class would be represented by a gait model that represents a representative gait for the given pathology. The pathology associated with a given probe gait model would be the one for which the distance would be the smallest. These surveillance and medical applications apply to the case where no new classes are encountered during the classification process, that is, the set of people or pathologies to recognize is fixed. This is known as *closed set classification*, whereas the case where new classes are encountered during the classification process is known as *opened set classification*. The latter is much more complicated, and is thus not considered in most of the work on gait analysis and recognition.

For both surveillance and medical applications, there can be a learning phase where an improved representation for the gait models is learned. Learning an improved representation for the gait models can be performed by using one of the many machine learning techniques that are available in the literature [101, 102, 103]. *Linear Discriminant Analysis* (LDA) is used here since it provides a transform that projects the gait models into a lower dimensional feature space where the overall separability of the classes is optimal. Indeed, LDA deals directly with multi-class problems, unlike other methods (e.g. Support Vector Machines) that only works on two-class problems, and thus requires a one-against-all or one-against-one strategy when they are used on multi-class problems.

Figure 4.4 shows an overview of the gait model comparison method used in this thesis. Without loss of generality, the gait comparison method will be described here in the context of surveillance applications. First, a LDA is performed on the set of all gait models in the gallery in order to learn an improved and more efficient representation of the gait models. A probe gait model is then compared to a gait model in the gallery

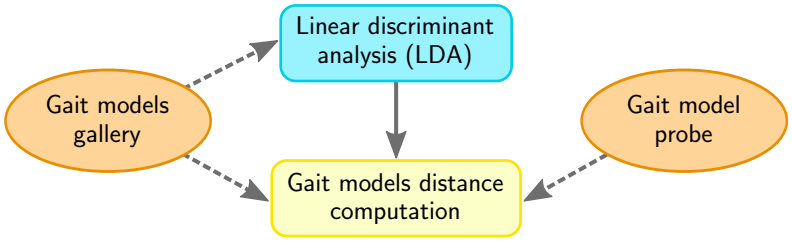

Figure 4.4 – Gait models comparison overview.

by computing a distance between the improved representation of both the gallery gait model and the probe gait model. The learning process is described in Section 4.3.1, while the gait models distance computation is detailed in Section 4.3.2.

4.3.1 Linear Discriminant Analysis

An improved representation for the gait models is learned from all the gait models in the gallery using the LDA method. The gallery consists in a two-part gait model for each of the R considered subjects (classes) in a surveillance systems. The two-part gait model in the gallery for subject r is denoted $(\overline{\mathbf{g}}_{\mathsf{A},r}, \overline{\mathbf{g}}_{\mathsf{B},r})$, where $\overline{\mathbf{g}}_{\mathsf{A},r}$ and $\overline{\mathbf{g}}_{\mathsf{B},r}$ are the parts A and B of the gait model, respectively. As mentioned previously, each part of the gait model is defined as the average gait feature vectors computed from half-cycles of type A and B:

$$\overline{\mathbf{g}}_{\mathsf{A},r} = \frac{1}{G_{\mathsf{A},r}} \sum_{\alpha=1}^{G_{\mathsf{A},r}} \mathbf{g}_{\mathsf{A},r}[\alpha], \tag{4.20}$$

$$\overline{\mathbf{g}}_{\mathsf{B},r} = \frac{1}{G_{\mathsf{B},r}} \sum_{\beta=1}^{G_{\mathsf{B},r}} \mathbf{g}_{\mathsf{B},r}[\beta], \tag{4.21}$$

where $\mathbf{g}_{\mathsf{A},r}[\alpha]$ and $\mathbf{g}_{\mathsf{B},r}[\beta]$ are gait feature vectors, and $G_{\mathsf{A},r}$ and $G_{\mathsf{B},r}$ are the number of gait feature vectors of type A and B, respectively. One must note that the gait feature vectors may be obtained from more than one walk for a given subject.

The LDA method consists in determining a transform matrix $\mathbf{W}$ that projects the feature vectors of all subjects into a lower dimensional feature space where the overall linear separability between the subjects is optimal. Here, two transform matrices, $\mathbf{W}_{\mathsf{A}}$ and $\mathbf{W}_{\mathsf{B}}$, will be determined independently for parts A and B of the gait models. These transform matrices will project the gait feature vectors of part A and B into two new

feature spaces as follows:

$$\mathbf{g}'_{\mathsf{A},r}[\alpha] = \mathbf{W}_{\mathsf{A}}^{\mathsf{T}}\, \mathbf{g}_{\mathsf{A},r}[\alpha], \quad \alpha = 1, 2, \ldots, G_{\mathsf{A},r}, \tag{4.22}$$

$$\mathbf{g}'_{\mathsf{B},r}[\beta] = \mathbf{W}_{\mathsf{B}}^{\mathsf{T}}\, \mathbf{g}_{\mathsf{B},r}[\beta], \quad \beta = 1, 2, \ldots, G_{\mathsf{B},r}, \tag{4.23}$$

where $\mathbf{g}'_{\mathsf{A},r}[\alpha]$ and $\mathbf{g}'_{\mathsf{B},r}[\beta]$ are the projected gait feature vectors, and $r = 1, 2, \ldots, R$. Since the matrices $\mathbf{W}_{\mathsf{A}}$ and $\mathbf{W}_{\mathsf{B}}$ are determined independently in the same way, the notation A and B will be temporarily dropped in the following.

The transform matrix that leads to the optimal linear separability between the subjects is the matrix $\mathbf{W}^*$ such that

$$\mathbf{W}^* = \arg\max_{\mathbf{W}} \left(\frac{\det\left(\mathbf{W}^{\mathsf{T}}\, \mathbf{S}_{\mathrm{B}}\, \mathbf{W}\right)}{\det\left(\mathbf{W}^{\mathsf{T}}\, \mathbf{S}_{\mathrm{W}}\, \mathbf{W}\right)} \right), \tag{4.24}$$

where $\det(\,\cdot\,)$ is the determinant operator, and where $\mathbf{S}_{\mathrm{B}}$ and $\mathbf{S}_{\mathrm{W}}$ are respectively the *between-subject scatter matrix* and the *within-subject scatter matrix*, which are going to be defined shortly. The matrix $\mathbf{W}^*$ is $D \times (R-1)$ in size, where D is the dimensionality of the gait feature vectors (number of components), and R is the number of subjects. This matrix is comprised of the eigenvectors of $\mathbf{S}_{\mathrm{W}}^{-1}\mathbf{S}_{\mathrm{B}}$ that corresponds to its $R-1$ largest eigenvalues.

The within-subject scatter matrix $\mathbf{S}_{\mathrm{W}}$, which is known in the literature as the *within-class scatter matrix*, is defined as

$$\mathbf{S}_{\mathrm{W}} = \sum_{r=1}^{R} \mathbf{S}_r, \tag{4.25}$$

where the scatter matrix $\mathbf{S}_r$ for subject r is defined as

$$\mathbf{S}_r = \sum_{j=1}^{G_r} \left(\mathbf{g}_r[j] - \overline{\mathbf{g}}_r\right) \left(\mathbf{g}_r[j] - \overline{\mathbf{g}}_r\right)^{\mathsf{T}}, \tag{4.26}$$

with $\overline{\mathbf{g}}_r$ being the mean of the gait feature vectors $\mathbf{g}_r[j]$ for subject r, which is the gait model of subject r as well:

$$\overline{\mathbf{g}}_r = \frac{1}{G_r} \sum_{j=1}^{G_r} \mathbf{g}_r[j]. \tag{4.27}$$

The between-subject scatter matrix $\mathbf{S}_{\mathrm{B}}$, which is known in the literature as the *between-class scatter matrix*, is defined as

$$\mathbf{S}_{\mathrm{B}} = \sum_{r=1}^{R} G_r \left(\overline{\mathbf{g}}_r - \boldsymbol{\mu}\right) \left(\overline{\mathbf{g}}_r - \boldsymbol{\mu}\right)^{\mathsf{T}}, \tag{4.28}$$

where G_r is the number of gait feature vectors for subject r, and $\boldsymbol{\mu}$ is the mean of the gait feature vectors of all the subjects, that is,

$$\boldsymbol{\mu} = \frac{\sum_{r=1}^{R} G_r \overline{\mathbf{g}}_r}{\sum_{r=1}^{R} G_r}. \tag{4.29}$$

Once the matrices $\mathbf{W}_{\mathsf{A}}$ and $\mathbf{W}_{\mathsf{B}}$ are obtained, the two-part gait model $(\overline{\mathbf{g}}_{\mathsf{A},r}, \overline{\mathbf{g}}_{\mathsf{B},r})$ of each subject is projected into the lower dimensional feature spaces as follows:

$$\overline{\mathbf{g}}'_{\mathsf{A},r} = \mathbf{W}_{\mathsf{A}}^{\mathsf{T}} \overline{\mathbf{g}}_{\mathsf{A},r}, \tag{4.30}$$

$$\overline{\mathbf{g}}'_{\mathsf{B},r} = \mathbf{W}_{\mathsf{B}}^{\mathsf{T}} \overline{\mathbf{g}}_{\mathsf{B},r}. \tag{4.31}$$

The two-part projected gait models $(\overline{\mathbf{g}}'_{\mathsf{A},r}, \overline{\mathbf{g}}'_{\mathsf{B},r})$ will be used in the following for gait model distance computation.

4.3.2 Gait Model Distance Computation

As mentioned previously, gait comparison is performed by computing distances between a probe gait model and the gait models in the gallery. The main objective of gait comparison is the classification of a probe gait model for which the class (i.e subject identity) is presumably unknown. First, the two parts of the probe gait model, which is denoted $(\overline{\mathbf{x}}_{\mathsf{A}}, \overline{\mathbf{x}}_{\mathsf{B}})$, are projected in their respective lower dimensional feature space as follows:

$$\overline{\mathbf{x}}'_{\mathsf{A}} = \mathbf{W}_{\mathsf{A}}^{\mathsf{T}} \overline{\mathbf{x}}_{\mathsf{A}}, \tag{4.32}$$

$$\overline{\mathbf{x}}'_{\mathsf{B}} = \mathbf{W}_{\mathsf{B}}^{\mathsf{T}} \overline{\mathbf{x}}_{\mathsf{B}}. \tag{4.33}$$

A distance $\Delta\left((\overline{\mathbf{g}}'_{\mathsf{A},r}, \overline{\mathbf{g}}'_{\mathsf{B},r}); (\overline{\mathbf{x}}'_{\mathsf{A}}, \overline{\mathbf{x}}'_{\mathsf{B}})\right)$ between the projected probe gait model and the projected gait model of subject r in the gallery can be computed as

$$\Delta\left((\overline{\mathbf{g}}'_{\mathsf{A},r}, \overline{\mathbf{g}}'_{\mathsf{B},r}); (\overline{\mathbf{x}}'_{\mathsf{A}}, \overline{\mathbf{x}}'_{\mathsf{B}})\right) = \left\|\overline{\mathbf{g}}'_{\mathsf{A},r} - \overline{\mathbf{x}}'_{\mathsf{A}}\right\| + \left\|\overline{\mathbf{g}}'_{\mathsf{B},r} - \overline{\mathbf{x}}'_{\mathsf{B}}\right\|, \tag{4.34}$$

where $\|\cdot\|$ denotes the Euclidean distance. One can see here that the distance is defined as the sum of the Euclidean distances computed independently on the part A and B of the gait models. Therefore, each of the two parts of the probe gait model is compared with the corresponding part of a gait model in the gallery. As discussed previously, this permits to take into account the possible differences between the gait half-cycles of types A and B.

4.4 Conclusion

The gait analysis, modelling and comparison methods presented in this chapter show that it is possible to extract useful measurements and features from the view-rectified body-part trajectories. Gait is analyzed by extracting gait measurements from the view-rectified extremities and other intermediate results from the view-rectification process. Gait modelling is performed by extracting dynamic gait features from two types of gait half-cycles. Gait models are compared by first performing a LDA to learn an improved representation for which the overall separability of the different gait classes is optimal, and then by computing a distance between gait models projected in the learned feature space.

It is important to see that the computed gait measurements and gait models will be expressed in the same units that are used in the view-rectification process described in Chapter 3. Performing the view-rectification process in scene units (in meters) provides a physical meaning for the gait measurements and allows for the comparison of gait models obtained from different camera setups. If the units are arbitrary, the gait measurements lose their physical meaning but can still be used for comparison with other gait measurements obtained from the same camera. For instance, it is possible to determine that a certain subject has strides lengths that are x times greater than another subject. Also, the gait models obtained with arbitrary units can still be used for gait comparison as long as the gait models have been extracted from the same camera setup.

The following chapter presents the experimental results obtained from the gait analysis, modelling and comparison methods presented in this chapter. Although the gait modelling and comparison experiments are performed in the context of surveillance applications, one must note that the proposed methods apply to medical applications as well since the only difference is the nature of the classes.

Chapter 5

Experimental Results

"In a very large part of morphology,
our essential task lies in the
comparison of related forms rather
than in the precise definition of each."

D'Arcy Thompson
"On Growth and Form", 1917

This chapter presents the results of the experiments that were performed as part of this thesis. The experimental results presented here show that the approach proposed in this thesis is well suited for gait analysis, modelling and comparison from unconstrained walks and viewpoints. In order to do so, both synthetic and real walks are used. Overall, the experiments are aimed at validating and characterizing the performance and the robustness of the view-rectification method presented in Chapter 3, as well as the suitability of the gait analysis, modelling, and comparison methods presented in Chapter 4. The quality of the body-part trajectories produced by the body-part tracking method presented in Chapter 2 is indirectly assessed in experiments involving real walks.

The proposed view-rectification method is first validated using *synthetic walks*, that is, walks that are generated so that both the 3-D positions of the body parts and their imaged counterpart are known. This permits to confirm that the view-rectified body-part trajectories represent what can be observed from a fronto-parallel viewpoint, and that the gait measurements extracted from them correspond to the measurements in the *synthetic scene*. The validation results of the view-rectification method using synthetic walks are presented and discussed in Section 5.1.

Secondly, the view-rectification method is tested on a gait database consisting in real walks performed by several subjects observed from a single fixed camera. This gait database consists in walks with changes in the walk direction, and thus the subjects are viewed from an extensive range of viewpoints. The view-rectified body-part trajectories obtained from these real walks is then used to perform gait analysis, modelling and comparison. Firstly, the gait measurements extracted from the view-rectified body-part trajectories is presented and discussed. Gait models is then learned for all subjects and gait comparison experiments is performed with the goal of identifying the subjects using their gait. The experimental results obtained on the real walks are presented and discussed in Section 5.2.

5.1 Validation of the View-rectification Method

The view-rectification method is validated using synthetic walks since it is the most convenient way to assess its performance and the validity of the view-rectified body-part trajectories. Indeed, the validation of the view-rectification using real walks would imply that the 3-D positions of each body parts are known, along with the corresponding imaged body-part positions. This would necessitate the use of an expensive motion capture system, and one would have to ensure that there is a correspondence between the acquired 3-D body-part positions and the imaged body-part positions, which is not a trivial task. Therefore, the generation of synthetic walks in a synthetic scene is the selected approach.

A synthetic walk consists in generated 3-D body-parts trajectories that are realistic enough to be processed by the proposed view-rectification algorithm. Here, "realistic enough" means that the generated body-part trajectories are designed to represent as much as possible real body-part trajectories, but without being a perfect reproduction of the motion made by real body-parts. As it will be shown shortly, these synthetic 3-D body-parts trajectories, along with their synthetic imaged counterpart, are suitable for validating the view-rectification method.

The validation of the view-rectification method consists in extracting gait measurements from the view-rectified body-part trajectories and comparing these measurements with the corresponding ground truth measurements, that is, the gait measurements performed on the generated 3-D body-part trajectories. This first validation is performed for different noise levels added to the imaged body-part trajectories. A second validation process consists in computing error statistics between the view-rectified body-part positions and the ground truth positions in the scene. Finally, the ground vanishing

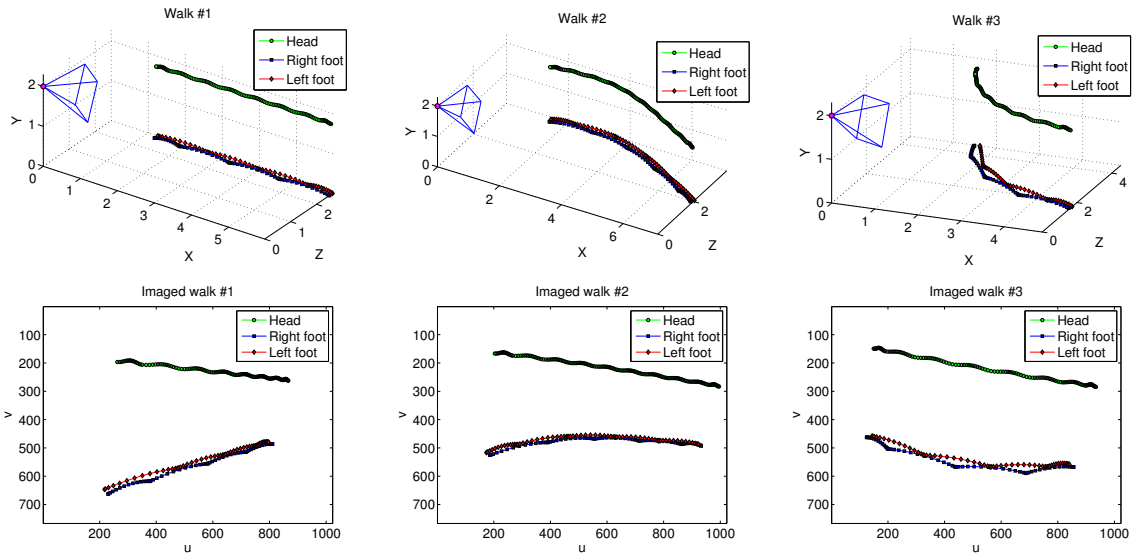

Figure 5.1 – The three synthetic walks used for the validation of the proposed view-rectification method. The first row shows the body-part trajectories in the synthetic scene, along with the orientation (blue pyramid) and the position of the synthetic camera (magenta point, pyramid's apex). The second row shows the imaged body-part trajectories for each walk.

line estimated in the step 0 of the proposed view-rectification method (see Section 3.9) is compared to the ground truth vanishing line for the different noise levels.

The synthetic walks that were generated for this thesis are presented in Section 5.1.1. The validation results of the view-rectified body part-trajectories are presented in Section 5.1.2, while the validation results of the estimated ground vanishing line are presented in Section 5.1.3.

5.1.1 Synthetic Walks Generation

Synthetic walks are generated using the method detailed in Appendix A, which was developed as part of this thesis. This method first generates the 3-D trajectories of the head and the feet using user-provided parameters describing the desired walk path and the "synthetic walker" gait parameters. The 2-D imaged body-part trajectories are then generated using a synthetic camera in the synthetic scene. As explained in Appendix A, the method generates the trajectory of body-part extremities. Thus, minor changes are required to the view-rectification method since no body-part mass centres and bounding

boxes are generated (see Section A.4).

The validation process is performed using the three synthetic walks presented in Figure 5.1. The first row of Figure 5.1 shows the 3-D body-part trajectories in the synthetic scene. The Y axis in the scene represents the vertical direction, while the $X-Z$ plane ($Y=0$) represents the ground plane. The orientation and the position of the synthetic camera is depicted as a blue pyramid for which the apex represents the camera position in the scene. The second row of Figure 5.1 shows the images generated using this synthetic camera. One may see the perspective distortion in the imaged body-part trajectories, which is induced by the camera viewpoint and the changes in the walk direction.

The parameters of each synthetic walk are summarized in Table 5.1. These synthetic walks are designed to provide different viewpoints from which the effects of perspective distortion cannot be neglected. For instance, the first walk consists in a straight walk defined at an angle of 45° with respect to the camera optical axis. In the second walk, there is one smooth change in the walk direction, whereas in the third walk, the direction of walk is continuously changing.

Walk (#)	Leading foot $l \in \{\mathsf{L},\mathsf{R}\}$	Initial position $\mathbf{O}$	Motion directions $\{\theta_j\}$
1	R	$(1.25, 0, 2.5)^{\mathsf{T}}$	$\{0°, 0°, 0°, 0°\}$
2	L	$(1.5, 0, 3.75)^{\mathsf{T}}$	$\{10°, 0°, -20°, -30°, -30°\}$
3	R	$(1.5, 0, 4.5)^{\mathsf{T}}$	$\{-75°, -55°, -35°, -15°\}$

Table 5.1 – Synthetic walk parameters.

The gait parameters for the three walks of the "synthetic walker" are summarized in Table 5.2. These parameters represent a realistic gait and are supported by the values reported in clinical studies [94, 95]. For instance, the average parameters for a normal person are a stride length of 1.41 m, a stride width between 5 cm and 13 cm, a vertical amplitude of 4.2 cm for the head (here the vertical amplitude is about 3.5 cm), and a cadence of 113 steps/min (here, the cadence is $60/(\delta_{\mathrm{t}}/f_{\mathrm{s}}) = 60/(15/30) = 120$ steps/min). For the walker's height, it is set to an arbitrary, but realistic value of 1.8 m. The vertical foot amplitude is set to 3% of the walker's height.

Height h (m)	Stride length δ_{s} (m)	Stride width δ_{w} (m)	Duration δ_{t} (frames)	Head amplitude ν_{H} (%)	Foot amplitude ν_{F} (%)
1.80	1.35	0.12	15	1.94	3.00

Table 5.2 – Synthetic gait parameters.

The synthetic camera parameters are summarized in Table 5.3. The position and

the orientation parameters are chosen so that the three walks fit within the field of view of the synthetic camera. The camera is positioned at 2 m from the ground plane and it is oriented to look downward, with a slight roll component. The focal length, image size, frame rate, and principal point have realistic values for a camera. One must note that radial and tangential distortion are not included in the synthetic camera model.

focal length f	fps f_s	image size width × height	principal point (u_0, v_0)	pixel size ζ	orientation $(\alpha_y, \alpha_x, \alpha_z)$	position $\mathbf{X}_c$
8 mm	30	1024×768	$(512, 384)$	10 µm	$(-45°, -15°, -10°)$	$(0, 2, 0)^T$

Table 5.3 – Synthetic camera intrinsic and extrinsic parameters.

5.1.2 Validation of the View-rectified Trajectories

The validation aims at confirming that the proposed view-rectification method works as intended using imaged body-part trajectories for which the ground truth (3-D) body-part trajectories are known. It also aims at evaluating the robustness of the proposed view-rectification method in case of noisy imaged body-part trajectories. The added noise simulates the noise coming from the acquisition process of the imaged body-part trajectories, that is, the noise induced by the background subtraction and the body-part tracking methods described in Chapter 2. For completeness purposes, the proposed view-rectification method is also evaluated on filtered and unfiltered versions of the body-part trajectories in order to see if filtering can improve the results.

Six experiments are performed on each of the generated synthetic walks. The first two experiments consist in view-rectifying the imaged body-part trajectories without added noise ($\sigma_N = 0$), with and without filtering of the body-part trajectories (see first and second row of Figure 5.2). In the third and fourth experiments, Gaussian noise (zero mean) with standard deviation of $\sigma_N = 5$ pixels is added to each body-part position in each imaged body-part trajectory (see third and fourth rows of Figure 5.2). Similarly, Gaussian noise with standard deviation of $\sigma_N = 10$ pixels is added to each body-part position in each imaged body-part trajectory in the fifth and sixth experiments (see fifth and sixth rows of Figure 5.2). In the second, fourth, and sixth experiments, the body-part trajectories are post-filtered using the filtering process described in Section 2.7.3. One must note that the filter parameters are the same for these three experiments, that is, the kernel size is fixed to $\Psi = 5$ and the standard deviation is $\sigma = 1$ pixel.

The body-parts trajectories in the six experiments are processed using the proposed view-rectification method described in Chapter 3 along with the minor modifications to

the method described in Section A.4. These modifications simply ensure that the view-rectification method treats the body-part trajectory points as extremities and not as mass centres. The computation of the head and foot extremities is thus simplified since the synthetic body-part trajectories already represent body-part extremity positions. The fixed parameters that are used for the view-rectification method are the same as the ones mentioned in Chapter 3, that is, the maximum cadence parameter is set to $f_c = 240$ steps/min and the feet distance filter is a Gaussian kernel with $\Psi = 5$ and $\sigma = 1$. The ground vanishing line is estimated for each experiment using the corresponding synthetic walks (see Section 3.9.1). The validation of the obtained ground vanishing lines are presented in Section 5.1.3. In the case of the ground scale factor, it is computed once for all experiments by defining four 3-D points representing a one meter square on the ground plane in the synthetic scene, and the image of each point is computed using the camera projection matrix (see Equation A.14 and Section 3.9.2).

5.1.2.1 Imaged Body-part Trajectories and Head Motion Planes

In Figure 5.2, the head motion planes computed by the view-rectification method are shown along with the imaged body-part trajectories for the six experiments. First, one may notice that filtering has almost no visible effect on the computed motion planes with noise-free imaged body-part trajectories. However, the filtering has a clear effect on both the body-part trajectories and the head motion planes in the presence of noise, even when the fixed standard deviation of the filter is much smaller than the standard deviation of the added noise. Indeed, the head motion planes of the noisy body-part trajectories become more similar to the head motion planes of the noise-free body-part trajectories after filtering. It is also possible to notice that one gait half-cycle is not detected in experiments 5 and 6 (indicated by arrows). The last gait half-cycle is not detected for walks #1 and #2 (experiments 5 and 6), and the first gait cycle is not detected for walk #3 (experiment 6). In the case of walks #1 and #2, the last gait half-cycle is performed far from the camera. Moreover, the viewpoint for the last gait half-cycle in walk #1 is almost frontal. Given that the noise level is the same across all gait-half-cycles, this means that the signal-to-noise ratio is low in the body-part trajectories, which makes the last gait half-cycle harder to detect and analyze. In the case of the first cycle of walk #3, it is possible to see that in the case of the first gait half-cycle, the two "blobs" of points (indicated by magenta ellipses) representing the feet extremities at the first key time are very close, which makes the feet distance maximum hard to detect. In conclusion, the effect of noise on the detection of the gait half-cycles increases when the distance to the camera increases, and when the viewpoint gets close to a frontal view.

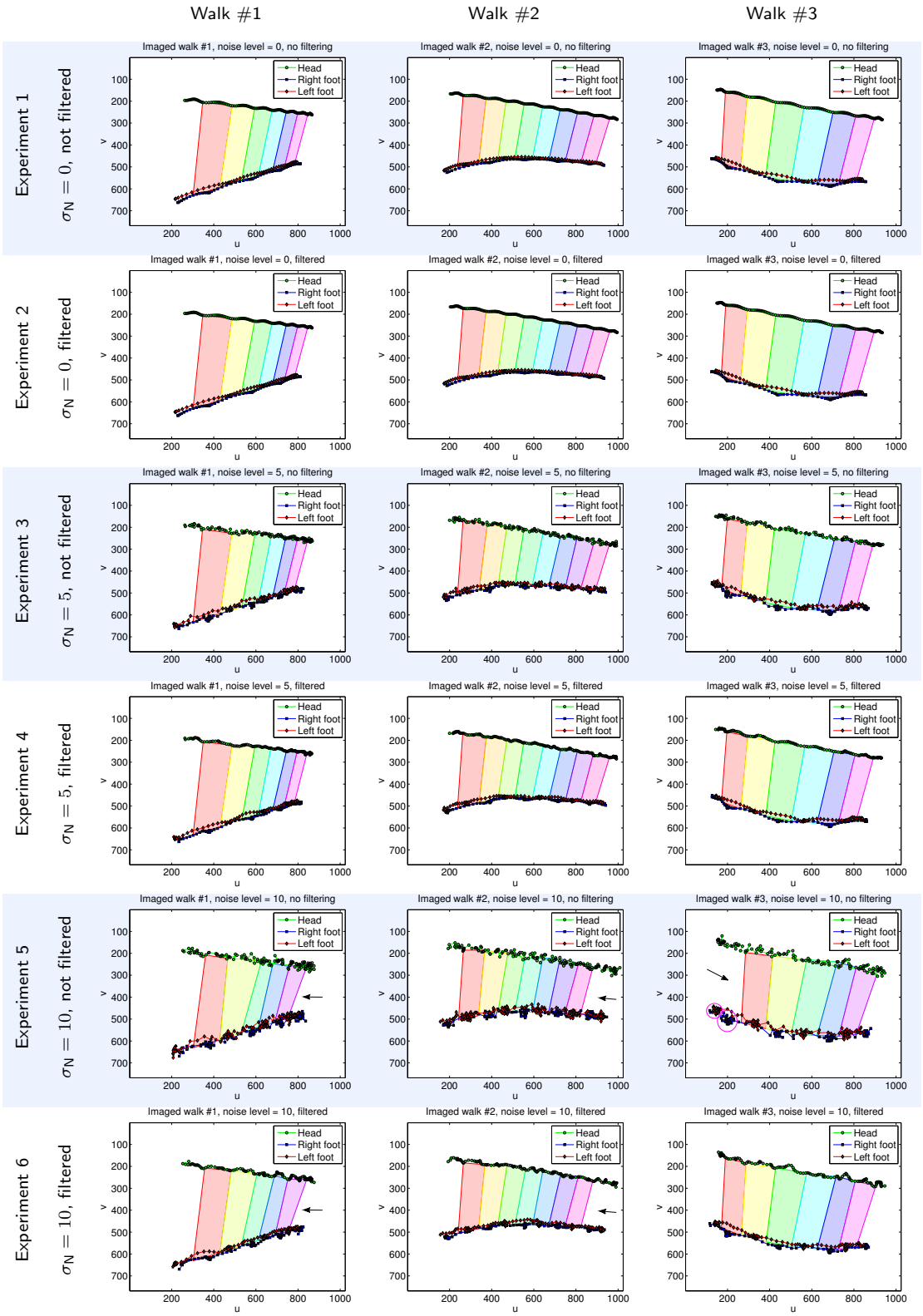

Figure 5.2 – Imaged body-part trajectories of synthetic walks with three different levels of noise (0, 5, and 10 pixels), filtered and non-filtered. The head motion planes obtained with the view-rectification method are also shown.

5.1.2.2 View-rectified Body-part Trajectories and Head Motion Planes

Figure 5.3 shows the rectified body-part trajectories along with the rectified head motion planes for the six experiments. In the first two experiments, there is no visible difference between the rectified motion planes and the rectified body-part trajectories. This means that the filtering of the noise-free trajectories does not change the behaviour of the view-rectification method. Besides, the rectified body-part trajectories in all experiments appear as if they where observed from a fronto-parallel viewpoint. However, the imaged body-part positions that are farthest from the camera appear more noisy in the rectified body-part trajectories than they are in the imaged body-part trajectories. This is what one would expect since the same level of noise was added to all imaged body-part positions regardless of the position they represent in the scene. Therefore, the relative noise amplitude is scaled down for imaged positions representing points close to the camera, and scaled up for imaged positions representing points far from the camera.

5.1.2.3 Average Error in the View-rectified Trajectories

The *ground truth fronto-parallel body-part trajectories* can be obtained on a half-cycle basis since the generated motion of each body part is designed to lie in a known plane in the scene (see Section A.2). Therefore, one can compare the computed view-rectified body-part trajectories to the ground truth fronto-parallel body-part trajectories at each gait half-cycle of a synthetic walk. In order to perform this comparison on a gait half-cycle basis, each detected gait half-cycle must be assigned to a ground truth gait half-cycle. Here, a ground truth half-cycle is assigned to the detected gait half-cycle for which the temporal overlap is the greatest.

Table 5.4 presents the point-to-point distance statistics that were computed on a gait half-cycle basis between the view-rectified body-part trajectories and the ground truth fronto-parallel body-part trajectories. In order to compute these error statistics for a given body-part, a least-squares fitting process is performed between the view-rectified body-part trajectory and its corresponding ground truth counterpart. The least-squares fitting process corresponds to an optimal alignment between an ordered set of view-rectified positions and the corresponding set of ground truth positions. This is performed using the algorithm presented in [104], which was adapted to work on sets of 2-D points. This algorithm finds the optimal rigid transformation (rotation and translation) aligning two sets of ordered points by minimizing the sum of the squared distances between the pairs of corresponding points. Here, the two sets of ordered points are defined as the positions for the overlapping frames of the detected gait half-cycle

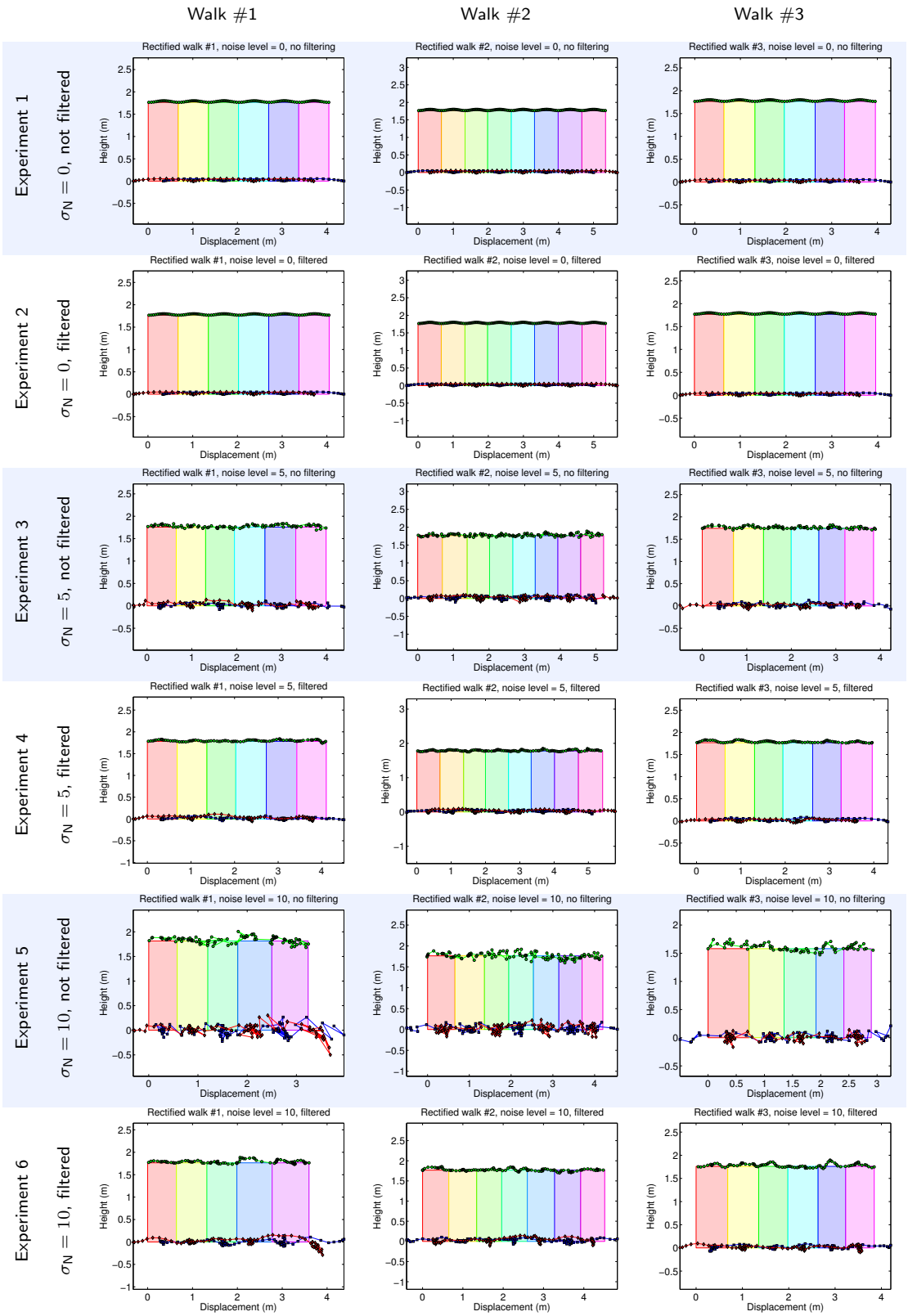

Figure 5.3 – The view-rectified body-part trajectories corresponding to the imaged body-part in Figure 5.2. The view-rectified head motion planes are also shown.

Walk #	Noise (pixels)	Filtered (Y/N)	Head (mm) mean	std	median	min	max	Feet (mm) mean	std	median	min	max
1	0	N	1.422	1.781	0.810	0.038	8.515	0.189	0.160	0.157	0.014	0.685
	0	Y	2.294	2.063	1.684	0.526	15.729	8.325	3.542	8.388	1.690	13.608
	5	N	44.534	32.571	34.533	4.978	169.779	47.092	28.376	41.256	3.793	141.262
	5	Y	22.208	14.192	19.333	2.194	55.447	25.533	14.641	22.304	1.714	63.770
	10	N	111.778	77.872	88.102	8.609	398.850	123.401	76.383	108.462	20.223	486.962
	10	Y	72.770	63.354	47.574	6.785	277.982	62.166	44.771	52.685	2.845	264.643
2	0	N	0.640	0.825	0.337	0.006	4.032	0.091	0.073	0.073	0.004	0.335
	0	Y	1.733	1.423	1.422	0.480	11.799	8.214	3.512	8.426	1.924	13.090
	5	N	46.306	29.473	41.713	1.189	142.739	49.542	30.948	41.855	5.809	209.974
	5	Y	20.950	12.589	19.467	1.459	56.860	24.715	13.921	23.229	2.305	78.482
	10	N	80.043	40.746	71.224	7.754	198.295	104.643	58.846	95.152	11.795	307.808
	10	Y	40.559	20.787	37.045	3.761	123.290	54.657	31.607	51.254	3.009	138.718
3	0	N	1.735	1.546	1.322	0.018	6.871	0.206	0.139	0.186	0.007	0.569
	0	Y	2.608	2.221	1.743	0.428	15.030	8.162	3.512	8.607	1.736	13.275
	5	N	37.149	22.811	33.211	3.574	113.859	47.515	26.938	40.714	8.070	145.961
	5	Y	17.523	10.800	14.856	2.752	44.385	19.332	9.924	19.085	3.136	53.020
	10	N	65.216	37.716	61.453	1.304	171.361	98.660	52.070	88.179	17.402	222.092
	10	Y	34.533	19.657	33.015	3.543	88.216	38.856	20.833	35.819	2.562	95.229

Table 5.4 – Point to point distance statistics of the view-rectified body-part trajectories and the ground truth fronto-parallel body-part trajectories. The statistics are computed over the point-to-point distance of the optimally aligned view-rectified trajectories and ground truth fronto-parallel trajectories.

and its assigned ground truth gait half-cycle.

The values presented for each experiment in Table 5.4 are statistics computed over the point-to-point distance of the view-rectified trajectories and their corresponding ground truth fronto-parallel trajectories. The statistics were computed independently for the head and the feet. In the case of the feet, the statistics were computed from the point-to-point distances of both feet. The feet point-to-point distances are computed for the moving foot in each gait half-cycle. The view-rectified trajectory and the ground truth trajectory of the still foot were not aligned since the foot positions in these trajectories are all equal in the case of the synthetic walks (the foot is really, completely still).

The point-to-point distance statistics are presented in order to show that the view-rectified body-part trajectories correspond on a point-to-point basis to what can be observed in the scene from a fronto-parallel viewpoint. This means that the view-rectified trajectories are suitable for gait analysis and modelling. For instance, the point-to-point distance statistics in the case of the first experiment (no noise, no filtering) is at most of the order of 10 mm. In the case of the second experiment, the point-to-point distance statistics is slightly greater since the body-part trajectories are filtered. The statistics for the experiments with added noise in the imaged body-part trajectories are shown here for completeness. As one would expect, the view-rectified trajectories in these experiments do not fit well to the ground truth fronto-parallel trajectories. Nonetheless, the statistics show that for a given amount of noise in the acquisition process, the point-to-point distance between the view-rectified trajectories

Walk #	Exp. #	Noise (pixels)	Filtered (Y/N)	Half-cycles (detected/real)	Duration (%)	Stride (%)	Displacement (%)	Height (%)
1	1	0	N	6/6	0.988 ± 0.851	0.006 ± 0.005	0.006 ± 0.005	0.020 ± 0.013
	2	0	Y	6/6	1.323 ± 1.159	0.028 ± 0.016	0.028 ± 0.016	0.038 ± 0.019
	3	5	N	6/6	5.818 ± 3.309	2.401 ± 1.542	2.349 ± 1.611	1.353 ± 0.578
	4	5	Y	6/6	5.212 ± 3.018	1.966 ± 1.492	1.903 ± 1.425	1.105 ± 0.750
	5	10	N	5/6	24.704 ± 37.868	9.051 ± 4.209	8.740 ± 4.276	7.395 ± 2.576
	6	10	Y	5/6	22.091 ± 38.655	9.312 ± 10.011	8.990 ± 9.620	1.744 ± 1.864
2	1	0	N	8/8	0.624 ± 0.855	0.004 ± 0.001	0.004 ± 0.001	0.022 ± 0.011
	2	0	Y	8/8	0.854 ± 1.216	0.017 ± 0.012	0.017 ± 0.012	0.040 ± 0.016
	3	5	N	8/8	3.478 ± 2.374	4.344 ± 1.206	4.368 ± 1.231	2.455 ± 1.461
	4	5	Y	8/8	3.306 ± 1.892	1.810 ± 1.424	1.801 ± 1.413	1.520 ± 0.798
	5	10	N	7/8	5.288 ± 5.098	11.263 ± 8.631	11.311 ± 8.628	3.527 ± 2.375
	6	10	Y	7/8	3.847 ± 4.428	4.549 ± 3.411	4.575 ± 3.469	1.337 ± 1.145
3	1	0	N	6/6	1.055 ± 0.558	0.003 ± 0.002	0.003 ± 0.002	0.095 ± 0.030
	2	0	Y	6/6	1.389 ± 0.724	0.011 ± 0.006	0.011 ± 0.006	0.027 ± 0.018
	3	5	N	6/6	3.424 ± 2.529	5.802 ± 3.670	5.852 ± 3.642	0.855 ± 0.483
	4	5	Y	6/6	2.814 ± 1.982	1.172 ± 1.419	1.165 ± 1.423	0.933 ± 0.719
	5	10	N	5/6	7.585 ± 3.579	15.916 ± 9.977	15.777 ± 10.103	6.089 ± 2.908
	6	10	Y	6/6	5.388 ± 3.421	4.764 ± 3.103	4.817 ± 3.132	2.701 ± 1.379

Table 5.5 – Gait analysis results on the synthetic walks. The results are the *average* ± *standard deviation* percentage of difference with respect to the corresponding ground truth values. The number of detected gait half-cycles is also shown along with the real number of gait half-cycles.

and the ground truth fronto-parallel trajectories is higher for body-part positions that are far from the camera or from a viewpoint that is close to a frontal view.

5.1.2.4 Gait Measurements

Gait measurements were extracted from the rectified body-part trajectories and compared to their known ground truth values. Table 5.5 shows the results for the six experiments. The number of detected gait half-cycles are shown along with the actual number of gait half-cycles for each synthetic walk. For each detected gait half-cycle, the duration, the stride length, the displacement, and the height were computed from the view-rectified body-part trajectories. The percentage of difference between the computed gait measurements and corresponding ground truth gait measurements was computed on a gait half-cycle basis. A ground truth gait-half-cycle was assigned to each detected gait half-cycle, as described previously in Section 5.1.2.3. The values shown in the table are the averages and the standard deviations of the percentage of difference for all detected gait half-cycles.

One may notice that the results are quite good given the amount of noise that was added to the trajectories. Indeed, the performance of the view-rectification method degrades quite gracefully when the noise level is increased. As one would expect, filtering the body-trajectory, even with a narrow band Gaussian kernel, limits the degradation of the performance in most cases. Filtering noise-free body-part trajectories leads however

to a small error in the gait measurements. One can also notice that the percentage of difference of the stride lengths and the displacements for walk #1 are greater in experiment #6 (filtered) than in experiment #5 (unfiltered). This is due to the fact that the gait measurement errors in the last gait half-cycle are greater in the sixth experiment than in the fifth experiment. These erroneous measurements coming from one gait half-cycle greatly affects the average values.

Overall, the above results confirm that the view-rectification method works as intended; that is, it generates a fronto-parallel view of the imaged body-part trajectories. The reason the percentages of difference are not zero even when there is no noise and no filtering is that the key times are not precisely recovered since the feet distance signal is computed from the imaged position of the feet, which are under perspective projection. Thus, the times when the feet are at maximum distance in the image do not exactly correspond to the times when feet are at maximum distance in the scene. Nonetheless, the estimated times only lead to small errors on the gait half-cycle durations and the other gait measurements. For instance, a 2% error on a 15-frame (500 ms) gait half-cycle corresponds to an error of 0.3 frame or 10 ms ($15 \times 0.02/30$). The error incurred by the other gait measurements is, on average, less than 0.1%.

5.1.3 Validation of the Ground Vanishing Line

The ground vanishing line is used several times in the view-rectification method. As described in Section 3.9.1, the ground vanishing line is estimated using multiple walks. It is thus important to validate the estimation process of the ground vanishing line as well as to assess its performance in the presence of noise in the imaged body-part trajectories. The validation of the estimation process is performed by comparing the estimated vanishing line in each experiment with the ground truth vanishing line. The latter can be precisely computed as follow:

$$\mathbf{l}_\infty = \mathbf{K}^{-\mathsf{T}}\,\mathbf{R}\,\mathbf{n}_\mathrm{G}, \tag{5.1}$$

where $\mathbf{n}_\mathrm{G}$ is the normal vector of the ground plane in the scene's Euclidean coordinate frame, $\mathbf{R}$ is the rotation matrix representing the orientation of the camera in the scene, and $\mathbf{K}$ is the matrix of the camera's intrinsic parameters. Here, the ground plane's normal vector in the synthetic scene is defined as $\mathbf{n}_\mathrm{G} = (0,\, 1,\, 0)^\mathsf{T}$, that is, a unit vector pointing in the same direction as the Y axis.

Table 5.6 shows the validation results of the estimation of the ground vanishing line on each experiment. As mentioned previously in Section 5.1.2, the three synthetic walks were used to estimate the ground vanishing line for a given experiment. The value of

Experiment (#)	Noise	Filtered	$\hat{l}_a$	$\hat{l}_b$	$\hat{l}_c$	$\left\langle (l_a, l_b)^\mathsf{T}, (\hat{l}_a, \hat{l}_b)^\mathsf{T} \right\rangle$	$\left\lvert \frac{\hat{l}_c - l_c}{l_c} \right\rvert \times 100$
Ground truth line $\mathbf{l}_\infty$			0.174	-0.985	74.899	–	–
1	0	N	0.174	-0.985	74.976	1.00000	0.103
2	0	Y	0.174	-0.985	75.017	1.00000	0.158
3	5	N	0.137	-0.991	142.785	0.99930	90.637
4	5	Y	0.181	-0.984	68.863	0.99997	8.058
5	10	N	0.069	-0.998	225.094	0.99447	200.530
6	10	Y	0.147	-0.989	113.653	0.99963	51.741

Table 5.6 – Results of the validation of the ground vanishing line. An estimated line is represented by the parameters $(\hat{l}_a, \hat{l}_b, \hat{l}_c)^\mathsf{T}$, and the ground truth vanishing line is represented by the parameters $(l_a, l_b, l_c)^\mathsf{T}$. The ground truth vanishing line parameters are presented along with the estimated line's parameters for each experiment. The inner product between the estimated line's normal and the ground truth line's normal are present in the next to last column. The percentage of difference between the parameters l_c and $\hat{l}_c$ is shown in the last column.

the estimated line's parameters are presented for each experiment. The parameters of the ground truth vanishing line computed using Equation 5.1 are also shown. In order to compare an estimated line $\hat{\mathbf{l}}_\infty = (\hat{l}_a, \hat{l}_b, \hat{l}_c)^\mathsf{T}$ to the ground truth line $\mathbf{l}_\infty = (l_a, l_b, l_c)^\mathsf{T}$, both the estimated and the ground truth lines are multiplied by the normalizing factor $1/\|(\hat{l}_a, \hat{l}_c)^\mathsf{T}\| = 1$ and $1/\|(l_a, l_b)^\mathsf{T}\|$, respectively. Therefore, the vector $(\hat{l}_a, \hat{l}_b)^\mathsf{T}$ of a normalized line represents a unit vector normal to the line, while the parameter $\hat{l}_c$ directly represents the distance of the line to the origin (the top-left corner of the synthetic camera image). The orientation of the estimated line is compared to the orientation of the ground truth line by computing the inner product between the lines' normals. The distance to the origin of the estimated line is compared to the ground truth by computing the percentage of difference between the parameters $\hat{l}_c$ and l_c.

One may first notice that in the case of the first and second experiments (no added noise), the parameters are very close to the ground truth parameters, thus showing that the estimation process works as intended. The differences with the ground truth can be explained again by the slight errors made in the estimation of the key times, which lead to small errors in the computation of the body-part extremity positions at these key times. The experiments with added noise in the imaged body-part trajectories show that the parameter that is the most influenced by the presence of noise is the parameter $\hat{l}_c$. This means that the distance of the line to the origin is more influenced by the presence of noise in the imaged body-part trajectories than the orientation of the line in the image. As before, filtering improves the estimated parameters.

5.2 Gait Analysis, Modelling and Comparison on Real Walks

The experiments on gait analysis, modelling, and comparison using the view-rectified body-part trajectories were performed on a gait database that was designed as part of this thesis. As discussed in Sections 1.3.3 and 1.4, the databases that are commonly used in the literature mostly consist in outdoor walks observed at a distance or walks that are performed on straight lines. The perspective distortion induced by the viewpoints in some of these databases is limited since the distance between the subject and the camera is such that the weak perspective assumption holds. Moreover, there are no significant changes in viewpoints for walks performed on a straight line. These public databases are thus not appropriate to test all the unique aspects of the view-rectification method proposed in this thesis.

The acquisition process and the characteristics of the proposed gait database are described in detail in Appendix B. The gait database is comprised of 520 video sequences each representing a walk performed by a subject following a given *path*. Five walking *tracks* were designed to provide a wide range of viewpoints induced by both the distance range and the changes in the walk direction. Each of the 52 subjects walked twice on each track, that is, once in each direction. There are thus 10 paths that were followed by each subject. A path is denoted by the track number (1 to 5) and the direction (1 or 2): paths 1-1, 1-2, 2-1, 2-2, 3-1, 3-2, 4-1, 4-2, 5-1, and 5-2. All the walks were observed by a single, fixed, and calibrated camera that was positioned as in a typical surveillance scenario. The body part tracking method was performed on each of the 520 walks using the parameters and thresholds mentioned in Chapter 2. The parameters used for the view-rectification method are the same as in the validation process, that is, the maximum cadence parameter is set to $f_c = 240$ steps/min and the feet distance filter is a Gaussian kernel with $\Psi = 5$ and $\sigma = 1$. The ground scale factor was estimated as explained in Section 3.9.2, and the ground vanishing line was estimated using all the walks from subjects 1 to 10 (100 walks).

The acquisition conditions for the gait database were controlled in order to limit as much as possible some perturbing factors that are of no interest in this thesis, as the changes in lighting and complex, dynamic backgrounds. Indeed, the gait database was designed to test the proposed approach on challenging walks, not on challenging acquisition conditions. Thus, the lighting was maintained constant and the background was simple and static during the acquisition process. However, these factors could not be completely eliminated. For instance, the white curtains used as the background were not completely static since they were moving a little bit when the subjects were

walking in the acquisition room. Also, the floor of the acquisition room was highly specular, which led to reflections of the subjects on the floor and cast shadows. These remaining factors have led in some cases to errors in the foreground segmentation by either adding or subtracting parts of the subject's silhouette. The body-part tracking method is thus the part of the proposed approach that is directly influenced by these factors. The view-rectification method and the gait analysis, modelling and comparison methods are thus indirectly influenced by these factors.

The results of the experiments performed on the gait database show that the proposed approach is able to perform gait analysis, modelling, and comparison on unconstrained walks. The experiments performed on the gait database and the results that were obtained are presented as follows. First, qualitative results depicting both the imaged and the view-rectified trajectories are presented in Section 5.2.1. Next, Section 5.2.2 presents the gait analysis results of all the walks in the gait database. Finally, the gait modelling and comparison results are presented in 5.2.3.

5.2.1 View-Rectification Results

A set of 20 walks were selected from the database in order to visually assess the behaviour of the body-part tracking and the view-rectification methods. Figure 5.4 presents the imaged body-part trajectories and the computed head motion planes of these walks. The foot motion planes are not shown here since the head motion planes provide all the visual information needed to assess the behaviour of the view-rectification method with respect to the motion planes. The results in each row present two example walks for each of the two paths of a given walking track. For instance, the first row shows two example walks for path 1-1, and two example walks for path 1-2. The 20 walks belong to ten different subjects in order to have each subject appearing twice in the results. Each continuous tracking interval is identified by a label of the form "int. #", which is located close the corresponding imaged body-part trajectories. It is also possible to visually assess the result of the foot labelling process since each foot trajectory is coloured according to the foot label that was assigned to it: blue for the right foot, red for the left foot.

The results presented in Figure 5.4 show that both the body-part tracking method and the view-rectification method performed well on real walks. Indeed, the body-part trajectories and the head motion planes are realistic and provide enough visual information to easily deduce the motion performed and the path followed by the subjects. Moreover, one can verify that the foot trajectories were correctly labelled by considering the direction of walk and the respective location of the foot trajectories. For instance,

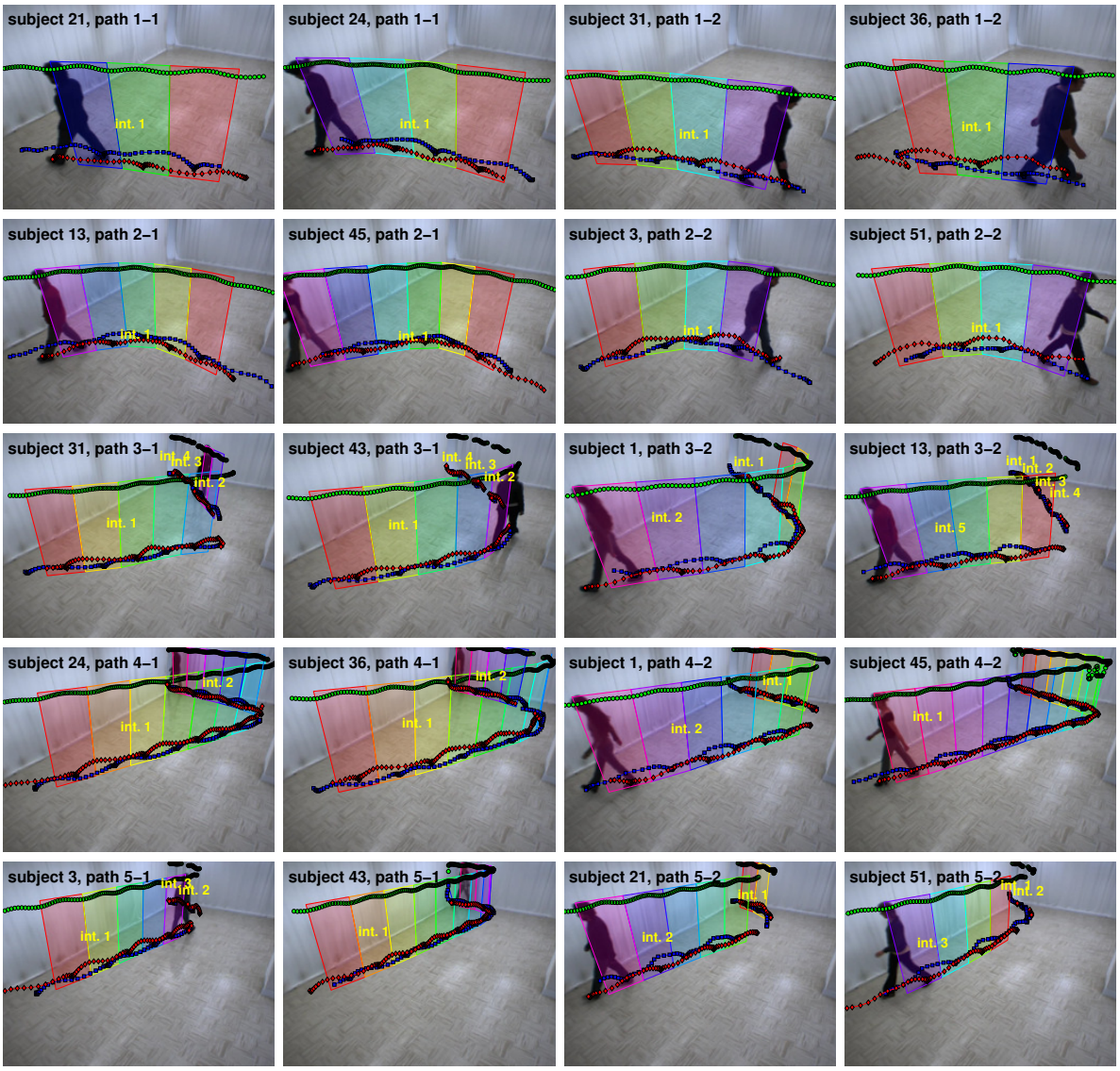

Figure 5.4 – Imaged body-part trajectories and computed head motion planes for 20 walks of the gait database. Each row presents two examples for each of the two paths on a given walking track: paths 1-1 and 1-2, 2-1 and 2-2, 3-1 and 3-2, 4-1 and 4-2, 5-1 and 5-2. The walks presented here come from 10 subjects of the gait database (subjects 1, 3, 13, 21, 24, 31, 36, 43, 45, and 51). Each subject appears twice in these walk examples. The blue and red trajectories represent the foot that was labelled "right and "left" by the view-rectification method, respectively. Each continuous tracking interval is identified directly in the sub-figure (int.1, int.2, etc).

if the walk is performed from left to right in the image, the right foot trajectory should be located a little bit lower in the image than the left foot trajectory, especially for the points representing the positions of each foot when they are still (blobs of positions). One can also observe the qualitative differences in the way subjects are walking on the same path, that is, the body-part trajectories are somewhat different.

It is possible to see that in general, the track 3 and 5 are harder than the other track when it comes to body-part tracking. At some positions on these two tracks, the viewpoint is close to the frontal viewpoint, which makes the feet occlusion last several frames. The feet tracking is thus lost until both legs can be separated again. This leads to many continuous tracking intervals that are not long enough to contain a complete gait half-cycle. Some tracking errors and erroneous positions are also visible for the walk of subject 36 on path 1-2, and for the walk of subject 45 on path 4-2. In the former, the correspondence between the feet was swapped just before the beginning of the first gait half-cycle because of an erroneous position found for one of the feet. This has no impact on the view-rectified trajectories since it occurred before the first detectable gait half-cycle. In the latter, the part of the silhouette representing the head was lost for more than a gait half-cycle, which led to a series of erroneous positions in the head trajectories (see the head trajectory, close to the upper right corner of the image). It will be shown shortly that these erroneous positions only have an effect on the gait half-cycles to which they belong.

Figure 5.5 presents the view-rectified body-part trajectories and the view-rectified head motion planes that correspond to the imaged body-part trajectories and the computed head motion planes presented in Figure 5.4. The trajectories and the motion planes for the different continuous tracking intervals are shown in the same sub-figure but are separated by a gap. Only the continuous tracking intervals that were not discarded by the view-rectification method are presented (intervals with at least one gait half-cycle). It is possible to see that the body-part trajectories appear to have been observed from a fronto-parallel viewpoint. Also, the view-rectified walks appear to have been performed from left to right, even if the direction of walk changed. One may notice that some parts of the head and/or the foot trajectories are distorted for some gait half-cycles in the following view-rectified walk: subject 1, path 3-2; subject 36, path 4-1; subject 45, path 4-2; subject 43, path 5-1. Except for subject 45 on path 4-2, the distortion can be explained by first noticing that the viewpoint during the problematic gait half-cycles was almost frontal (see corresponding sub-figures in Figure 5.4). Also, the body parts were successfully tracked in these cases since the change in direction was very sharp, and thus the feet occlusion did not last long. As one may recall, the view-rectification of body-part trajectories for nearly frontal views is problematic since the view-rectifying homography matrix is almost singular. The view-rectified trajectories

for these problematic gait half-cycles are distorted. In the case of subject 45 on path 4-2, the erroneous head positions led to erroneous head and foot planes from which an erroneous rectifying homography was defined. Is is important however to note that these distortions effects are confined to the gait half-cycles were they occurred, and thus the view-rectified trajectories in the unaffected gait half-cycles reflects what would have been observed from a fronto-parallel viewpoint.

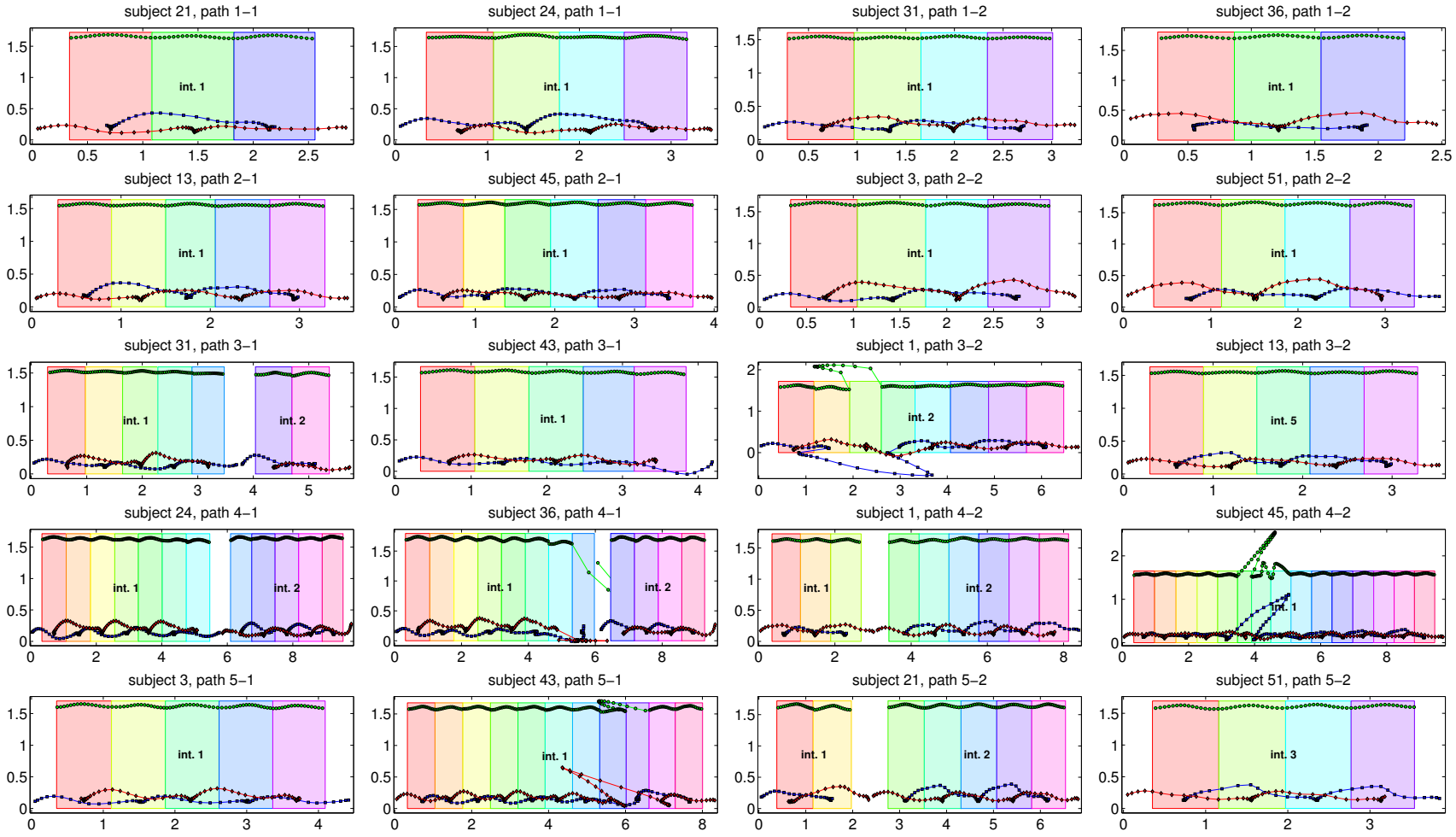

Figure 5.5 – The view-rectified body-part trajectories and view-rectified head motion planes corresponding to the examples presented in Figure 5.4. All the intervals of a walk are shown on the same sub-figure and are separated by a gap in the head motion planes and the trajectories. For presentation purposes, the vertical and the horizontal axes were not made equal.

The imaged body-part trajectories and the view-rectified body-part trajectories cannot be quantitatively assessed in the case of real walks since the ground truth 3-D body-part trajectories are not available. Hence, it is not possible to directly evaluate the performance of the body-part tracking method. Similarly, the view-rectified trajectories and the measurements performed on them cannot be directly evaluated as it was done for synthetic walks in Section 5.1). Nonetheless, the results of gait analysis, modelling, and comparison show that the body-part tracking and view-rectification methods provide valid results on real walks.

5.2.2 Gait Analysis Results

Gait analysis was performed on each walk for each subject of the gait database using the methods described in Section 4.1. The 520 sets of gait measurements thus obtained is presented in a table of Appendix C. Other information provided in this table are:

- the number of frames where the subject is entirely visible during the walk;
- the percentage of these frames that are part of a detected gait half-cycle;
- the number of continuous tracking intervals;
- the total number of detected gait half-cycles across all tracking intervals.

Since gait measurements such as the stride lengths, the displacement, the duration and the height are computed on a gait half-cycle basis, the mean and the standard deviation of these measurements are given for a specific subject's walk. The table also presents the stature (height) that each subject reported during the acquisition process. The precision of the stature values is thus variable from a subject to another. The percentage of difference between the stature and the computed mean height is presented in the last column of the table in appendix C. The processing time required for analyzing the gait of the 520 walks was about 4 seconds on a computer with a dual core 2.66 GHz CPU running non-optimized and non-parallelized MATLAB™ code. Gait analysis can thus be performed in real time since the processing time is about 8 ms per walk.

Tables 5.7 and 5.8 present gait measurement statistics on a subject basis and on a path basis, respectively. The results presented in Table 5.7 are the mean and the standard deviation of the gait measurements over all the walks performed by a given subject. The total number of gait half-cycles across all walks is presented, as well as the percentage of difference between the stature and the computed mean height. In the case of Table 5.8, the presented results are the mean and standard deviation of the gait measurements over all subjects for a given path. The statistics on the number of detected gait half-cycles for each path is also reported in this table.

Subject (ID)	Gender (M/F)	Stature (m)	½ Cycles (num.)	Cadence (steps/min)	Speed (m/min)	Duration (s)	Strides (m)	Displacement (m)	Height (m)	ΔHeight (%)
1	F	1.78	53	125.4 ± 2.5	95.5 ± 3.5	0.477 ± 0.016	1.528 ± 0.064	0.763 ± 0.033	1.777 ± 0.034	0.19
2	M	1.75	56	105.6 ± 1.9	79.4 ± 2.1	0.569 ± 0.019	1.508 ± 0.081	0.753 ± 0.041	1.738 ± 0.019	0.68
3	M	1.73	49	109.6 ± 4.0	76.3 ± 5.8	0.547 ± 0.030	1.398 ± 0.089	0.699 ± 0.045	1.752 ± 0.021	1.25
4	M	1.85	52	106.9 ± 2.2	78.3 ± 3.7	0.560 ± 0.024	1.467 ± 0.077	0.733 ± 0.039	1.822 ± 0.019	1.51
5	M	1.62	65	108.1 ± 3.9	67.0 ± 4.4	0.556 ± 0.022	1.237 ± 0.049	0.618 ± 0.024	1.646 ± 0.034	1.63
6	M	1.83	46	102.9 ± 2.6	79.4 ± 4.7	0.583 ± 0.021	1.568 ± 0.083	0.774 ± 0.037	1.777 ± 0.275	2.91
7	M	1.83	63	98.1 ± 2.9	67.3 ± 4.0	0.611 ± 0.028	1.371 ± 0.101	0.685 ± 0.051	1.797 ± 0.020	1.80
8	M	1.70	54	107.6 ± 2.7	76.7 ± 3.8	0.557 ± 0.023	1.439 ± 0.099	0.719 ± 0.050	1.649 ± 0.022	3.00
9	M	1.80	68	95.6 ± 1.7	68.2 ± 4.0	0.625 ± 0.036	1.453 ± 0.136	0.726 ± 0.066	1.865 ± 0.185	3.63
10	M	1.73	50	102.7 ± 2.4	71.3 ± 3.5	0.584 ± 0.025	1.386 ± 0.075	0.693 ± 0.038	1.758 ± 0.016	1.65
11	M	1.82	53	100.1 ± 4.0	63.9 ± 5.1	0.597 ± 0.032	1.278 ± 0.067	0.639 ± 0.034	1.809 ± 0.013	0.58
12	M	1.74	56	109.3 ± 2.3	79.1 ± 3.6	0.547 ± 0.022	1.457 ± 0.100	0.727 ± 0.057	1.744 ± 0.034	0.21
13	M	1.68	71	115.6 ± 1.8	70.9 ± 2.9	0.517 ± 0.022	1.236 ± 0.144	0.618 ± 0.070	1.663 ± 0.019	1.04
14	M	1.85	55	98.1 ± 2.4	86.0 ± 3.3	0.609 ± 0.025	1.760 ± 0.050	0.880 ± 0.026	1.889 ± 0.046	2.11
15	M	1.80	51	97.7 ± 2.4	73.5 ± 2.6	0.618 ± 0.027	1.504 ± 0.085	0.752 ± 0.043	1.831 ± 0.016	1.72
16	M	1.75	53	98.8 ± 5.4	71.5 ± 5.9	0.602 ± 0.037	1.456 ± 0.061	0.728 ± 0.030	1.776 ± 0.017	1.49
17	M	1.74	62	104.4 ± 2.5	64.7 ± 3.2	0.575 ± 0.029	1.245 ± 0.044	0.623 ± 0.022	1.736 ± 0.018	0.24
18	M	1.63	54	111.8 ± 2.6	77.8 ± 4.7	0.538 ± 0.023	1.391 ± 0.072	0.695 ± 0.035	1.630 ± 0.031	0.00
19	M	1.70	62	99.7 ± 3.0	69.1 ± 3.8	0.597 ± 0.024	1.383 ± 0.067	0.691 ± 0.033	1.727 ± 0.035	1.61
20	M	1.85	61	94.6 ± 4.2	67.6 ± 6.5	0.640 ± 0.032	1.408 ± 0.187	0.704 ± 0.091	1.874 ± 0.008	1.29
21	M	1.77	58	102.2 ± 3.2	77.4 ± 2.7	0.586 ± 0.075	1.530 ± 0.115	0.765 ± 0.058	1.792 ± 0.047	1.22
22	F	1.63	83	93.1 ± 1.8	51.9 ± 2.8	0.646 ± 0.024	1.114 ± 0.080	0.557 ± 0.039	1.594 ± 0.035	2.18
23	M	1.71	60	85.0 ± 2.6	55.0 ± 4.1	0.705 ± 0.033	1.289 ± 0.095	0.644 ± 0.047	1.728 ± 0.028	1.08
24	M	1.77	65	84.0 ± 6.3	59.7 ± 3.5	0.704 ± 0.090	1.420 ± 0.112	0.710 ± 0.056	1.736 ± 0.020	1.92
25	M	1.78	61	113.8 ± 2.6	84.5 ± 5.0	0.528 ± 0.033	1.472 ± 0.146	0.730 ± 0.076	1.779 ± 0.149	0.05
26	M	1.64	71	106.2 ± 3.5	67.7 ± 4.9	0.568 ± 0.090	1.299 ± 0.174	0.648 ± 0.086	1.645 ± 0.213	0.30
27	F	1.57	67	96.9 ± 4.1	55.7 ± 4.0	0.616 ± 0.033	1.155 ± 0.046	0.578 ± 0.023	1.570 ± 0.012	0.03
28	M	1.88	46	104.5 ± 4.0	81.6 ± 5.1	0.571 ± 0.027	1.571 ± 0.056	0.785 ± 0.028	1.888 ± 0.013	0.43
29	F	1.57	70	119.0 ± 4.2	73.6 ± 4.0	0.500 ± 0.027	1.242 ± 0.062	0.621 ± 0.031	1.550 ± 0.015	1.25
30	F	1.68	74	105.5 ± 3.1	66.9 ± 6.0	0.568 ± 0.028	1.286 ± 0.094	0.643 ± 0.047	1.675 ± 0.015	0.28
31	F	1.62	66	112.7 ± 3.2	75.0 ± 3.7	0.536 ± 0.021	1.325 ± 0.066	0.662 ± 0.033	1.620 ± 0.010	0.02
32	M	1.65	57	105.1 ± 3.2	75.9 ± 4.3	0.569 ± 0.021	1.442 ± 0.057	0.721 ± 0.029	1.661 ± 0.010	0.64
33	M	1.85	58	110.2 ± 5.5	90.7 ± 7.7	0.544 ± 0.097	1.671 ± 0.186	0.836 ± 0.093	1.856 ± 0.032	0.34
34	M	1.78	44	90.8 ± 12.1	73.4 ± 19.2	0.662 ± 0.191	1.698 ± 0.716	0.844 ± 0.349	1.738 ± 0.066	2.34
35	F	1.75	70	122.4 ± 4.6	93.1 ± 3.8	0.493 ± 0.063	1.521 ± 0.101	0.760 ± 0.050	1.784 ± 0.034	1.93
36	M	1.83	60	103.4 ± 3.1	70.6 ± 3.6	0.582 ± 0.036	1.366 ± 0.156	0.692 ± 0.037	1.889 ± 0.366	3.22
37	M	1.80	60	99.0 ± 1.7	74.6 ± 1.7	0.605 ± 0.018	1.511 ± 0.064	0.755 ± 0.032	1.827 ± 0.030	1.52
38	F	1.70	66	105.0 ± 3.6	71.4 ± 3.4	0.571 ± 0.027	1.371 ± 0.090	0.685 ± 0.045	1.690 ± 0.030	0.61
39	F	1.62	76	112.2 ± 2.5	71.2 ± 3.7	0.537 ± 0.029	1.271 ± 0.140	0.635 ± 0.067	1.607 ± 0.013	0.80
40	F	1.65	65	107.0 ± 6.4	73.9 ± 6.2	0.557 ± 0.033	1.383 ± 0.070	0.691 ± 0.035	1.683 ± 0.018	2.00
41	M	1.85	58	103.3 ± 2.4	74.7 ± 3.5	0.583 ± 0.026	1.435 ± 0.074	0.717 ± 0.037	1.868 ± 0.019	0.98
42	F	1.67	76	108.6 ± 3.1	67.2 ± 3.0	0.553 ± 0.030	1.234 ± 0.093	0.615 ± 0.047	1.642 ± 0.101	1.70
43	F	1.70	67	113.5 ± 1.9	78.8 ± 2.6	0.526 ± 0.019	1.396 ± 0.049	0.698 ± 0.024	1.711 ± 0.019	0.63
44	F	1.65	79	104.2 ± 2.9	61.1 ± 2.1	0.574 ± 0.024	1.167 ± 0.055	0.583 ± 0.028	1.614 ± 0.013	2.19
45	F	1.65	80	105.2 ± 3.5	64.0 ± 3.1	0.570 ± 0.050	1.220 ± 0.065	0.610 ± 0.033	1.718 ± 0.102	4.13
46	F	1.68	58	102.8 ± 6.4	67.2 ± 7.0	0.582 ± 0.040	1.336 ± 0.088	0.654 ± 0.032	1.575 ± 0.239	6.23
47	F	1.68	69	118.4 ± 4.0	73.7 ± 4.9	0.504 ± 0.022	1.249 ± 0.046	0.625 ± 0.023	1.685 ± 0.018	0.30
48	F	1.55	80	110.5 ± 3.0	67.7 ± 3.4	0.539 ± 0.017	1.228 ± 0.055	0.614 ± 0.028	1.557 ± 0.016	0.48
49	F	1.70	51	111.1 ± 1.7	77.6 ± 3.4	0.540 ± 0.017	1.402 ± 0.057	0.701 ± 0.029	1.631 ± 0.017	4.09
50	F	1.55	76	116.8 ± 6.7	71.6 ± 3.4	0.519 ± 0.119	1.236 ± 0.154	0.618 ± 0.077	1.590 ± 0.016	2.58
51	F	1.76	47	111.6 ± 15.8	97.7 ± 12.1	0.532 ± 0.088	1.811 ± 0.723	0.898 ± 0.332	1.764 ± 0.051	0.24
52	F	1.54	61	111.7 ± 3.7	74.0 ± 4.7	0.538 ± 0.022	1.330 ± 0.070	0.662 ± 0.034	1.595 ± 0.076	3.58

Table 5.7 – Gait measurement statistics for each subject. The column "½ Cycles" presents the total number of detected gait half-cycles in the database for a given subject. The column "ΔHeight" presents the percentage of difference between the stature and the mean height in the first to last column.

The percentage of difference between the stature and the computed mean height can be used to some extent to determine the validity of the other gait measurements. One must recall that the height is computed from the view-rectified positions of the top of the silhouette, which in turn depends on the height of the view-rectified head motion planes (see Section 4.1.6). The width of the head motion planes on the ground plane is used along with the aspect ratio to compute the height of the motion plane in the scene (see Section 3.7.3). Ultimately, the computed subject's height depends on the imaged

Path (ID)	$\frac{1}{2}$ Cycles (num.)	Cadence (steps/min)	Speed (m/min)	Duration (s)	Strides (m)	Displacement (m)	Height (m)
1-1	3.5 ± 0.7	105.3 ± 9.0	72.4 ± 9.6	0.574 ± 0.055	1.361 ± 0.172	0.679 ± 0.083	1.692 ± 0.110
1-2	3.4 ± 0.8	106.1 ± 9.8	74.4 ± 10.1	0.572 ± 0.074	1.381 ± 0.156	0.689 ± 0.078	1.700 ± 0.110
2-1	4.7 ± 0.9	101.8 ± 9.3	67.9 ± 10.3	0.594 ± 0.060	1.314 ± 0.148	0.656 ± 0.073	1.689 ± 0.123
2-2	4.7 ± 0.9	102.7 ± 9.6	69.4 ± 10.2	0.589 ± 0.059	1.329 ± 0.148	0.664 ± 0.074	1.683 ± 0.109
3-1	5.8 ± 1.9	106.2 ± 8.2	72.9 ± 11.0	0.569 ± 0.076	1.371 ± 0.253	0.684 ± 0.125	1.716 ± 0.105
3-2	5.3 ± 1.6	105.8 ± 8.6	72.1 ± 9.7	0.568 ± 0.069	1.368 ± 0.233	0.682 ± 0.116	1.720 ± 0.142
4-1	11.1 ± 2.3	107.0 ± 8.7	75.9 ± 11.3	0.564 ± 0.063	1.400 ± 0.261	0.699 ± 0.121	1.721 ± 0.167
4-2	10.7 ± 2.4	106.4 ± 9.0	75.1 ± 10.6	0.568 ± 0.067	1.386 ± 0.213	0.692 ± 0.104	1.728 ± 0.124
5-1	6.6 ± 2.0	107.0 ± 11.4	76.7 ± 9.3	0.565 ± 0.081	1.421 ± 0.214	0.709 ± 0.106	1.732 ± 0.143
5-2	5.8 ± 2.0	107.6 ± 8.7	74.5 ± 9.8	0.561 ± 0.051	1.373 ± 0.145	0.686 ± 0.072	1.712 ± 0.097

Table 5.8 – Gait measurement statistics for each path. The column "$\frac{1}{2}$ Cycles" presents the statistics on the number of detected gait half-cycles in the database for a given path.

head and feet extremities at each key time, which are used to compute the stride lengths and the displacement, among other things. Therefore, a low percentage of difference between the stature and the computed height indicates that the body-part extremity positions were correctly estimated and view-rectified, which in turn indicates that the other gait measurements that are derived from the extremity positions are presumably representative of the real gait measurements. The stature can thus act as a ground truth measurement for gait analysis, although one must keep in mind there is an inherent error in the value reported by the subjects. Moreover, a high percentage of difference for a given walk does not necessarily means that all the other gait measurements are erroneous. Indeed, this difference in height might be due to erroneous head extremities positions, which does not have an influence on the computed gait half-cycle durations, strides lengths, displacement, cadence and speed.

The percentage of differences in the table of Appendix C vary from a minimum of 5.3×10^{-3}% to a maximum of 26.4%, with an average value of 1.9%, a standard deviation of 2.8%, and a median of 1.2%. The results thus suggest that the gait analysis results are quite good, considering that these measurements were automatically extracted from unconstrained walks, without using any markers on the subjects' body parts. Another observation that indicates that the gait measurements are valid is the fact that gait measurements obtained on different paths for a given subject are similar, minus small, normal variations across the paths. These variations are visible in Table 5.8, where the speeds are lower or higher on some paths. For instance, the subjects clearly walked slower on the paths 2-1 and 2-2, which can be explained by the continuous change in the walk direction that had to be performed by the subjects. Also, the walks were performed faster for the paths 4-1, 4-2, 5-1, and 5-2. Indeed, the changes in direction on these two tracks are performed close to the beginning or close to the end of the tracks, which make the walk divided in a short and a long walk on a straight line. The

Gender (M/F/A)	Type (R/C)	Cadence (steps/min)	Speed (m/min)	Strides (m)
Males	reference	111.0	86.0	1.46
	computed	102.4 ± 8.2	73.4 ± 9.1	1.43 ± 0.20
Females	reference	117.0	77.0	1.28
	computed	110.2 ± 9.1	72.8 ± 12.2	1.31 ± 0.21
All	reference	113.0	82.0	1.41
	computed	105.6 ± 9.4	73.1 ± 10.5	1.38 ± 0.21

Table 5.9 – Comparison between reference and computed gait measurements. The reference gait measurements are the average values reported in [95]. The computed gait measurements were obtained using all the walks of all the subjects in the gait database. The gait measurements are also shown for male and females separately.

subjects thus had more space to accelerate on the long straight line walk. One can also see in Table 5.7 some differences between the gait measurements of different subjects. These differences already indicate that each subject has his own way of walking and that to some extent it will be possible to recognize some subjects by the dynamics of their gait.

The consistency of the gait measurements can also be assessed to some extent by performing a comparison with the normal gait measurements found in clinical gait analysis references [95]. Table 5.9 presents the cadence, the speed and the stride lengths statistics computed over all paths and subjects, as well as over all males and females separately. The reference gait measurements shown in the table represent the average measurements that can be found in [95] (no standard deviations were reported in that study). One may see that the cadence and the speed obtained from the gait database are lower than the ones reported in [95]. This can be explained by the fact that the subjects could not reach their natural walking speed and cadence because of the short length of the paths and the changes in the walk direction the subjects had to perform. Nonetheless, one can see that the cadence difference between male and female is of the same order of magnitude. Also, the stride lengths are very close to the reference values. This observations indicates that the gait measurements computed with the proposed approach are valid.

There is only one walk in the whole gait database that could not be analyzed, which is the walk of subject 34 on the path 5-2. No gait half-cycle could be detected in this walk, as shown in Figure 5.6(a). The feet could not be tracked correctly because of repeated silhouette segmentation errors that are due to the colour of the subject's clothes. Indeed, the subject's shorts are of a colour similar to the background, which leads to silhouettes with missing parts. This was also problematic for the path 5-1, as shown in Figure 5.6(b), where gait half-cycles were detected but erroneous foot position

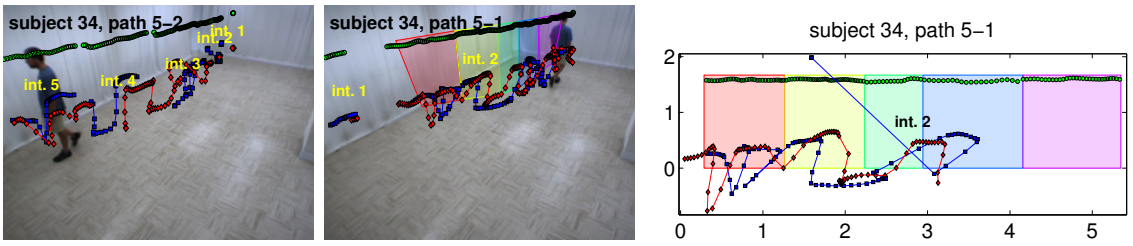

(a) (b) (c)

Figure 5.6 – Example of a problematic subject in the gait database (subject 34). In (a) the subject's feet could not be continuously tracked because of silhouettes segmentation error due to the subject's white cloths overlapping with the white curtains. In (b), the subject's foot positions are erroneous because of the same kind segmentation errors than in (a). The resulting view-rectified body-part trajectories are presented in (c).

were computed from the erroneous silhouettes. As one would expect in such a case, the view-rectified body-part trajectories are erroneous, as shown in Figure 5.6(c). There are other problematic walks in the gait database, as one may see by looking at the percentage of difference between the stature and the computed mean height in the table of Appendix C. For instance, there are some walks where segmentation errors led to erroneous height measurements for the following subjects: 6, 25, 46, and 51. In some cases, this segmentation errors had an erroneous effect on the other gait measurements as well. Another cause for erroneous gait measurements comes from the view-rectified body-part trajectories in gait half-cycles where the viewpoint is almost frontal, as shown previously in Figure 5.5 (subject 1, path 3-2; subject 36, path 4-1; subject 45, path 4-2; subject 43, path 5-1). It might be possible in future work to discard some gait half-cycles from the gait analysis, modelling and comparison process by evaluating if the height computed in those gait half-cycles is too different from the mean height, or if the normal vector of the head motion plane indicates that the viewpoint is too frontal.

5.2.3 Gait Modelling and Comparison Results

Gait modelling and comparison was performed on the gait database using the methods described in Sections 4.2 and 4.3, respectively. As one may recall, the proposed gait model is computed on a walk basis using either the position-based gait feature vectors or the velocity-based gait feature vectors. Also, a gait model consists in two parts, where the first part (part A) represents the gait when the left foot is moving, and the second part (part B) represents the gait when the right foot is moving. An improved representation for the gait models is learned using the gait feature vectors coming from

a subset of the walks for each subject and the LDA[1] algorithm. A gait model is then defined for each subject using the improved representation. The obtained models are part of what is called the *gallery*. The gait model of each walk not used in the learning process is called a *probe* and is compared to each gait model in the gallery using the improved representation. A gallery gait model and a probe gait model are compared by computing the sum of the Euclidean distance between the corresponding model parts (parts A and B). In the case where the gallery gait model and the probe gait model come from the same subject, the distance between the models should be low. Otherwise, the distance should vary according to the similarity between the gaits of the compared subjects.

Gait modelling was performed on the gait database using the position-based and the velocity-based gait models. In each case, 520 gait models were obtained, that is, one gait model for each walk of each subject. For each walk, the view-rectified body-part trajectories where sampled with the method described in Section 4.2.1, using $Q = 16$ samples. Using a higher number of samples did not lead to better results, whereas the performance started to degrade with a smaller number of samples. Computing a gait model for a walk takes on average 0.1 second on a computer with a dual core, 2.66 GHz CPU running non-optimized and non-parallelized MATLAB™ code. It would be realistic to perform gait modelling in real-time, by either performing it each x seconds or performing it once the subject exits the field of view of the camera.

Figures 5.7 and 5.8 present examples of gait models obtained for 4 different subjects and 4 different walks. A gait model is shown by plotting the value of each component of its feature vector. The vector of a position-based gait model has 64 components, while the vector of a velocity-based gait model has 60 components. In the case of position-based gait models, the components 1 to 16 and 17 to 32 are the x and y components of the head position, respectively, whereas the components 33 to 48 and 49 to 64 are the x and y components of the moving foot position, respectively. For the velocity-based gait models, the range are 1 to 15, 16 to 30, 31 to 45, and 46 to 60, respectively, and the components' value represents the x and y component of the velocity instead of the position.

One can see that the gait models are relatively similar in Figures 5.7 and 5.8. The parts A and B of the gait models also look similar. This is expected since the subjects are all performing the same action (walk) and all subjects in the database seemed to have a normal walk at acquisition time. The differences between the subjects' gait are subtle, but still visible. For instance, it is possible to see in the position-based gait models in Figure 5.7 that the amplitude of motion for subject 1 is higher than for

[1]The implementation of the LDA algorithm available in [105] was used in this thesis.

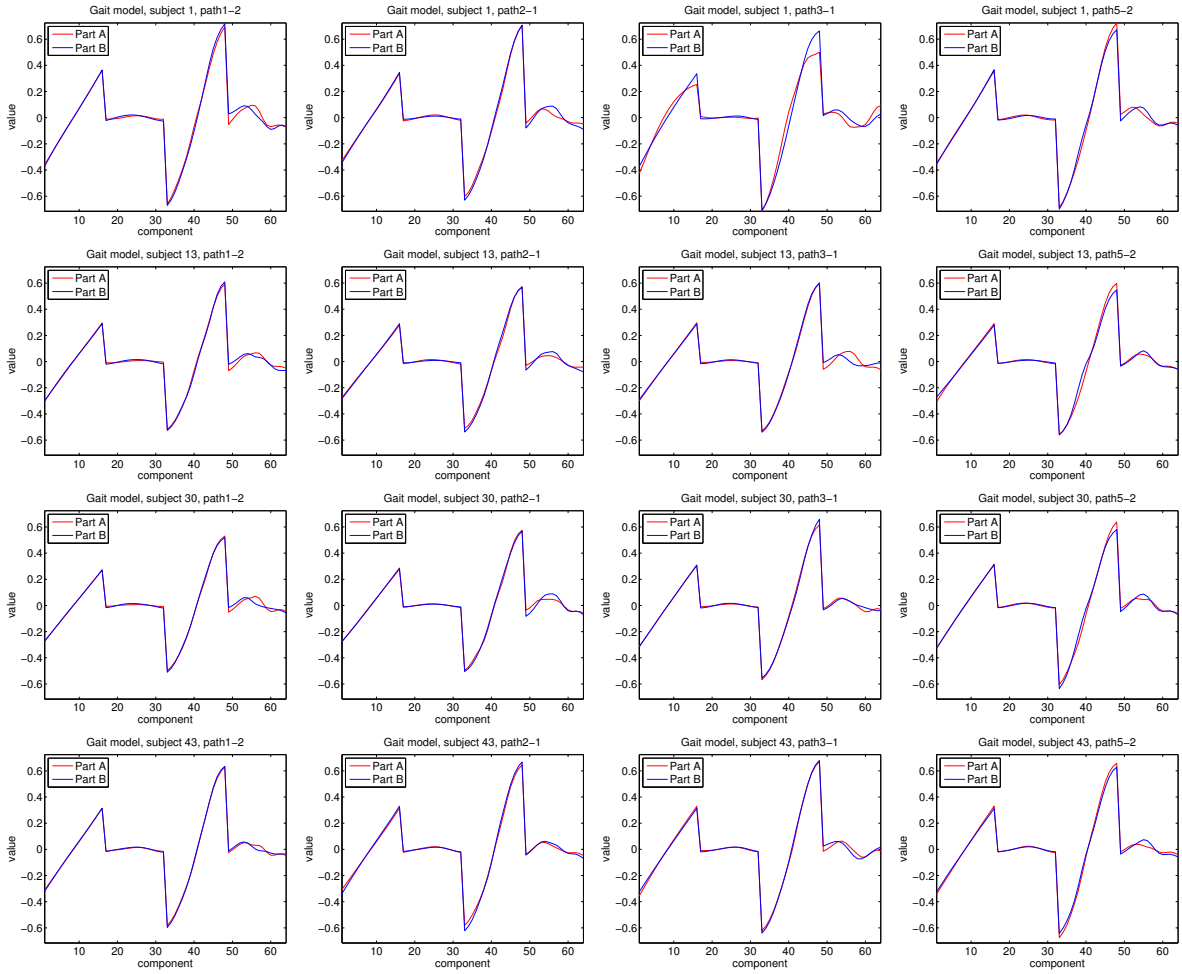

Figure 5.7 – Example of position-based gait models for four different subjects (rows) and four different paths (columns). Parts A and B of the gait models are shown on the same graphic. Each gait model a is 64-vector, which is shown by plotting the value of each vector's component. The paths are, from left to right, 1-2, 2-1, 3-1, and 5-2. The subjects are, from top to bottom, 1, 13, 30, and 43.

the other three subjects (longer head displacement, longer strides). The amplitude of motion for subject 43 is higher than for subject 13 and 30, and the amplitude of motion for subject 30 is higher than subject 30. In the case of velocity-based gait models, the velocity of subject 1 is the highest (fastest head and foot displacement), followed by subject 43. The two other subjects have similar velocity.

Gait modelling and comparison is difficult to assess since there is no ground truth available for the subjects gait similarity. The only ground truth that can be used here is the person identity. The comparison results are thus presented in the context of subjects recognition by their gait. The usual way of presenting gait recognition results consists in using *Cumulative Match Curves* (CMCs) [5]. A CMC shows recognition

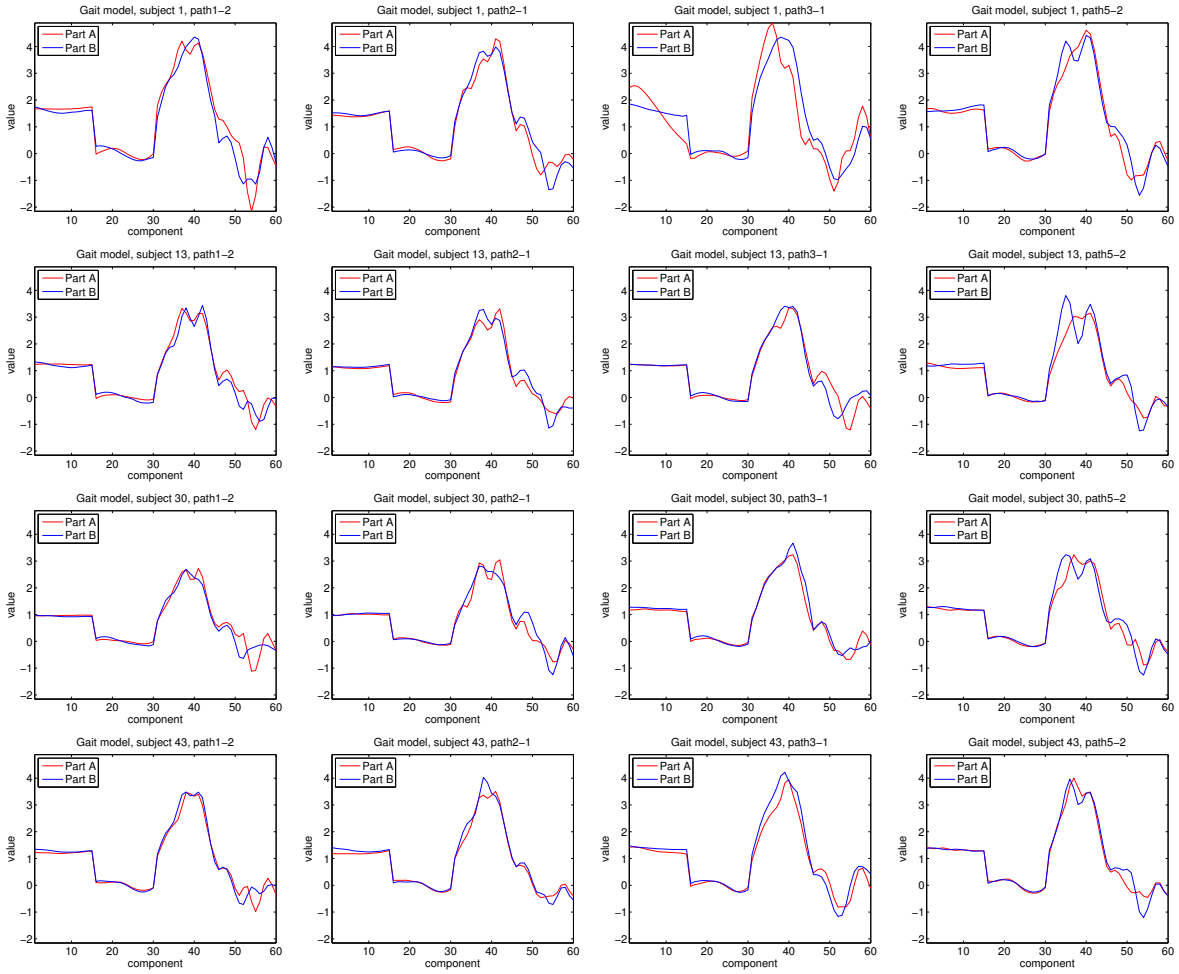

Figure 5.8 – Example of velocity-based gait models for four different subjects (rows) and four different paths (columns). Parts A and B of the gait models are shown on the same graphic. Each gait model a is 60-vector, which is shown by plotting the value of each vector's component. The paths are, from left to right, 1-2, 2-1, 3-1, and 5-2. The subjects are, from top to bottom, 1, 13, 30, and 43.

rate as a function of the rank, which is ranging from 1 to 52 (the number of subjects in the database). The subject corresponding to a given probe gait model is considered as recognized at rank k if the gallery gait model of the subject is in the k closest matches. The subject is also necessarily considered recognized for ranks greater than k. The CMC is thus a curve for which the value can only increase or remain the same between rank k and rank $k+1$. One must note that the recognition rate at rank 52 is necessarily 100%.

Figures 5.9(a) and 5.9(b) present examples of CMCs for position-based and velocity-based gait models, respectively. In these examples, the gait feature vectors from path 2-2 and 4-2 were used to obtain the gallery gait models. The gait model of the other

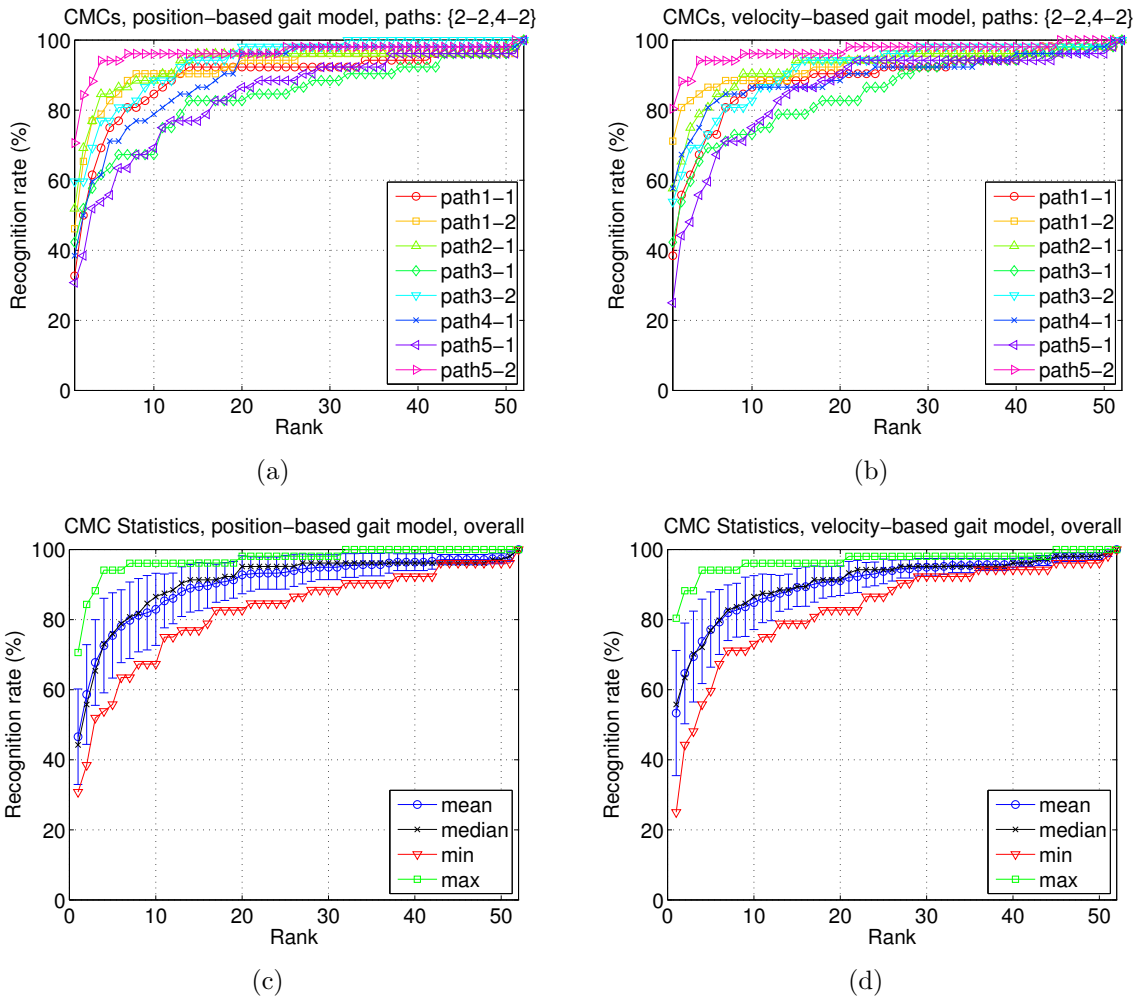

Figure 5.9 – Examples of Cumulative Match Curves (CMCs) obtained using the paths 2-2 and 4-2 as the gallery, and the other paths as the probes. In (a), the CMCs for the position-based gait models, and in (b), the CMCs for the velocity-based gait models. In (c) and (d), the CMC statistics of the CMCs in (a) and (b), respectively. The standard deviation is shown as error bars around be mean.

paths were used as probes, and the CMCs were computed on a path basis. For instance, the CMC for path 1-2 was obtained by computing the distance between each of the 52 probe gait models and the 52 gallery gait models, thus leading to $52 \times 52 = 2704$ gait model distances. Figures 5.9(c) and 5.9(d) present the statistics on the CMCs for the position-based and velocity-based gait models, respectively. These curves show the gait recognition statistics obtained at each rank from the CMCs of Figures 5.9(a) and 5.9(b).

It is possible to see from these results that the recognition rates are on average better for the velocity-based gait models than for the position-based gait models. One can also notice that recognition rates are lower for some probe paths than other ones.

For instance, the results for the probe paths 5-1 and 5-2 are significantly different, even if these two paths are on the same track. Indeed, the former has one of the lowest recognition rate, while the latter has the best recognition rate. It is possible to see in Table 5.8 that there is a significant difference between paths 5-1 and 5-2 with respect to the average strides lengths and cadence standard deviation. The values for the path 5-2 are close to the values of the paths 2-2 and 4-2 (the paths used for the gallery), while they are significantly different for path 5-1. This means there are significant difference between the probe gait model of path 5-1 and the gallery gait models, which makes the subjects harder to recognize by their gait. This is an expected conclusion since neither the position-based models nor the velocity-based models were designed to be invariant to changes in the cadence or in the stride length.

The above results have shown that the obtained recognition rates most likely depend on the paths used for the gallery. Therefore, all galleries formed by the combinations of 2, 3, and 4 paths where experimented independently for the position-based gait models and the velocity-based gait models. For each case, the number of experimented galleries is $\binom{10}{2} + \binom{10}{3} + \binom{10}{4} = 375$, where $\binom{n}{k}$ is the number of subsets of k elements in a set of n elements, without ordering (binomial coefficient). The total number of obtained CMCs is

$$\sum_{i=2}^{4} \binom{10}{i} (10 - i) = 2460, \tag{5.2}$$

where $(10 - i)$ is the number of probe paths, which depends on the number of paths used for the gallery. The total number of gait model comparisons is thus $2460 \times 52^2 = 6\,651\,840$. This high number of galleries and comparisons allows for obtaining a good estimate of the average time to perform the learning phase of a gallery, as well as the average time to make the 52×52 comparisons. On a computer with a dual core 2.66 GHz CPU running non-optimized and non-parallelized MATLAB™ code, the learning phase took on average 0.6 second, while 52×52 gait model comparisons took on average 28 seconds. Although the gait comparison process is the heaviest part of the whole process, it could still be performed in a real-time surveillance system since it doesn't need to be performed after each frame, as for the gait modelling process.

Figures 5.10 and 5.11 present the CMC statistics for the position-based gait model and the velocity-based gait model, respectively. The CMC statistics are shown independently for galleries formed with two paths, three paths and four paths. The overall CMC statistics is also presented. These results clearly show that the velocity-based gait model leads on average to higher recognition rates than the position-based gait model. Also, one may see that the use of more paths to form the gallery leads on average to slightly better recognition rates.

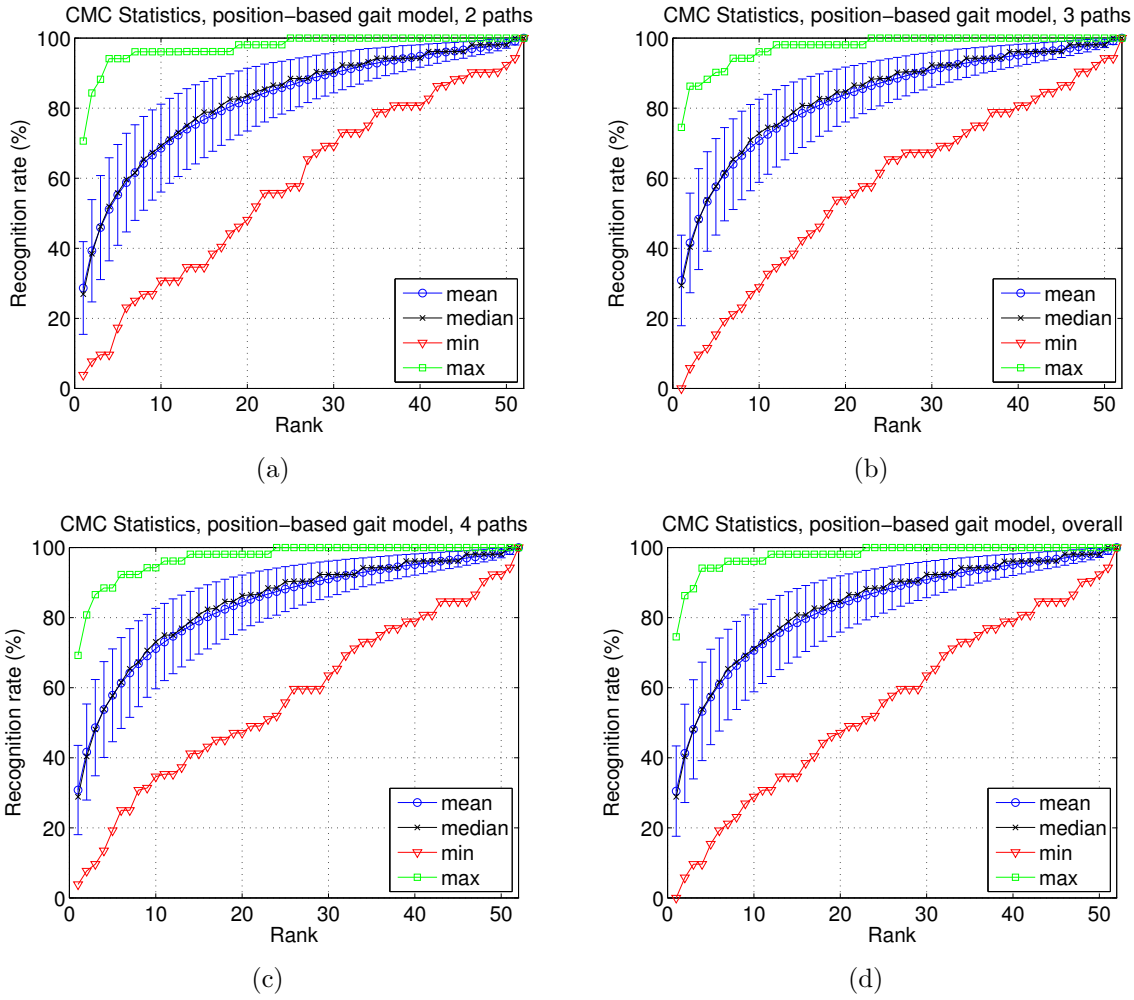

Figure 5.10 – Cumulative match curve statistics for position-based gait models. In (a), (b), and (c), the CMC statistics of using as the gallery all the combinations of two, three and four paths, respectively. In (d), the combined CMC statistics from (a), (b), and (c). The standard deviation is shown as error bars around be mean.

Overall, the above results highlight the fact that it is quite challenging to recognize people simply by their gait. Indeed, the differences between gaits of normal subjects is subtle, and the variations that are due to changes in walking speed make the recognition process even more difficult. Different combinations of paths for the gallery/probes also lead to different recognition rates. As mentioned previously, there is no ground truth available that could confirm that some subjects have similar gaits and thus cannot be easily set apart solely by their gait.

In terms of the robustness of the proposed method, there are cases where the view-rectified body-part trajectories are erroneous, as seen in Section 5.2.2. The view-rectified body-part trajectories in these cases clearly have a bad effect on the obtained

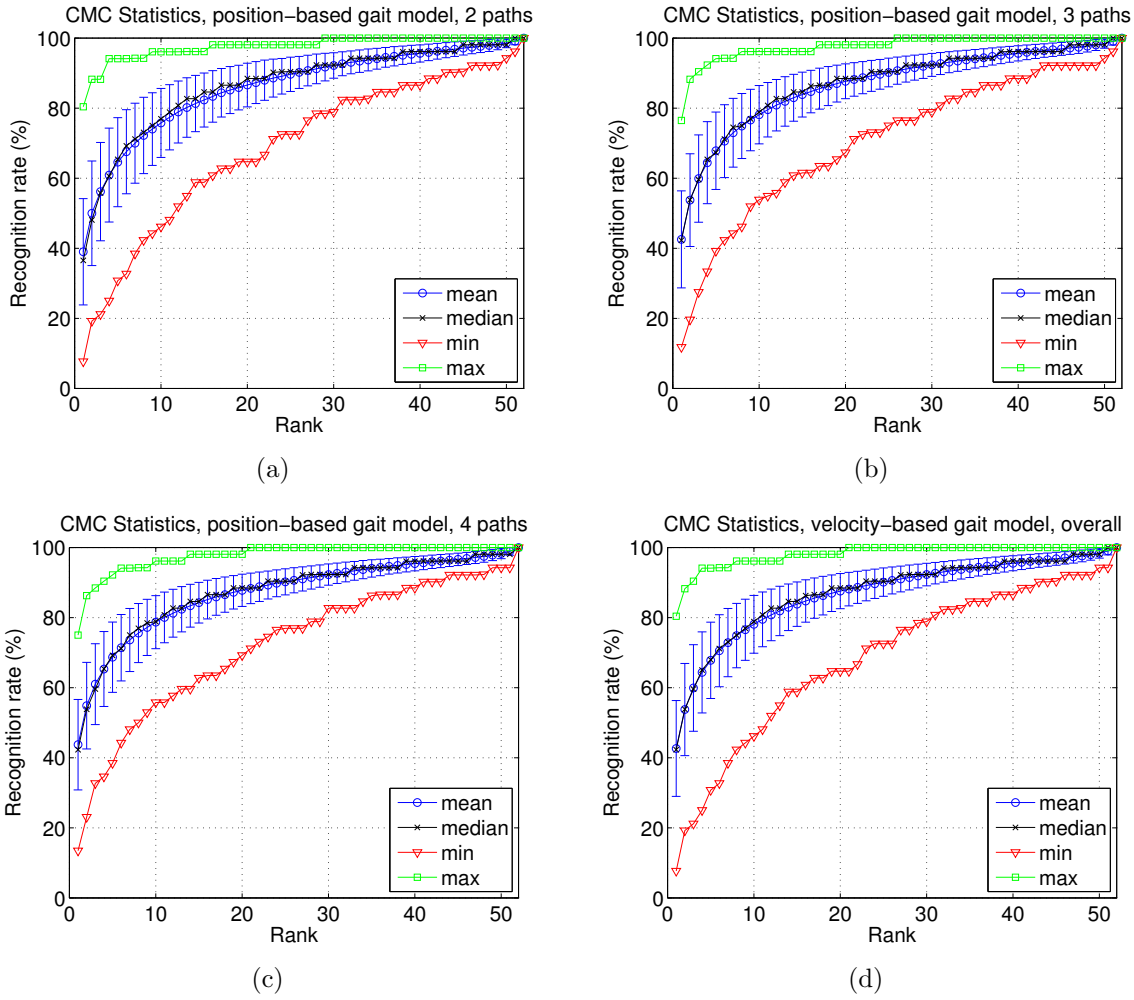

Figure 5.11 – Cumulative match curve statistics for velocity-based gait models. In (a), (b), and (c), the CMC statistics of using as the gallery all the combinations of two, three and four paths, respectively. In (d), the combined CMC statistics from (a), (b), and (c). The standard deviation is shown as error bars around be mean.

gait models for some subjects. The gait models are thus harder to match against other gait models of the same subjects. Fortunately, the gait half-cycles where these cases occur could potentially be discarded by analyzing the height and the orientation of the head motion plane. It might also be possible to discard the gait half-cycles for which the view-rectified trajectories do not lead to a realistic or possible motion. These two post-processing steps would help improving the results obtained with the gait analysis, modelling and comparison methods presented in this thesis.

The results presented here for gait modelling and comparison methods are quite good considering the difficult conditions in which they were obtained. For instance, these results were obtained only by considering the motion of the head and the feet.

There is thus no global appearance information used in the approach proposed in this thesis, which is in contrast with most of the gait modelling and comparison methods in the literature. As discussed previously in Section 1.3.1, it is still unclear to what extent the appearance-based methods benefit from the appearance information provided by the subjects' silhouettes. It is however clear that these methods would hardly work on the gait database used in this thesis since many of their assumptions would not hold. Indeed, in the proposed gait database the viewpoint is not fronto-parallel most of the time and it is continuously changing given the distance of the subjects to the camera. The silhouettes at the basis of the modelling and comparison in standard gait recognition methods are thus severely distorted by the perspective distortion. Moreover, these silhouettes could not be properly rectified since their contour points do not represent the same physical points on the scene from one gait cycle to another. The standard methods proposed in the literature are not invariant to changes in walk directions and walking speed. Although the gait models proposed in this thesis are not invariant to changes in walking speed, the view-rectification method is not influenced by them, and thus it returns a valid fronto-parallel view of the body-part trajectories. Therefore, it could be possible in future works to develop a gait model that is invariant to the walking speed by using the view-rectified body-part trajectories provided by the proposed view-rectification method.

Chapter 6

Conclusion

"I may not have gone where I intended
to go, but I think I have ended up
where I needed to be."

Douglas Adams

The approach proposed in this thesis aims at performing gait analysis, modelling, and comparison from unconstrained walks and viewpoints. Since the fronto-parallel viewpoint is optimal for gait analysis, modelling and comparison, a novel view-rectification method has been proposed in order to generate a fronto-parallel view of a person's walk from a monocular video sequence. The view-rectified walk can then be analyzed, modelled and compared as if the walk was continuously observed from a fronto-parallel viewpoint.

The proposed approach first consists in determining the imaged trajectory of the head and the feet from the monocular video sequence that represents a person's walk. This is performed by tracking the positions of the head and feet in each frame of the video sequence. The imaged feet trajectories are used to detect the gait half-cycles by detecting the times when the distance between the feet is maximal. The imaged motion planes, which are the image of the planes in which each body part motion is performed during a gait half-cycle, are determined using the estimated head and feet extremities at the beginning and end of the gait half-cycle. A fronto-parallel viewpoint of each motion plane is then computed using the camera intrinsic parameters and the estimated ground vanishing line. The homography that maps an imaged motion plane to its view-rectified counterpart is used to compute the view-rectified trajectory of the corresponding body part in a gait half-cycle. The obtained view-rectified trajectories thus represent what could be observed from a fronto-parallel view point.

View-rectified trajectories are used to perform gait analysis by extracting common gait measurements as cadence, speed, stride length, displacement, gait half-cycle duration, and height. Two gait models that are computed from the view-rectified trajectories are also proposed. The first gait model is based on the view-rectified position of the head and the feet, while the second gait model is based on the velocity of the head and the feet. Each gait model is formed of two parts, each part representing the gait when the left and the right feet are moving, respectively. An improved representation of the gait models is then learned using the LDA method on a subset of the available walks. The improved gait models are then compared by computing the Euclidean distance between each corresponding model part.

The proposed approach was first validated using synthetic walks comprising different viewpoints and changes in the walk direction. The validation results showed that the proposed view-rectification method works as expected, that is, valid gait measurements can be extracted from the view-rectified body-part trajectories. The proposed approach was used next to perform gait analysis, modelling, and comparison on real unconstrained walks, which were acquired as part of this thesis. The results first showed that the obtained gait measurements are realistic and correspond to the gait measurements found in references on clinical gait analysis. The gait comparison results then showed that the proposed approach can be used to perform gait modelling and comparison in the context of surveillance applications. The obtained recognition rate are quite good considering the challenging walks of the gait database.

6.1 Contributions

The approach proposed in this thesis provides significant contributions. These contributions are categorized here as theoretical, algorithmic and experimental:

1. Theoretical contributions
   (a) A novel walk model based on projective geometry that provides the spatio-temporal links between a normal walk performed in the scene and the corresponding imaged walk. The walk model only requires the knowledge of the imaged head and feet extremities at the beginning and at the end of the gait half-cycles. This walk model is used by the view-rectification method in order to compute view-rectified body-part trajectories.
   (b) Two novel gait models based on the view-rectified body-part positions and velocities, which are interpretable features (have a physical meaning). The

gait models are formed of two parts, each part representing the gait during a gait half-cycle. Features that are extracted from body-part trajectories have not been used before for gait modelling and comparison. Also, gait models in the literature are based on complete gait half-cycles and uses features that are not easily interpretable.

2. Algorithmic contributions
   (a) An automatic view-rectification method that generates a metric fronto-parallel viewpoint of body-part trajectories. The view-rectified body-part trajectories allow for extracting gait measurements and models in scene units. The proposed method works for non-frontal viewpoints as well as for walks with changes in direction and in speed. The obtained view-rectified body-part trajectories can be used for medical applications as well as for surveillance applications. The methods found in the literature are restricted to one of these applications.
   (b) An automatic, real-time body parts tracking method that tracks the head and the feet positions in the images while maintaining correspondence between the feet. It is based on silhouette analysis and motion correspondence.
   (c) A method for generating 3-D synthetic walks with changes in the walk direction. Synthetic 3-D body-part trajectories are generated and are imaged using a synthetic camera. The synthetic body-part trajectories are useful for validating a model-based, view-invariant gait analysis method.

3. Experimental contribution
   (a) A novel gait database consisting of walks containing changes in the walk direction and in the walk speed. Ten walks were performed by 52 subjects, leading to 520 walks. In comparison to existing database, the walks are less constrained in the proposed gait database and thus are more similar to a real indoor surveillance scenario.

6.2 Future Work

Future work would be focused on improving some aspects of the proposed approach, using it in other contexts, and performing further validation experiments on it. More precisely, the following elements could be part of future work:

- Validating the view-rectification method on real walk for which ground truth body-part positions are obtained with a motion capture system (e.g. a Vicon™

system). This would imply much work for the acquisition process since one would have to synchronize the motion capture system with the camera and define the camera position in the Euclidean coordinates frame of the motion capture system. Moreover, some methods would have to be developed to detect the gait half-cycles in the 3-D body-part trajectories obtained with the motion capture system. This would be necessary in order to validate the view-rectified body-part trajectories obtained with the view-rectification method proposed in this thesis.

- Performing gender recognition using the gait. A male gait model and a female gait model could be learned using a subset of walks in the gait database proposed in this thesis. The gender of a subject would be determined by comparing his or her gait model (probe) to the two gait models in the gallery.
- Performing gait modelling and comparison in the context of medical applications. This would require to learn a gait model for each considered gait pathology using a representative set of walks. A subject's gait pathology would then be identified by comparing his gait model (probe) to each gait pathology model in the gallery.
- Performing view-rectification of other body parts such as knees and hips. These two body parts could indeed be view-rectified with the foot motion planes since their motion is performed in those motion planes.
- Extending the gait models to include new body-parts as knees and hips. New gait models based on the angles between the foot, knee and hip could also be defined.
- Detecting and discarding bad gait half-cycles, that is, gait half-cycles for which the view is too frontal or for which the body-part trajectories do not represent a possible motion. Viewpoints that are too frontal would be detected by analyzing the orientation of the normal vector of the head motion plane. Impossible motion would be detected by putting constraints on the difference in position that is possible to obtained between two consecutive body-part positions in the view-rectified body-part trajectories.
- Performing automatic camera calibration using a subset of walks. This would be a extension of the parameters estimation process of the view-rectification method. Camera intrinsic parameters can by estimated by computing the Image of the Absolute Conic (IAC). The IAC can be computed using constraints defined using the horizontal and the vertical vanishing points obtained from the subset of walks.

6.3 Related Publications

The proposed approach led to several publications in peer-reviewed conference proceedings and in journals. These publications cover some parts of the proposed approach, and some of them are earlier attempts for the methods proposed in this thesis.

The body-part tracking method is presented in [106]. A method for tracking the hands is also proposed in this publication, but it is not used in this thesis since the hands can not be reliably used for gait modelling. Indeed, the hand motion is not constrained during walk, that is, the subjects can do many different actions with their hands while walking.

The first version of the view-rectification method is presented in [107, 108]. This method doesn't use the concept of gait half-cycle. It computes one plane for each linear walk direction and uses it to perform view-rectification on both the head and feet trajectories. The obtained view-rectified trajectories are not metric, and the relative position of the head and feet in the scene is not recovered because their motion was considered as performed in the same plane.

The second version of the view-rectification method was presented in [109, 110]. This version of the method introduced the concept of view-rectification on a gait half-cycle basis. As in the first version of the method, only one plane was used to perform view-rectification of both head and feet trajectories.

The view-rectification method proposed in this thesis is presented in [111]. The proposed gait analysis, modelling and comparison methods will constitute the subject of future publications.

Appendix A

Generation of a Synthetic Walk

This appendix describes the method used to generate synthetic walks. Synthetic walks are used in Section 5.1 in order to validate the view-rectification method proposed in Chapter 3.

The generation of a synthetic walk consists in three steps: (i) synthetic path definition (Section A.1), (ii) 3-D body-part trajectories generation (Section A.2), and (iii), synthetic camera viewpoint definition (Section A.3). The method proposed here is based on the walk model presented in Section 3.3. The 3-D body-part trajectories are thus generated so that they lie in the motion planes described in the walk model.

In order to generate a 3-D synthetic walk, several parameters must be defined:

- h, the height of the synthetic walker;
- l, the label of the leading foot ($l \in \{\mathsf{R}, \mathsf{L}\}$), which is the foot that will move first in the synthetic walk;
- δ_{s}, the stride length of the leading foot;
- δ_{w}, the stride width;
- δ_{t}, the duration in frames of a gait half-cycle;
- ν_{H}, the vertical amplitude of the head motion as a percentage of the height h;
- ν_{F}, the vertical amplitude of the foot motion as a percentage of the height h;
- $\mathbf{O}$, the initial 3-D position of the leading foot;
- $\{\theta_j\}$, $j = 1, 2, \cdots, J$, the angles representing the direction of motion of the leading foot for each gait half-cycle in which it is moving.

Algorithm A.1: Extremity positions of the leading foot.

$\mathbf{E}_l[1] = \mathbf{O}$ ⇒ *initial extremity position*
$\mathbf{E}_l[2] = \mathbf{O} + \left(\frac{\delta_\mathrm{s}}{2}\cos\theta_1,\ 0,\ \frac{\delta_\mathrm{s}}{2}\sin\theta_1\right)^\mathsf{T}$ ⇒ *foot is moving, half stride*
$\mathbf{E}_l[3] = \mathbf{E}_l[2]$ ⇒ *foot is still*
$K = 3$
for $j = 2, \ldots, J$ **do**
  $K = K + 1$
  $\mathbf{E}_l[K] = \mathbf{E}_l[K-1] + (\delta_\mathrm{s}\cos\theta_j,\ 0,\ \delta_\mathrm{s}\sin\theta_j)^\mathsf{T}$ ⇒ *foot is moving*
  $K = K + 1$
  $\mathbf{E}_l[K] = \mathbf{E}_l[K-1]$ ⇒ *foot is still*
end for

Also, some parameters are needed in order to define a synthetic camera viewpoint:

- f, the focal length of the camera (in meters);
- ζ, the size (in meters) of a pixel on the synthetic camera sensor (pixels are square);
- (u_0, v_0), the coordinate of the camera principal point in the image (in pixels);
- $\mathbf{X}_\mathrm{c}$, the 3-D position of the camera in the scene;
- $(\alpha_y, \alpha_x, \alpha_z)$, the orientation of the camera in the scene, defined as the rotation angles around the scene axes Y, X, and Z (in that order).

Each required step for the generation of a synthetic walk is presented in the following sections. This appendix is then concluded by describing the minor modifications to some of the steps of the view-rectification method so that synthetic body-part trajectories can be processed.

A.1 Synthetic Path Definition

The first step of the generation of a synthetic walk consists in defining a synthetic path followed by the "synthetic walker"; that is, the direction of motion of the head and the feet are defined in the scene for each key time of a walk. This is performed by first defining on a key time basis the extremity positions of the leading foot on the ground plane using the provided 3-D initial position $\mathbf{O}$ and the set of J directions $\{\theta_j\}$, $j = 1, 2, \cdots, J$. One must note that the leading foot is defined here as the foot that moves in the first gait half-cycle. It is the foot for which the initial position and the direction of motion are specified as parameters. All the other 3-D body-part extremities and trajectories will be defined with respect to the leading foot extremity

Algorithm A.2: Extremity positions of the trailing foot.

if $l = \mathsf{L}$ **then** ⇒ *leading foot is the left foot*
  $\epsilon = 1$
else if $l = \mathsf{R}$ **then** ⇒ *leading foot is the right foot*
  $\epsilon = -1$
end if
$\mathbf{D} = \text{unit}\,(\mathbf{E}_l[2] - \mathbf{E}_l[1])$ ⇒ *unit vector on the leading foot stride line*
$\mathbf{D}_\perp = \text{perp}\,(\mathbf{D})$ ⇒ *perpendicular vector in the $X - Z$ plane*
$\mathbf{E}_{\bar{l}}[1] = \mathbf{E}_l[1] + \epsilon\delta_\text{w}\mathbf{D}_\perp$ ⇒ *position for first key time*
for $k = 2, \ldots, K-1$ **do**
  if k is even **then** ⇒ *trailing foot is still*
    $\mathbf{E}_{\bar{l}}[K] = \mathbf{E}_{\bar{l}}[K-1]$
  else if k is odd **then** ⇒ *trailing foot is moving*
    $\mathbf{D} = \text{unit}\,(\mathbf{E}_l[k+1] - \mathbf{E}_l[k])$
    $\mathbf{D}_\perp = \text{perp}\,(\mathbf{D})$
    $\mathbf{E}_{\bar{l}}[k] = \frac{1}{2}\,(\mathbf{E}_l[k] + \mathbf{E}_l[k+1]) + \epsilon\delta_\text{w}\mathbf{D}_\perp$ ⇒ *position for kth key time*
  end if
end for
$\mathbf{D} = \text{unit}\,(\mathbf{E}_l[K-1] - \mathbf{E}_l[K-2])$
$\mathbf{D}_\perp = \text{perp}\,(\mathbf{D})$
$\mathbf{E}_{\bar{l}}[K] = \mathbf{E}_l[K] + \epsilon\delta_\text{w}\mathbf{D}_\perp$ ⇒ *position for last key time*

positions. Also, the coordinates in the synthetic scene are defined using three axes, X, Y, and Z, where the Y axis represents the vertical direction and the plane $Y = 0$ (the $X - Z$ plane) represents the ground plane.

The definition of the leading foot extremity position at each key time is performed using Algorithm A.1, and an example of defined extremity positions is shown in Figure A.1(a). One should note that the length of the first stride performed by the leading foot is $\delta_\text{s}/2$ since the walk is simulated from a standing position where both feet are side by side and are in contact with the ground plane. Beside the initial extremity position $\mathbf{E}_l[1]$ and the extremity position $\mathbf{E}_l[2]$, the other extremity positions of the leading foot are defined as per the walk model described in Section 3.3 (if the leading foot is moving in a given gait half-cycle, then it is still in the previous and the next gait half-cycles). One must note that by providing J directions for the leading foot, the synthetic walk will consist in $K = 2J + 1$ key times, and therefore $C = K - 1 = 2J$ gait half-cycles.

The extremity positions of the trailing foot l are computed using Algorithm A.2, and an example of the computed trailing foot extremity positions is shown in Figure A.1(b). The extremity positions of the trailing foot for the first and the last key times

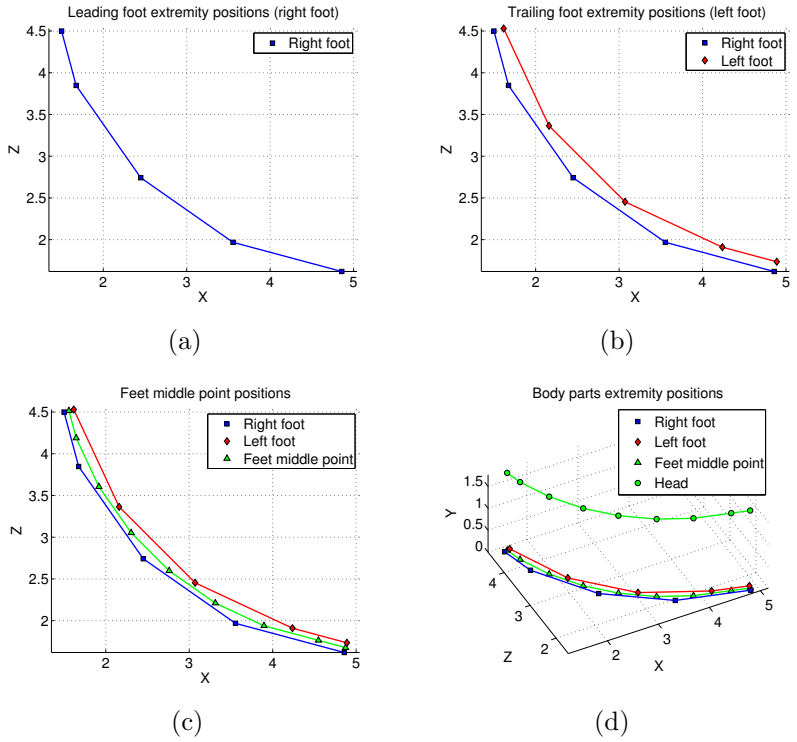

Figure A.1 – Example of computed 3-D body-part extremities. The parameters that are used in this example are $h = 1.8\,\mathrm{m}$, $\delta_\mathrm{s} = 1.35\,\mathrm{m}$, $\delta_\mathrm{w} = 0.12\,\mathrm{m}$, and the leading foot is the right foot ($l = \mathsf{R}$). In (a), the extremity positions of the leading foot on the ground plane $X - Z$ are computed for an initial position $\mathbf{O} = (1.5,\, 0,\, 4.5)^\mathsf{T}$ and for direction angles $\{-75°, -55°, -35°, -15°\}$. In (b), the computed trailing foot extremity positions are shown along with the extremity positions of the leading foot, and in (c), the computed feet middle point are shown. In (d), the computed feet extremity positions, the feet middle points and the head extremity positions are shown in the synthetic scene.

are computed such that the synthetic walker stands still; that is, the trailing foot position is at a distance δ_w (the stride width) from the leading foot, in the direction perpendicular to the motion of the leading foot in the first and the last gait half-cycles. Besides these two cases, the kth trailing foot extremity position is computed such that it is at a distance of δ_w from the middle point on the line segment joining the kth and the $(k+1)$th leading foot extremity positions.

Once the extremity positions of both feet are computed, it is possible to compute the feet middle point positions $\mathbf{E}_\mathsf{M}[k]$ as

$$\mathbf{E}_\mathsf{M}[k] = \frac{1}{2}\left(\mathbf{E}_\mathsf{L}[k] + \mathbf{E}_\mathsf{R}[k]\right). \tag{A.1}$$

The head extremity positions are then computed as the positions at a distance of

$h(1-\nu_{\mathsf{H}})$ above the feet middle point positions:

$$\mathbf{E}_{\mathsf{H}}[k] = \mathbf{E}_{\mathsf{M}}[k] + \big(0,\, h(1-\nu_{\mathsf{H}}),\, 0\big)^{\mathsf{T}}. \tag{A.2}$$

As described in the walk model, the head is not at its highest position with respect to the ground plane at each key time since the feet are further apart at these times, and thus the walker should appear a little bit shorter. Examples of computed feet middle positions and head extremity positions are shown in Figures A.1(c) and A.1(d).

Finally, the key times are defined as follow:

$$t_k = \begin{cases} 1 & \text{if } k = 1, \\ t_{k-1} + \delta_{\mathrm{t}} & \text{otherwise.} \end{cases} \tag{A.3}$$

One must note that a key time might not be an integer frame number depending on the value of the duration parameter δ_{t}.

A.2 3-D Body-part Trajectories Generation

The 3-D body-part trajectories are generated on a gait half-cycle basis once the head and the feet extremity positions are determined at each key time. The body-part positions that are going to be generated at each frame in a gait half-cycle will represent the body-part extremity positions at each frame, and not the body-part mass centre as in the case of a real walk. This simplifies the synthetic walk generation process by only having to generate one position per frame per body part, instead of having to generate a mass centre position along with a bounding box for each body part at each frame. The implications of this simplification on the use of the view-rectification method with the synthetic imaged body-part trajectories will be discussed in Section A.4.

A.2.1 3-D Head Trajectory Generation

A 3-D head trajectory is generated as a 3-D curve having a sinusoidal motion component in the direction of the walk as well as a sinusoidal motion component in the vertical direction. There is no lateral motion component, which means that the 3-D head trajectory lies in a plane perpendicular to the ground plane and parallel to the direction of the walk for a given gait half-cycle (i.e the head trajectory lies in the head motion plane as defined in the walk model). For a gait half-cycle c, the *normalized* position of

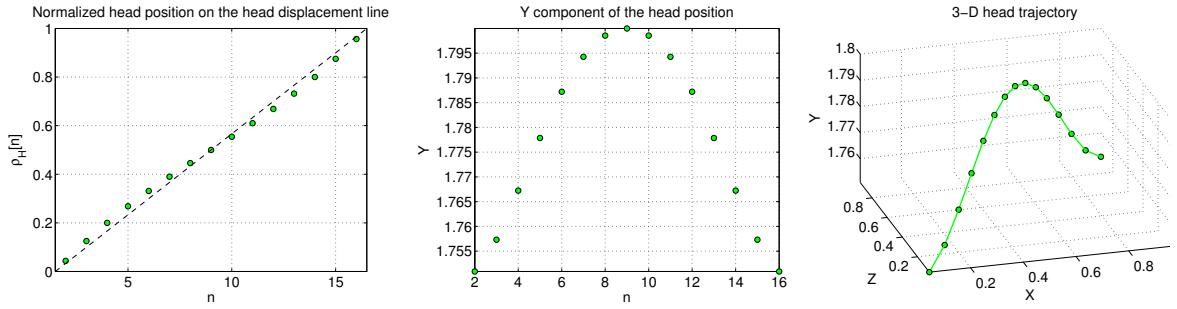

(a) (b) (c)

Figure A.2 – Example of 3-D head trajectory for a gait half-cycle c that starts at key time $t_c = 1.5$ and ends at key time $t_{c+1} = 16.5$ ($\delta_t = 15$). The parameters are the same as in Figure A.1, and $\nu_H = 0.0278$. In (a), the normalized positions of the head on the head displacement line. This represents the sinusoidal motion component in the direction of walk. The vertical motion component of the head is shown in (b), and the 3-D head trajectory is shown in (c).

the head on the head line segment defined by the extremity positions $\mathbf{E}_H[c]$ and $\mathbf{E}_H[c+1]$ (i.e. the head displacement line) is defined as

$$\rho_H[n] = \frac{8\tau[n] + \cos(\pi\tau[n]) - 1}{6}, \tag{A.4}$$

where $\tau[n]$ is the *normalized* time in gait half-cycle c and is defined as

$$\tau[n] = \frac{n - \lceil t_c \rceil}{\lfloor t_{c+1} \rfloor - \lceil t_c \rceil}, \quad \lceil t_c \rceil \leq n \leq \lfloor t_{c+1} \rfloor . \tag{A.5}$$

The normalized time $\tau[n]$ represents the percentage of the gait cycle c in function of the frame number such that $\tau[\lceil t_c \rceil] = 0$ and $\tau[\lfloor t_{c+1} \rfloor] = 1$. Similarly, $\rho_H[n]$ represents the normalized position of the head on the head displacement line such that $\rho_H[\lceil t_c \rceil] = 0$ and $\rho_H[\lfloor t_{c+1} \rfloor] = 1$. This represents the head sinusoidal motion component in the direction of the walk and it is designed so that the velocity of the head is faster at the beginning and at the end of the gait half-cycle, and slower in the middle of the gait half-cycle. An example of the normalized position of the head is shown in Figure A.2(a).

The 3-D head trajectory $\mathbf{P}_H[n]$ in gait half-cycle c starting at key time t_c and ending at key time t_{c+1} is then computed using the normalized time and the normalized position of the head on the head displacement line as

$$\mathbf{P}_H[n] = \begin{bmatrix} E_{H,x}[c] + \rho_H[n]\big(E_{H,x}[c+1] - E_{H,x}[c]\big) \\ E_{H,y}[c] + \frac{h\nu_H}{2}\big(1 - \cos(2\pi\rho_H[n])\big) \\ E_{H,z}[c] + \rho_H[n]\big(E_{H,z}[c+1] - E_{H,z}[c]\big) \end{bmatrix}, \tag{A.6}$$

where $E_{H,x}[c]$, $E_{H,y}[c]$, and $E_{H,z}[c]$ are the X, Y, and Z component of the head extremity position at key time t_c, and $\lceil t_c \rceil \leq n \leq \lfloor t_{c+1} \rfloor$. It is possible to see that the vertical

component of the head trajectory is designed such that it is maximal at the middle of the gait half-cycle (equals to h), and minimal at the beginning and at end of the gait half-cycle (equals to $h(1-\nu_{\mathsf{H}})$). An example of the vertical component of the head is shown in Figure A.2(b), and the 3-D trajectory of the head is shown in Figure A.2(c).

A.2.2 3-D Foot Trajectory Generation

The 3-D foot trajectory is generated such that the motion component in the direction of the walk is at a complete stop at the beginning and at the end of the gait half-cycles, and at a maximum velocity in the middle of the gait half-cycle. The vertical component of the foot is designed such that it is at the ground level ($Y = 0$) at the beginning and at the end of the gait half-cycle, and at a maximal height in the middle of the gait half-cycle. There will be no lateral motion component, which means that the 3-D foot trajectory will lie in a plane slightly slanted with respect to the vertical (i.e the foot trajectory lies in the foot motion plane as defined in the walk model).

For a gait half-cycle c, the positions of the still foot (with label $\bar{m}$) are defined as

$$\mathbf{P}_{\bar{m}}[n] = \mathbf{E}_{\bar{m}}[c], \quad \lceil t_c \rceil \leq n \leq \lfloor t_{c+1} \rfloor, \tag{A.7}$$

that is, all the foot positions in the gait half-cycle are equal to the foot extremity position at the beginning of the gait half-cycle. In the case of the moving foot (with label m), the normalized position of the foot on the stride line is defined as

$$\rho_{\mathsf{F}}[n] = \frac{1-\cos\left(\pi\tau[n]\right)}{2}, \tag{A.8}$$

where $\tau[n]$ is the normalized time in the gait half-cycle c, as defined in Equation A.4. An example of the normalized positions of the foot is shown in Figure A.3(a).

The 3-D foot trajectory for the moving foot in gait half-cycle c is defined using the normalized time $\tau[n]$ and the normalized foot positions on the stride line $\rho_{\mathsf{F}}[n]$:

$$\mathbf{P}_m[n] = \begin{bmatrix} E_{m,x}[c] + \rho_{\mathsf{F}}[n]\big(E_{m,x}[c+1] - E_{m,x}[c]\big) \\ 0 \\ E_{m,z}[c] + \rho_{\mathsf{F}}[n]\big(E_{m,z}[c+1] - E_{m,z}[c]\big) \end{bmatrix} + \frac{h\nu_{\mathsf{F}}\big(1-\cos\left(2\pi\rho_{\mathsf{F}}[n]\right)\big)}{2}\mathbf{V}[c], \tag{A.9}$$

where the vector $\mathbf{V}[c]$ is defined for a gait half-cycle c as

$$\begin{aligned}\mathbf{V}[c] = \mathrm{unit}\Big\{ & \mathbf{E}_{\mathsf{H}}[c] - \mathbf{E}_m[c] - \\ & \big\langle \mathbf{E}_{\mathsf{M}}[c] - \mathbf{E}_m[c], \mathrm{unit}\left(\mathbf{E}_m[c+1] - \mathbf{E}_m[c]\right)\big\rangle \,\mathrm{unit}\big(\mathbf{E}_m[c+1] - \mathbf{E}_m[c]\big)\Big\},\end{aligned} \tag{A.10}$$

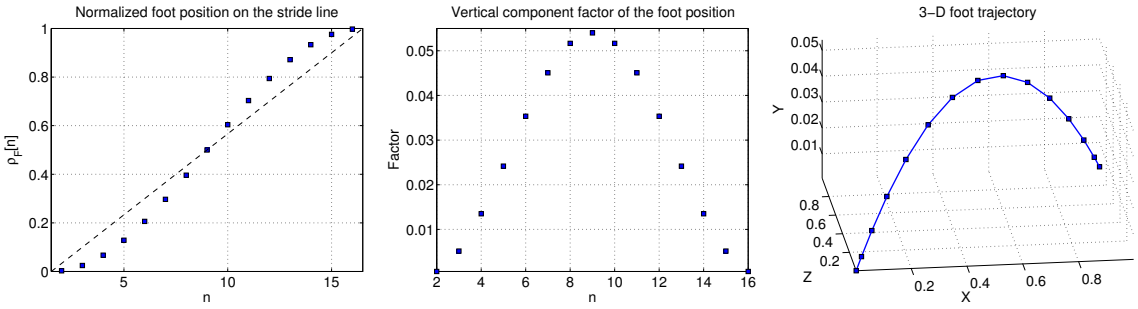

(a) (b) (c)

Figure A.3 – Example of 3-D foot trajectory for a gait half-cycle c that starts at key time $t_c = 1.5$ and ends at key time $t_{c+1} = 16.5$ ($\delta_t = 15$). The parameters are the same as in Figure A.1, and $\nu_F = 0.03$. In (a), the normalized positions of the foot on the stride line. The vertical motion component of the foot is shown in (b), and the 3-D foot trajectory is shown in (c).

where $\text{unit}(\mathbf{X}) = \mathbf{X}/\|\mathbf{X}\|$, and $\langle \mathbf{X}, \mathbf{Y} \rangle$ is the inner product of vectors $\mathbf{X}$ and $\mathbf{Y}$. The first term of Equation A.9 defines a position on the $X - Z$ plane (ground plane), which is also a position on the stride line. The second term of Equation A.9 defines a vector perpendicular to the stride line but slightly slanted with respect to the vertical direction such that it points towards the head displacement line. The length of this vector is defined according to the factor $\frac{1}{2}h\nu_F\big(1 - \cos(2\pi\rho_F[n])\big)$, which equals zero at the beginning and at the end of the gait half-cycle, and equals $h\nu_F$ in the middle of the gait half-cycle. An example of the values taken by this factor is shown in Figure A.3(b), and an example of a 3-D foot trajectory is presented in Figure A.3(c).

An example of the 3-D body-part trajectories obtained for a synthetic walk are presented in Figure A.4. The synthetic walk consists in 8 gait half-cycles where the synthetic walker changes the direction of walk by about 10° for each gait half-cycle (except the last one). The vertical component of the head motion is sinusoidal and is similar to what can be observed from a real walk. Moreover, the foot trajectories respect the typical dynamics of the walk pattern, that is, when a foot is moving, the other foot is still. The synthetic walk starts and ends with the two feet side by side, and thus, the first and the last "half-cycles" are not complete.

A.3 Synthetic Camera Viewpoint Definition

An image of the 3-D body-part trajectories can be generated from a given position and orientation by defining a synthetic camera viewpoint in the synthetic scene. This is

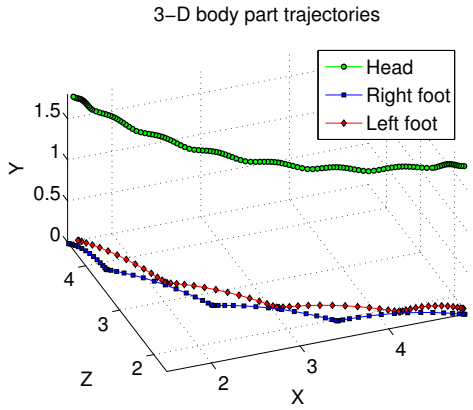

Figure A.4 – Example of generated 3-D body-part trajectories obtained for a synthetic walk. The parameters are $h = 1.8$ m, $\delta_{\mathrm{s}} = 1.35$ m, $\delta_{\mathrm{w}} = 0.12$ m, $\delta_{\mathrm{t}} = 15$, $l = \mathsf{R}$, $\nu_{\mathsf{H}} = 0.0194$, $\nu_{\mathsf{F}} = 0.03$, $\mathbf{O} = (1.5,\, 0,\, 4.5)^{\mathsf{T}}$ and the direction angles are $\{-75°, -55°, -35°, -15°\}$.

performed by defining a projection matrix $\mathbf{M}$ that transforms the 3-D points in the scene into 2-D points in the synthetic camera image [98]. The matrix $\mathbf{M}$ is defined as

$$\mathbf{M} = \mathbf{K}\,\mathbf{R}\,\big[\mathbf{I}_{3\times 3}\big|{-\mathbf{X}_{\mathrm{c}}}\big], \tag{A.11}$$

where $\mathbf{K}$ is the synthetic camera intrinsic parameters, $\mathbf{X}_{\mathrm{c}}$ is the 3-D position of the camera in scene coordinates, $\mathbf{I}_{3\times 3}$ is a 3×3 identity matrix, and $\mathbf{R}$ is a rotation matrix that defines the orientation of the camera in the scene. The camera intrinsic parameters matrix is defined as

$$\mathbf{K} = \begin{bmatrix} f\zeta^{-1} & 0 & u_0 \\ 0 & -f\zeta^{-1} & v_0 \\ 0 & 0 & 1 \end{bmatrix}, \tag{A.12}$$

where f is the camera focal length (in meters), ζ is the size of a pixel (in meters), and (u_0, v_0) is the coordinate in pixels of the principal point. One must note here that the synthetic camera has square pixels (no skew). The rotation matrix $\mathbf{R}$ is defined as the product of three rotation matrices $\mathbf{R}_z$, $\mathbf{R}_x$, and $\mathbf{R}_y$:

$$\mathbf{R} = \underbrace{\begin{bmatrix} \cos\alpha_z & -\sin\alpha_z & 0 \\ \sin\alpha_z & \cos\alpha_z & 0 \\ 0 & 0 & 1 \end{bmatrix}}_{\mathbf{R}_z} \underbrace{\begin{bmatrix} 1 & 0 & 0 \\ 0 & \cos\alpha_x & -\sin\alpha_x \\ 0 & \sin\alpha_x & \cos\alpha_x \end{bmatrix}}_{\mathbf{R}_x} \underbrace{\begin{bmatrix} \cos\alpha_y & 0 & \sin\alpha_y \\ 0 & 1 & 0 \\ -\sin\alpha_y & 0 & \cos\alpha_y \end{bmatrix}}_{\mathbf{R}_y}, \tag{A.13}$$

where α_y, α_x, and α_z are the rotation angle to apply to the scene axes Y, X, and Z in order to define the orientation of the camera.

Once the synthetic camera projection matrix is defined, the imaged position $\mathbf{p}_\ell[n]$ of each 3-D position $\mathbf{P}_\ell[n]$ of a body part $\ell \in \{\mathsf{H}, \mathsf{L}, \mathsf{R}\}$ is computed as

$$\widetilde{\mathbf{p}}_\ell[n] = \mathbf{M}\,\widetilde{\mathbf{P}}_\ell[n], \tag{A.14}$$

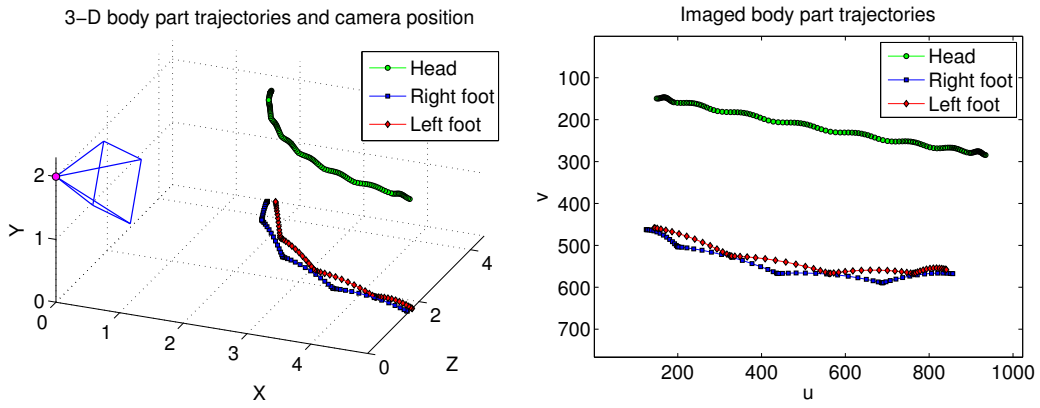

(a) (b)

Figure A.5 – Example of 3-D and imaged body-part trajectories. In (a), the 3-D body-part trajectories of a synthetic walk are shown along with the camera position (magenta point) and orientation (blue pyramid). In (b), the imaged body-part trajectories are shown in the synthetic camera image (1024×768). The synthetic walk parameters are the same as in Figure A.4. The synthetic camera parameters are $\mathbf{X}_{\mathrm{c}} = (0, 2, 0)^{\mathsf{T}}$, $f = 8$ mm, $\zeta = 10$ µm, $(u_0, v_0) = (512, 384)$, and $(\alpha_y, \alpha_x, \alpha_z) = (-45°, -15°, -10°)$.

where $\widetilde{\mathbf{P}}_\ell[n]$ and $\widetilde{\mathbf{p}}_\ell[n]$ are the homogeneous coordinates representation of $\mathbf{P}_\ell[n]$ and $\mathbf{p}_\ell[n]$, respectively. An example of 3-D body-part trajectories and their imaged counterpart is shown in Figure A.5.

A.4 Conclusion

The proposed method for generating a synthetic walk is used in Section 5.1 in order to validate the view-rectification method. The view-rectified body-part trajectories are obtained using the proposed view-rectification method on the synthetic imaged body-part trajectories. Validation of the view-rectified body-part trajectories is possible since all the ground truth gait measurements (stride lengths, gait half-cycle durations, displacements, heights, cadence, speed) can be obtained from the generated 3-D body-part extremities and the parameters of the synthetic walk. Moreover, the ground truth fronto-parallel body-part trajectories can be obtained from the 3-D body-part trajectories since the plane in which each 3-D body-part trajectory lie is known. The view-rectified body-part trajectories can thus be validated on a gait half-cycle basis by performing a point to point comparison with the ground truth body-part trajectories.

There are two remarks to make on the processing of the synthetic body-part tra-

jectories by the proposed view-rectification method. Firstly, one should note that the first and the last gait half-cycle are not complete, and thus are not be processed by the view-rectification method. Indeed, the first and the last "key times" t_1 and t_K are not valid key times, that is, the feet distance is not maximal at these times. Thus, the view-rectification method will process the body-part trajectories from t_2 to t_{K-1}. Secondly, minor changes to the view-rectification method are also needed since the generated body-part trajectories represent body-part extremity positions instead of mass centre positions, and no body-part bounding boxes are generated. For these reasons, the foot extremity position (Section 3.5.1.1) at frame n is now defined as $\mathbf{p}_{\ell\mathsf{B}}[n] = \mathbf{p}_{\ell}[n]$, $\ell \in \{\mathsf{L}, \mathsf{R}\}$. Similarly, the position of the top of the silhouette (Section 3.5.1.3) at frame n is now defined as $\mathbf{p}_{\mathsf{HT}}[n] = \mathbf{p}_{\mathsf{H}}[n]$. The head extremity at key time t_c is thus defined as $\mathbf{e}_{\mathsf{H}}[c] = \mathbf{p}_{\mathsf{HT}}(t_c)$, which is a linear interpolation of the position of the top of the silhouette. All other steps of the proposed view-rectification method remain unchanged.

Appendix B

Gait Database Acquisition Setup

This appendix presents the gait database that was acquired in the context of this thesis. The acquisition process was performed in the acquisition room of the Computer Vision and Systems Laboratory at Université Laval. As discussed in section 1.3.3, this database has some characteristics not found in other gait databases, and as such, it is a contribution of the thesis. The main characteristic of the database is the wide range of viewpoints that is induced by the direction of the walks and the direction change during the walks with respect to the camera optical axis.

The remaining of this appendix is structured as follow. The acquisition room layout is presented in Section B.1 and the hardware used in the acquisition process is described in Section B.2. The camera calibration procedure is detailed in Section B.3. The walk tracks on which the subjects walked and the data that was acquired during the acquisition process are described in Sections B.4 and B.5 respectively.

B.1 Acquisition Room Layout

The acquisition room layout is presented in Figure B.1, and some photos are presented in Figure B.2. Since this thesis in not focused on improving background subtraction algorithms, a simple white background was used in order to get good contrast between the background and the subjects. The white background was obtained by using curtains that delineate the workspace needed for the acquisition process. The curtains were attached to the ceiling and were fixed to the floor in order to limit their motion when a subject walked in the workspace (see Figures B.2(a), B.2(b), and B.2(c)). The same

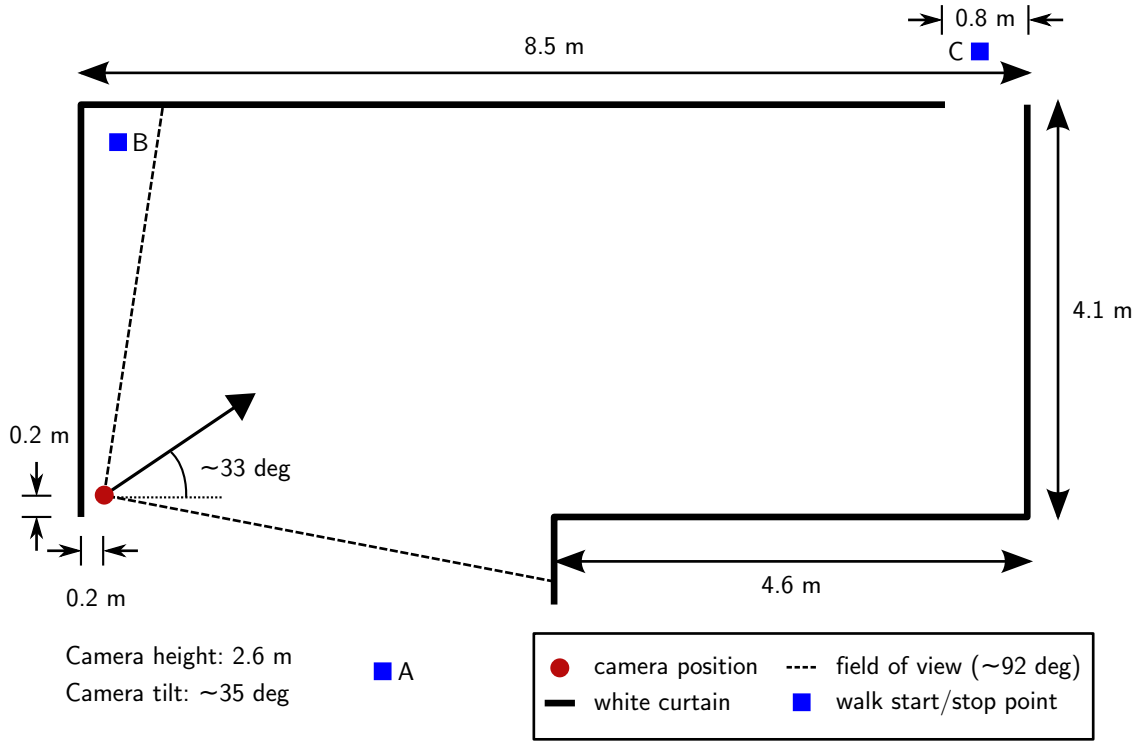

Figure B.1 – A scale representation of the acquisition room layout with position of the camera and the walk start/stop points. The approximated line of sight and field of view of the camera are also shown.

clothing was used just below the strip lighting in order to decrease the specular effect on the floor induced by the direct lighting. The camera was positioned close to the ceiling (see Figures B.2(b) and B.2(d)) in order to simulate the view obtained by surveillance cameras. The walk start/stop points (where the subject starts or stops walking) were positioned in order to obtain the greatest number of non-frontal gait cycles in the camera field of view.

B.2 Hardware

The camera used in the acquisition process is a Dragonfly®2 model DR2-HICOL-CSBOX from Point Grey Research, mounted on a Manfrotto 161MK2 tripod with a Manfrotto 329RC4 3-way head. This camera uses a 1/3" Sony® CCD sensor and is connected to a computer through a Firewire 400 bus.

The acquisition of the video sequences were made at a resolution of 1024×768

(a) (b) (c) (d)

Figure B.2 – Photos of the acquisition room setup. In (a), a photo taken close to the camera position towards start/stop point C and in (b), a photo taken close to the start/stop point C towards the camera. A photo toward start/stop point B is shown in (c). The photo in (d) shows a close-up of the camera that is positioned close to the ceiling, as it can be seen in (b).

pixels and at an approximate frame rate of 30 fps. To obtain colour video sequences at the mentioned resolution and frame rate, one have to use this camera in a special mode where frames are sent unprocessed to the computer in BAYER pattern format (1024×768, 8 bits per pixel). The frames have to be post-processed by software (using some functions provided by the *PGRFlyCapture* library) upon reception by the computer in order to obtain RGB colour frames.

The computer used for the acquisition process is a Windows® XP PC with two Dual Core AMD Opteron™ at 1.81 GHz. An in-house software was developed in order to the perform the acquisitions since it is the only way to perform it at the desired resolution and frame rate. The software is built in C++ and uses the *PGRFlyCapture* library provided by Point Grey Research. It performs the acquisition at the maximum speed permitted by a Firewire 400 bus (which is about 30 fps for the wanted resolution) and also extract a timestamp for each of the acquired frame (more details in section B.5).

B.3 Camera Calibration

The camera calibration process consists in computing the camera intrinsic parameters along with some distortion parameters. The method necessitates the use of a calibration target on which a grid of black dots is printed. In this work, the target that was used is a print laminated on a piece of MDF (Medium Density Fibreboard). The dots are of the same size and are equidistant, except for a special dot pattern in the middle of the target used to determine the target orientation (those dots are bigger and closer than the normal ones). An image collection of the calibration target is acquired with the camera, and each image represents the target in a different pose with respect to the

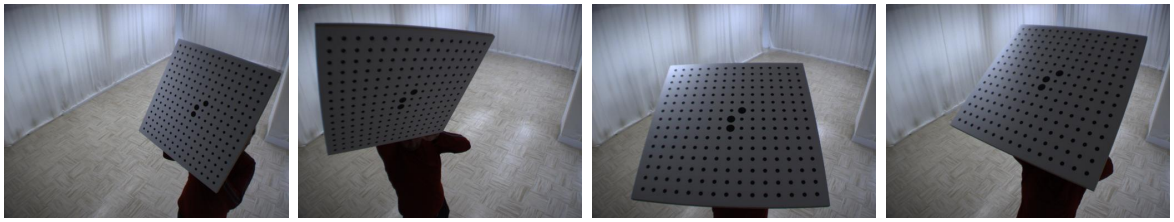

Figure B.3 – Different camera images of the calibration target.

camera. Examples of the calibration target images acquired with the camera are shown in Figure B.3.

The algorithm presented in [85] is used in order to compute the camera intrinsic and distortion parameters from the collected images of the target. The intrinsic parameters computed by this algorithm[1] are the focal length f (in pixels), the pixel aspect ratio s, and the coordinates of the principal point (u_0, v_0). It is known from the camera specifications that the camera has a pixel size of $\zeta = 10$ µm. The calibration algorithm also accounts for two sorts of distortion induced by the lens system, namely the radial distortion and the tangential distortion. The former is represented by two coefficients, k_1 and k_2, and the latter is represented by two coefficients, p_1 and p_2. The camera intrinsic and distortion parameters obtained from the camera calibration process are presented in Table B.1. The underlying method for estimating all those parameters from the collected images of the target is out of the scope of this thesis. The interested reader may refer to [85] for more details.

f	u_0	v_0	s	k_1	k_2	p_1	p_2
762.72	528.83	402.31	1.00027	4.36×10^{-3}	2.26×10^{-5}	2.77×10^{-5}	-2.51×10^{-4}

Table B.1 – Camera intrinsic and distortion parameters obtained by camera calibration.

B.4 Walk Tracks

Figure B.4 shows the layout of the tracks, that is, the approximate "paths" on which the subjects were asked to walk. The tracks were not "drawn" on the floor; they were indicated to the subject by the start/stop points and a control point at the position of highest curvature of the track shape. This was made in order to have the subjects execute a normal walk while having the wanted changes in walk direction and viewpoints

[1] It is supposed that the pixels are not skewed, that is, the intrinsic skew parameter is zero.

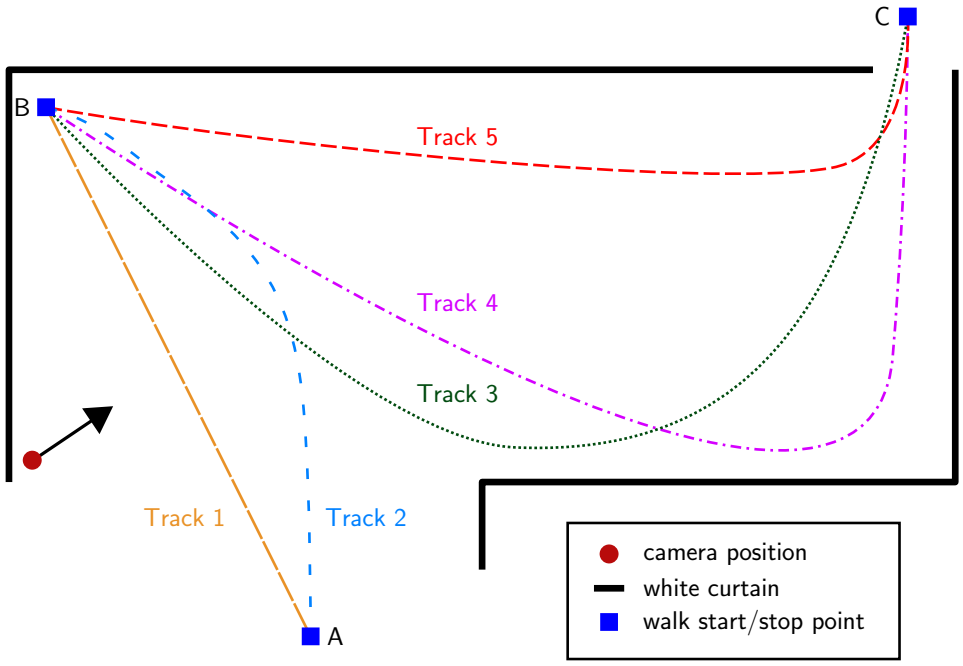

Figure B.4 – Walk tracks layout.

for the gait database. The track's control point was indicated on the floor using a piece of white tape. The subjects were asked to walk normally at a constant pace from a given start point to a given stop point while changing smoothly their walk direction to pass close to the indicated control point.

The track #1 provides a close fronto-parallel view of the subjects, that is, the angles between the track and the camera optical axis is about 90°and the subjects walked very close to the camera. It is worth noting that there is no control point for track #1 since it represents a straight line walk. Track #2 has the subjects change constantly but smoothly their walk direction while remaining close to the camera. For the tracks #3, #4, and #5, the subjects are close to the camera at one end point and are far from the camera at the other end point. This makes the apparent height of a subject very different (by a factor of 2) within the same video sequence. These three tracks contain a change in the walk direction that occurs at different positions in the acquisition room. The smoothness of the direction change is also different in each of these tracks.

Label	Track	From	To	Duration (frames)	Duration (seconds)
path 1-1	1	A	B	297 ± 40	9.8 ± 1.3
path 1-2	1	B	A	276 ± 34	9.1 ± 1.1
path 2-1	2	A	B	311 ± 37	10.2 ± 1.2
path 2-2	2	B	A	305 ± 41	10.0 ± 1.3
path 3-1	3	B	C	429 ± 47	14.1 ± 1.5
path 3-2	3	C	B	443 ± 51	14.6 ± 1.7
path 4-1	4	B	C	436 ± 48	14.4 ± 1.6
path 4-2	4	C	B	456 ± 54	15.0 ± 1.8
path 5-1	5	B	C	381 ± 43	12.6 ± 1.4
path 5-2	5	C	B	399 ± 45	13.1 ± 1.5

Table B.2 – Acquired video sequences with details about corresponding tracks, origin and destination points, and average duration statistics.

B.5 Acquired Data

The proposed database consists in 52 volunteers (31 males, 21 females) who walked on each of the tracks presented in Figure B.4. Each subject was given an ID number from 1 to 52. The subjects were aged from 20 to 55, with an average[2] of 29.5 ± 8.1 years old. The average subject height[3] was 1.72 m $\pm$ 0.09 m (males: 1.76 m $\pm$ 0.08 m; females: 1.65 m $\pm$ 0.09 m).

For each subject, ten separate video sequences were acquired. The Table B.2 presents the label given to each of the video sequences along with the track number and the origin/destination point to which they correspond. The average duration statistics are also presented for each sequence and were computed by considering the sequence duration of the 52 subjects. The subjects walked twice on each track, one time in a direction and the other time in the opposite direction. This makes 10 sequences per subject, for a total of 520 video sequences.

Each video sequence starts with at least 100 frames ($\sim$3 seconds) of static background, that is, frames in which the acquisition room is observed while nobody is visible in the field of view of the camera. This is necessary for the background subtraction algorithms considered in this work (see section 2.3.2). Finally, a timestamp was retrieved for each frame of each video sequence, with an accuracy of 1 ms. The timestamps are used by the proposed view-rectification method presented in Chapter 3 and by the proposed gait analysis and modelling methods presented in 4.

[2]The notation used here for the statistics is defined as *average* $\pm$ *standard deviation*.
[3]Statistics based on approximate heights reported by the subjects.

Appendix C

Gait Analysis Results

This appendix presents the gait analysis results for all the walks in the gait database described in Appendix B. The results are presented in the table in the following pages. Each row of the table presents the gait analysis results for a given subject and a given walk (path). Each column of the table represent a different information or result as follow:

Subject : The unique ID of the subject, which is a number between 1 and 52;

Gender : The gender of the subject, either male (M) or female (F);

Stature : The subject's stature, which is the height reported by the subject during the gait database acquisition process;

Path : The label of the path, which corresponds to a walk defined by a track number and an origin and a destination point (see Table B.2); The walk is entirely contained in a video file;

Frames : The number of frames in the walk where the subject is completely visible in the field of view of the camera;

Use : The percentage of the number of frames in the walk that are part of a detected gait half-cycle;

Intervals : The number of continuous tracking intervals in the walk;

$\frac{1}{2}$ Cycles : The total number of detected gait half-cycles in the walk (all intervals);

Cadence : The cadence computed for the whole walk using Equation 4.6;

Speed : The speed computed for the whole walk using Equation 4.7;

Duration : The mean and the standard deviation of the gait half-cycle durations, where the duration of a gait half-cycle is computed using Equation 4.5;

Strides : The mean and the standard deviation of the stride lengths, where the stride length for a gait half-cycle is computed using Equation 4.1;

Displacement : The mean and the standard deviation of the displacements, where the displacement for a gait half-cycle is computed using Equation 4.2;

Height : The mean and the standard deviation of the computed subject's heights, where the subject's height for a gait half-cycle is computed using Equation 4.8.

ΔHeight : The percentage of difference between the computed mean height and the stature, which is computed as

$$100 \times \frac{|\text{height} - \text{stature}|}{\text{stature}},$$

where $|\cdot|$ is the absolute value.

The gait analysis results are further analyzed and discussed in Section 5.2.2.

Subject (ID)	Gender (M/F)	Stature (m)	Path (ID)	Frames (num.)	Use (%)	Intervals (num.)	½ Cycles (num.)	Cadence (steps/min)	Speed (m/min)	Duration (s)	Strides (m)	Displacement (m)	Height (m)	ΔHeight (%)
1	F	1.78	1-1	61	72.1	1	3	123.4	92.98	0.486 ± 0.009	1.507 ± 0.012	0.754 ± 0.006	1.764 ± 0.013	0.89
			1-2	53	54.7	1	2	125.0	98.31	0.480 ± 0.029	1.573 ± 0.038	0.786 ± 0.019	1.786 ± 0.014	0.35
			2-1	85	70.6	1	4	121.1	88.36	0.496 ± 0.008	1.460 ± 0.043	0.730 ± 0.021	1.744 ± 0.015	2.09
			2-2	81	72.8	1	4	122.5	91.82	0.490 ± 0.009	1.500 ± 0.060	0.750 ± 0.030	1.738 ± 0.006	2.40
			3-1	181	39.2	1	5	127.0	94.15	0.472 ± 0.006	1.483 ± 0.117	0.741 ± 0.059	1.759 ± 0.012	1.20
			3-2	179	63.1	1	8	128.7	97.46	0.466 ± 0.022	1.522 ± 0.080	0.757 ± 0.047	1.766 ± 0.032	0.80
			4-1	196	73.0	2	10	127.2	98.02	0.472 ± 0.011	1.542 ± 0.049	0.771 ± 0.025	1.836 ± 0.004	3.05
			4-2	201	64.7	2	9	125.5	98.38	0.478 ± 0.017	1.568 ± 0.033	0.784 ± 0.017	1.765 ± 0.009	0.84
			5-1	148	39.2	1	4	125.5	97.63	0.478 ± 0.007	1.556 ± 0.035	0.778 ± 0.017	1.774 ± 0.010	0.35
			5-2	150	38.0	1	4	128.1	98.05	0.468 ± 0.011	1.530 ± 0.030	0.765 ± 0.015	1.777 ± 0.007	0.16
2	M	1.75	1-1	76	69.7	1	3	104.2	76.07	0.576 ± 0.001	1.460 ± 0.053	0.730 ± 0.027	1.736 ± 0.012	0.81
			1-2	65	80.0	1	3	106.3	82.06	0.565 ± 0.005	1.544 ± 0.015	0.772 ± 0.008	1.751 ± 0.009	0.08
			2-1	101	68.3	1	4	105.0	78.51	0.572 ± 0.009	1.496 ± 0.044	0.748 ± 0.022	1.723 ± 0.009	1.59
			2-2	90	76.7	1	4	104.9	82.02	0.572 ± 0.021	1.564 ± 0.051	0.782 ± 0.026	1.719 ± 0.008	1.80
			3-1	226	29.2	1	4	109.9	80.20	0.546 ± 0.012	1.463 ± 0.179	0.730 ± 0.093	1.726 ± 0.015	1.42
			3-2	215	47.9	1	6	105.8	80.33	0.567 ± 0.019	1.530 ± 0.034	0.759 ± 0.029	1.768 ± 0.038	1.03
			4-1	245	70.2	2	10	105.4	79.82	0.570 ± 0.023	1.515 ± 0.106	0.758 ± 0.053	1.737 ± 0.011	0.77
			4-2	252	69.4	2	10	104.0	79.71	0.577 ± 0.015	1.533 ± 0.042	0.766 ± 0.021	1.741 ± 0.007	0.51
			5-1	191	62.3	2	7	107.2	79.17	0.560 ± 0.023	1.477 ± 0.100	0.738 ± 0.050	1.729 ± 0.006	1.21
			5-2	203	43.3	1	5	103.0	75.90	0.583 ± 0.022	1.474 ± 0.032	0.737 ± 0.016	1.743 ± 0.007	0.41
3	M	1.73	1-1	78	66.7	1	3	106.0	69.92	0.566 ± 0.022	1.319 ± 0.036	0.659 ± 0.018	1.750 ± 0.017	1.15
			1-2	71	69.0	1	3	112.1	80.64	0.535 ± 0.015	1.438 ± 0.057	0.719 ± 0.029	1.736 ± 0.004	0.37
			2-1	100	70.0	1	4	104.5	70.21	0.574 ± 0.005	1.344 ± 0.044	0.672 ± 0.022	1.713 ± 0.013	0.99
			2-2	98	72.4	1	4	103.4	71.61	0.580 ± 0.035	1.385 ± 0.070	0.692 ± 0.035	1.733 ± 0.008	0.16
			3-1	249	33.3	1	5	109.6	70.12	0.548 ± 0.024	1.282 ± 0.148	0.640 ± 0.076	1.742 ± 0.013	0.69
			3-2	223	22.0	1	3	110.8	77.76	0.542 ± 0.015	1.404 ± 0.037	0.702 ± 0.018	1.779 ± 0.009	2.77
			4-1	231	71.9	2	10	109.7	77.06	0.547 ± 0.035	1.406 ± 0.080	0.703 ± 0.040	1.762 ± 0.008	1.80
			4-2	220	59.5	2	8	111.0	80.59	0.540 ± 0.027	1.452 ± 0.045	0.726 ± 0.022	1.778 ± 0.008	2.67
			5-1	192	40.6	1	5	116.7	87.40	0.514 ± 0.023	1.498 ± 0.024	0.749 ± 0.012	1.748 ± 0.005	1.01
			5-2	198	32.8	1	4	112.5	77.57	0.533 ± 0.031	1.379 ± 0.046	0.689 ± 0.023	1.742 ± 0.013	0.69
4	M	1.85	1-1	74	70.3	1	3	104.6	78.16	0.574 ± 0.017	1.494 ± 0.025	0.747 ± 0.012	1.820 ± 0.018	1.65
			1-2	61	55.7	1	2	108.0	79.96	0.556 ± 0.026	1.482 ± 0.029	0.741 ± 0.014	1.834 ± 0.025	0.85
			2-1	98	72.4	1	4	103.2	73.62	0.582 ± 0.019	1.427 ± 0.052	0.714 ± 0.026	1.812 ± 0.017	2.10
			2-2	98	71.4	1	4	104.3	75.53	0.575 ± 0.018	1.449 ± 0.061	0.724 ± 0.031	1.807 ± 0.014	2.40
			3-1	240	28.3	1	4	107.0	75.25	0.561 ± 0.006	1.408 ± 0.039	0.703 ± 0.020	1.808 ± 0.015	2.30
			3-2	258	32.9	1	5	107.1	73.82	0.560 ± 0.034	1.378 ± 0.099	0.689 ± 0.049	1.807 ± 0.017	2.39
			4-1	241	84.2	2	12	108.1	79.14	0.555 ± 0.026	1.466 ± 0.107	0.732 ± 0.054	1.846 ± 0.009	0.22
			4-2	250	67.6	2	10	107.8	80.85	0.557 ± 0.025	1.500 ± 0.025	0.750 ± 0.012	1.822 ± 0.009	1.51
			5-1	177	37.3	1	4	110.4	84.88	0.543 ± 0.019	1.538 ± 0.021	0.769 ± 0.010	1.821 ± 0.010	1.61
			5-2	187	35.8	1	4	108.4	82.03	0.553 ± 0.022	1.513 ± 0.033	0.757 ± 0.017	1.804 ± 0.008	2.53
5	M	1.62	1-1	85	55.3	1	3	114.8	74.72	0.523 ± 0.016	1.302 ± 0.012	0.651 ± 0.006	1.635 ± 0.008	0.94
			1-2	95	71.6	1	4	106.1	66.11	0.565 ± 0.014	1.246 ± 0.015	0.623 ± 0.008	1.647 ± 0.009	1.64
			2-1	124	72.6	1	5	101.7	59.33	0.590 ± 0.017	1.167 ± 0.074	0.584 ± 0.037	1.622 ± 0.012	0.12
			2-2	121	71.9	1	5	104.7	63.04	0.573 ± 0.021	1.204 ± 0.065	0.602 ± 0.032	1.564 ± 0.010	3.59
			3-1	271	37.3	1	6	107.5	66.37	0.558 ± 0.015	1.235 ± 0.057	0.618 ± 0.029	1.639 ± 0.006	1.16
			3-2	272	31.2	1	5	107.3	65.70	0.559 ± 0.010	1.225 ± 0.012	0.613 ± 0.006	1.619 ± 0.011	0.04
			4-1	288	76.0	2	13	107.7	66.64	0.557 ± 0.020	1.238 ± 0.028	0.619 ± 0.014	1.668 ± 0.007	2.85
			4-2	289	69.2	2	12	109.2	67.42	0.550 ± 0.016	1.235 ± 0.049	0.618 ± 0.024	1.684 ± 0.010	3.82
			5-1	219	43.8	1	6	113.9	73.17	0.527 ± 0.009	1.285 ± 0.022	0.643 ± 0.011	1.632 ± 0.003	0.71
			5-2	231	43.7	1	6	108.6	67.60	0.552 ± 0.018	1.245 ± 0.014	0.622 ± 0.007	1.664 ± 0.008	2.67

Subject (ID)	Gender (M/F)	Stature (m)	Path (ID)	Frames (num.)	Use (%)	Intervals (num.)	½ Cycles (num.)	Cadence (steps/min)	Speed (m/min)	Duration (s)	Strides (m)	Displacement (m)	Height (m)	ΔHeight (%)
6	M	1.83	1-1	85	85.9	1	4	99.7	69.04	0.602 ± 0.025	1.418 ± 0.044	0.692 ± 0.014	1.506 ± 0.191	21.51
			1-2	77	68.8	1	3	102.3	80.26	0.586 ± 0.018	1.568 ± 0.014	0.784 ± 0.007	1.837 ± 0.012	0.40
			2-1	99	74.7	1	4	98.1	76.37	0.612 ± 0.027	1.586 ± 0.061	0.779 ± 0.011	1.846 ± 0.214	0.86
			2-2	94	56.4	1	3	103.0	79.18	0.582 ± 0.020	1.537 ± 0.042	0.769 ± 0.021	1.793 ± 0.007	2.05
			3-1	208	34.1	1	4	102.8	79.32	0.584 ± 0.010	1.558 ± 0.059	0.772 ± 0.019	1.468 ± 0.142	24.63
			3-2	210	41.4	1	5	103.6	77.46	0.579 ± 0.024	1.496 ± 0.076	0.748 ± 0.038	1.829 ± 0.013	0.06
			4-1	221	38.9	1	5	105.4	85.58	0.569 ± 0.015	1.636 ± 0.044	0.812 ± 0.018	1.537 ± 0.195	19.09
			4-2	243	72.8	2	10	103.1	81.21	0.582 ± 0.017	1.631 ± 0.081	0.787 ± 0.032	2.012 ± 0.389	9.04
			5-1	168	40.5	1	4	107.2	85.69	0.560 ± 0.010	1.598 ± 0.016	0.799 ± 0.008	1.823 ± 0.009	0.40
			5-2	181	38.7	1	4	103.6	80.13	0.579 ± 0.011	1.547 ± 0.010	0.773 ± 0.005	1.829 ± 0.008	0.05
7	M	1.83	1-1	101	57.4	1	3	94.5	62.80	0.635 ± 0.021	1.329 ± 0.038	0.665 ± 0.019	1.810 ± 0.022	1.11
			1-2	88	86.4	1	4	96.5	68.70	0.622 ± 0.017	1.425 ± 0.025	0.712 ± 0.013	1.795 ± 0.014	1.95
			2-1	120	80.8	1	5	93.8	59.91	0.640 ± 0.022	1.278 ± 0.058	0.639 ± 0.029	1.811 ± 0.013	1.08
			2-2	110	85.5	1	5	96.6	65.64	0.621 ± 0.023	1.359 ± 0.047	0.679 ± 0.024	1.787 ± 0.018	2.41
			3-1	274	67.2	2	10	98.6	65.32	0.609 ± 0.033	1.326 ± 0.169	0.663 ± 0.086	1.780 ± 0.011	2.82
			3-2	261	28.0	1	4	100.1	68.59	0.600 ± 0.018	1.371 ± 0.017	0.685 ± 0.008	1.787 ± 0.013	2.39
			4-1	288	70.8	2	11	98.2	68.46	0.611 ± 0.023	1.395 ± 0.053	0.697 ± 0.027	1.793 ± 0.014	2.09
			4-2	278	73.4	2	11	98.4	68.18	0.610 ± 0.032	1.386 ± 0.084	0.693 ± 0.042	1.806 ± 0.029	1.34
			5-1	206	51.5	1	6	103.0	71.90	0.583 ± 0.023	1.397 ± 0.165	0.698 ± 0.083	1.813 ± 0.010	0.94
			5-2	210	34.3	1	4	101.1	73.23	0.593 ± 0.015	1.448 ± 0.010	0.724 ± 0.005	1.802 ± 0.010	1.57
8	M	1.70	1-1	83	80.7	1	4	107.9	75.12	0.556 ± 0.017	1.393 ± 0.030	0.696 ± 0.015	1.666 ± 0.018	2.07
			1-2	74	44.6	1	2	110.2	80.57	0.545 ± 0.019	1.464 ± 0.018	0.731 ± 0.009	1.652 ± 0.013	2.93
			2-1	102	68.6	1	4	104.3	72.18	0.575 ± 0.012	1.384 ± 0.033	0.692 ± 0.017	1.639 ± 0.024	3.74
			2-2	100	71.0	1	4	102.6	71.91	0.585 ± 0.011	1.402 ± 0.057	0.701 ± 0.029	1.626 ± 0.012	4.52
			3-1	222	29.3	1	4	111.7	72.65	0.537 ± 0.041	1.304 ± 0.243	0.651 ± 0.123	1.686 ± 0.019	0.85
			3-2	214	47.7	1	6	107.1	75.09	0.560 ± 0.018	1.406 ± 0.046	0.701 ± 0.026	1.623 ± 0.018	4.75
			4-1	227	66.1	2	9	109.4	82.50	0.548 ± 0.023	1.509 ± 0.040	0.754 ± 0.020	1.661 ± 0.014	2.37
			4-2	236	64.4	2	9	108.4	79.46	0.553 ± 0.020	1.466 ± 0.027	0.733 ± 0.014	1.658 ± 0.007	2.53
			5-1	212	55.7	2	7	107.3	79.70	0.559 ± 0.019	1.488 ± 0.139	0.743 ± 0.068	1.644 ± 0.008	3.41
			5-2	195	43.1	1	5	107.6	77.98	0.558 ± 0.026	1.450 ± 0.044	0.725 ± 0.022	1.633 ± 0.015	4.08
9	M	1.80	1-1	98	59.2	1	3	93.8	64.24	0.640 ± 0.023	1.370 ± 0.058	0.685 ± 0.029	1.823 ± 0.016	1.28
			1-2	90	84.4	1	4	95.4	67.96	0.629 ± 0.011	1.424 ± 0.013	0.712 ± 0.006	1.826 ± 0.011	1.43
			2-1	120	80.8	1	5	93.5	63.78	0.642 ± 0.019	1.365 ± 0.039	0.682 ± 0.020	1.818 ± 0.015	0.98
			2-2	118	82.2	1	5	93.0	63.58	0.645 ± 0.017	1.367 ± 0.071	0.684 ± 0.035	1.825 ± 0.009	1.36
			3-1	265	42.6	1	6	96.2	68.48	0.624 ± 0.016	1.424 ± 0.043	0.712 ± 0.021	1.834 ± 0.015	1.85
			3-2	265	28.3	1	4	96.2	66.50	0.624 ± 0.014	1.383 ± 0.023	0.691 ± 0.011	1.840 ± 0.015	2.18
			4-1	276	93.8	1	14	98.3	76.04	0.610 ± 0.049	1.551 ± 0.250	0.774 ± 0.120	1.843 ± 0.012	2.36
			4-2	273	76.6	2	11	95.6	69.44	0.628 ± 0.049	1.452 ± 0.071	0.726 ± 0.034	1.902 ± 0.150	5.35
			5-1	223	67.7	1	8	96.4	69.65	0.622 ± 0.030	1.444 ± 0.046	0.722 ± 0.023	2.008 ± 0.512	10.34
			5-2	213	70.4	1	8	97.2	72.66	0.617 ± 0.045	1.498 ± 0.085	0.748 ± 0.043	1.837 ± 0.012	2.02
10	M	1.73	1-1	88	61.4	1	3	101.1	71.61	0.594 ± 0.010	1.417 ± 0.023	0.708 ± 0.011	1.739 ± 0.002	0.51
			1-2	75	68.0	1	3	106.4	77.76	0.564 ± 0.021	1.462 ± 0.012	0.731 ± 0.006	1.755 ± 0.006	1.43
			2-1	100	75.0	1	4	98.1	67.69	0.612 ± 0.017	1.381 ± 0.019	0.690 ± 0.009	1.744 ± 0.006	0.80
			2-2	96	74.0	1	4	101.6	70.45	0.590 ± 0.010	1.387 ± 0.076	0.693 ± 0.038	1.742 ± 0.009	0.69
			3-1	243	36.2	1	5	103.3	66.33	0.581 ± 0.035	1.284 ± 0.173	0.642 ± 0.087	1.739 ± 0.013	0.52
			3-2	242	29.3	1	4	102.3	70.30	0.586 ± 0.015	1.374 ± 0.020	0.687 ± 0.010	1.763 ± 0.005	1.88
			4-1	255	69.8	2	10	101.7	70.35	0.590 ± 0.029	1.383 ± 0.047	0.692 ± 0.024	1.770 ± 0.007	2.28
			4-2	249	62.7	2	9	105.5	73.63	0.569 ± 0.025	1.397 ± 0.042	0.698 ± 0.021	1.777 ± 0.006	2.63
			5-1	206	34.0	1	4	104.2	75.81	0.576 ± 0.012	1.455 ± 0.035	0.728 ± 0.018	1.752 ± 0.009	1.28
			5-2	217	32.7	1	4	102.3	69.37	0.586 ± 0.023	1.357 ± 0.024	0.678 ± 0.012	1.762 ± 0.005	1.82

Subject (ID)	Gender (M/F)	Stature (m)	Path (ID)	Frames (num.)	Use (%)	Intervals (num.)	½ Cycles (num.)	Cadence (steps/min)	Speed (m/min)	Duration (s)	Strides (m)	Displacement (m)	Height (m)	ΔHeight (%)
11	M	1.82	1-1	91	61.5	1	3	97.8	60.98	0.614 ± 0.013	1.248 ± 0.035	0.624 ± 0.018	1.812 ± 0.006	0.43
			1-2	92	79.3	1	4	98.8	64.85	0.607 ± 0.029	1.313 ± 0.063	0.656 ± 0.031	1.802 ± 0.012	1.01
			2-1	125	76.0	1	5	95.4	57.94	0.629 ± 0.028	1.215 ± 0.042	0.608 ± 0.021	1.800 ± 0.008	1.11
			2-2	135	85.9	1	6	93.9	56.89	0.639 ± 0.020	1.212 ± 0.052	0.606 ± 0.026	1.791 ± 0.005	1.61
			3-1	275	25.5	1	4	103.5	68.95	0.580 ± 0.018	1.332 ± 0.072	0.666 ± 0.036	1.797 ± 0.006	1.28
			3-2	270	26.3	1	4	101.7	67.10	0.590 ± 0.032	1.319 ± 0.021	0.660 ± 0.011	1.799 ± 0.005	1.19
			4-1	299	58.5	2	10	104.2	68.24	0.576 ± 0.021	1.310 ± 0.071	0.655 ± 0.035	1.826 ± 0.005	0.35
			4-2	297	59.9	2	10	102.5	65.76	0.585 ± 0.022	1.283 ± 0.037	0.642 ± 0.018	1.816 ± 0.007	0.22
			5-1	230	30.0	1	4	105.9	70.60	0.566 ± 0.022	1.333 ± 0.023	0.667 ± 0.011	1.814 ± 0.006	0.35
			5-2	249	22.5	1	3	97.6	57.57	0.615 ± 0.029	1.179 ± 0.031	0.590 ± 0.015	1.816 ± 0.004	0.23
12	M	1.74	1-1	77	66.2	1	3	106.1	72.10	0.565 ± 0.019	1.359 ± 0.013	0.679 ± 0.006	1.742 ± 0.010	0.13
			1-2	70	71.4	1	3	108.3	79.18	0.554 ± 0.008	1.463 ± 0.027	0.731 ± 0.013	1.732 ± 0.009	0.44
			2-1	94	72.3	1	4	106.3	75.38	0.564 ± 0.014	1.418 ± 0.030	0.709 ± 0.015	1.715 ± 0.011	1.47
			2-2	88	77.3	1	4	106.7	78.07	0.562 ± 0.005	1.463 ± 0.036	0.732 ± 0.018	1.728 ± 0.006	0.70
			3-1	222	51.8	2	7	110.0	80.48	0.545 ± 0.013	1.463 ± 0.025	0.731 ± 0.012	1.739 ± 0.007	0.05
			3-2	213	45.5	1	6	112.2	77.89	0.535 ± 0.057	1.425 ± 0.286	0.694 ± 0.167	1.791 ± 0.087	2.82
			4-1	223	66.4	2	9	110.6	81.99	0.543 ± 0.008	1.483 ± 0.040	0.742 ± 0.020	1.756 ± 0.007	0.90
			4-2	236	63.1	2	9	109.7	79.56	0.547 ± 0.015	1.450 ± 0.059	0.725 ± 0.030	1.727 ± 0.010	0.75
			5-1	184	53.3	1	6	111.8	85.40	0.537 ± 0.009	1.528 ± 0.024	0.764 ± 0.012	1.752 ± 0.008	0.66
			5-2	176	46.0	1	5	111.7	80.88	0.537 ± 0.014	1.449 ± 0.040	0.724 ± 0.020	1.736 ± 0.008	0.24
13	M	1.68	1-1	90	71.1	1	4	112.9	67.27	0.531 ± 0.002	1.192 ± 0.019	0.596 ± 0.010	1.668 ± 0.011	0.74
			1-2	81	58.0	1	3	117.1	73.54	0.512 ± 0.015	1.256 ± 0.022	0.628 ± 0.011	1.656 ± 0.013	1.48
			2-1	108	74.1	1	5	113.8	68.08	0.527 ± 0.008	1.197 ± 0.049	0.598 ± 0.024	1.665 ± 0.009	0.89
			2-2	106	75.5	1	5	114.2	67.93	0.525 ± 0.016	1.189 ± 0.049	0.595 ± 0.024	1.620 ± 0.011	3.72
			3-1	263	24.0	1	4	115.7	72.48	0.519 ± 0.007	1.253 ± 0.070	0.627 ± 0.035	1.658 ± 0.008	1.30
			3-2	260	30.8	1	5	113.7	68.05	0.528 ± 0.021	1.197 ± 0.008	0.599 ± 0.004	1.660 ± 0.007	1.20
			4-1	273	79.1	2	14	118.2	72.57	0.508 ± 0.023	1.228 ± 0.137	0.614 ± 0.068	1.674 ± 0.019	0.36
			4-2	274	79.6	2	14	117.2	75.71	0.512 ± 0.026	1.294 ± 0.268	0.646 ± 0.129	1.668 ± 0.007	0.71
			5-1	229	47.2	2	7	117.4	72.86	0.511 ± 0.013	1.244 ± 0.151	0.621 ± 0.072	1.641 ± 0.006	2.36
			5-2	222	70.7	2	10	115.5	70.99	0.519 ± 0.031	1.229 ± 0.040	0.614 ± 0.020	1.676 ± 0.006	0.22
14	M	1.85	1-1	80	72.5	1	3	93.4	78.19	0.642 ± 0.025	1.674 ± 0.058	0.837 ± 0.029	1.871 ± 0.009	1.12
			1-2	64	57.8	1	2	98.1	85.61	0.612 ± 0.010	1.745 ± 0.032	0.873 ± 0.016	1.868 ± 0.010	0.97
			2-1	92	60.9	1	3	97.1	84.14	0.618 ± 0.017	1.733 ± 0.040	0.866 ± 0.020	1.861 ± 0.009	0.57
			2-2	90	62.2	1	3	97.1	85.75	0.618 ± 0.028	1.767 ± 0.012	0.883 ± 0.006	1.848 ± 0.007	0.11
			3-1	218	60.6	2	7	96.7	85.52	0.620 ± 0.016	1.768 ± 0.051	0.884 ± 0.025	1.868 ± 0.006	0.96
			3-2	212	52.4	2	6	98.0	87.73	0.613 ± 0.012	1.791 ± 0.059	0.896 ± 0.029	1.864 ± 0.009	0.73
			4-1	222	66.7	2	8	99.0	87.80	0.606 ± 0.013	1.773 ± 0.027	0.887 ± 0.013	1.883 ± 0.004	1.77
			4-2	226	73.9	2	9	98.4	85.99	0.610 ± 0.029	1.748 ± 0.059	0.874 ± 0.029	1.873 ± 0.012	1.24
			5-1	183	88.0	1	9	101.4	89.84	0.592 ± 0.031	1.775 ± 0.047	0.886 ± 0.026	1.987 ± 0.025	6.88
			5-2	173	51.4	1	5	101.8	89.25	0.589 ± 0.022	1.753 ± 0.042	0.877 ± 0.021	1.871 ± 0.008	1.13
15	M	1.80	1-1	81	67.9	1	3	99.7	75.44	0.602 ± 0.008	1.514 ± 0.024	0.757 ± 0.012	1.828 ± 0.007	1.52
			1-2	80	68.8	1	3	98.7	77.09	0.608 ± 0.023	1.563 ± 0.018	0.781 ± 0.009	1.812 ± 0.016	0.67
			2-1	94	78.7	1	4	97.8	76.06	0.614 ± 0.021	1.556 ± 0.024	0.778 ± 0.012	1.820 ± 0.009	1.09
			2-2	101	75.2	1	4	95.5	73.60	0.628 ± 0.011	1.542 ± 0.053	0.771 ± 0.026	1.815 ± 0.020	0.85
			3-1	247	36.0	1	5	101.7	70.10	0.590 ± 0.049	1.382 ± 0.227	0.689 ± 0.117	1.823 ± 0.016	1.27
			3-2	244	23.4	1	3	95.6	70.24	0.628 ± 0.006	1.469 ± 0.018	0.735 ± 0.009	1.837 ± 0.001	2.00
			4-1	276	68.5	2	10	96.4	72.08	0.622 ± 0.028	1.495 ± 0.041	0.748 ± 0.021	1.836 ± 0.011	1.97
			4-2	268	72.0	2	10	94.6	71.85	0.634 ± 0.027	1.519 ± 0.039	0.759 ± 0.019	1.830 ± 0.013	1.62
			5-1	205	35.1	1	4	100.4	76.44	0.598 ± 0.006	1.522 ± 0.014	0.761 ± 0.007	1.844 ± 0.011	2.39
			5-2	207	45.9	1	5	96.2	72.55	0.624 ± 0.012	1.508 ± 0.029	0.754 ± 0.014	1.852 ± 0.005	2.79

Subject (ID)	Gender (M/F)	Stature (m)	Path (ID)	Frames (num.)	Use (%)	Intervals (num.)	½ Cycles (num.)	Cadence (steps/min)	Speed (m/min)	Duration (s)	Strides (m)	Displacement (m)	Height (m)	ΔHeight (%)
16	M	1.75	1-1	86	67.4	1	3	94.3	66.99	0.636 ± 0.022	1.420 ± 0.024	0.710 ± 0.012	1.782 ± 0.019	1.78
			1-2	79	49.4	1	2	95.1	67.06	0.631 ± 0.036	1.411 ± 0.043	0.705 ± 0.022	1.789 ± 0.019	2.19
			2-1	115	87.0	1	5	91.4	63.05	0.657 ± 0.021	1.381 ± 0.026	0.690 ± 0.013	1.754 ± 0.012	0.24
			2-2	113	69.9	1	4	91.4	65.61	0.657 ± 0.013	1.436 ± 0.012	0.718 ± 0.006	1.753 ± 0.015	0.15
			3-1	244	36.5	1	5	102.1	71.61	0.588 ± 0.016	1.403 ± 0.066	0.701 ± 0.033	1.763 ± 0.011	0.72
			3-2	260	42.7	2	6	98.5	69.73	0.609 ± 0.023	1.416 ± 0.070	0.708 ± 0.035	1.786 ± 0.008	1.99
			4-1	256	68.8	2	10	103.3	76.42	0.581 ± 0.022	1.480 ± 0.026	0.740 ± 0.013	1.780 ± 0.007	1.69
			4-2	248	64.1	2	9	102.7	78.21	0.584 ± 0.024	1.523 ± 0.026	0.761 ± 0.013	1.786 ± 0.008	2.02
			5-1	193	44.6	1	5	106.2	79.40	0.565 ± 0.026	1.496 ± 0.023	0.748 ± 0.011	1.794 ± 0.004	2.46
			5-2	199	35.2	1	4	103.1	76.70	0.582 ± 0.024	1.489 ± 0.058	0.744 ± 0.029	1.763 ± 0.009	0.74
17	M	1.74	1-1	98	71.4	1	4	104.9	63.77	0.572 ± 0.011	1.217 ± 0.022	0.608 ± 0.011	1.727 ± 0.020	0.73
			1-2	99	70.7	1	4	103.1	61.69	0.582 ± 0.016	1.197 ± 0.036	0.599 ± 0.018	1.747 ± 0.013	0.38
			2-1	129	83.7	1	6	100.9	59.43	0.595 ± 0.020	1.178 ± 0.030	0.589 ± 0.015	1.731 ± 0.014	0.52
			2-2	125	71.2	1	5	102.1	62.17	0.587 ± 0.015	1.217 ± 0.033	0.609 ± 0.017	1.713 ± 0.010	1.56
			3-1	293	41.6	2	7	105.1	65.84	0.571 ± 0.035	1.254 ± 0.052	0.627 ± 0.026	1.755 ± 0.011	0.84
			3-2	286	24.5	1	4	102.7	63.84	0.584 ± 0.020	1.243 ± 0.019	0.622 ± 0.009	1.754 ± 0.019	0.78
			4-1	300	63.3	2	11	105.5	67.19	0.569 ± 0.029	1.274 ± 0.034	0.637 ± 0.017	1.733 ± 0.008	0.41
			4-2	308	74.0	2	13	103.6	65.50	0.579 ± 0.037	1.264 ± 0.025	0.632 ± 0.013	1.745 ± 0.011	0.31
			5-1	226	29.6	1	4	109.2	70.42	0.549 ± 0.017	1.290 ± 0.009	0.645 ± 0.004	1.712 ± 0.010	1.61
			5-2	219	31.1	1	4	107.1	67.47	0.560 ± 0.040	1.261 ± 0.025	0.630 ± 0.013	1.719 ± 0.014	1.24
18	M	1.63	1-1	78	82.1	1	4	113.3	80.31	0.530 ± 0.017	1.418 ± 0.035	0.709 ± 0.017	1.626 ± 0.024	0.22
			1-2	71	69.0	1	3	111.9	80.30	0.536 ± 0.023	1.435 ± 0.058	0.717 ± 0.029	1.622 ± 0.030	0.50
			2-1	104	80.8	1	5	109.0	71.01	0.550 ± 0.022	1.303 ± 0.052	0.651 ± 0.026	1.619 ± 0.017	0.71
			2-2	95	68.4	1	4	110.8	75.38	0.542 ± 0.023	1.361 ± 0.037	0.680 ± 0.019	1.580 ± 0.023	3.19
			3-1	219	28.8	1	4	116.3	83.89	0.516 ± 0.010	1.444 ± 0.029	0.721 ± 0.015	1.660 ± 0.018	1.82
			3-2	239	35.1	1	5	108.0	69.76	0.556 ± 0.030	1.291 ± 0.130	0.646 ± 0.064	1.625 ± 0.019	0.29
			4-1	252	57.9	2	9	111.6	78.63	0.538 ± 0.019	1.412 ± 0.058	0.705 ± 0.026	1.610 ± 0.012	1.26
			4-2	248	66.1	2	10	110.5	77.40	0.543 ± 0.020	1.401 ± 0.039	0.700 ± 0.020	1.628 ± 0.014	0.12
			5-1	187	42.2	1	5	115.3	83.30	0.520 ± 0.012	1.445 ± 0.018	0.723 ± 0.009	1.687 ± 0.015	3.39
			5-2	197	41.6	1	5	111.0	77.65	0.540 ± 0.032	1.399 ± 0.026	0.699 ± 0.013	1.653 ± 0.010	1.41
19	M	1.70	1-1	87	63.2	1	3	99.5	74.97	0.603 ± 0.010	1.511 ± 0.137	0.754 ± 0.066	1.708 ± 0.011	0.49
			1-2	86	64.0	1	3	99.1	70.97	0.606 ± 0.007	1.433 ± 0.033	0.716 ± 0.016	1.714 ± 0.009	0.82
			2-1	118	65.3	1	4	94.1	61.72	0.638 ± 0.006	1.313 ± 0.010	0.656 ± 0.005	1.724 ± 0.007	1.38
			2-2	109	68.8	1	4	96.1	65.48	0.624 ± 0.020	1.363 ± 0.016	0.681 ± 0.008	1.714 ± 0.011	0.83
			3-1	253	36.8	1	5	97.5	66.53	0.615 ± 0.013	1.365 ± 0.051	0.682 ± 0.025	1.711 ± 0.008	0.67
			3-2	231	45.9	1	6	102.9	68.22	0.583 ± 0.016	1.326 ± 0.063	0.663 ± 0.032	1.724 ± 0.010	1.42
			4-1	265	61.1	2	9	101.1	69.40	0.593 ± 0.012	1.373 ± 0.059	0.686 ± 0.030	1.719 ± 0.007	1.12
			4-2	252	69.8	2	10	103.3	71.95	0.581 ± 0.016	1.394 ± 0.045	0.697 ± 0.022	1.733 ± 0.009	1.89
			5-1	208	69.2	2	8	101.3	70.95	0.592 ± 0.017	1.401 ± 0.078	0.701 ± 0.039	1.749 ± 0.093	2.83
			5-2	212	84.0	2	10	102.0	70.99	0.588 ± 0.033	1.392 ± 0.038	0.696 ± 0.019	1.738 ± 0.006	2.18
20	M	1.85	1-1	79	67.1	1	3	101.3	78.55	0.592 ± 0.013	1.551 ± 0.032	0.775 ± 0.016	1.864 ± 0.013	0.77
			1-2	74	73.0	1	3	101.8	79.62	0.590 ± 0.012	1.565 ± 0.017	0.782 ± 0.009	1.882 ± 0.006	1.68
			2-1	116	69.8	1	4	90.1	61.06	0.666 ± 0.012	1.355 ± 0.035	0.678 ± 0.017	1.867 ± 0.008	0.89
			2-2	112	71.4	1	4	91.3	63.95	0.657 ± 0.019	1.401 ± 0.070	0.701 ± 0.035	1.874 ± 0.008	1.27
			3-1	269	58.0	2	8	93.5	64.24	0.642 ± 0.030	1.374 ± 0.064	0.687 ± 0.032	1.866 ± 0.007	0.85
			3-2	290	49.0	2	7	89.4	67.56	0.671 ± 0.038	1.518 ± 0.528	0.755 ± 0.255	1.882 ± 0.005	1.70
			4-1	297	71.0	2	11	94.8	65.97	0.633 ± 0.020	1.392 ± 0.047	0.696 ± 0.023	1.872 ± 0.004	1.16
			4-2	318	74.2	2	12	92.5	61.77	0.648 ± 0.031	1.335 ± 0.047	0.667 ± 0.023	1.876 ± 0.005	1.37
			5-1	218	44.0	1	5	95.4	68.32	0.629 ± 0.013	1.432 ± 0.024	0.716 ± 0.012	1.882 ± 0.004	1.71
			5-2	241	31.5	1	4	95.7	64.85	0.627 ± 0.021	1.355 ± 0.009	0.678 ± 0.004	1.873 ± 0.006	1.23

Subject (ID)	Gender (M/F)	Stature (m)	Path (ID)	Frames (num.)	Use (%)	Intervals (num.)	½ Cycles (num.)	Cadence (steps/min)	Speed (m/min)	Duration (s)	Strides (m)	Displacement (m)	Height (m)	ΔHeight (%)
21	M	1.77	1-1	80	66.2	1	3	103.2	76.48	0.581 ± 0.008	1.482 ± 0.013	0.741 ± 0.007	1.772 ± 0.011	0.13
			1-2	76	68.4	1	3	103.2	76.74	0.581 ± 0.011	1.487 ± 0.032	0.743 ± 0.016	1.782 ± 0.012	0.66
			2-1	99	73.7	1	4	100.0	71.66	0.600 ± 0.017	1.433 ± 0.056	0.717 ± 0.028	1.745 ± 0.011	1.45
			2-2	96	76.0	1	4	100.8	77.87	0.595 ± 0.013	1.545 ± 0.060	0.772 ± 0.030	1.756 ± 0.011	0.81
			3-1	235	29.8	1	4	103.5	76.75	0.580 ± 0.013	1.483 ± 0.069	0.741 ± 0.035	1.779 ± 0.013	0.50
			3-2	239	22.6	1	3	100.9	75.14	0.595 ± 0.006	1.490 ± 0.041	0.745 ± 0.020	1.777 ± 0.007	0.38
			4-1	261	67.4	2	10	103.6	78.03	0.579 ± 0.017	1.507 ± 0.040	0.753 ± 0.020	1.780 ± 0.010	0.57
			4-2	253	73.9	2	11	106.3	80.24	0.564 ± 0.010	1.509 ± 0.069	0.755 ± 0.034	1.777 ± 0.007	0.38
			5-1	197	87.3	1	9	95.3	79.77	0.630 ± 0.189	1.676 ± 0.213	0.837 ± 0.108	1.892 ± 0.034	6.47
			5-2	198	60.6	2	7	105.7	81.09	0.568 ± 0.012	1.534 ± 0.059	0.767 ± 0.029	1.775 ± 0.009	0.25
22	F	1.63	1-1	135	72.6	1	5	92.5	53.11	0.649 ± 0.028	1.149 ± 0.028	0.574 ± 0.014	1.584 ± 0.006	2.93
			1-2	123	78.9	1	5	93.4	55.46	0.643 ± 0.011	1.188 ± 0.022	0.594 ± 0.011	1.587 ± 0.007	2.71
			2-1	164	86.0	1	7	90.2	47.86	0.665 ± 0.011	1.061 ± 0.032	0.531 ± 0.016	1.579 ± 0.005	3.20
			2-2	162	86.4	1	7	90.9	47.98	0.660 ± 0.012	1.055 ± 0.056	0.528 ± 0.028	1.579 ± 0.007	3.22
			3-1	357	26.6	1	5	95.0	53.95	0.631 ± 0.006	1.135 ± 0.038	0.568 ± 0.019	1.590 ± 0.007	2.55
			3-2	369	31.7	1	6	93.3	49.80	0.643 ± 0.011	1.068 ± 0.014	0.534 ± 0.007	1.593 ± 0.004	2.32
			4-1	385	86.8	2	17	92.4	53.46	0.649 ± 0.029	1.159 ± 0.120	0.579 ± 0.058	1.624 ± 0.064	0.40
			4-2	394	85.0	2	17	92.3	49.75	0.650 ± 0.029	1.078 ± 0.072	0.539 ± 0.036	1.595 ± 0.025	2.17
			5-1	286	60.5	2	9	94.8	54.33	0.633 ± 0.023	1.147 ± 0.041	0.573 ± 0.021	1.583 ± 0.007	3.00
			5-2	287	32.8	1	5	96.0	52.97	0.625 ± 0.009	1.103 ± 0.012	0.552 ± 0.006	1.580 ± 0.004	3.14
23	M	1.71	1-1	122	69.7	1	4	85.4	54.86	0.702 ± 0.020	1.285 ± 0.021	0.642 ± 0.010	1.714 ± 0.019	0.26
			1-2	97	86.6	1	4	87.3	64.58	0.687 ± 0.027	1.477 ± 0.160	0.740 ± 0.081	1.674 ± 0.014	2.18
			2-1	152	75.0	1	5	79.9	49.53	0.751 ± 0.023	1.239 ± 0.042	0.620 ± 0.021	1.703 ± 0.014	0.41
			2-2	144	77.8	1	5	81.0	51.58	0.741 ± 0.033	1.274 ± 0.032	0.637 ± 0.016	1.718 ± 0.014	0.47
			3-1	337	49.0	2	8	87.9	54.38	0.682 ± 0.025	1.236 ± 0.096	0.618 ± 0.048	1.775 ± 0.013	3.67
			3-2	336	25.6	1	4	84.7	52.00	0.708 ± 0.020	1.228 ± 0.014	0.614 ± 0.007	1.727 ± 0.014	0.99
			4-1	364	58.8	2	10	84.7	54.50	0.708 ± 0.024	1.287 ± 0.026	0.643 ± 0.013	1.725 ± 0.009	0.89
			4-2	364	58.0	2	10	86.4	55.60	0.695 ± 0.022	1.288 ± 0.035	0.644 ± 0.018	1.731 ± 0.010	1.19
			5-1	293	43.3	2	6	85.8	57.88	0.699 ± 0.051	1.351 ± 0.171	0.675 ± 0.083	1.749 ± 0.013	2.24
			5-2	280	30.0	1	4	86.6	54.76	0.693 ± 0.014	1.266 ± 0.020	0.633 ± 0.010	1.721 ± 0.012	0.66
24	M	1.77	1-1	99	86.9	1	4	84.7	60.14	0.708 ± 0.034	1.420 ± 0.041	0.710 ± 0.021	1.762 ± 0.020	0.44
			1-2	95	85.3	1	3	67.9	58.07	0.883 ± 0.388	1.708 ± 0.334	0.855 ± 0.168	1.716 ± 0.016	3.14
			2-1	133	85.7	1	5	79.8	52.94	0.752 ± 0.032	1.326 ± 0.078	0.663 ± 0.039	1.716 ± 0.015	3.13
			2-2	129	69.0	1	4	82.0	55.48	0.732 ± 0.043	1.354 ± 0.062	0.677 ± 0.031	1.717 ± 0.017	3.11
			3-1	274	29.6	1	4	89.1	63.54	0.673 ± 0.025	1.426 ± 0.028	0.713 ± 0.014	1.731 ± 0.010	2.24
			3-2	293	28.7	1	4	86.3	58.84	0.695 ± 0.022	1.363 ± 0.027	0.682 ± 0.013	1.718 ± 0.017	3.05
			4-1	323	76.8	2	12	87.9	62.67	0.683 ± 0.037	1.426 ± 0.071	0.713 ± 0.035	1.748 ± 0.009	1.24
			4-2	308	81.2	2	12	87.4	62.89	0.686 ± 0.034	1.439 ± 0.050	0.719 ± 0.025	1.742 ± 0.009	1.59
			5-1	257	64.6	2	8	87.5	61.96	0.686 ± 0.063	1.416 ± 0.102	0.708 ± 0.051	1.757 ± 0.010	0.73
			5-2	268	70.5	2	9	87.1	60.91	0.689 ± 0.043	1.399 ± 0.073	0.699 ± 0.037	1.717 ± 0.011	3.07
25	M	1.78	1-1	61	50.8	1	2	117.3	91.71	0.511 ± 0.004	1.608 ± 0.083	0.782 ± 0.010	1.389 ± 0.089	28.17
			1-2	61	80.3	1	3	113.0	89.61	0.531 ± 0.015	1.587 ± 0.025	0.793 ± 0.012	1.769 ± 0.018	0.60
			2-1	83	80.7	1	4	109.9	81.93	0.546 ± 0.013	1.491 ± 0.029	0.745 ± 0.015	1.747 ± 0.019	1.87
			2-2	85	76.5	1	4	111.9	83.59	0.536 ± 0.015	1.496 ± 0.055	0.747 ± 0.027	1.714 ± 0.011	3.88
			3-1	218	22.5	1	3	112.5	84.39	0.533 ± 0.003	1.529 ± 0.039	0.750 ± 0.007	1.761 ± 0.021	1.08
			3-2	204	53.4	2	7	116.6	76.73	0.515 ± 0.068	1.314 ± 0.240	0.658 ± 0.119	1.845 ± 0.022	3.52
			4-1	229	91.7	1	13	113.0	80.90	0.531 ± 0.023	1.467 ± 0.101	0.716 ± 0.074	1.767 ± 0.236	0.71
			4-2	229	85.2	1	12	111.8	81.57	0.537 ± 0.041	1.464 ± 0.106	0.730 ± 0.060	1.822 ± 0.124	2.29
			5-1	176	43.8	1	5	117.6	91.89	0.510 ± 0.012	1.583 ± 0.042	0.782 ± 0.017	1.819 ± 0.148	2.16
			5-2	182	69.8	2	8	114.7	82.87	0.523 ± 0.028	1.444 ± 0.217	0.723 ± 0.107	1.807 ± 0.014	1.52

Subject (ID)	Gender (M/F)	Stature (m)	Path (ID)	Frames (num.)	Use (%)	Intervals (num.)	½ Cycles (num.)	Cadence (steps/min)	Speed (m/min)	Duration (s)	Strides (m)	Displacement (m)	Height (m)	ΔHeight (%)
26	M	1.64	1-1	90	56.7	1	3	107.6	65.40	0.558 ± 0.015	1.216 ± 0.022	0.608 ± 0.011	1.631 ± 0.038	0.55
			1-2	95	87.4	1	5	109.5	70.02	0.548 ± 0.014	1.278 ± 0.097	0.640 ± 0.049	1.601 ± 0.015	2.41
			2-1	147	74.1	1	6	99.8	58.62	0.601 ± 0.026	1.174 ± 0.052	0.587 ± 0.026	1.615 ± 0.013	1.53
			2-2	125	84.8	1	6	102.9	60.84	0.583 ± 0.027	1.182 ± 0.051	0.591 ± 0.025	1.599 ± 0.011	2.56
			3-1	267	43.4	1	7	109.6	68.48	0.548 ± 0.018	1.250 ± 0.056	0.625 ± 0.028	1.644 ± 0.010	0.27
			3-2	265	44.5	1	7	107.7	66.97	0.557 ± 0.050	1.255 ± 0.081	0.622 ± 0.031	1.863 ± 0.682	11.99
			4-1	271	77.1	2	12	104.4	72.76	0.574 ± 0.151	1.394 ± 0.194	0.697 ± 0.097	1.620 ± 0.009	1.23
			4-2	275	77.5	2	12	102.6	71.68	0.585 ± 0.154	1.397 ± 0.268	0.698 ± 0.134	1.637 ± 0.010	0.19
			5-1	239	41.8	2	6	109.2	73.11	0.549 ± 0.043	1.347 ± 0.253	0.669 ± 0.118	1.623 ± 0.008	1.03
			5-2	231	50.6	1	7	108.6	69.13	0.553 ± 0.032	1.273 ± 0.035	0.637 ± 0.017	1.604 ± 0.009	2.27
27	F	1.57	1-1	135	74.8	1	5	90.8	49.75	0.661 ± 0.021	1.095 ± 0.023	0.548 ± 0.012	1.571 ± 0.008	0.04
			1-2	134	73.1	1	5	92.6	51.13	0.648 ± 0.024	1.104 ± 0.023	0.552 ± 0.012	1.570 ± 0.008	0.01
			2-1	125	76.8	1	5	95.3	53.90	0.629 ± 0.037	1.131 ± 0.043	0.565 ± 0.022	1.578 ± 0.010	0.48
			2-2	137	70.1	1	5	94.5	52.62	0.635 ± 0.023	1.113 ± 0.050	0.557 ± 0.025	1.570 ± 0.009	0.01
			3-1	297	32.0	1	5	96.4	55.21	0.622 ± 0.016	1.145 ± 0.065	0.573 ± 0.033	1.557 ± 0.009	0.86
			3-2	316	29.7	1	5	96.7	55.81	0.621 ± 0.012	1.155 ± 0.032	0.577 ± 0.016	1.571 ± 0.005	0.08
			4-1	319	69.0	2	12	99.0	58.63	0.606 ± 0.034	1.185 ± 0.034	0.592 ± 0.017	1.588 ± 0.006	1.11
			4-2	333	61.6	2	11	97.7	56.95	0.614 ± 0.020	1.166 ± 0.021	0.583 ± 0.010	1.560 ± 0.006	0.63
			5-1	238	51.3	2	7	104.3	62.59	0.575 ± 0.029	1.200 ± 0.031	0.600 ± 0.015	1.560 ± 0.006	0.62
			5-2	259	48.3	1	7	102.0	59.97	0.589 ± 0.019	1.176 ± 0.021	0.588 ± 0.010	1.564 ± 0.005	0.39
28	M	1.88	1-1	74	68.9	1	3	105.8	80.96	0.567 ± 0.024	1.530 ± 0.010	0.765 ± 0.005	1.896 ± 0.006	0.86
			1-2	71	77.5	1	3	99.4	76.88	0.604 ± 0.015	1.547 ± 0.031	0.774 ± 0.015	1.890 ± 0.009	0.55
			2-1	93	78.5	1	4	99.9	75.68	0.601 ± 0.026	1.516 ± 0.065	0.758 ± 0.033	1.879 ± 0.008	0.06
			2-2	96	77.1	1	4	97.8	72.89	0.613 ± 0.026	1.490 ± 0.033	0.745 ± 0.017	1.862 ± 0.009	0.99
			3-1	205	24.9	1	3	106.4	81.18	0.564 ± 0.006	1.526 ± 0.019	0.763 ± 0.009	1.874 ± 0.008	0.29
			3-2	224	30.8	1	4	105.6	83.65	0.568 ± 0.004	1.584 ± 0.023	0.792 ± 0.012	1.889 ± 0.004	0.47
			4-1	220	67.7	2	9	109.9	88.93	0.546 ± 0.016	1.619 ± 0.047	0.809 ± 0.024	1.899 ± 0.009	1.02
			4-2	227	45.4	2	6	105.9	83.69	0.567 ± 0.022	1.581 ± 0.035	0.790 ± 0.018	1.895 ± 0.003	0.79
			5-1	181	46.4	1	5	108.2	85.81	0.554 ± 0.007	1.586 ± 0.040	0.793 ± 0.020	1.885 ± 0.009	0.28
			5-2	173	49.7	1	5	105.9	85.88	0.566 ± 0.020	1.622 ± 0.029	0.811 ± 0.015	1.892 ± 0.003	0.62
29	F	1.57	1-1	85	77.6	1	4	110.8	67.96	0.542 ± 0.013	1.227 ± 0.019	0.613 ± 0.009	1.548 ± 0.007	1.39
			1-2	84	72.6	1	4	119.0	74.43	0.504 ± 0.012	1.251 ± 0.038	0.625 ± 0.019	1.551 ± 0.007	1.23
			2-1	100	79.0	1	5	115.6	70.79	0.519 ± 0.011	1.225 ± 0.036	0.612 ± 0.018	1.537 ± 0.007	2.13
			2-2	107	89.7	1	6	114.2	67.19	0.525 ± 0.027	1.177 ± 0.056	0.588 ± 0.028	1.525 ± 0.004	2.98
			3-1	229	39.3	1	6	122.5	74.55	0.490 ± 0.022	1.217 ± 0.120	0.609 ± 0.060	1.558 ± 0.008	0.77
			3-2	226	40.3	1	6	119.8	72.11	0.501 ± 0.025	1.204 ± 0.089	0.602 ± 0.045	1.561 ± 0.019	0.55
			4-1	252	76.2	2	13	123.8	79.42	0.485 ± 0.022	1.284 ± 0.045	0.642 ± 0.023	1.550 ± 0.005	1.28
			4-2	261	74.3	2	13	121.7	75.95	0.493 ± 0.034	1.249 ± 0.041	0.624 ± 0.021	1.568 ± 0.006	0.14
			5-1	197	45.2	1	6	121.4	77.60	0.494 ± 0.008	1.278 ± 0.024	0.639 ± 0.012	1.553 ± 0.004	1.12
			5-2	204	51.5	1	7	121.1	75.79	0.495 ± 0.019	1.251 ± 0.025	0.626 ± 0.012	1.532 ± 0.003	2.50
30	F	1.68	1-1	106	66.0	1	4	104.0	60.75	0.577 ± 0.009	1.168 ± 0.040	0.584 ± 0.020	1.673 ± 0.010	0.40
			1-2	104	70.2	1	4	99.6	57.35	0.603 ± 0.014	1.152 ± 0.015	0.576 ± 0.008	1.666 ± 0.013	0.84
			2-1	122	86.9	1	6	103.2	60.64	0.581 ± 0.027	1.175 ± 0.050	0.588 ± 0.025	1.660 ± 0.008	1.23
			2-2	118	89.0	1	6	104.4	62.40	0.575 ± 0.014	1.196 ± 0.096	0.598 ± 0.048	1.646 ± 0.009	2.05
			3-1	252	46.4	2	7	109.0	72.01	0.551 ± 0.009	1.322 ± 0.047	0.661 ± 0.024	1.678 ± 0.010	0.15
			3-2	263	44.9	2	7	107.8	71.07	0.557 ± 0.040	1.319 ± 0.046	0.659 ± 0.023	1.691 ± 0.005	0.67
			4-1	279	93.2	1	15	105.0	68.89	0.572 ± 0.028	1.313 ± 0.080	0.656 ± 0.040	1.673 ± 0.009	0.44
			4-2	277	74.7	2	12	105.1	70.06	0.571 ± 0.023	1.334 ± 0.048	0.667 ± 0.024	1.689 ± 0.005	0.55
			5-1	219	37.9	1	5	110.1	73.43	0.545 ± 0.012	1.333 ± 0.120	0.667 ± 0.060	1.679 ± 0.010	0.03
			5-2	226	60.2	2	8	107.1	72.54	0.560 ± 0.037	1.355 ± 0.070	0.678 ± 0.035	1.681 ± 0.006	0.05

Subject (ID)	Gender (M/F)	Stature (m)	Path (ID)	Frames (num.)	Use (%)	Intervals (num.)	½ Cycles (num.)	Cadence (steps/min)	Speed (m/min)	Duration (s)	Strides (m)	Displacement (m)	Height (m)	ΔHeight (%)
31	F	1.62	1-1	80	78.8	1	4	116.0	78.35	0.517 ± 0.013	1.351 ± 0.014	0.676 ± 0.007	1.623 ± 0.011	0.19
			1-2	80	80.0	1	4	113.3	77.29	0.529 ± 0.012	1.364 ± 0.015	0.682 ± 0.008	1.637 ± 0.008	1.07
			2-1	108	75.0	1	5	112.2	71.51	0.535 ± 0.013	1.275 ± 0.043	0.637 ± 0.021	1.612 ± 0.008	0.48
			2-2	93	66.7	1	4	116.9	79.92	0.513 ± 0.006	1.367 ± 0.040	0.683 ± 0.020	1.609 ± 0.006	0.70
			3-1	263	45.2	2	7	106.6	68.73	0.563 ± 0.032	1.290 ± 0.072	0.645 ± 0.036	1.615 ± 0.008	0.32
			3-2	263	25.1	1	4	111.0	74.68	0.541 ± 0.007	1.346 ± 0.024	0.673 ± 0.012	1.621 ± 0.007	0.07
			4-1	261	74.3	2	12	112.5	73.90	0.533 ± 0.012	1.314 ± 0.073	0.657 ± 0.036	1.627 ± 0.006	0.41
			4-2	274	66.8	2	11	109.5	71.78	0.548 ± 0.020	1.311 ± 0.076	0.655 ± 0.038	1.620 ± 0.005	0.01
			5-1	216	67.1	2	9	112.5	74.40	0.533 ± 0.018	1.322 ± 0.084	0.661 ± 0.042	1.627 ± 0.004	0.41
			5-2	200	47.0	1	6	116.0	79.68	0.517 ± 0.012	1.373 ± 0.030	0.687 ± 0.015	1.606 ± 0.006	0.85
32	M	1.65	1-1	78	67.9	1	3	102.9	77.54	0.583 ± 0.006	1.507 ± 0.034	0.753 ± 0.017	1.659 ± 0.008	0.51
			1-2	77	64.9	1	3	107.4	79.14	0.559 ± 0.015	1.474 ± 0.006	0.737 ± 0.003	1.660 ± 0.011	0.61
			2-1	98	74.5	1	4	99.5	71.89	0.603 ± 0.005	1.445 ± 0.024	0.722 ± 0.012	1.661 ± 0.011	0.65
			2-2	104	86.5	1	5	101.0	68.70	0.594 ± 0.015	1.362 ± 0.016	0.680 ± 0.008	1.645 ± 0.008	0.32
			3-1	229	52.8	2	7	105.3	76.36	0.570 ± 0.025	1.450 ± 0.049	0.725 ± 0.024	1.665 ± 0.007	0.91
			3-2	232	30.2	1	4	105.0	73.31	0.572 ± 0.006	1.397 ± 0.041	0.698 ± 0.020	1.660 ± 0.005	0.57
			4-1	244	69.7	2	10	107.0	77.61	0.561 ± 0.016	1.451 ± 0.041	0.725 ± 0.020	1.666 ± 0.005	0.94
			4-2	241	49.0	2	7	107.9	80.10	0.556 ± 0.008	1.484 ± 0.022	0.742 ± 0.011	1.670 ± 0.007	1.18
			5-1	199	49.7	1	6	110.1	82.36	0.545 ± 0.010	1.497 ± 0.024	0.748 ± 0.012	1.659 ± 0.003	0.52
			5-2	243	57.2	2	8	104.9	72.35	0.572 ± 0.022	1.379 ± 0.048	0.689 ± 0.024	1.655 ± 0.010	0.30
33	M	1.85	1-1	84	88.1	1	4	99.3	73.14	0.604 ± 0.015	1.473 ± 0.026	0.737 ± 0.013	1.832 ± 0.013	0.96
			1-2	72	68.1	1	3	111.6	88.99	0.538 ± 0.009	1.595 ± 0.034	0.797 ± 0.017	1.826 ± 0.011	1.33
			2-1	95	71.6	1	4	107.5	83.73	0.558 ± 0.013	1.557 ± 0.036	0.779 ± 0.018	1.821 ± 0.010	1.59
			2-2	91	72.5	1	4	111.0	86.99	0.540 ± 0.009	1.567 ± 0.060	0.783 ± 0.030	1.832 ± 0.011	0.97
			3-1	206	53.4	3	7	115.1	93.01	0.521 ± 0.049	1.616 ± 0.159	0.808 ± 0.079	1.853 ± 0.009	0.16
			3-2	203	45.8	2	6	115.5	97.64	0.520 ± 0.015	1.691 ± 0.037	0.846 ± 0.018	1.834 ± 0.008	0.87
			4-1	206	83.5	2	10	105.6	95.73	0.568 ± 0.175	1.813 ± 0.220	0.907 ± 0.110	1.874 ± 0.007	1.28
			4-2	209	67.9	2	9	115.1	95.75	0.521 ± 0.007	1.664 ± 0.050	0.832 ± 0.025	1.851 ± 0.007	0.04
			5-1	169	60.9	2	6	106.0	97.07	0.566 ± 0.200	1.830 ± 0.368	0.916 ± 0.186	1.935 ± 0.010	4.40
			5-2	166	47.6	1	5	115.3	94.54	0.520 ± 0.010	1.640 ± 0.031	0.820 ± 0.016	1.852 ± 0.005	0.13
34	M	1.78	1-1	105	55.2	1	3	93.6	80.74	0.641 ± 0.117	1.760 ± 0.828	0.863 ± 0.385	1.777 ± 0.015	0.16
			1-2	107	47.7	1	3	106.5	64.93	0.564 ± 0.051	1.220 ± 0.022	0.610 ± 0.011	1.784 ± 0.005	0.23
			2-1	146	47.3	1	3	79.3	51.85	0.756 ± 0.144	1.309 ± 0.181	0.654 ± 0.090	1.799 ± 0.005	1.04
			2-2	156	59.0	1	4	79.1	49.49	0.759 ± 0.047	1.255 ± 0.203	0.626 ± 0.100	1.754 ± 0.009	1.50
			3-1	269	27.9	1	4	96.5	58.80	0.621 ± 0.026	1.218 ± 0.052	0.609 ± 0.026	1.791 ± 0.007	0.60
			3-2	247	72.9	1	10	100.7	83.99	0.596 ± 0.178	1.676 ± 0.697	0.834 ± 0.346	1.640 ± 0.015	8.54
			4-1	228	54.8	1	7	101.8	93.33	0.589 ± 0.164	1.854 ± 0.759	0.917 ± 0.379	1.753 ± 0.017	1.56
			4-2	244	42.2	1	5	88.4	105.89	0.679 ± 0.341	2.413 ± 1.205	1.198 ± 0.569	1.821 ± 0.026	2.23
			5-1	218	58.7	1	5	70.9	71.78	0.846 ± 0.230	2.035 ± 0.422	1.013 ± 0.205	1.691 ± 0.012	5.25
			5-2	171	0.0	0	0	–	–	–	–	–	–	–
35	F	1.75	1-1	73	80.8	1	4	122.5	91.99	0.490 ± 0.006	1.502 ± 0.016	0.751 ± 0.008	1.776 ± 0.012	1.44
			1-2	61	70.5	1	3	127.0	100.38	0.472 ± 0.005	1.581 ± 0.009	0.790 ± 0.005	1.739 ± 0.008	0.65
			2-1	89	84.3	1	5	121.2	89.97	0.495 ± 0.008	1.484 ± 0.032	0.742 ± 0.016	1.764 ± 0.009	0.82
			2-2	85	70.6	1	4	122.8	93.53	0.489 ± 0.011	1.524 ± 0.048	0.762 ± 0.024	1.744 ± 0.007	0.32
			3-1	212	78.3	2	11	120.7	90.20	0.497 ± 0.032	1.494 ± 0.052	0.747 ± 0.026	1.831 ± 0.011	4.41
			3-2	213	69.5	2	9	110.6	87.15	0.543 ± 0.168	1.576 ± 0.251	0.788 ± 0.125	1.768 ± 0.013	1.01
			4-1	213	68.1	2	10	124.9	95.10	0.480 ± 0.009	1.523 ± 0.039	0.761 ± 0.019	1.787 ± 0.006	2.05
			4-2	217	67.3	2	10	124.1	93.86	0.483 ± 0.010	1.513 ± 0.034	0.756 ± 0.017	1.780 ± 0.004	1.69
			5-1	180	63.9	2	8	126.4	97.16	0.475 ± 0.019	1.538 ± 0.094	0.768 ± 0.046	1.783 ± 0.009	1.85
			5-2	190	46.3	1	6	124.0	92.07	0.484 ± 0.020	1.490 ± 0.029	0.743 ± 0.019	1.794 ± 0.079	2.46

Subject (ID)	Gender (M/F)	Stature (m)	Path (ID)	Frames (num.)	Use (%)	Intervals (num.)	½ Cycles (num.)	Cadence (steps/min)	Speed (m/min)	Duration (s)	Strides (m)	Displacement (m)	Height (m)	ΔHeight (%)
36	M	1.83	1-1	79	43.0	1	2	104.2	70.56	0.576 ± 0.019	1.354 ± 0.019	0.677 ± 0.010	1.854 ± 0.010	1.30
			1-2	79	63.3	1	3	108.9	70.64	0.551 ± 0.027	1.297 ± 0.080	0.648 ± 0.040	1.857 ± 0.005	1.43
			2-1	116	78.4	1	5	99.5	65.18	0.603 ± 0.030	1.310 ± 0.035	0.655 ± 0.018	1.828 ± 0.007	0.09
			2-2	116	77.6	1	5	100.8	66.44	0.595 ± 0.014	1.318 ± 0.048	0.659 ± 0.024	1.807 ± 0.004	1.29
			3-1	249	34.9	1	5	104.8	69.79	0.572 ± 0.016	1.332 ± 0.057	0.666 ± 0.029	1.842 ± 0.008	0.65
			3-2	264	27.7	1	4	99.7	67.14	0.602 ± 0.008	1.346 ± 0.052	0.673 ± 0.026	1.840 ± 0.006	0.56
			4-1	266	80.8	2	12	101.6	71.64	0.590 ± 0.067	1.326 ± 0.320	0.705 ± 0.019	2.084 ± 0.817	12.20
			4-2	254	69.7	2	10	103.5	74.02	0.580 ± 0.023	1.431 ± 0.047	0.715 ± 0.023	1.846 ± 0.007	0.89
			5-1	205	66.8	2	8	106.9	77.02	0.561 ± 0.021	1.441 ± 0.096	0.720 ± 0.048	1.849 ± 0.012	1.05
			5-2	218	48.6	2	6	103.7	73.10	0.578 ± 0.015	1.409 ± 0.059	0.705 ± 0.030	1.840 ± 0.008	0.54
37	M	1.80	1-1	78	70.5	1	3	99.2	75.39	0.605 ± 0.005	1.521 ± 0.009	0.760 ± 0.004	1.811 ± 0.015	0.61
			1-2	80	68.8	1	3	98.1	74.53	0.612 ± 0.003	1.520 ± 0.024	0.760 ± 0.012	1.812 ± 0.009	0.69
			2-1	100	76.0	1	4	95.1	71.40	0.631 ± 0.012	1.502 ± 0.033	0.751 ± 0.016	1.797 ± 0.013	0.15
			2-2	101	73.3	1	4	97.8	72.28	0.613 ± 0.005	1.477 ± 0.053	0.739 ± 0.027	1.803 ± 0.010	0.17
			3-1	229	40.2	1	5	99.2	74.48	0.605 ± 0.007	1.502 ± 0.076	0.751 ± 0.038	1.803 ± 0.010	0.18
			3-2	226	31.9	1	4	100.5	74.59	0.597 ± 0.016	1.485 ± 0.031	0.742 ± 0.015	1.799 ± 0.011	0.06
			4-1	246	96.3	1	13	99.6	75.69	0.602 ± 0.022	1.520 ± 0.092	0.760 ± 0.046	1.864 ± 0.009	3.45
			4-2	255	71.4	2	10	99.8	75.49	0.601 ± 0.016	1.513 ± 0.079	0.756 ± 0.039	1.815 ± 0.011	0.82
			5-1	193	85.5	1	9	99.6	75.55	0.602 ± 0.023	1.518 ± 0.063	0.758 ± 0.033	1.856 ± 0.027	3.02
			5-2	192	46.9	1	5	100.9	77.00	0.595 ± 0.013	1.527 ± 0.028	0.763 ± 0.014	1.813 ± 0.012	0.74
38	F	1.70	1-1	86	77.9	1	4	108.9	75.96	0.551 ± 0.013	1.396 ± 0.008	0.698 ± 0.004	1.680 ± 0.008	1.22
			1-2	82	84.1	1	4	104.8	71.92	0.573 ± 0.009	1.373 ± 0.019	0.687 ± 0.009	1.707 ± 0.007	0.40
			2-1	108	65.7	1	4	102.2	66.31	0.587 ± 0.009	1.297 ± 0.034	0.649 ± 0.017	1.709 ± 0.009	0.50
			2-2	105	88.6	1	5	97.7	65.11	0.614 ± 0.015	1.333 ± 0.033	0.666 ± 0.017	1.666 ± 0.009	2.05
			3-1	239	34.3	1	5	110.3	71.07	0.544 ± 0.040	1.290 ± 0.177	0.644 ± 0.090	1.690 ± 0.008	0.58
			3-2	244	34.8	1	5	106.5	72.44	0.563 ± 0.009	1.361 ± 0.015	0.680 ± 0.008	1.654 ± 0.006	2.75
			4-1	260	78.8	2	12	107.1	74.68	0.560 ± 0.032	1.397 ± 0.152	0.697 ± 0.076	1.683 ± 0.007	1.01
			4-2	263	65.8	2	10	104.9	72.51	0.572 ± 0.023	1.385 ± 0.037	0.692 ± 0.017	1.703 ± 0.048	0.18
			5-1	225	69.3	2	9	105.3	72.67	0.570 ± 0.019	1.380 ± 0.048	0.690 ± 0.024	1.707 ± 0.008	0.43
			5-2	223	63.7	2	8	102.2	71.73	0.587 ± 0.011	1.405 ± 0.048	0.702 ± 0.023	1.686 ± 0.050	0.84
39	F	1.62	1-1	88	72.7	1	4	113.9	75.94	0.527 ± 0.013	1.333 ± 0.014	0.667 ± 0.007	1.602 ± 0.006	1.11
			1-2	86	73.3	1	4	114.0	74.48	0.526 ± 0.013	1.307 ± 0.024	0.653 ± 0.012	1.625 ± 0.004	0.31
			2-1	121	82.6	1	6	109.5	65.36	0.548 ± 0.023	1.194 ± 0.043	0.597 ± 0.022	1.591 ± 0.007	1.85
			2-2	112	85.7	1	6	113.2	68.81	0.530 ± 0.031	1.216 ± 0.047	0.608 ± 0.023	1.586 ± 0.006	2.14
			3-1	282	54.3	2	9	107.2	65.13	0.560 ± 0.043	1.215 ± 0.086	0.608 ± 0.043	1.610 ± 0.005	0.59
			3-2	258	36.8	1	6	115.1	72.16	0.521 ± 0.049	1.257 ± 0.142	0.627 ± 0.074	1.629 ± 0.007	0.56
			4-1	293	82.6	2	15	112.7	74.14	0.532 ± 0.019	1.320 ± 0.268	0.658 ± 0.127	1.607 ± 0.005	0.79
			4-2	291	78.7	2	14	111.1	70.50	0.540 ± 0.025	1.269 ± 0.094	0.635 ± 0.047	1.612 ± 0.006	0.47
			5-1	214	44.4	1	6	114.0	73.42	0.526 ± 0.013	1.288 ± 0.015	0.644 ± 0.007	1.612 ± 0.007	0.50
			5-2	225	43.6	1	6	110.9	71.76	0.541 ± 0.026	1.294 ± 0.049	0.647 ± 0.024	1.591 ± 0.006	1.82
40	F	1.65	1-1	83	60.2	1	3	109.6	77.74	0.547 ± 0.004	1.418 ± 0.006	0.709 ± 0.003	1.673 ± 0.011	1.35
			1-2	84	76.2	1	4	113.0	78.06	0.531 ± 0.009	1.381 ± 0.010	0.691 ± 0.005	1.678 ± 0.007	1.66
			2-1	117	65.0	1	4	94.7	63.01	0.634 ± 0.025	1.331 ± 0.049	0.665 ± 0.024	1.651 ± 0.009	0.05
			2-2	117	81.2	1	5	96.2	64.44	0.624 ± 0.010	1.340 ± 0.033	0.670 ± 0.017	1.672 ± 0.011	1.32
			3-1	255	53.3	2	8	106.7	71.35	0.562 ± 0.030	1.338 ± 0.100	0.669 ± 0.050	1.707 ± 0.009	3.32
			3-2	252	40.1	1	6	107.6	70.13	0.558 ± 0.009	1.304 ± 0.131	0.652 ± 0.066	1.674 ± 0.018	1.44
			4-1	259	75.3	2	12	111.5	79.07	0.538 ± 0.010	1.419 ± 0.027	0.709 ± 0.013	1.690 ± 0.009	2.37
			4-2	260	69.6	2	11	110.1	76.73	0.545 ± 0.012	1.394 ± 0.033	0.697 ± 0.016	1.694 ± 0.007	2.57
			5-1	197	58.4	1	7	111.4	79.71	0.539 ± 0.006	1.431 ± 0.022	0.716 ± 0.011	1.665 ± 0.010	0.90
			5-2	219	37.9	1	5	109.1	78.26	0.550 ± 0.022	1.434 ± 0.017	0.717 ± 0.008	1.688 ± 0.006	2.25

Subject (ID)	Gender (M/F)	Stature (m)	Path (ID)	Frames (num.)	Use (%)	Intervals (num.)	½ Cycles (num.)	Cadence (steps/min)	Speed (m/min)	Duration (s)	Strides (m)	Displacement (m)	Height (m)	ΔHeight (%)
41	M	1.85	1-1	82	63.4	1	3	104.8	78.44	0.573 ± 0.011	1.498 ± 0.014	0.749 ± 0.007	1.850 ± 0.008	0.01
			1-2	72	69.4	1	3	108.1	82.30	0.555 ± 0.006	1.522 ± 0.046	0.761 ± 0.023	1.864 ± 0.017	0.76
			2-1	106	67.0	1	4	102.3	73.10	0.586 ± 0.012	1.429 ± 0.047	0.715 ± 0.024	1.843 ± 0.006	0.37
			2-2	103	69.9	1	4	101.2	73.65	0.593 ± 0.014	1.456 ± 0.048	0.728 ± 0.024	1.852 ± 0.016	0.12
			3-1	250	27.6	1	4	104.7	76.42	0.573 ± 0.005	1.460 ± 0.029	0.730 ± 0.015	1.854 ± 0.011	0.21
			3-2	243	29.6	1	4	101.0	71.97	0.594 ± 0.013	1.426 ± 0.024	0.713 ± 0.012	1.855 ± 0.007	0.24
			4-1	282	70.2	2	11	100.8	71.63	0.595 ± 0.020	1.422 ± 0.057	0.711 ± 0.028	1.875 ± 0.006	1.35
			4-2	268	72.4	2	11	103.0	74.15	0.582 ± 0.014	1.440 ± 0.040	0.720 ± 0.020	1.863 ± 0.008	0.69
			5-1	218	71.1	2	9	105.3	73.31	0.570 ± 0.053	1.393 ± 0.150	0.696 ± 0.075	1.897 ± 0.013	2.50
			5-2	218	41.3	1	5	101.6	71.57	0.590 ± 0.023	1.409 ± 0.027	0.704 ± 0.013	1.880 ± 0.007	1.57
42	F	1.67	1-1	88	73.9	1	4	111.6	70.68	0.538 ± 0.010	1.266 ± 0.045	0.633 ± 0.022	1.636 ± 0.006	2.10
			1-2	89	75.3	1	4	108.4	69.62	0.553 ± 0.025	1.284 ± 0.013	0.642 ± 0.007	1.641 ± 0.007	1.77
			2-1	112	75.0	1	5	107.3	67.04	0.559 ± 0.017	1.249 ± 0.051	0.625 ± 0.026	1.599 ± 0.016	4.42
			2-2	119	87.4	1	6	104.4	64.02	0.575 ± 0.017	1.226 ± 0.046	0.613 ± 0.023	1.616 ± 0.017	3.34
			3-1	259	45.6	1	7	108.6	68.39	0.552 ± 0.012	1.288 ± 0.063	0.630 ± 0.052	1.683 ± 0.208	0.74
			3-2	277	24.5	1	4	107.8	66.82	0.556 ± 0.006	1.239 ± 0.019	0.620 ± 0.010	1.616 ± 0.005	3.32
			4-1	287	80.5	2	14	110.4	69.51	0.543 ± 0.031	1.261 ± 0.075	0.630 ± 0.038	1.616 ± 0.060	3.33
			4-2	305	78.4	2	14	106.5	64.18	0.564 ± 0.037	1.209 ± 0.091	0.603 ± 0.047	1.686 ± 0.153	0.93
			5-1	229	62.0	2	9	115.1	69.82	0.521 ± 0.021	1.210 ± 0.114	0.607 ± 0.052	1.618 ± 0.049	3.24
			5-2	248	62.9	2	9	105.5	61.78	0.569 ± 0.038	1.173 ± 0.165	0.586 ± 0.080	1.660 ± 0.086	0.61
43	F	1.70	1-1	82	58.5	1	3	112.7	77.80	0.532 ± 0.009	1.381 ± 0.026	0.690 ± 0.013	1.699 ± 0.010	0.06
			1-2	86	75.6	1	4	111.7	75.20	0.537 ± 0.013	1.346 ± 0.020	0.673 ± 0.010	1.715 ± 0.004	0.85
			2-1	101	82.2	1	5	110.3	74.72	0.544 ± 0.012	1.355 ± 0.043	0.677 ± 0.022	1.692 ± 0.007	0.46
			2-2	97	84.5	1	5	111.6	77.78	0.538 ± 0.010	1.395 ± 0.032	0.697 ± 0.016	1.689 ± 0.004	0.67
			3-1	220	35.9	1	5	114.9	80.66	0.522 ± 0.015	1.404 ± 0.042	0.702 ± 0.021	1.705 ± 0.004	0.29
			3-2	230	27.8	1	4	114.3	78.20	0.525 ± 0.016	1.368 ± 0.035	0.684 ± 0.017	1.700 ± 0.010	0.01
			4-1	238	72.3	2	11	116.1	83.27	0.517 ± 0.013	1.434 ± 0.025	0.717 ± 0.012	1.703 ± 0.005	0.16
			4-2	248	69.8	2	11	115.1	80.80	0.521 ± 0.015	1.404 ± 0.027	0.702 ± 0.014	1.715 ± 0.007	0.90
			5-1	202	86.6	1	11	114.0	79.55	0.526 ± 0.031	1.396 ± 0.073	0.698 ± 0.037	1.731 ± 0.032	1.81
			5-2	197	64.5	2	8	114.5	80.10	0.524 ± 0.018	1.399 ± 0.061	0.700 ± 0.030	1.723 ± 0.007	1.34
44	F	1.65	1-1	88	77.3	1	4	107.7	64.41	0.557 ± 0.010	1.197 ± 0.021	0.598 ± 0.011	1.628 ± 0.008	1.34
			1-2	90	78.9	1	4	102.5	62.16	0.586 ± 0.012	1.213 ± 0.011	0.607 ± 0.006	1.608 ± 0.005	2.62
			2-1	138	78.3	1	6	100.9	57.77	0.595 ± 0.013	1.145 ± 0.033	0.573 ± 0.017	1.595 ± 0.008	3.48
			2-2	135	80.7	1	6	100.0	58.50	0.600 ± 0.012	1.170 ± 0.021	0.585 ± 0.011	1.591 ± 0.006	3.73
			3-1	305	33.8	1	6	105.9	61.05	0.567 ± 0.009	1.153 ± 0.028	0.576 ± 0.014	1.609 ± 0.006	2.56
			3-2	309	40.1	2	7	102.4	60.80	0.586 ± 0.032	1.188 ± 0.079	0.594 ± 0.039	1.609 ± 0.006	2.55
			4-1	318	73.9	2	14	108.3	62.71	0.554 ± 0.021	1.158 ± 0.086	0.579 ± 0.043	1.627 ± 0.006	1.39
			4-2	334	79.3	2	15	103.1	59.23	0.582 ± 0.019	1.149 ± 0.036	0.575 ± 0.018	1.614 ± 0.005	2.24
			5-1	268	64.2	2	10	105.5	62.24	0.569 ± 0.024	1.180 ± 0.053	0.590 ± 0.026	1.611 ± 0.005	2.42
			5-2	271	44.3	2	7	106.1	61.78	0.565 ± 0.028	1.164 ± 0.061	0.582 ± 0.030	1.631 ± 0.005	1.16
45	F	1.65	1-1	102	68.6	1	4	103.7	63.68	0.578 ± 0.027	1.228 ± 0.034	0.614 ± 0.017	1.699 ± 0.003	2.86
			1-2	109	81.7	1	5	102.3	61.89	0.586 ± 0.015	1.210 ± 0.058	0.605 ± 0.029	1.696 ± 0.003	2.69
			2-1	128	85.9	1	6	99.3	57.18	0.604 ± 0.026	1.152 ± 0.061	0.576 ± 0.031	1.688 ± 0.006	2.24
			2-2	117	91.5	1	6	102.6	62.69	0.585 ± 0.020	1.222 ± 0.041	0.611 ± 0.020	1.707 ± 0.006	3.34
			3-1	268	31.0	1	5	109.1	67.25	0.550 ± 0.017	1.234 ± 0.071	0.617 ± 0.036	1.693 ± 0.006	2.56
			3-2	281	42.3	2	7	107.1	65.04	0.560 ± 0.046	1.214 ± 0.025	0.607 ± 0.013	1.698 ± 0.004	2.85
			4-1	301	79.4	2	14	106.8	66.28	0.562 ± 0.029	1.242 ± 0.043	0.621 ± 0.021	1.703 ± 0.005	3.09
			4-2	302	87.7	1	15	103.0	62.57	0.582 ± 0.099	1.217 ± 0.103	0.607 ± 0.053	1.784 ± 0.222	7.53
			5-1	222	75.7	2	10	108.2	66.52	0.554 ± 0.022	1.230 ± 0.072	0.615 ± 0.036	1.715 ± 0.004	3.78
			5-2	230	57.8	1	8	110.0	67.33	0.546 ± 0.009	1.228 ± 0.028	0.612 ± 0.016	1.713 ± 0.086	3.66

Subject (ID)	Gender (M/F)	Stature (m)	Path (ID)	Frames (num.)	Use (%)	Intervals (num.)	½ Cycles (num.)	Cadence (steps/min)	Speed (m/min)	Duration (s)	Strides (m)	Displacement (m)	Height (m)	ΔHeight (%)
46	F	1.68	1-1	100	73.0	1	4	99.6	64.00	0.602 ± 0.018	1.323 ± 0.079	0.642 ± 0.010	1.589 ± 0.214	5.71
			1-2	81	81.5	1	4	110.7	74.53	0.542 ± 0.013	1.422 ± 0.122	0.673 ± 0.016	1.397 ± 0.235	20.23
			2-1	127	87.4	1	6	97.8	61.31	0.614 ± 0.015	1.291 ± 0.075	0.627 ± 0.023	1.237 ± 0.144	35.86
			2-2	128	73.4	1	5	95.9	60.04	0.626 ± 0.012	1.291 ± 0.077	0.626 ± 0.025	1.376 ± 0.206	22.05
			3-1	262	43.1	1	6	96.9	60.02	0.619 ± 0.017	1.276 ± 0.104	0.620 ± 0.026	1.665 ± 0.260	0.91
			3-2	265	35.8	1	5	95.2	58.90	0.630 ± 0.027	1.249 ± 0.035	0.619 ± 0.008	1.763 ± 0.176	4.72
			4-1	227	45.8	1	6	104.9	70.12	0.572 ± 0.015	1.358 ± 0.062	0.669 ± 0.009	1.409 ± 0.190	19.26
			4-2	225	44.0	1	6	110.8	76.70	0.542 ± 0.016	1.404 ± 0.033	0.692 ± 0.009	1.740 ± 0.081	3.46
			5-1	178	92.7	1	10	110.1	74.51	0.545 ± 0.028	1.378 ± 0.095	0.677 ± 0.028	1.705 ± 0.118	1.47
			5-2	179	57.5	1	6	106.4	71.54	0.564 ± 0.023	1.344 ± 0.008	0.672 ± 0.004	1.729 ± 0.006	2.82
47	F	1.68	1-1	103	77.7	1	5	113.7	65.06	0.528 ± 0.014	1.144 ± 0.021	0.572 ± 0.010	1.671 ± 0.006	0.55
			1-2	89	69.7	1	4	117.1	73.37	0.512 ± 0.010	1.253 ± 0.027	0.626 ± 0.013	1.674 ± 0.008	0.37
			2-1	113	86.7	1	6	111.4	66.47	0.539 ± 0.015	1.194 ± 0.036	0.597 ± 0.018	1.661 ± 0.007	1.12
			2-2	103	76.7	1	5	115.5	72.04	0.520 ± 0.008	1.248 ± 0.025	0.624 ± 0.012	1.661 ± 0.007	1.13
			3-2	242	31.8	1	5	117.2	72.37	0.512 ± 0.023	1.235 ± 0.009	0.617 ± 0.004	1.682 ± 0.002	0.10
			3-1	237	57.8	2	9	119.8	75.62	0.501 ± 0.015	1.262 ± 0.037	0.631 ± 0.018	1.719 ± 0.007	2.26
			4-1	260	74.2	2	13	122.5	77.31	0.490 ± 0.015	1.262 ± 0.033	0.631 ± 0.016	1.690 ± 0.007	0.58
			4-2	255	58.8	2	10	121.2	76.79	0.495 ± 0.018	1.267 ± 0.021	0.633 ± 0.011	1.693 ± 0.006	0.76
			5-1	201	44.8	1	6	122.4	78.01	0.490 ± 0.016	1.274 ± 0.026	0.637 ± 0.013	1.680 ± 0.012	0.01
			5-2	187	47.1	1	6	123.0	79.87	0.488 ± 0.023	1.299 ± 0.019	0.650 ± 0.010	1.681 ± 0.005	0.05
48	F	1.55	1-1	103	82.5	1	5	108.2	64.10	0.555 ± 0.009	1.185 ± 0.011	0.593 ± 0.006	1.535 ± 0.009	0.97
			1-2	106	65.1	1	4	105.7	68.78	0.568 ± 0.011	1.299 ± 0.134	0.651 ± 0.066	1.537 ± 0.005	0.87
			2-1	132	77.3	1	6	106.1	60.80	0.566 ± 0.011	1.147 ± 0.024	0.573 ± 0.012	1.537 ± 0.004	0.85
			2-2	121	82.6	1	6	109.2	65.86	0.549 ± 0.007	1.206 ± 0.025	0.603 ± 0.012	1.532 ± 0.003	1.16
			3-1	273	30.0	1	5	111.6	67.75	0.538 ± 0.004	1.214 ± 0.032	0.607 ± 0.016	1.558 ± 0.004	0.53
			3-2	277	52.0	2	9	112.9	68.21	0.531 ± 0.017	1.209 ± 0.036	0.604 ± 0.018	1.577 ± 0.005	1.69
			4-1	290	77.9	2	14	112.5	69.36	0.533 ± 0.010	1.233 ± 0.031	0.617 ± 0.015	1.558 ± 0.005	0.49
			4-2	274	75.9	2	13	114.0	72.49	0.526 ± 0.014	1.272 ± 0.037	0.636 ± 0.018	1.575 ± 0.007	1.59
			5-1	230	56.5	2	8	112.6	70.81	0.533 ± 0.014	1.258 ± 0.030	0.629 ± 0.015	1.557 ± 0.003	0.46
			5-2	225	71.6	2	10	112.5	68.44	0.533 ± 0.011	1.217 ± 0.048	0.608 ± 0.024	1.563 ± 0.007	0.86
49	F	1.70	1-1	80	81.2	1	4	112.0	76.72	0.536 ± 0.013	1.371 ± 0.013	0.685 ± 0.007	1.617 ± 0.009	5.16
			1-2	74	66.2	1	3	112.0	79.82	0.536 ± 0.008	1.426 ± 0.010	0.713 ± 0.005	1.641 ± 0.012	3.59
			2-1	96	86.5	1	5	109.4	73.11	0.548 ± 0.008	1.336 ± 0.063	0.668 ± 0.031	1.599 ± 0.006	6.32
			2-2	93	73.1	1	4	107.8	74.64	0.557 ± 0.011	1.385 ± 0.046	0.692 ± 0.023	1.619 ± 0.009	5.02
			3-1	217	30.4	1	4	111.2	79.66	0.540 ± 0.011	1.433 ± 0.071	0.716 ± 0.036	1.630 ± 0.008	4.28
			3-2	216	30.6	1	4	110.3	71.82	0.544 ± 0.020	1.302 ± 0.051	0.651 ± 0.025	1.617 ± 0.007	5.14
			4-1	232	63.4	2	9	111.5	79.70	0.538 ± 0.021	1.429 ± 0.040	0.715 ± 0.020	1.633 ± 0.008	4.11
			4-2	221	59.7	2	8	110.3	78.34	0.544 ± 0.022	1.420 ± 0.032	0.710 ± 0.016	1.651 ± 0.007	2.97
			5-1	181	44.2	1	5	114.0	82.36	0.526 ± 0.007	1.444 ± 0.014	0.722 ± 0.007	1.634 ± 0.007	4.05
			5-2	180	45.0	1	5	112.4	80.28	0.534 ± 0.015	1.429 ± 0.024	0.714 ± 0.012	1.647 ± 0.006	3.20
50	F	1.55	1-1	94	79.8	1	5	121.2	74.18	0.495 ± 0.015	1.224 ± 0.041	0.612 ± 0.021	1.576 ± 0.008	1.63
			1-2	92	66.3	1	4	120.0	72.60	0.500 ± 0.017	1.210 ± 0.029	0.605 ± 0.015	1.579 ± 0.007	1.83
			2-1	110	74.5	1	5	111.3	66.18	0.539 ± 0.006	1.189 ± 0.011	0.594 ± 0.006	1.579 ± 0.008	1.86
			2-2	108	86.1	1	6	117.0	68.80	0.513 ± 0.013	1.176 ± 0.034	0.588 ± 0.017	1.557 ± 0.008	0.46
			3-1	258	77.5	2	11	100.3	68.86	0.598 ± 0.309	1.372 ± 0.382	0.687 ± 0.191	1.602 ± 0.012	3.24
			3-2	260	48.1	2	8	115.8	67.61	0.518 ± 0.020	1.168 ± 0.047	0.584 ± 0.023	1.606 ± 0.009	3.47
			4-1	263	63.9	2	11	118.8	72.81	0.505 ± 0.011	1.226 ± 0.020	0.613 ± 0.010	1.585 ± 0.006	2.22
			4-2	256	75.8	2	13	121.2	74.57	0.495 ± 0.020	1.230 ± 0.033	0.615 ± 0.016	1.599 ± 0.007	3.04
			5-1	200	53.0	1	7	119.9	73.87	0.500 ± 0.013	1.232 ± 0.013	0.616 ± 0.006	1.600 ± 0.006	3.12
			5-2	198	44.9	1	6	122.4	76.12	0.490 ± 0.018	1.243 ± 0.019	0.622 ± 0.009	1.587 ± 0.008	2.33

Subject (ID)	Gender (M/F)	Stature (m)	Path (ID)	Frames (num.)	Use (%)	Intervals (num.)	$\frac{1}{2}$ Cycles (num.)	Cadence (steps/min)	Speed (m/min)	Duration (s)	Strides (m)	Displacement (m)	Height (m)	ΔHeight (%)
51	F	1.76	1-1	67	68.7	1	3	118.4	96.79	0.507 ± 0.004	1.635 ± 0.053	0.817 ± 0.026	1.741 ± 0.011	1.07
			1-2	64	48.4	1	2	115.6	93.67	0.519 ± 0.001	1.620 ± 0.033	0.810 ± 0.016	1.790 ± 0.008	1.65
			2-1	79	78.5	1	4	118.5	96.04	0.506 ± 0.023	1.622 ± 0.059	0.811 ± 0.029	1.734 ± 0.008	1.53
			2-2	81	79.0	1	4	113.1	84.48	0.531 ± 0.002	1.494 ± 0.043	0.747 ± 0.022	1.758 ± 0.005	0.11
			3-1	194	53.1	2	6	106.4	118.04	0.564 ± 0.093	2.242 ± 1.126	1.109 ± 0.552	1.742 ± 0.008	1.04
			3-2	190	32.1	1	4	119.3	94.11	0.503 ± 0.013	1.580 ± 0.109	0.789 ± 0.053	1.744 ± 0.006	0.94
			4-1	200	76.0	2	10	119.7	120.13	0.501 ± 0.027	2.058 ± 1.209	1.004 ± 0.529	1.763 ± 0.008	0.19
			4-2	196	63.8	2	8	117.0	93.42	0.513 ± 0.011	1.598 ± 0.044	0.799 ± 0.022	1.766 ± 0.007	0.34
			5-1	161	33.5	1	2	68.0	84.65	0.882 ± 0.162	2.508 ± 0.534	1.245 ± 0.280	1.995 ± 0.012	11.77
			5-2	158	38.6	1	4	119.7	95.44	0.501 ± 0.018	1.594 ± 0.036	0.797 ± 0.018	1.744 ± 0.005	0.92
52	F	1.54	1-1	80	78.8	1	4	115.4	79.70	0.520 ± 0.016	1.397 ± 0.043	0.690 ± 0.011	1.585 ± 0.058	2.84
			1-2	83	77.1	1	4	112.1	75.94	0.535 ± 0.012	1.354 ± 0.036	0.677 ± 0.018	1.571 ± 0.010	1.95
			2-1	113	77.0	1	5	103.7	64.67	0.579 ± 0.024	1.267 ± 0.043	0.624 ± 0.015	1.684 ± 0.176	8.55
			2-2	110	76.4	1	5	107.6	68.47	0.558 ± 0.009	1.273 ± 0.038	0.636 ± 0.019	1.567 ± 0.009	1.71
			3-1	231	34.2	1	5	114.0	75.77	0.526 ± 0.010	1.329 ± 0.053	0.664 ± 0.027	1.583 ± 0.011	2.69
			3-2	222	29.3	1	4	112.6	72.38	0.533 ± 0.010	1.302 ± 0.053	0.643 ± 0.017	1.614 ± 0.091	4.56
			4-1	242	68.2	2	10	110.7	73.30	0.542 ± 0.017	1.336 ± 0.087	0.662 ± 0.038	1.617 ± 0.117	4.78
			4-2	254	77.2	2	12	111.0	72.95	0.541 ± 0.025	1.316 ± 0.095	0.657 ± 0.048	1.580 ± 0.012	2.55
			5-1	197	56.3	1	7	114.4	78.88	0.525 ± 0.011	1.380 ± 0.010	0.690 ± 0.005	1.580 ± 0.005	2.53
			5-2	202	39.1	1	5	115.3	77.95	0.520 ± 0.003	1.352 ± 0.009	0.676 ± 0.005	1.573 ± 0.007	2.07

Bibliography

[1] Ed Ayyappa. Normal human locomotion, part 1 : Basic concepts and terminology. *Journal of Prosthetics and Orthotics*, 9(1):10–17, 1997.

[2] Mary Patricia Murray. Gait as a total pattern of movement. *American Journal of Physical Medicine*, 13(1):290–332, 1967.

[3] Éric Viel. *La Marche Humaine, la Course et le Saut (Biomécanique, Explorations, Normes et Dysfonctionnements)*. Masson, Paris, 2000.

[4] Nikolaos V. Boulgouris, Dimitrios Hatzinakos, and Konstantinos N. Plataniotis. Gait recognition : A challening signal processing technology for biometric identification. *IEEE Signal Processing Magazine*, pages 78 – 90, November 2005.

[5] Sudeep Sarkar, P. Jonathon Phillips, Zongyi Liu, I. Rebledo Vega, Patrick Grother, and Kevin W. Bowyer. The HumanID gait challenge problem : Data sets, performance, and analysis. *IEEE Transactions on Pattern Analysis and Machine Intelligence*, 27(2):162 – 177, 2005.

[6] L. Sloman, M. Berridge, S. Homatidis, D. Hunter, and T. Duck. Gait patterns of depressed patients and normal subjects. *American Journal of Psychiatry*, 139(1):94–97, 1982.

[7] Liang Wang. Abnormal walking gait analysis using Silhouette-Masked flow histograms. In *Proceedings of the International Conference on Pattern Recognition*, volume 3, pages 473–476, 2006.

[8] Junius André F. Balista, Maricor N. Soriano, and Caesar A. Saloma. Compact time-independent pattern representation of entire human gait cycle for tracking of gait irregularities. *Pattern Recognition Letters*, 31(1):20–27, 2010.

[9] Heba Lakany. Extracting a diagnostic gait signature. *Pattern Recognition*, 41(5):1644–1654, May 2008.

[10] A. H. Khandoker, D. Lai, R. K. Begg, and M. Palaniswami. A Wavelet-Based approach for screening falls risk in the elderly using support vector machines. In *Proceedings of the Fourth International Conference on Intelligent Sensing and Information Processing*, pages 184–189, 2006.

[11] Rezaul Begg, Russell Best, Lisa Dell'Oro, and Simon Taylor. Minimum foot clearance during walking: Strategies for the minimisation of trip-related falls. *Gait & Posture*, 25(2):191–198, February 2007.

[12] David J. Hewson, Jacques Duchêne, François Charpillet, Jamal Saboune, Valérie Michel-Pellegrino, Hassan Amoud, Michel Doussot, Jean Paysant, Anne Boyer, and Jean-Yves Hogrel. The PARAChute project: Remote monitoring of posture and gait for fall prevention. *EURASIP Journal on Advances in Signal Processing*, 2007:15, 2007.

[13] Bai ling Zhang, Yanchun Zhang, and Rezaul K. Begg. Gait classification in children with cerebral palsy by bayesian approach. *Pattern Recognition*, 42(4):581–586, April 2009.

[14] Nigar Sen Köktas, Nese Yalabik, Günes Yavuzer, and Robert P.W. Duin. A multi-classifier for grading knee osteoarthritis using gait analysis. *Pattern Recognition Letters*, In Press, Corrected Proof, 2010.

[15] G. Johansson. Visual perception of biological motion and a model for its analysis. *Perception Psychophysics*, 14(2):201–211, 1973.

[16] J. E. Cutting and L. T. Kozlowski. Recognizing friends by their walk: Gait perception without familiarity cues. *Bulletin of the Psychonomic Society*, 9(5):353–356, 1977.

[17] Sarah V. Stevenage, Mark S. Nixon, and Kate Vince. Visual analysis of gait as a cue to identity. *Applied Cognitive Psychology*, (13):513–526, 1999.

[18] Bufu Huang, Meng Chen, Panfeng Huang, and Yangsheng Xu. Gait modeling for human identification. In *Proceedings of the IEEE International Conference on Robotics and Automation*, pages 4833–4838, 2007.

[19] Liu Rong, Duan Zhiguo, Zhou Jianzhong, and Liu Ming. Identification of individual walking patterns using gait acceleration. In *Proceedings of the First International Conference on Bioinformatics and Biomedical Engineering*, pages 543–546, 2007.

[20] Shuichi Enokida, Ryo Shimomoto, Tomohito Wada, and Toshiaki Ejima. A predictive model for gait recognition. In *Proceedings of the Special Session on Research at the Biometric Consortium Conference*, pages 1–6, 2006.

[21] Alexandra Branzan Albu, Denis Laurendeau, Sylvain Comtois, Denis Ouellet, Patrick Hébert, André Zaccarin, Marc Parizeau, Robert Bergevin, Xavier Maldague, Richard Drouin, Stéphane Drouin, Nicolas Martel-Brisson, Frédéric Jean, Hélène Torresan, Langis Gagnon, and France Laliberté. MONNET: Monitoring pedestrians with a network of loosely-coupled cameras. In *Proceedings of the IEEE International Conference on Pattern Recognition*, Hong Kong, China, 2006.

[22] R. Jafri and H.R. Arabnia. Fusion of face and gait for automatic human recognition. In *Proceedings of the Fifth International Conference on Information Technology: New Generations*, pages 167–173, 2008.

[23] Xiaohui Hou and Zhijing Liu. Fusion of face and gait for human recognition in video sequences. In *Proceedings of the International Conference on Information Technology and Computer Science*, volume 1, pages 577–580, 2009.

[24] Zongyi Liu and Sudeep Sarkar. Simplest representation yet for gait recognition: Averaged silhouette. In *International Conference on Pattern Recognition*, volume 4, pages 211– 214, 2004.

[25] Ju Han and Bir Bhanu. Statistical feature fusion for gait-based human recognition. In *Proceedings of the IEEE Conference on Computer Vision and Pattern Recognition*, volume 2, pages 842–847, 2004.

[26] Ju Han and Bir Bhanu. Individual recognition using gait energy image. *IEEE Transactions on Pattern Analysis and Machine Intelligence*, 28(2):316– 322, 2006.

[27] K. Bashir, Tao Xiang, and Shaogang Gong. Feature selection on gait energy image for human identification. In *Proceedings of the IEEE International Conference on Acoustics, Speech and Signal Processing*, pages 985–988, 2008.

[28] Yanmei Chai, Jinchang Ren, Rongchun Zhao, and Jingping Jia. Automatic gait recognition using dynamic variance features. In *Proceedings of the International Conference on Automatic Face and Gesture Recognition*, pages 475– 480, 2006.

[29] Qinyong Ma, Shenkang Wang, Dongdong Nie, and Jianfeng Qiu. Gait recognition at a distance based on energy deviation image. In *Proceedings of the First International Conference on Bioinformatics and Biomedical Engineering*, pages 621–624, 2007.

[30] Jianyi Liu and Nanning Zheng. Gait history image: A novel temporal template for gait recognition. In *Proceeding of the IEEE International Conference on Multimedia and Expo*, pages 663–666, 2007.

[31] R.T. Collins, R. Gross, and Jianbo Shi. Silhouette-based human identification from body shape and gait. In *Proceedings of the IEEE International Conference on Automatic Face and Gesture Recognition*, pages 351–356, 2002.

[32] Chiraz BenAbdelkader, Ross Cutler, and Larry Davis. Motion-based recognition of people in eigengait space. In *Proceedings of the IEEE Conference on Automatic Face and Gesture Recognition*, pages 254 – 259, Washington, DC, May 2002.

[33] Jeff P. Foster, Mark S. Nixon, and Adam Prügel-Bennett. Automatic gait recognition using area-based metrics. *Pattern Recognition Letters*, 24(14):2489 – 2497, 2003.

[34] Nikolaos V. Boulgouris, Konstantinos N. Plataniotis, and Dimitrios Hatzinakos. Gait recognition using linear time normalization. *Pattern Recognition Letters*, (39):969 – 979, 2005.

[35] Ming-Hsu Cheng, Meng-Fen Ho, and Chung-Lin Huang. Gait analysis for human identification through manifold learning and HMM. *Pattern Recognition*, 41(8):2541–2553, August 2008.

[36] Liang Wang, Huazhong Ning, Tieniu Tan, and Weiming Hu. Fusion of static and dynamic body biometrics for gait recognition. *IEEE Transactions on Circuits and Systems for Video Technology*, 14(2):149– 158, 2004.

[37] Erhu Zhang, Jiwen Lu, and Ganglong Duan. Gait recognition via independent component analysis based on support vector machine and neural network. In *Advances in Natural Computation*, volume 3610 of *LNCS*, pages 640–649. Springer, 2005.

[38] S. Rahati, R. Moravejian, and F.M. Kazemi. Gait recognition using wavelet transform. In *Proceedings of the Fifth International Conference on Information Technology: New Generations*, pages 932–936, 2008.

[39] Shiqi Yu, Liang Wang, Weiming Hu, and Tieniu Tan. Gait analysis for human identification in frequency domain. In *Proceedings of the International Conference on Image and Graphics*, pages 282–285, 2004.

[40] Nikolaos V. Boulgouris, Konstantinos N. Plataniotis, and Dimitrios Hatzinakos. Gait recognition using dynamic time warping. In *Proceedings of the IEEE International Symposium on Multimedia Signal Processing*, pages 263 – 266, Siena, Italy, September 2004.

[41] Amit Kale, N. Cuntoor, B. Yegnanarayana, A. N. Rajagopalan, and Rama Chellappa. Gait analysis for human identification. In *Proceedings of the International*

Conference on Audio- and Video-based Person Authentication, pages 706 – 714, Guilford, UK, June 2003.

[42] Toby H. W. Lam and Tony W. H. Ao Ieong. Silhouette spatio-temporal spectrum (SStS) for Gait-Based human recognition. In *Proceedings of the International Conference on Advances in Pattern Recognition*, volume LNCS 3687, pages 309 – 315, 2005.

[43] Sungjun Hong, Heesung Lee, Imran Fareed Nizami, and Euntai Kim. A new gait representation for human identification: Mass vector. In *Proceedings of the Second IEEE Conference on Industrial Electronics and Applications*, pages 669– 673, 2007.

[44] Murat Ekinci. Gait recognition using multiple projections. In *Proceedings of the International Conference on Automatic Face and Gesture Recognition*, pages 517–522. IEEE Computer Society, 2006.

[45] Guo-Chang Huang and Yun-Hong Wang. Human gait recognition based on X-T plane energy images. In *Proceedings of the International Conference on Wavelet Analysis and Pattern Recognition*, volume 3, pages 1134–1138, 2007.

[46] M. Goffredo, J.N. Carter, and M.S. Nixon. Front-view gait recognition. In *Proceedings of the 2nd IEEE International Conference on Biometrics: Theory, Applications and Systems*, pages 1–6, 2008.

[47] James J. Little and Jeffrey E. Boyd. Recognizing people by their gait: The shape of motion. *International Journal of Computer Vision*, 14(6):83 – 105, 1998.

[48] Ling-Feng Liu, Wei Jia, and Yi-Hai Zhu. Gait recognition using hough transform and principal component analysis. In *Emerging Intelligent Computing Technology and Applications*, pages 363–370. 2009.

[49] Amos Y. Johnson and Aaron F. Bobick. A multi-view method for gait recognition using static body parameters. In *Audio- and Video-Based Biometric Person Authentication*, volume 2091 of *LNCS*, pages 301–311. Springer, 2001.

[50] Chiraz BenAbdelkader, Ross Cutler, and Larry Davis. View-invariant estimation of height and stride for gait recognition. In *Proceedings of the International ECCV Workshop on Biometric Authentication*, volume LNCS 2359, pages 155 – 167, 2002.

[51] Yanmei Chai, Qing Wang, Jingping Jia, and Rongchun Zhao. A novel gait recognition method via fusing shape and kinematics features. *Advances in Visual Computing*, 4291:80–89, 2006.

[52] Imed Bouchrika and Mark Nixon. Model-Based feature extraction for gait analysis and recognition. In *Computer Vision/Computer Graphics Collaboration Techniques*, pages 150–160. 2007.

[53] I. Bouchrika and M.S. Nixon. Gait recognition by dynamic cues. In *Proceedings of the 19th International Conference on Pattern Recognition*, pages 1–4, 2008.

[54] I. Bouchrika and M.S. Nixon. Exploratory factor analysis of gait recognition. In *Proceedings of the 8th IEEE International Conference on Automatic Face & Gesture Recognition*, pages 1–6, 2008.

[55] I. Bouchrika, M. Goffredo, J. Carter, and M. Nixon. Covariate analysis for View-Point independent gait recognition. In *Advances in Biometrics*, pages 990–999. 2009.

[56] David Cunado, Mark S. Nixon, and John N. Carter. Automatic extraction and description of human gait models for recognition purposes. *Computer Vision and Image Understanding*, 90(1):1–41, 2003.

[57] L. Lee and W. Eric L. Grimson. Gait appearance for recognition. In *Biometric Authentication*, volume 2359 of *LNCS*, pages 143–154. Springer, 2002.

[58] Seungdo Jeong, Su-Sun Kim, and Byung-Uk Choi. Canonical view synthesis for gait recognition. In *Proceedings of Conference on Frontiers in the Convergence of Bioscience and Information Technologies*, pages 734–739, 2007.

[59] Rong Zhang, Christian Vogler, and Dimitris Metaxas. Human gait recognition at sagittal plane. *Image and Vision Computing*, 25(3):321–330, March 2007.

[60] Haiping Lu, Konstantinos N. Plataniotis, and Anastasios N. Venetsanopoulos. A full-body layered deformable model for automatic model-based gait recognition. *EURASIP Journal on Advances in Signal Processing*, 2008, 2008.

[61] Nikolaos V. Boulgouris and Zhiwei X. Chi. Human gait recognition based on matching of body components. *Pattern Recognition*, 40:1763–1770, 2007.

[62] Hee-Deok Yang and Seong-Whan Lee. Reconstruction of 3D human body pose for gait recognition. In *Advances in Biometrics*, volume 3932 of *LNCS*, pages 619–625. Springer, 2005.

[63] Guoying Zhao, Guoyi Liu, Hua Li, and Matti Pietikainen. 3D gait recognition using multiple cameras. In *Proceedings of the International Conference on Automatic Face and Gesture Recognition*, pages 529– 534, 2006.

[64] CASIA gait database. http://www.cbsr.ia.ac.cn/english/Gait%20Databases.asp, 2005.

[65] Jamie Shutler, Mike Grant, Mark S Nixon, and John N Carter. On a large Sequence-Based human gait database. In *Fourth International Conference on Recent Advances in Soft Computing*, pages 66–72, Nottingham UK, November 2002.

[66] Human identification at a distance – University of Maryland Database. http://www.umiacs.umd.edu/labs/pirl/hid/data.html, 2001.

[67] Ralph Gross and Jianbo Shi. The CMU motion of body (MoBo) database. Technical Report CMU-RI-TR-01-18, Robotics Institute, Pittsburgh, PA, USA, June 2001.

[68] Thomas B. Moeslund, Adrian Hilton, and Volker Kruger. A survey of advances in vision-based human motion capture and analysis. *Computer Vision and Image Understanding*, 104(2-3):90–126, 2006.

[69] Jérôme Vignola, Jean-François Lalonde, and Robert Bergevin. Progressive human skeleton fitting. In *Proceedings of the Conference on Vision Interface*, pages 35–42, 2003.

[70] Costas Panagiotakis and Georgios Tziritas. Recognition and tracking of the members of a moving human body. In *Proceedings of the International Workshop on Articulated Motion and Deformable Objects*, pages 86–98, September 2004.

[71] Huazhong Ning, Tieniu Tan, Liang Wang, and Weiming Hu. People tracking based on motion model and motion constraints with automatic initialization. *Pattern Recognition*, 37(7):1423–1440, July 2004.

[72] Rui M. Jesus, Arnaldo J. Abrantes, and Jorge S. Marques. Tracking the human body using multiple predictors. In *Workshop on Articulated Motion and Deformable Objects*, volume 2492 of *LNCS*, pages 155–164. Springer, 2002.

[73] David K. Wagg and Mark S. Nixon. Model-based gait enrolment in Real-World imagery. In *Proceedings of the Workshop on Multimodal User Authentication*, Santa Barbara, CA, USA, 2003.

[74] M. Andriluka, S. Roth, and B. Schiele. People-tracking-by-detection and people-detection-by-tracking. In *Proceedings of the IEEE Conference on Computer Vision and Pattern Recognition*, pages 1–8, 2008.

[75] Grégory Rogez, Carlos Orrite-Urunuela, and Jesus Martinez-del-Rincon. A spatio-temporal 2D-models framework for human pose recovery in monocular sequences. *Pattern Recognition*, 41(9):2926–2944, September 2008.

[76] Rafael C. Gonzalez and Richard E. Woods. *Digital Image Processing*, chapter 6. Prentice Hall, second edition, 2002.

[77] N. J. B. McFarlane and C. P. Schofield. Segmentation and tracking of piglets in images. *Machine Vision and Applications*, 8(3):187–193, May 1995.

[78] Christopher Richard Wren, Ali Azarbayejani, Trevor Darrell, and Alex Paul Pentland. Pfinder : Real-Time tracking of the human body. *IEEE Transaction on Pattern Analysis and Machine Intelligence*, 19(7):780 – 785, 1997.

[79] C. Stauffer and W.E.L. Grimson. Adaptive background mixture models for real-time tracking. In *Proceedings of the Conference on Computer Vision and Pattern Recognition*, pages 246–252, Fort Collins, CO, USA, 1999.

[80] N.M. Oliver, B. Rosario, and A.P. Pentland. A bayesian computer vision system for modeling human interactions. *IEEE Transactions on Pattern Analysis and Machine Intelligence*, 22(8):831–843, August 2000.

[81] Z. Zivkovic. Improved adaptive gaussian mixture model for background subtraction. In *Proceedings of the 17th International Conference on Pattern Recognition*, pages 28–31, Cambridge, UK, 2004.

[82] Simone Calderara, Rudy Melli, Andrea Prati, and Rita Cucchiara. Reliable background suppression for complex scenes. In *Proceedings of the 4th ACM international workshop on Video Surveillance and Sensor Networks*, pages 211–214, Santa Barbara, California, USA, 2006. ACM.

[83] K. Rangarajan and M. Shah. Establishing motion correspondence. In *Proceedings of the Conference on Computer Vision and Pattern Recognition*, pages 103–108, 1991.

[84] B.K.P Horn and B.G. Schunck. Determining optical flow. *Artificial Intelligence*, 17:185–203, 1981.

[85] Janne Heikkilä. Geometric camera calibration using circular control points. *IEEE Transactions on Pattern Analysis and Machine Intelligence*, 22(10):1066–1077, 2000.

[86] Chan-Su Lee and Ahmed Elgammal. Towards scalable View-Invariant gait recognition: Multilinear analysis for gait. In *Audio- and Video-Based Biometric Person Authentication*, volume 3546 of *LNCS*, pages 395–405. Springer, 2005.

[87] Jiwen Lu and Yap-Peng Tan. Uncorrelated discriminant simplex analysis for view-invariant gait signal computing. *Pattern Recognition Letters*, 31(5):382–393, April 2010.

[88] Ju Han, Bir Bhanu, and Amit K. Roy-Chowdhury. A study on View-Insensitive gait recognition. In *Proceedings of the IEEE International Conference on Image Processing*, volume 3, pages 297 – 300, September 2005.

[89] Amit Kale, Amit K. Roy Chowdhury, and Rama Chellappa. Towards a view invariant gait recognition algorithm. In *Proceedings of the IEEE Conference on Advanced Video and Signal Based Surveillance*, pages 143–150, 2003.

[90] Amit K. Roy Chowdhury, Amit Kale, and Rama Chellappa. Video synthesis of arbitrary views for approximately planar scenes. In *Proceedings of the IEEE International Conference on Acoustics, Speech, and Signal Processing*, volume 3, pages 497–500, 2003.

[91] Nicholas M. Spencer. *Pose Invariant Gait Analysis And Reconstruction*. Thesis, University of Southampton, December 2005.

[92] Nicholas M. Spencer and John Carter. Towards pose invariant gait reconstruction. In *Proceedings of the IEEE International Conference on Image Processing*, volume 3, pages 261–264, 2005.

[93] Michela Goffredo, Nicholas M. Spencer, Daniel Pearce, John N. Carter, and Mark S. Nixon. Human perambulation as a self calibrating biometric. In *Analysis and Modeling of Faces and Gestures*, volume 4778 of *LNCS*, pages 139–153. Springer Berlin, 2007.

[94] Michael W. Whittle. *Gait Analysis : An Introduction*. Butterworth-Heinemann, Edinburgh ; New York, 4th edition, 2007.

[95] Jacquelin Perry and Judith M. Burnfield. *Gait Analysis : Normal and Pathological Function*. SLACK, Thorofare, NJ, 2nd edition, 2010.

[96] Christopher Kirtley. *Clinical Gait Analysis : Theory and Practice*. Elsevier Churchill Livingstone, Edinburgh ; Toronto, 2006.

[97] Jessica Rose and James G. Gamble. *Human Walking*. Lippincott Williams and Wilkins, Philidelphia, 3rd edition, 2006.

[98] Richard I. Hartley and Andrew Zisserman. *Multiple View Geometry in Computer Vision*. Cambridge University Press, second edition, 2004.

[99] Robust regression – MATLAB. http://www.mathworks.com/help/toolbox/stats/robustfit.html, 2011.

[100] Cubic spline data interpolation – MATLAB. http://www.mathworks.com/help/techdoc/ref/spline.html, 2011.

[101] Richard O. Duda, Peter E. Hart, and David G. Stork. *Pattern Classification*. Wiley-Interscience, 2nd edition, November 2001.

[102] Christopher M. Bishop. *Pattern Recognition and Machine Learning*. Springer, 1st edition, October 2006.

[103] Ethem Alpaydin. *Introduction to machine learning*. Adaptive computation and machine learning. MIT Press, 2004.

[104] K. S. Arun, T. S. Huang, and S. D. Blostein. Least-Squares fitting of two 3-D point sets. *IEEE Transactions on Pattern Analysis and Machine Intelligence*, 9(5):698–700, 1987.

[105] Laurens van der Maaten. MATLAB toolbox for dimensionality reduction 0.7.2. http://homepage.tudelft.nl/19j49/Matlab_Toolbox_for_Dimensionality_Reduction.html, November 2010.

[106] Frédéric Jean, Robert Bergevin, and Alexandra Branzan-Albu. Body tracking in human walk from monocular video sequences. In *Proceedings of the Second Canadian Conference on Computer and Robot Vision (CRV)*, pages 144–151, Victoria, BC, Canada, May 9-11 2005.

[107] Frédéric Jean, Robert Bergevin, and Alexandra Branzan-Albu. Computing view-normalized body parts trajectories. In *Proceedings of the Fourth Canadian Conference on Computer and Robot Vision (CRV)*, pages 89–96, Montreal, QC, Canada, May 27-30 2007.

[108] Frédéric Jean, Robert Bergevin, and Alexandra Branzan-Albu. Computing and evaluating view-normalized body part trajectories. *Image and Vision Computing*, 27(9):1272–1284, August 2009.

[109] Frédéric Jean, Robert Bergevin, and Alexandra Branzan-Albu. Trajectories normalization for viewpoint invariant gait recognition. In *Proceedings of the 19th International Conference on Pattern Recognition*, Tampa, Florida, USA, December 8-11 2008.

[110] Frédéric Jean, Alexandra Branzan-Albu, and Robert Bergevin. Towards view-invariant gait modeling: Computing view-normalized body part trajectories. *Pattern Recognition*, 42(11):2936–2949, November 2009.

[111] Frédéric Jean, Robert Bergevin, and Alexandra Branzan-Albu. Human gait characteristics from unconstrained walks and viewpoints. In *Proceedings of the IEEE International Conference on Computer Vision Workshop on Visual Surveillance*, Barcelona, Spain, November 6-13 2011.